Chitosan Edible Films Crosslinked by Citric Acid

by

Joseph Khouri

A thesis
presented to the University of Waterloo
in fulfillment of the
thesis requirement for the degree of
Doctor of Philosophy
in
Chemical Engineering

Waterloo, Ontario, Canada, 2019

Examining Committee Membership

The following served on the Examining Committee for this thesis. The decision of the Examining Committee is by majority vote.

External Examiner: Loong-Tak Lim
Professor
Dept. of Food Science, University of Guelph

Supervisor(s): Christine Moresoli
Professor
Dept. of Chemical Engineering, University of Waterloo

Alexander Penlidis
Professor
Dept. of Chemical Engineering, University of Waterloo

Internal Member: Xianshe Feng
Professor
Dept. of Chemical Engineering, University of Waterloo

Internal Member: Boxin Zhao
Associate Professor
Dept. of Chemical Engineering, University of Waterloo

Internal-External Member: Scott Taylor
Professor
Dept. of Chemistry, University of Waterloo

Author's Declaration

This thesis consists of material all of which I authored or co-authored: see Statement of Contributions included in the thesis. This is a true copy of the thesis, including any required final revisions, as accepted by my examiners.

I understand that my thesis may be made electronically available to the public.

Statement of Contributions

A portion of the work presented in Chapter 5 has been published (*Processes* **2019**, 7(3), 157), of which I was the first author, and I conducted all experimental work presented in that article. Chapter 6 contains material that has been submitted for publication, of which I was the first author, and I conducted all experimental work presented in that manuscript.

Abstract

Chitosan offers an exciting potential as a safe, biodegradable material for niche food packaging and coating applications. Barriers to getting this crustacean-derived polysaccharide to the packaging market include poor processability and the competitive advantage of petroleum-based thermoplastics, which are cheaper, easier to produce, and have overall better mechanical and gas barrier properties. Crosslinking chitosan films with citric acid as a means of improving mechanical and moisture barrier properties was the objective of this research project.

Incorporating citric acid into chitosan films using the heterogeneous crosslinking procedure for food packaging applications was investigated for the first time. Briefly, the heterogeneous crosslinking methodology involves neutralizing a solvent cast neat chitosan film, then adding the crosslinker to the neutralized film. Chitosan films with 15 % citric acid (w/w), denoted as CA films, were characterized and their structure - property relationships were compared with neat and neutralized films.

Converting the crosslinking type between citric acid's carboxylates and chitosan's primary amine groups from ionic to covalent bonding requires thermal treatment. The CA films were heated at 150 °C for 0.5 h, denoted as CA-HT films. The covalent crosslinking was assessed by studying the temperature-dependent viscoelastic properties of the films from 30 to 200 °C using dynamic mechanical analysis (DMA) and by considering principles of the rubber elasticity theory. The viscoelastic properties of chitosan films homogeneously and heterogeneously crosslinked with a model crosslinker, glutaraldehyde (GLU), were also studied for comparative purposes. Covalent crosslinking of thermally treated CA films was not confirmed due to a non-significant difference between the storage modulus, E', of neutralized, CA and CA-HT films.

The DMA study also produced data that supports the notion that the tanδ relaxation peak of neat films near 165 °C is ascribable to structural relaxation caused by the acid present in the film, and is not a typical glass-rubber transition as it is often described in the literature. The tanδ relaxation peak diminished with neutralization and by increasing GLU concentration from 3 to 12 % (w/w). A partial resurgence of this tanδ peak occurred near 130 °C after the addition of citric acid, both in films prepared heterogeneously and in films cast with 15 % citric acid (w/w) in the filmogenic solution, providing further evidence of the relaxation mechanism source.

Following the DMA work, the physical properties of chitosan films ionically crosslinked with citric acid were studied. Thermogravimetric analysis (TGA) tests showed citric acid enhanced thermal stability by increasing the temperature of the maximum rate of degradation by 7 °C compared to a neutralized film. The tensile strength (TS) increased from 60 to 85 to 95 MPa, for neat, neutralized and CA films, respectively, while elongation capacity remained constant, demonstrating a positive effect of ionic crosslinking on the

mechanical properties. The crystallinity of CA films decreased relative to neutralized films, but were similar with respect to neat films, as estimated from x-ray diffraction (XRD).

The water vapor permeability (WVP) was lowest for neat films at 5.06×10^{-11} g/(m·s·Pa) and highest for neutralized films at 10.70×10^{-11} g/(m·s·Pa). Incorporating citric acid into neutralized films decreased the WVP to 7.38×10^{-11} g/(m·s·Pa) demonstrating the positive influence that organic acids have on the hydrogen bonding network of the film matrix in hindering moisture permeability. Moisture sorption isotherms supported the trends observed with the WVP measurements. Water contact angle measurements showed that the surface of CA films were slightly more hydrophobic, 79° compared to 72° for neat films, which is advantageous for packaging applications.

Citric acid shows some benefits as a crosslinker for chitosan, particularly with the heterogeneous crosslinking method. The mechanical, thermal stability, and moisture barrier properties improved relative to either neat or neutralized films. Suggestions for future work include modification or optimization of the crosslinked film formation methodology to further enhance film characteristics mechanical and gas barrier properties. Additional properties such as oxygen and carbon dioxide permeability and antimicrobial properties could be investigated.

Acknowledgements

I would like to thank my supervisors Dr. Christine Moresoli and Dr. Alex Penlidis for providing me with the opportunity to pursue a doctorate in chemical engineering, and for their guidance throughout the process. I would like to thank my committee members, Dr. Loong-Tak Lim, Dr. Scott Taylor, Dr. Xianshe Feng, and Dr. Boxin Zhao for their support and advice.

I appreciate the assistance of Ralph Dickhout and Bert Habicher for training, technical matters and helpful discussions. I also thank the Chemical Engineering Department staff for their help, including Judy Caron, Rose Guderian, Ingrid Sherrer, and Liz Bevan.

I appreciate the training, assistance and helpful discussions with Dr. Geoff Rivers and Dr. Allen Rogalsky for the DMA measurements. I also would like to thank Dr. Nina Heinig for the XRD measurements, Dr. Sigrid Peldszus for permission to use the drop shape analyzer, and Jennifer Moll for assistance with the light microscope.

I extend my best wishes to my group members and colleagues, past and present, for your insightful discussions, advice, and good company: Dr. Hasan Moussa, Dr. Rasool Nasseri, Nagma Zerin, Huayu Niu, Dr. Omar Al-Kubaisi, Chu Yin Huang, Dr. Katharina Hassel, and Priscilla Lai. And I can't forget to thank my former co-op students: Scotty, Kari, and Leo. Thank you to Kari for compiling the MATLAB code for film image analysis.

And finally, thanks to Lana and Nancy for their assistance in proof reading parts of this thesis.

Dedication

To Fadi, Lana, and Christine.

Table of Contents

List of Tables

List of Figures

List of Symbols

A	Film cross-sectional area [m^2]
A_a	Integrated diffractogram area, amorphous component
A_c	Integrated diffractogram area, crystalline component
a_w	Water activity
c	Gas concentration [mol/L]
C_G	Sorption monolayer constant
CrI	Degree of crystallinity/crystallinity index [%]
D	Diffusion coefficient [m^2/s]
d	Distance between parallel crystal lattices [Å]
E	Young's modulus of elasticity [Pa]
E'	Dynamic tensile storage modulus [Pa]
E''	Dynamic tensile loss modulus [Pa]
E^*	Complex tensile modulus [Pa]
E_∞	Unrelaxed modulus [Pa]
F	Free energy [J/mol]
G	Elastic shear modulus [Pa]
i	Imaginary number, $\sqrt{-1}$
K_a	Acid dissociation constant
k_B	Boltzmann's constant, 1.3806×10^{-23} J/K
K_G	Multilayer moisture sorption constant
L	Length, test specimen for tensile measurement [m]
l	Film thickness [μm]
M	Molar mass [g/mol]
m	Mass [g]
$\overline{M}_c$	Average molecular weight between crosslinks [g/mol]
$\overline{M}_v$	Viscosity average molecular weight [g/mol]
n	Number of replicate runs
$\tan\delta$	Dissipation factor
P	Permeability coefficient [$m^3 \cdot m/m^2 \cdot s \cdot Pa$]
P	Peak load or load at tensile failure [N]
p	Vapor pressure [Pa]

pH	Power of hydrogen
pK_a	Power of acid dissociation constant
R	Ideal gas constant [Pa·m^3/mol·K]
R_i	Resistance to gas permeation from component i [m^2·s·Pa/g]
S	Solubility coefficient [m^3/m^3·Pa]
S	Saturation vapor pressure [Pa]
T	Temperature [^{o}C]
t	Lapsed time [s]
T_{cure}	Cure temperature [^{o}C]
t_{cure}	Cure time [h]
T_g	Glass transition temperature [^{o}C]
u	Complex frequency [Hz]
V	Volume of network polymer [m^3]
v	Poisson's ratio
X	Percentage of moisture absorbed [g-H_2O/g-dry basis]
x_m	Monolayer moisture constant
α	Significance level [%]
α	Extension ratio
α_i	Grazing incidence angle [^{o}]
δ	Phase angle [^{o}]
ϵ	Tensile strain [%]
γ	Surface tension or surface energy [J/m^2]
λ	Principal extension ratio
λ	Incident of light wavelength [nm]
μ	Number of crosslink junctions
ν	Crosslink density [mol/L]
ρ	Density [g/L]
Π	Permeation [g/m^2·s·Pa]
ϕ	Crosslinking functionality
σ	Tensile stress [Pa]
θ	Light scattering angle [^{o}]
θ	Liquid contact angle [^{o}]
ω	Angular frequency [radians/s]
ξ	Network cycle rank

List of Acronyms

ATR	Attenuated Total Reflectance
BET	Brunauer-Emmett-Teller model
CA	Chitosan film containing citric acid
CA-HT	Heat treated chitosan film containing citric acid
CP	Carbon Dioxide Permeability [$cm^3/m{\cdot}s{\cdot}Pa$]
DD	Degree of Deacetylation
DMA	Dynamic Mechanical Analysis
DSC	Differential Scanning Calorimetry
DTGA	Differential Thermogravimetric Analysis
EBB	Elongation Before Break [%]
EDC	1-ethyl-3-(3-dimethylaminopropyl) carbodiimide
FDA	Food and Drug Administration
FTIR	Fourier Transform Infrared Spectroscopy
FWHM	Full Width at Half Maximum
GAB	Guggenheim-Anderson-de Boer model
GLU	Glutaraldehyde
GLU-HET	Chitosan-glutaraldehyde crosslinked film, heterogeneous method
GLU-HOM	Chitosan-glutaraldehyde crosslinked film, homogeneous method
GRAS	Generally Regarded as Safe
GIXRD	Grazing Incidence X-ray Diffraction
HPMC	Hydroxypropyl methylcellulose
HPN	Hybrid Polymer Network
IPN	Interpenetrating Polymer Network
OP	Oxygen Permeability [$cm^3/m{\cdot}s{\cdot}Pa$]
RH	Relative Humidity [%]
SHP	Sodium hypophosphite
TGA	Thermogravimetric Analysis
TS	Tensile Strength [MPa]
WVP	Water Vapor Permeability [$g/m{\cdot}s{\cdot}Pa$]
WVTR	Water Vapor Transmission Rate [$g/m^2{\cdot}s$]
XRD	X-ray Diffraction

Chapter 1

Thesis Introduction

1.1 Motivation

Natural and renewable resourced materials that are biodegradable, ecologically non-toxic, and non-harmful to human organs are desirable food packaging agents. While plastics are superior materials for the storage and preservation of food, they are toxic to the environment and are non-biodegradable. Polysaccharide edible films are therefore a high interest research topic for their potential to reduce the production and consumption of olefin-derived plastics commonly used for packaging. Efforts are being made to further develop a wider range of food-related products from cellulose-derivatives, starches, chitosan, and blends of these polysaccharides.

Chitosan is a particularly unique polysaccharide as it has good anti-microbial and anti-bacterial properties [1], which provides an additional incentive to develop it for niche food applications. Chitosan films, however, have poor thermo-processability, high water affinity and less durable mechanical properties [2] compared to common plastics (e.g., polyethylene terephthalate, low density polyethylene), and are still under-developed commercially. Physical or chemical modification is necessary to address these deficiencies and improve crucial technical properties such as tensile strength and resistance to water vapor permeability.

Modification could involve either composite formation with a hydrophobic compound [3], grafting of a hydrophobic compound on the polymer's reactive side groups [4, 5], or intermolecular crosslinking between the polymer chains [5–7]. While all these methods have benefits and shortcomings, crosslinking is a promising approach since it could potentially improve mechanical and gas barrier properties simultaneously. The criterion for a crosslinking agent is that the compound be Generally Regarded as Safe (GRAS), derived from a natural and renewable resource, and be capable of forming a minimum of two covalent bonds. Citric acid was selected as a crosslinker for this

study. Its potential for covalent crosslinking of chitosan films was investigated, and the physico-chemical properties of chitosan films with citric acid relevant to the target application were characterized.

1.2 Research Objectives

The objective of this project was to improve moisture barrier and mechanical properties of chitosan films using citric acid as a crosslinking agent. As part of the objective, it was deemed necessary to address a complication in the crosslinking procedure that appeared overlooked by previous studies on chitosan films crosslinked by citric acid. In brief, the films are prepared by the solvent casting method, with acetic acid as the solvating agent for chitosan. In chitosan-citric acid crosslinking studies [5, 8], a procedure referred to as *homogeneous crosslinking* was used, where the crosslinking agent is present in the film-forming solution. This causes competition between citric acid and acetic acid for a reaction with chitosan when the film is heated to induce covalent bonding. For this study, *heterogeneous crosslinking* was used, where residual acetic acid is removed from the dried film by neutralization prior to the addition of the crosslinker, thus providing exclusivity for reaction to citric acid. Heterogeneous crosslinking is an established procedure for other crosslinkers such as glutaraldehyde and epichlorohydrin [9]. To the best of the author's knowledge, this project utilized heterogeneous crosslinking method for crosslinking chitosan with citric acid for edible film applications for the first time.

The first step was to select the conditions in the preparation of chitosan films crosslinked with citric acid. This included mass ratio of citric acid to chitosan and duration of exposure of the chitosan film to a citric acid aqueous solution. The other factors were heat treatment conditions, temperature and duration, that are typically applied to polysaccharide-citric acid films to force covalent bonding. The second step was to assess crosslinking of heterogeneously prepared chitosan-citric acid crosslinked films. Dynamic mechanical analysis (DMA) was used to evaluate crosslinking and address the question of whether the chosen thermal conditions resulted in covalent crosslinking or whether citric acid-chitosan interaction remained ionic. The third step was to characterize the physico-chemical properties of the heterogeneously prepared chitosan-citric acid films and compare them with neat and neutralized films. Characterization included thermogravimetric analysis (TGA), water vapor permeability (WVP) and mechanical properties for tensile strength (TS) and elongation before break (EBB). To elucidate changes in the physico-chemical properties associated with structural changes stemming from the inclusion of citric acid, the crystalline structure of the films was investigated using x-ray diffraction (XRD). And to further elicit information on the hydrophilic character of the films, liquid contact angle (sessile drop method) and moisture sorption isotherm measurements were performed.

To summarize, the research objectives are to identify appropriate film formation conditions, investigate covalent crosslinking *via* DMA, and characterize the physical properties of the films. A schematic of these project steps and objectives is given in Figure 1.1.

1.3 Thesis Layout

A literature review is provided in Chapter 2 of relevant background information pertaining to the different facets of the research project and materials involved. This includes the structure and chemistry of chitosan, a review on the properties of polysaccharide and chitosan films, general information on polymer crosslinking, and a summary of the experimental conditions of chitosan/polysaccharide crosslinking with citric acid.

Chapter 3 details the film-forming procedures, and the experimental procedures of the analytical DMA, WVP, mechanical, XRD, and contact angle measurements. Theoretical and applicable background information on these analytical techniques are included.

Chapter 4 presents preliminary experimental work that was conducted to select the film-forming factors that were used for the remainder of the work. This includes citric acid concentration in the films and the temperature and time of thermal treatment.

Chapter 5 presents the results from DMA measurements for the crosslinked and non-crosslinked films, including films prepared with a model crosslinker, glutaraldehyde. An assessment is given on the final bonding state of films with citric acid after heat treatment (i.e. covalent or other). An in-depth analysis on the question of the glass transition of chitosan films is also provided.

Chapter 6 presents the TGA, WVP, mechanical, XRD and contact angle measurements of films with citric acid and without citric acid (neat, neutralized films). The results are cross-analyzed to offer insights on structure-property relationships by assessing the influence of neutralization and citric acid on the physico-chemical properties.

Chapter 7 provides a summary of the thesis, contributions to the field, and a list of suggestions for short- and long-term experimental work to build upon based on the findings presented in the preceding chapters.

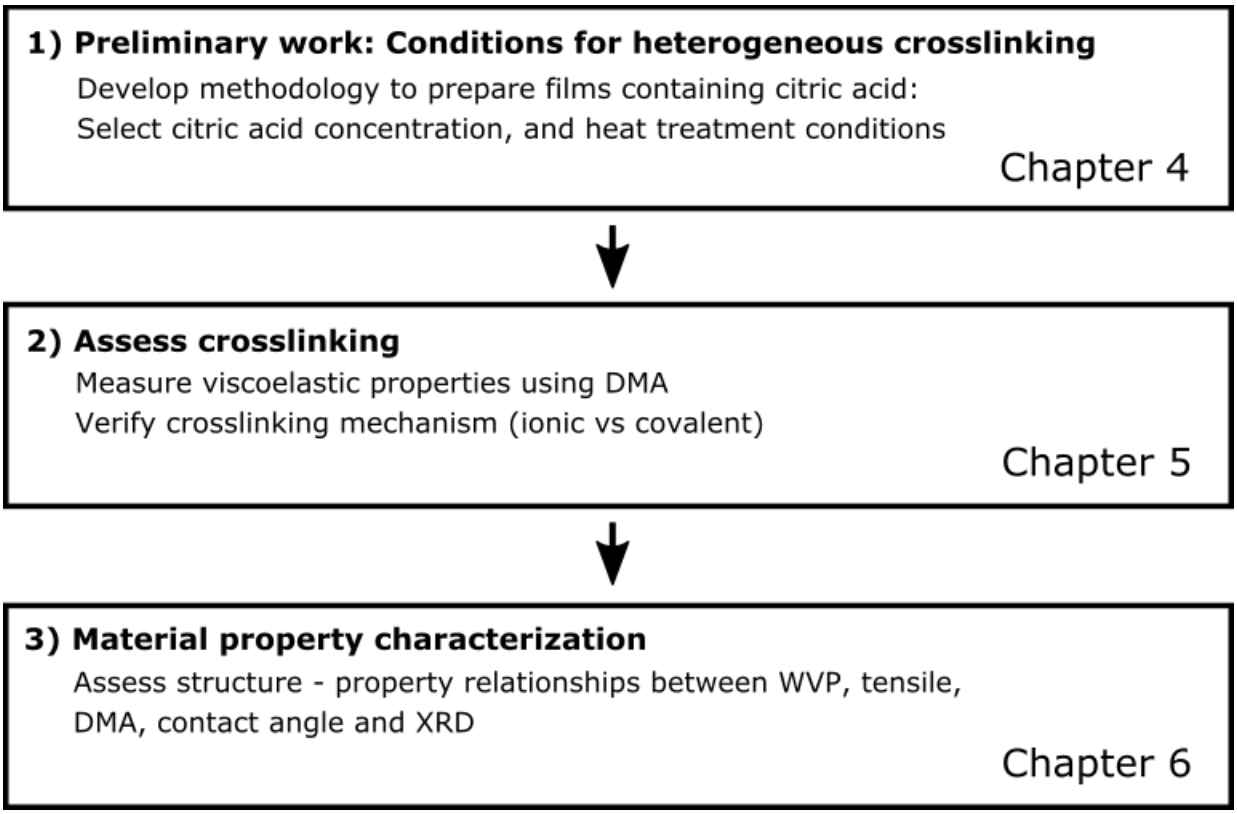

Figure 1.1: Research objectives of chitosan heterogeneous crosslinking project and associated thesis chapters.

Chapter 2

Background and Literature Review

2.1 Edible Films

2.1.1 Background

An edible film is any membrane made from an aqueous hydrocolloid or polymer that serves as a protective cover for food, is also itself consumable [10], and is approved by the US Food and Drug Administration (FDA). Films can either be in the form of a coating, where the film-forming solution is applied directly on the food (by dipping, brushing, or spraying), or as a stand-alone film where the film is prepared separately by solvent casting or extrusion [11]. The functions of an edible film can range from shelf life extension, aesthetic enhancement, texture enhancement, or delivery of antimicrobial, flavor, or nutritional agents [12, 13]. Typical sources for edible films include proteins such as gelatin, casein and whey, cellulose ethers, and modified starches. Lipids are employed for moisture control, while polysaccharides provide good structure stability and barrier against O_2, CO_2, and ethylene gas diffusion [10]. Coatings on meats, seafood, nuts, confectionery, fruits and vegetables, often result in prolonged firmness, and reduction of respiration rate and ethylene production [12].

Stand-alone films can be applied as packages (e.g. pouches for vitamin packs, food additives, color additives, or beverage mixes) or as free-standing films (e.g. dental applications, labels, nutraceuticals) [10]. Polysaccharide films are most often made from solvent casting, with thermoforming being less common due to difficulties with molding from degradation at high temperatures. Hydroxypropyl methylcellulose, thermoplastic starch and polylactic acid can be thermo-molded more easily than chitosan and other natural polymers. Commercial films are produced by casting on a disposable substrate or rotating stainless steel belt [10].

2.1.2 Polysaccharide Films

Commercial polysaccharide films emerged in the 1960's, beginning with hydroxypropyl methylcellulose [10]. Today, starch-based bags, bagasse-based containers, and plant fiber-based plates are being manufactured [14]. Pectins, alginates, gums (arabica, xanthan) and pullulan are examples of other common polysaccharides used for edible films [10]. The food industry is already reliant on native and modified starch and cellulose-ethers for rheological, adhesive, and texture-additive purposes. A brief discussion is given here on edible films from the most abundant polysaccharides, starch, cellulose, and chitosan.

Starch yields films that are odorless, colorless, and tasteless. Durable and isotropic films can also be prepared from pure amylose [15]. Starch films can be processed by either wet (solvent casting) or dry (shearing) methods. Wet processing involves gelatinization at high temperatures in water, and dry processing requires a plasticizer such as sorbitol or glycerol, and a minimal amount of water using a batch mixer (e.g. Brabender instruments) to yield thermoplastic starch (TPS). The TPS pellets are further processed by a molding process, such as injection, foam, and reactive molding [15, 16]. Cellulose-based films are typically produced from water-soluble derivatives such as methyl-cellulose, ethylmethyl cellulose, cellulose-acetate, cellulose-nitrate, hydroxypropyl methylcellulose (HPMC), and hydroxypropyl cellulose (HPC). Native cellulose is not readily soluble in aqueous solutions. HPMC and HPC can form sturdy, flexible and transparent films [17], and can also be molded by hot extrusion. Non-modified microfibrillated cellulose films have good properties but are high in cost and energy consumption [16].

Chitosan films are mostly made by wet processing from dilute acid aqueous solutions, but lately there have been developments in creating thermoplastic chitosan by thermomechanical processing [18–22]. Mechanical kneading with a plasticizer such as sorbitol [19] can form rigid and processable chitosan materials. Additionally, chitosan could be extruded at low concentrations by blending with a conventional thermoplastic, but requires a compatibilizing agent to reduce phase separation.

Polysaccharide films in general display a similar range of properties: high barrier to gases (CO_2, O_2, ethylene), poor barrier to moisture, high tensile strength, and low ductility. Due to the hydrophilic nature of polysaccharide films, the high barrier to gases is conditional on the test temperature and relative humidity, whereby humid environments reduce the barrier properties. Table 2.1 provides a brief list of gas barrier and mechanical properties, namely water vapor permeability (WVP), tensile strength (TS), elongation before break (EBB), carbon dioxide permeability (CP), and oxygen permeability (OP), for films of chitosan, starches, and cellulose-derivatives, along with some plastics for comparative purposes. For additional information on the film and test variables corresponding to the properties listed in the table, i.e. conditioning, film content, fillers, or plasticizer content, readers may consult the respective references.

Table 2.1: Mechanical and barrier properties of polysaccharide and thermoplastic films.

Material	Test conditions		WVP	TS	EBB	OP	CP
	T [°C]	ΔRH [%]	$\times 10^{-11}$ [g/m·s·Pa]	[MPa]	[%]	$\times 10^{-12}$ [cm^3/m·s·Pa]	$\times 10^{-12}$ [cm^3/m·s·Pa]
Starch (yam, cassava, rice, corn) + plasticizer (glycerol, sorbitol) [15] and references within	20 - 25	0 - 70 (WVP, OP, CP)	2.7 - 44.6	1.6 - 30.0	3 - 60	248 - 1,592	4,190 - 29,210
Starch + MC + plasticizer (glycerol, xylose) [23]	25	60 (WVP)	0.48 - 26.5	12.6 - 61.2	4.2 - 24.5	0.5 - 6,500	4.3 - 70,000
Starch (corn, rice) + chitosan + plasticizer [24–26]	20 - 25	60 - 75 (WVP)	4 - 23	5.0 - 38.0	3 - 22	n.g.	n.g.
Starch + CMC [27]	25	100	6.5 - 6.81	6.6 - 16.1	60 - 65	n.g.	n.g.
Chitosan [28–31]	25	50 (WVP), 0 - 60 (OP, CP)	1 - 33	14 - 150	4 - 42	0.1 - 10.5	0.2
MC [32–35]	25 - 30	0 (OP), 10 - 50 (WVP)	8.4 - 12.1	48.0 - 66.3	2 - 26	1	n.g.
HPC, HPMC [32, 35, 36]	23 - 30	0 (OP), 10 - 50 (WVP)	2.5 - 6.6	11.0 - 86	4 - 64.3	3	n.g.
Cellophane [26, 31, 37]	n.g.	n.g.	8.4	86	14	6 - 14,480	620
LDPE, HDPE [15, 26, 32, 35]	25 - 30	0 - 100 (WVP, OP)	0.02 - 0.09	9 - 35	150 - 965	5 - 21	n.g.
PP [15]	25 - 30	0 - 100 (WVP)	n.g.	42	300	n.g.	n.g.
PVA [38]	n.g.	n.g.	n.g.	60	105	n.g.	n.g.
PVC, PET [15, 31, 35]	25 - 30	0 - 100 (WVP)	0.2 - 0.7	n.g.	n.g.	2×10^{-5} - 0.1	n.g.

Properties: WVP - water vapor permeability, TS - tensile strength, EBB - elongation before break, OP - O_2 permeability, CP - CO_2 permeability
Materials: CMC - carboxy methylcellulose, HDPE - high density polyethylene, HPC - hydroxypropyl cellulose, LDPE - low density polyethylene, MC - methyl cellulose, PET - polyethylene terephthalate, PP - polypropylene, PVA - polyvinyl alcohol, PVC - polyvinyl chloride. Some unit conversions had to be made from the values listed in the references to those listed here. n.g. - not given in respective references

2.2 Background on Chitosan

2.2.1 Sources and Production

Chitosan is the deacetylated form of chitin. Commercial chitosan is mainly produced from the chemical derivation of chitin, which comprises 50 to 85 % [37] of exoskeletal shells of crustaceans (shrimps, crabs, crayfish, mollusk etc.). Chitin is also present in other sea creatures (squid pen, cuttlefish) [39, 40], and some fungi and insect species. Chitosan can be found in pure form in the cell walls of some fungi species (see [41] for more details), but is far less prevalent in nature than chitin. Isolating fungous chitosan has advantages of lower production cost and greater consistency of properties [41], but quantities are too low for significant production. By contrast, chitin harvested from seafood waste is economical, yet polymeric characteristics such as molecular weight may vary widely, from 1 to 2 MDa (M_v, viscosity average molecular weight) [37].

Chitin is purified from interlaced minerals and proteins by a series of alkaline and acid treatments [41] before it is converted to chitosan. The exoskeletal shells are ground, and the minerals (typically $CaCO_3$) are removed using a dilute acid solution [40, 41]. The acid and temperature conditions for de-mineralization depend on the mineral content which may vary with the source of chitin. After de-mineralization, the residuals are de-proteinated in dilute basic solution [41]. Residual color may be dealt with using acetone reflux [42] or light oxidizing treatment [39, 41] to yield a near white or slightly beige product. More specific isolation and preparation conditions are given elsewhere [40, 41] and schematically in Figure 2.1.

Chitin is reduced to chitosan by boiling in strong NaOH solutions of 40 - 50 % at temperatures of 90 - 120 ^{o}C for several hours [41] under nitrogen atmosphere. The NaOH concentration, temperature, and duration of treatment affect the extent of conversion of chitin to chitosan. Higher treatment times result in lower molecular weights and higher degree of deacetylation [42]. Enzymatic chitin-to-chitosan reactions are also possible with deacetylase chitin or acetyl xylan esterase [41]. The structural and chemical distinctions between chitin and chitosan are discussed in the following section.

2.2.2 Molecular and Crystal Structures

Chitosan is a linear aminopolysaccharide, (1,4)-2-amino-2-deoxy-β-D-glucan. Chitosan and chitin are copolymers of D-glucosamine and *N*-acetyl-D-glucosamine residues, which are glucose units with the second carbon (C2) hydroxyl side group replaced by an amine (-NH_2) or an acetamide side group (CH_3CONH-), respectively, as depicted in Figure 2.2. The two polymers are differentiated by the percentage of D-glucosamine

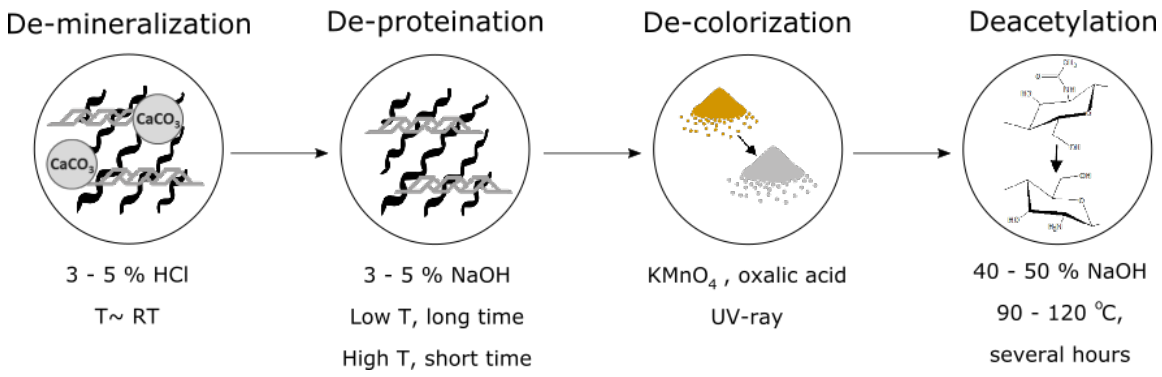

Figure 2.1: General procedure for the isolation of chitin and conversion to chitosan. Black squiggles represent polymer chains, and grey squiggles represent proteins.

units, termed the degree of deacetylation (DD). The polysaccharide is called chitosan when the DD is greater than 60 % and called chitin when it is less than that. They may also be classified by nitrogen content; 7 % nitrogen or greater for chitosan [37]. The residues alternate by a 180° rotation from one unit to the next along the polymer chain, and are linked through $\beta(1\rightarrow4)$ glycosidic bonds as shown in Figure 2.2. Molecular weight and DD of chitosan may vary widely from 8 to 375 kDa (M_v) [43, 44] and 75 to 99 % [38, 43], respectively, depending on the source of chitin and deacetylation process [43] (Section 2.2.1).

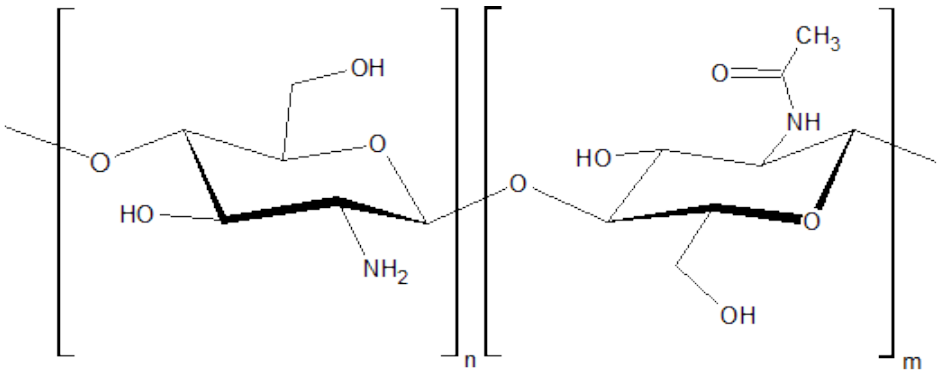

Figure 2.2: Structure of chitosan/chitin; D-glucosamine units and *N*-acetyl-D-glucosamine. For $n > 0.6$, the polymer is called chitosan, and for $n < 0.6$, the polymer is chitin.

The crystal structures and hydrogen bonding features of chitosan and chitin are briefly reviewed here. Chitin occurs naturally as a semi-crystal, and two allomorphs have been identified, with a possible third still in question [45] (not discussed here). α-chitin is extracted primarily from crustaceans [46], while β-chitin is found in squid pen. Both structures consist of long oriented fibers but the two polymorphs differ in their chain folding pattern and crystal unit structures. The α-chitin chains are arranged in an anti-parallel configuration, just as with cellulose II, and their unit cells are a tightly packed orthorhombic

structure with a $P2_12_12_1$ space group [47]. The β-chitin structure consists of chains arranged in a parallel manner in a monoclinic crystal also of $P2_12_12_1$. The rigid hydrogen bonding network prevents α-chitin from swelling in water [47], whereas the β-chitin is more susceptible to chemical reactions and has a greater affinity to solvents than its counterpart, as it lacks certain stabilizing hydroxymethyl hydrogen bonds [45].

Chitosan is semi-crystalline [48] with two main polymorphs, one hydrated, one anhydrous, and several secondary forms which are considered to be blends of the main two [45]. The polymorph and degree of crystallinity vary with the chitin source, deacetylation and other treatment conditions. The 'tendon' structure, shown in Figure 2.3, is the most prevalent form. It has similar characteristics with α-chitin, from which it is derived, notably the extended two-fold helix (zig-zag) chain configuration, packed in an anti-parallel manner and of orthorhombic unit cells [45, 49]. The chain repetition length and zig-zag chain conformation is secured by intramolecular O3$'\cdots$O5 hydrogen bonds. Adjacent (anti-parallel) chains are bound together by intermolecular O$\cdots$H-N2 bonds to form sheets (bc plane in Figure 2.3). The tendon lattice is hydrated by interstitial H_2O molecules that form intermediate hydrogen bonds between parallel sheets along the a-axis [49]; no direct hydrogen bonding occurs between the sheets of polymer chains.

Annealed chitosan, the anhydrous polymorph, is also of a zig-zag, anti-parallel structure with sheets held together by intrasheet N2$\cdots$O6 and O3$\cdots$O5 hydrogen bonds, as well as weak O3$\cdots$O6 bonds [45, 50]. No hydrogen bonding occurs along the a-axis (Figure 2.4) between chains in parallel sheets. Annealed chitosan can be converted from tendon chitosan by boiling chitosan in water near 240 ^{o}C [51]. Tendon and annealed polymorphs are distinguished via powder diffraction by a (020) reflection at approximately 10^{o} for tendon and (120) reflection at 15^{o} for the anhydrous form [51]. Other polymorphs of chitosan include mixed hydrated/anhydrous structures, such as '1-2' [45, 51, 52]. The structure of annealed chitosan is shown in Figure 2.4.

Solvent casting of a chitosan film using an organic or mineral acid produces a salt complex between the amine and conjugate base (discussed in Section 2.2.3), and the acid influences chitosan's microstructure in film compared to chitosan powder. Four different chitosan-salt arrangements have been identified [45, 50]. Briefly, films formed with a monocarboxylic acid yield a hydrated structure called Type II, shown in Figure 2.5. The original anti-parallel arrangement of chitosan chains remains unchanged [45], but the helical structure is altered to a 8/5 structure, which is also referred to as a relaxed twofold [53]. The length of this crystal lattice along the c-axis is roughly four times that of an ordinary tendon chitosan [50]. Additionally, when both the acid and water evaporate out of the crystal of a chitosan salt, the unit cell changes from a Type II to an annealed chitosan [50, 53, 54]. If the chitosan salt is heated past the boiling point of water it will similarly convert to the annealed form, but then reverses back due to reabsorption of moisture once it is cooled [54]. A comparison of the extended and relaxed two fold forms of the tendon and Type II structures is shown in Figure 2.5.

The crystallinity of α-chitin ranges between 56 to 90 % [39, 40, 55] and chitosan powder between 36 to 63 % [39, 56], depending on the calculation method [55]. Some degree of crystallinity is retained after film formation, from 10 to 22 % [9, 57, 58] typically, or occasionally reported up to 30 to 40 % [55, 59].

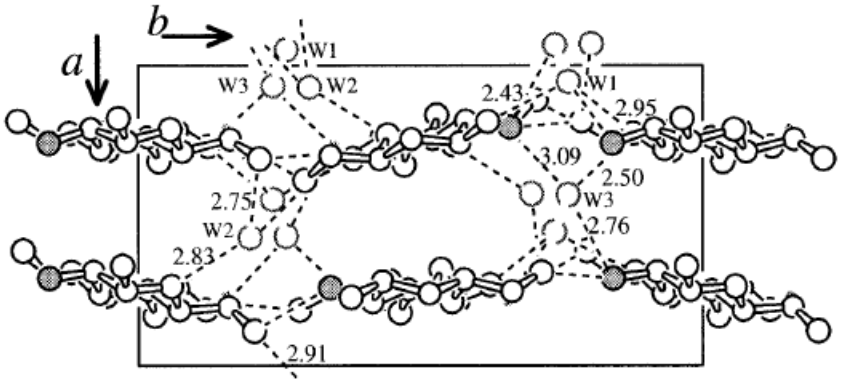

(A)

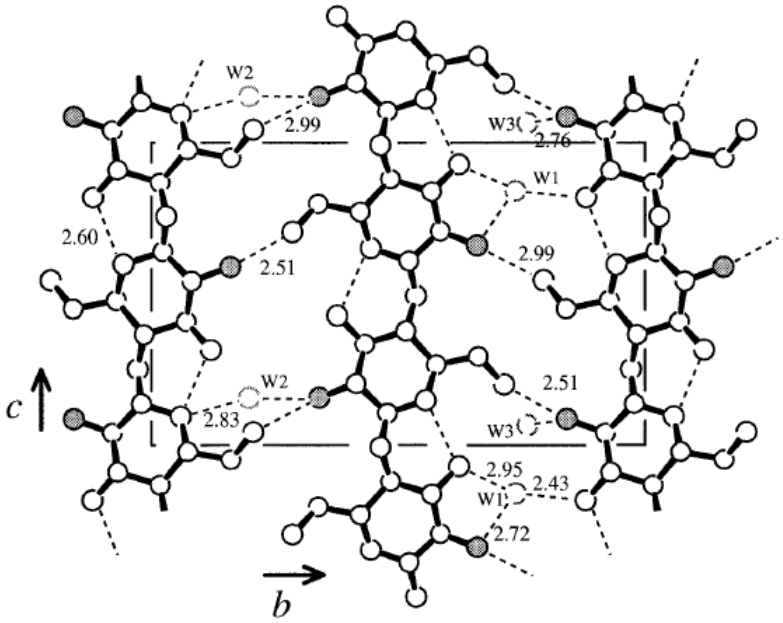

(B)

Figure 2.3: The molecular packing of 'tendon' chitosan crystal structure. (A) a-axis projection and (B) c-axis projection. Nitrogen atoms are represented by circles. For brevity, only three polymer chains from the a-axis projection are shown in the c-axis projection. There are three positions for H_2O molecules. Figure taken from Okuyama et al. [49].

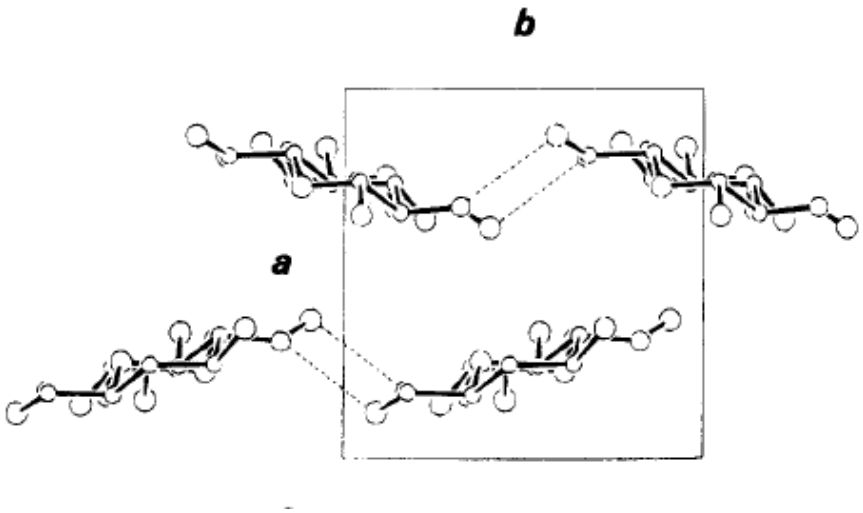

(A)

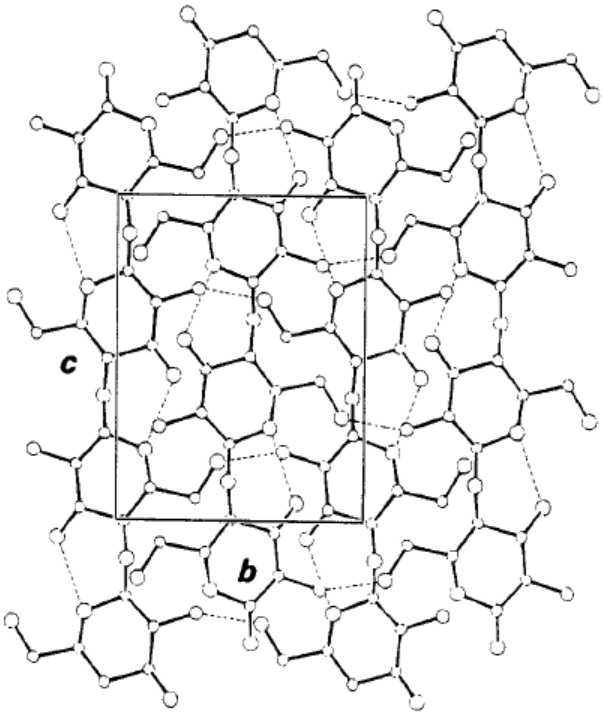

(B)

Figure 2.4: The molecular packing of 'annealed' chitosan crystal structure. (A) ab base plane and (B) bc base plane. Hydrogen atoms have been removed, and hydrogen bonds are represented by dashed lines. Figure taken from Yui et al. [60].

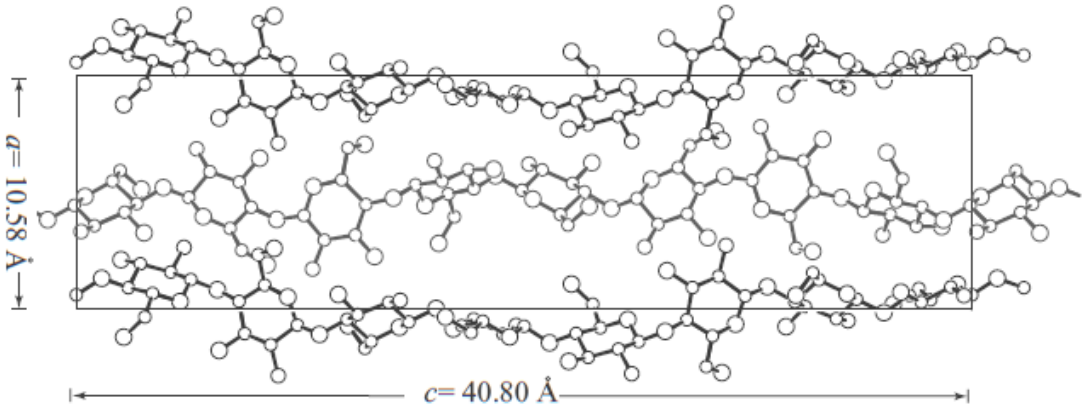

(A)

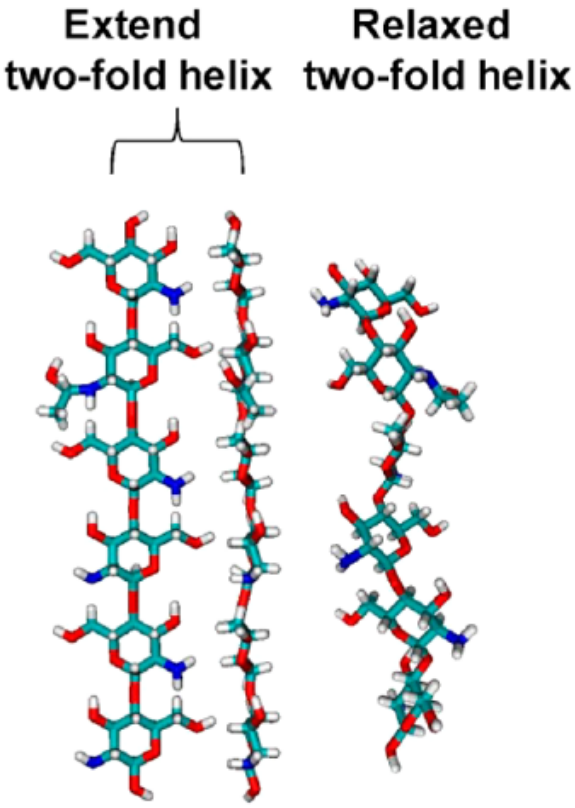

(B)

Figure 2.5: (A) The ac plane projection of the model for the Type II crystal structure of a chitosan-monocarboxylic acid salt; Figure taken from Ogawa et al. [50]. (B) A comparison of a tendon structure (extended two fold chains) and a Type II structure (relaxed two fold chains); Figure taken from Lee et al. [61].

2.2.3 Chitosan Solubility, Acid Solvents and Their Effects on Solution and Chitosan Film Properties

The dissolution of chitosan is critical for producing films by the solvent casting method. Chitosan is insoluble in water or basic solutions due to its high molecular weight, partial crystal structure, and extensive inter- and intra-molecular hydrogen bonding network. Nor is chitosan readily soluble in halogenated, aromatic or common organic solvents such as DMSO, DMF, THF, etc. [62], unless functionalized by alkylation or acylation [62, 63]. Salt complex formation with *p*-toluene-sulfonic acid or 10-camphorsulfonic acid allows dissolution in DMSO [64, 65]. Otherwise, chitosan readily dissolves in dilute aqueous organic and mineral acid solutions, such as acetic, formic, lactic, citric, phosphoric and hydrochloric acid, etc. [66]. As a weak polybase, chitosan becomes protonated at the amine side group, and the electrostatic repulsion partially disrupts the hydrogen bonds and crystal structure, enabling the chitosan flakes to swell and dissolve. The equilibrium reactions for the carboxylic acid and polyelectrolyte chitosan are:

$$\mathrm{R{-}COOH + H_2O \longrightarrow R{-}COO^- + H_3O^+}$$
$$\mathrm{Cht{-}NH_2 + H_3O^+ \longrightarrow Cht{-}NH_3{}^+ + H_2O}$$

where Cht represents the chitosan glucosamine unit. The acid dissociation constant for the protonation of chitosan, K_a, its logarithmic form, pK_a, and its relation to pH are given by the following equations:

$$\mathrm{p}K_a = -\log K_a = -\log\left(\frac{[\text{Cht-NH}_2][\mathrm{H_3O^+}]}{[\text{Cht-NH}_3^+]}\right) \tag{2.1}$$

$$\mathrm{pH} = \mathrm{p}K_a + \log\left(\frac{[\text{Cht-NH}_2]}{[\text{Cht-NH}_3^+]}\right) \tag{2.2}$$

As Equation 2.2 indicates, at pH's below the pKa, chitosan is mostly protonated ([Cht-NH_2] < [Cht-NH_3^+]) and is thus in a soluble state. Chitosan has an intrinsic dissociation constant (the pK_a at zero net charge), pK_0, approximately between 6.0 and 6.5 [67, 68], and requires a minimum of 50 % degree of protonation for dissolution, irrespective of the acid type and the acid's dissociation constant [67, 69]. Chitosan's extent of solubility is affected by the degree of deacetylation and distribution of acetyl groups. A random distribution of acetyl and amine groups improves solubility [70].

The film microstructure, thickness, and material properties are affected by residual acid counterions. When water evaporates during the casting process, the concentrations of the polymer and acid increase, leading to gel formation and ultimately a solid membrane. Compatible compounds with a molecular size less than 60 Å, e.g. acetate ion, can be confined within the crystal lattice without interfering significantly with molecular

rearrangement as the film dries and the chains recrystallize [71]. Larger sized acids result in a thicker film [71] and reduce chain packing and crystallization. Mechanical properties of the chitosan films are influenced by acid type [71], displaying differences in tensile modulus, elongation, stress-strain relationship (i.e. Hookian, non-Hookian behavior), and mode of deformation.

Chitosan films cast with acetic acid often fare better overall in elastic modulus, tensile strength, and barrier against moisture, oxygen, and carbon dioxide permeability relative to casting with other organic acids [29, 66, 72, 73]. Citric acid makes for a poor chitosan film casting agent, resulting in brittle films [29, 66]. This is partly due to how the acid affects the polymer chains' spatial conformation and junction density. Regarding the effect of film-forming solution pH on film characteristics, correlations and trends between pH and physical properties such as TS and EBB do not appear to be consistent with the different solvents of acetic, formic and lactic acid [73].

2.2.4 Modification of Chitosan Films: Composites and Grafting

A graphical depiction of the different modification methods, crosslinking, blending, grafting, and composite formation, is shown in Figure 2.6. Composite formation with lipids and fatty acids is undertaken to reduce chitosan film hydrophilicity and hence WVP. Poor compatibility with palmitic, stearic, octanoic, beeswax and other fatty acids and esters imparts a more porous microstructure resulting in an undesirable increase in WVP [74–76]. Some improvement in moisture barrier properties occurred with lauric and butyric acid [75] by 25 to 50 %. No correlation was found between WVP or gas barrier properties with increasing fatty acid chain length [75]. The previously mentioned fatty acids, however, significantly decreased the films' O_2 [74, 75] and CO_2 [75] permeation properties. Mechanical properties were also found to be compromised; increasing palmitic acid content from 0.05 to 0.25 % (wt) reduced TS and EBB [76] from 47 to 11 MPa, and 4.0 to 1.2 %, respectively.

Blends with proteins have mixed results. Whey proteins increased WVP of chitosan films drastically, regardless of crosslinking the protein by transglutaminase [77], while barrier properties against permeability of O_2 and CO_2 improved steadily. Composite chitosan-ovalbumin protein films were more mechanically durable than neat chitosan films, but with reduced barrier levels to moisture [78].

Compatibility issues with blends and composites can be avoided by chemical modification and grafting of the chitosan side groups. Stearic acid grafted onto chitosan in chitosan-HPMC composite films increased hydrophobicity. Film solubility in water decreased to 55 % compared to a totally soluble, unmodified composite film, and the water contact angle increased to 90°, up from 65° [5]. Functionality such as enhanced antioxidant properties can additionally be imparted to chitosan by grafting. Polyalcohols gallic acid

or octyl gallate grafted onto chitosan have a positive synergistic effect in scavenging activity against hydrogen peroxide [79], 2,2-diphenyl-1-picrylhydrazyl [79–82] and improved inhibition against *E.coli* cell growth [81]. Wu et al. [82] prepared chitosan-gallate films without an enzyme or carbodiimide intermediary by first preparing the chitosan-gallate derivative from free radical reactions with gallic acid, followed by film casting. Gallate modification increased shear modulus of the film-forming solution relative to an unmodified solution, akin to a polymer with a higher crosslink density. At low concentrations of gallate substitution, tensile strength and barrier against moisture permeability improved relative to unmodified chitosan films, but subsequently declined with further grafting of gallic acid.

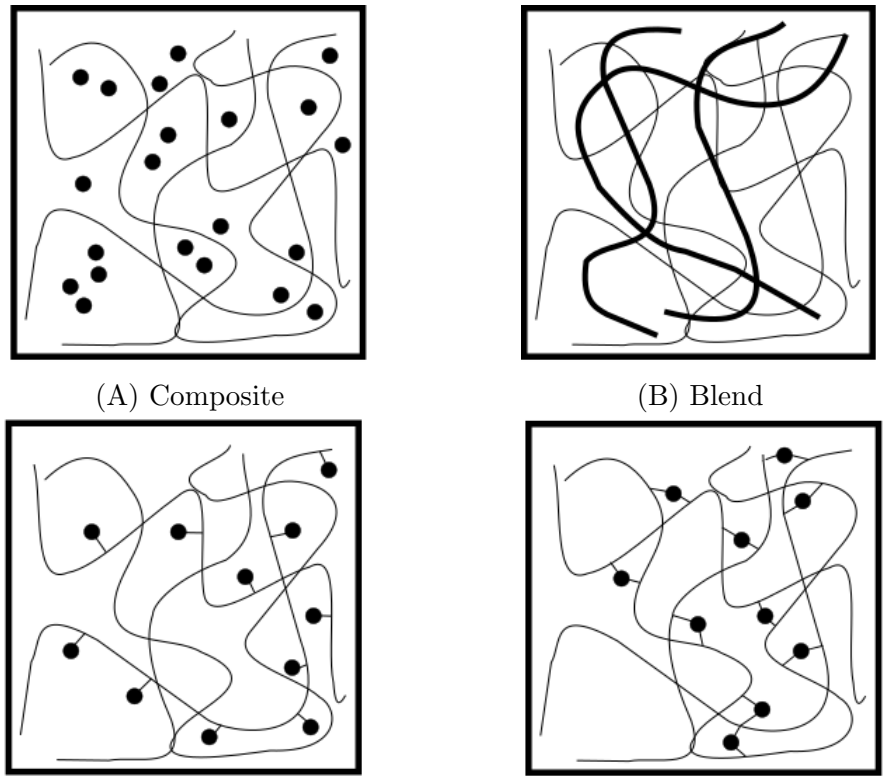

(A) Composite (B) Blend

(C) Graft (D) Crosslinking

Figure 2.6: Graphical depictions of the different methods for polymer modification: (A) composite, (B) polymer-polymer blend, (B) graft, and (C) crosslinking. Solid lines represent polymer chains. Black dots represent fillers or reacted compounds.

N-acylation of chitosan by fatty acids such as palmitic, lauric, hexanoic, decanoic acid etc., improves chitosan solubility in water [4, 68, 83] by weakening the intermolecular hydrogen bonding network. As it pertains to edible films, the grafting procedures of the compounds mentioned in this paragraph and the preceding paragraph use non-food grade compounds such as 1-ethyl-3-(3-dimethylaminopropyl) carbodiimide [4, 84], pyridine [37, 65], or monoalcohols like ethanol and methanol [65, 83]. These modified chitosans are poor film-formers [85, 86]; their solubility in aqueous acid solutions is reduced, and they yield

films too soft when cast from benzene or THF [62]. Chitosan films can be acylated after film formation, but this also involves non-food grade solvents such as methanol [85].

2.2.5 Reaction Chemistry

The reactive groups of chitosan are -NH_2 (C2), -OH (C3), and -OH (C6, methyl hydroxide). The primary amino group can react twice to yield a secondary and tertiary amine [65], giving chitosan a theoretical maximum degree of substitution of 4 [62]. While numerical values of the reaction rates or reaction rate constants could not be found by searching through the literature, the general consensus on the relative reactivity is NH_2 > OH (C6)> OH (C3) [65]. The activation energy, E_a, for the reaction of chitosan-NH_2 with genipin or isobutyric anhydride, determined from rheological measurements, is 41 to 68 kJ/mol [87, 88]. By contrast, the E_a of chitosan decomposition estimated from thermogravimetric measurements is typically between 138 to 166 kJ/mol [89, 90]. The reaction order for the *N*-acylation of chitosan is close to 2 [87, 88].

Chitosan can be modified by sulfation, xanthation, acylation from anhydrides, fatty acids or acid chlorides, alkylation with epoxies and monohalogencarboxylic acids, and these derivatives have been reviewed by Muzzarelli [37] and Mourya and Inamdar [65]. While *N*-acyl derivatives are the dominant products [86], *O*-acylation is achievable under certain conditions, including using a protection group on the amine prior to *O*-functionalization [65]. Specific solvents (e.g. 10 % acetic acid), and shorter fatty acids chains (e.g. acetyl, butyl anhydrides) allow for partial *O*-acylation [86], as well as prolonging the reaction time and increasing reaction temperature (e.g. 3 days, 70 °C) [64]. Small fractions of *O*-acylated were detected at bands of 1750 cm^{-1} with infrared spectroscopy when chitosan was prepared with smaller anhydrides in acetic acid solution. Aromatic anhydrides are more reactive towards chitosan than aliphatic anhydrides [64], and reactions with aldehydes and ketones result in a Schiff base (-C=N-).

2.3 Crosslinked Films

2.3.1 Introductory Remarks on Crosslinking

Classical elasticity theory, as first described by Flory [91], defines an ideal covalent crosslink (of a rubber) as a tetrafunctional junction where the four molecular strands are of equal length, and the crosslinks move affinely when sample geometry is disturbed by external stimuli [92]. Non-ideally, tri- or other multi-functional crosslinks exist, and the network could be comprised of a distribution of strand lengths. Physical crosslinks also cause restraint in polymer chain mobility, which stores elastic energy and increases entropy change and mechanical modulus with deformation. (Dangling ends and sol fractions do

not contribute to energy storage.) These include coupling entanglements [92] and ionic crosslinking. A graphical depiction of chemical (covalent) and physical crosslink types (ionic, entanglements) is given in Figure 2.7. Entanglements are temporary twists, loops, or long-range contours arising from chemical or structural heterogeneities. Their existence is independent of the polar or intermolecular bonding characteristics of the polymer (e.g. they occur in cellulose and polystyrene, two macromolecules with widely contrasting secondary bond architectures) [92]. Physical crosslinks tend to be more responsive in a degradative manner to external or environmental stimuli, making covalent bonding preferable for the production of more thermally and mechanically robust materials [93]. Chitosan is capable of both ionic and covalent crosslinking [93].

Additional modes of crosslinking include crosslinking between two chains of different polymer types to yield a hybrid polymer network (HPN). Semi- or full-interpenetrating polymer networks (IPN) are composed of a non-reacting polymer made into a composite with a reacting polymer. After crosslinking of chains of the reacting polymer, the non-reacting polymer becomes entrapped in the crosslinked matrix of the other. Two functionalized polymers may also be directly crosslinked at their functional sites without the aid of an intermediary molecule bridging the two. For this project, the crosslinked chitosan films are neither of the HPN or IPN forms.

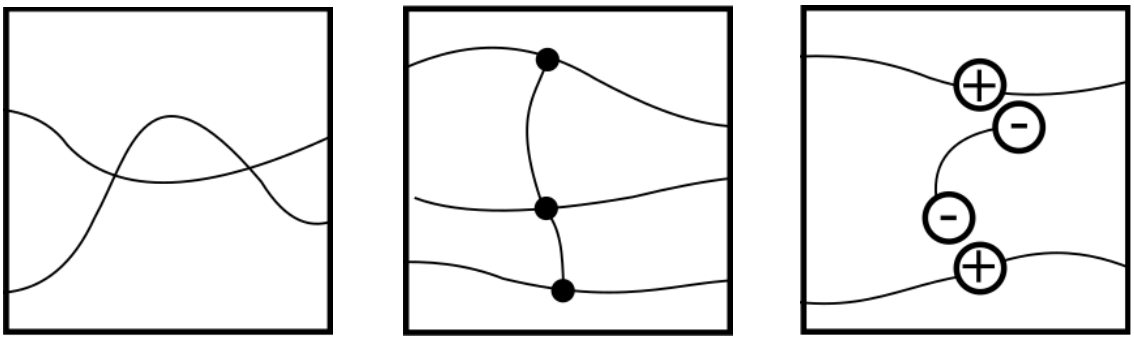

(A) Physical (B) Covalent (C) Electrostatic

Figure 2.7: Graphical depictions of crosslinking mechanisms: (A) physical entanglements between two polymer chains, (B) covalent crosslinking between three polymer chains (tetra- and tri-functional crosslinking) and (C) ionic crosslinking. Solid lines represent polymer chains. Black dots represent covalently bonded junctures.

2.3.2 Methods of Characterizing Crosslinking

Selection of an appropriate analytical technique to discern the crosslinking between chitosan and citric acid is an important facet of this project. Several experimental options are reviewed and tabulated in Table 2.2. Crosslinking of polysaccharide films can be

assessed by chemical analysis, or by testing physical properties affected by crosslinking such as mechanical damping or the glass transition [94]. While differential scanning calorimetry (DSC) is standard in observing thermally-induced phase changes such as the glass-rubber transition of polymers, the strong semi-crystalline nature of chitosan makes its glass transition temperature, T_g, difficult to detect [95, 96]. Biological macromolecules can have a large distribution of molecular weights that yield DSC scans with highly broad and unrecognizable glass transition endotherms [97]. Although the T_g of chitosan using calorimetry has been observed [98, 99], the sensitivity of DSC is generally insufficient for this polymer and is not suitable for chitosan-crosslinking studies.

Fourier Transform Infrared (FTIR) spectroscopy offers the advantage of observing the chemical signatures of amides and esters formed by reacting with chitosan's amine [5, 100–102] and hydroxyl side groups [103] at approximately 1,645 and 1,730 cm^{-1} [104], respectively. An example is given in Figure 2.8 for a crosslinked starch-citric acid film displaying the emergence of an ester carbonyl band at 1,724 cm^{-1}. While the spectrum's band intensity is representative of a local concentration of the accessible chemical substituents, it is not indicative of structural arrangement. And although FTIR is regularly employed to comment on "crosslinking" with chitosan [105], starch [6], cellulose-ethers [34] etc., the technique does not enable a distinction between grafts and crosslinks. Therefore, FTIR is not utilized here as a tool to analyze crosslinking with citric acid.

The chemical analysis of ninhydrin assay selectively targets and quantifies primary amines of amino acids, peptides, or proteins but may also be applied to characterize glucosamine [106], chitosan [101, 107] and crosslinked amino acids [108]. The sample is heated in ninhydrin solution, where ninhydrin hydrate reacts with free amino groups to yield colored ninhydrin (Ruhemann's purple), which has an optical absorbance at 570 nm [108]. Prochazkova et al. [107] deemed the method to be dependable with the detection of chitosan amine groups, and concluded that *N*-acetyl glucosamine units do not interfere in the measurements. Quantitative analysis was recommended only when accurate calibration can be performed using a reference with a similar DD [107]. Overall, ninhydrin assay is time efficient and sensitive, but only measures available amine groups, and does not reveal information on the character of amide linkages, be they graft or crosslink.

Swelling is a characteristic trait of polysaccharides and polymers in non-dissolving, thermodynamically compatible solutions. As networking constricts polymer expansion, polymer-liquid interaction and absorption of the solution molecules by the polymer decrease. The extent of swelling is determined by the mass change of the specimen after submersion for an extended period of time, e.g. 24 h. It is applicable to both ionic and covalent crosslinking [109, 110].

Material stiffness is also in part responsive to the degree of crosslinking when the material is mechanically deformed. As per rubber elasticity theory, stress of a polymeric specimen is proportional to material density (which increases with

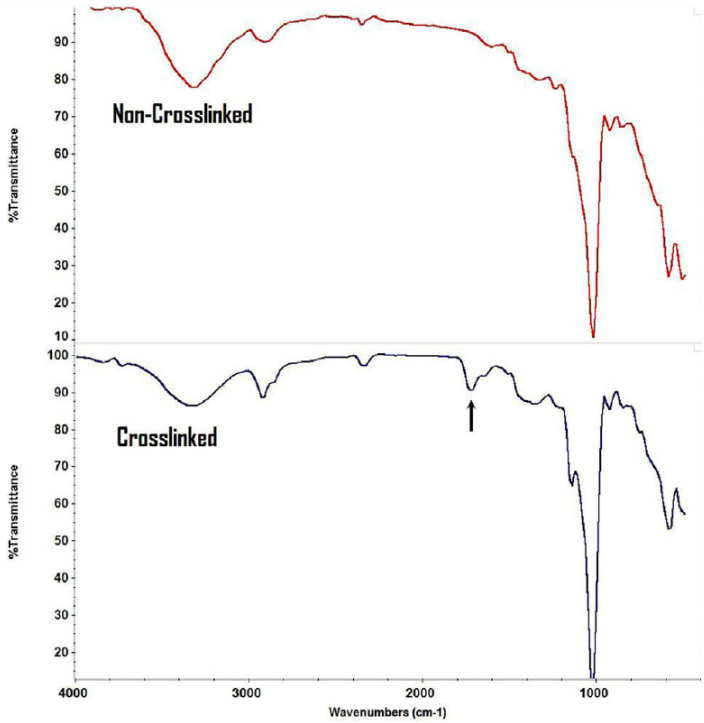

Figure 2.8: FTIR spectra of a neat starch film (top) and a starch film crosslinked with 5 % citric acid (bottom). An ester carbonyl band appears at 1724 cm^{-1} following the reaction between starch hydroxyl groups and citric acid. Figure taken from Reddy and Yang [6].

crosslinking) and inversely proportional to the number-average molecular weight of polymer between crosslinks. Tensile strength of crosslinked materials increases at low concentrations of crosslinking agent, while EBB decreases steadily with increasing crosslinker content, as demonstrated in Figure 2.9. While static and transient experiments such as creep and stress relaxation are simpler to conduct, they do not provide as wide of an analysis or interpretation as dynamic measurements [111]. This is a common technique used to assess the influence of a crosslinking agent on a polymer in the rubbery state, and is successful in characterizing thermoplastics with a strong glass transition [112, 113], as demonstrated in Figure 2.10. Characterizing crosslinked biopolymers has also been performed with this method. Examples include methyl cellulose-glutaraldehyde [33], whey proteins-formaldehyde [114], starch-trisodium trimetaphosphate [115], and chitosan-genipin [116]. Predictability of behavior from rubber elasticity theory on polysaccharide gels is difficult because the entropic assumption of the theory is violated by the high stiffness of polysaccharide chains that cause an internal energy dependence to the net change in free energy under stress [117] (see Section 3.3.2 for theory details). Despite this, viscoelastic characterization is advantageous because storage modulus reflects changes in crosslinking density of a material, and poses less doubt on whether the reactions are due to grafting or possibly crosslinking. Therefore, this technique is used here to characterize the crosslinking of chitosan with citric acid.

Table 2.2: Summary of techniques used to assess crosslinking of polysaccharides and their applicability to chitosan.

Technique (Target)	**Advantages and Limitations**
Ninhydrin (Primary amines)	**Advantages** - Direct detection of primary amines, reproducible, fast, and sensitive (3 %) [107], - Independent of molecular weight above degree of polymerization of 20, independent of reaction time **Limitations** - Lower detection of amines from chitosan than monosaccharide glucosamine, - Detection limit decreases with increasing DD from chitosan polymer [107], - Detection of monomer>oligomer>polymer, 40 % accuracy, requires calibration using different DD chitosan
FTIR (Chemical constituents, primary amines, secondary amines, esters, amides, etc.)	**Advantages** - Fast, easy to perform, and non-destructive, - Rough quantitative calculation if coupled with water loss measurements/knowledge of reaction mechanism [118] **Limitations** - Difficulty in differentiating between graft and crosslink - Estimation of DD skewed by water content [119], especially by amide I and II bands, - Difficulty in making adequate calibration curve [120]
DSC (Thermal transitions, water evaporation, glass transition)	**Advantages** - Easy to perform, high reproducibility of results **Limitations** - Low to no-detection of glass transition of chitosan

DMA (Storage modulus, glass transition)	**Advantages** - Easy to perform **Limitations** - Less reliable in detecting glass transition of polysaccharides than with thermoplastics, - Sensitive to small aberrations in sample dimensions/shape, leading to measurements errors
Swelling (Mass increase)	**Advantages** - Easy to perform, and degree of crosslinking can be estimated using Flory relationship [121] **Limitations** - Low reproducibility, high error due to other characteristics (hydrophilicity/hydrophobicity) which may impact swelling, - Estimating degree of crosslinking requires knowledge of molecular weight between crosslinks from a different technique via Flory-Huggins-solvent interaction parameter [121], less accurate with polysaccharides

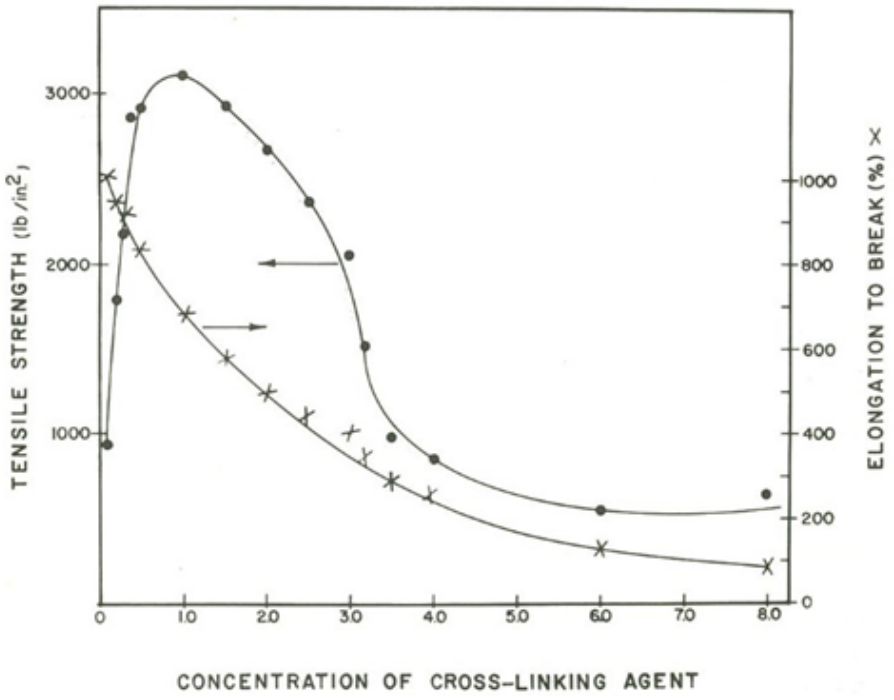

Figure 2.9: Stress-strain properties of a rubber as a function of the percent of crosslinking agent. Image taken from Nielsen [94].

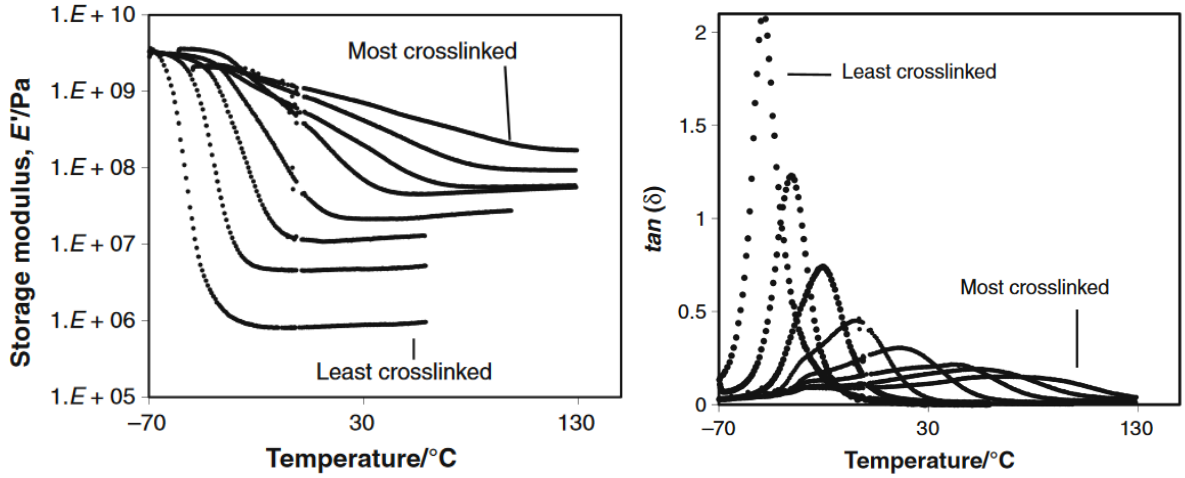

(A) (B)

Figure 2.10: Depiction of the effect of crosslinking on the viscoelastic properties of a crosslinked polyacrylate polymer. Plots of (A) storage modulus and (B) dissipation factor against temperature. Images taken from Krongrauz [112].

2.3.3 Crosslinking Agents with Chitosan

A variety of classes of compounds are available to crosslink chitosan, either ionically or covalently [93], and these include linear and aromatic dialdehydes, epoxies, inorganics, and organic acids. These crosslinking agents are utilized to enhance mechanical properties or alter the crystallinity [9] for a variety of biological, medical and industrial applications. A list of some common crosslinking compounds for chitosan is given in Table 2.3, along with information on bonding mechanism with chitosan, applications of the crosslinked chitosan films/membranes, and toxicity of the crosslinking agent.

Glutaraldehyde is a common crosslinking agent associated with chitosan, but mostly for microsphere, membrane or sorption [105] applications. Crosslinking with glutaraldehyde proceeds *via* formation of imine and alkene groups [105], as confirmed by FTIR. Glutaraldehyde should not be used in edible films because of its potentially chronic toxic effects towards the human reproductive system and some organs. Toxic and adverse health effects also prevent epichlorohydrin from being used in edible films. The same applies for carbodiimides which have been reported to form crosslinks between chitosan and gelatin [122].

Less toxic and bio-derived crosslinking agents such as genipin have been tested [123, 124] as a safer alternative to glutaraldehyde and epichlorohydrin. Muzzarelli [123] has reviewed the reaction mechanism between chitosan and genipin, and states that the two compounds can react under acidic or neutral conditions to form a tertiary amine, or under basic conditions to form an amide with genipin's ester group. Genipin however has not been FDA-approved as a GRAS material. Publications on crosslinked chitosan-genipin materials specific to food packaging or edible films are scarce. Augstina Aldana et al. [125] report the WVP of solvent cast chitosan-genipin films but did not compare the properties with non-crosslinked chitosan films. Mi et al. [126] report a decrease in WVP from heterogeneously crosslinked chitosan-glutaraldehyde and chitosan-genipin films from 835 g/m^2·day·atm of a neutralized film to 724 g/m^2·day·atm to a 684 g/m^2·day·atm, respectively.

Crosslinking chitosan with HPMC has been investigated by Möller et al. [5] using citric acid as a crosslinking agent. Solubility tests and Kjeldahl nitrogen analysis suggest that much of the crosslinking occurs with chitosan, and to a lesser extent with the cellulose-ether. Film solubility in water and moisture content in the films decreased compared to unmodified films and stearic acid grafted-chitosan films. Furthermore, crosslinking significantly reduced the WVTR rate compared to unmodified chitosan-HPMC films. Adipic acid was tested as a crosslinker by Cai et al. [102] where reactant ratios were kept constant but post-drying thermal treatment conditions were varied.

Table 2.3: Crosslinking agents used with chitosan, their toxicity, bonding type with chitosan, and applications.

Class	**Compound**	**Bond Type**	**Film Applications**	**Toxicity***	**Ref.**
Aldehydes	Glutaraldehyde	Schiff base (–C=N–), Michael type adduct	- Heavy ion/heavy metal compound capture - Ion transport in solution	Oral - Cat. 4 Inhalation - Cat. 4	[9, 105, 127]
	Glyoxal	Schiff base	Wound dressing	Oral - Cat. 4 Mutagenicity - Cat. 4	[128]
	Pyromellitic dianhydride	Imide (–N–)	Drug delivery	Oral - Cat. 5	[129]
Epoxies	Epichlorohydrin	Ether (–C-O-C–), secondary amine (–NH-C–)	- Heavy ion/heavy metal compound capture - Dye capture - Ion transport in solution	Not reported in SDS	[65, 130, 131]
	Poly(ethylene) glycol diglycidyl ether	Ether, secondary amine	- Heavy ion/heavy metal compound capture - Dye capture	Not reported in SDS	[130]
Organic and mineral acids	Sulfuric acid	Ionic	- Pervaporation	Skin corrosion - Cat. 1	[110, 132]
	Citric acid	Ionic, amide	- Textiles - Food packaging - Drug delivery	Dermal, Cat. 5	[133–135]
	Adipic acid	Ionic, amide	- Biomedical	Not reported in SDS	[102]
	Oxalic acid	Ionic	- Drug delivery/hydrogel	Oral - Cat. 4 Dermal - Cat. 4	[136]
Other	Tannic acid	Covalent	- Food packaging	Ora - Cat. 5	[7]
	Proanthocyanidin	Covalent, amide	- Biomedical - Drug delivery	Not reported in SDS	[137]
	Genipin	Covalent	- Biomedical - Drug delivery	Oral - Cat. 3	[7]
	Tripolyphosphate	Ionic	- Drug delivery - Heavy ion capture	Dermal - Cat. 5	[7, 110]

*GHS (Global Harmonized System) Classification. Health hazards listed are for 'acute toxicity'. Info extracted from safety data sheets (SDS).

2.3.4 Crosslinking with Citric Acid

Citric acid (2-hydroxy,1,2,3-propanetricarboxylic acid) can function as an ionic or covalent crosslinker with several polysaccharides (chitosan, starch, alginic acid) for various applications including drug delivery [138], edible films [5, 6, 139, 140] and digestion-resistant starch [141]. Citric acid, as well as other polycarboxylic acids, has been extensively researched as a crosslinking agent for textiles, providing a safe replacement of formaldehyde finishing, by grafting chitosan [142, 143] and cyclodextrins [144] to fabrics. Grafting of chitosan improves fabric durability and antimicrobial resistance. Alternative polycarboxylic acids include synthetic compounds such as 1,2,3,4-butanetetracarboxylic acid and 1,2,3,4-cyclopentanetetracarboxylic acid, which are decomposition and ozonation-derivatives of olefins. Carballylic acid (1,2,3-propanetricarboxylic acid) can be found in natural sources such as corn, beets and maple syrup. It chemically differs from citric acid by only one additional hydroxyl group.

The crosslinking reaction mechanism described in the literature has been derived from theory of citric acid esterification [145]. The reaction begins when two of citric acid's three carboxylic groups combine and eject a water molecule to transform citric acid into a cyclic anhydride. The cyclic anhydride then reacts with one of the polysaccharide's functional groups, either amine or hydroxyl, to yield an amide or ester, respectively, resulting in the loss of a second water molecule. The same citric acid-derivative moiety forms another cyclic anhydride, which reacts with a second functional group from an adjacent residue to complete the crosslink bridge. After this, the bridge does not have two carboxylic groups to form a cyclic anhydride for a third reaction. Thus, citric acid has a covalent functionality of 2 despite having three carboxylates, and can form three ionic links. See Figure 2.11.

A compilation of reaction (curing) conditions of cure temperature, T_{cure}, and curing time, t_{cure}, associated with citric acid crosslinking of polysaccharides is presented in Table 2.4. The conditions can be described as elevated temperature, above 100 °C, and short durations, less than an 1 h. Crosslinking of starch films [6] was confirmed by FTIR, evidenced by an absorbance band at 1724 cm^{-1} attributable to ester carbonyl groups, as shown in Figure 2.8. Catalysts are often employed to facilitate the covalent crosslinking of citric acid. Phosphorous-based salts generally outperformed carbonate salts [145], based on factors like fabric weight gain. Sodium hypophosphite (SHP) performed better than other sodium phosphorous-based salts with several of the polycarboxylic acids tested [145]. (SHP is designated as GRAS by the FDA.) Crosslinking can proceed without a catalyst [135, 144], and Gu and Yang [146] observed cyclic anhydride formation of a polycarboxylic acid in the absence of SHP at temperatures near its melting point of 190 °C. The catalytic mechanism is not fully developed, but one theory suggests that a disruption of hydrogen bonds is the main factor. The possibility of a reaction between the catalyst and citric acid-formed cyclic anhydride was evidenced at temperatures below the melting point of the carboxylic acids [146].

Citric acid promotes positive changes to the physico-chemical properties of films. Thermally treated HPMC-citric acid films [139] exhibited lower water vapor transmission rates when compared to films lacking citric acid, decreasing the transmission rate from 269 to 184 g/(m^2·day^2) from citric acid concentrations of 0 to 15 % (w/w HPMC), respectively. When the films were prepared with citric acid and a catalyst, the WVTR decreased to as low as 177 g/(m^2·day^2). For peanut protein films [140], citric acid crosslinking did not affect WVP or TS significantly, but EBB decreased by nearly 50 % of the original value.

Table 2.4: Curing conditions (temperature, T_{cure}, and time, t_{cure}) of polysaccharide films and fabrics with citric acid, ratio of citric acid to polymer, and ratio of citric acid to catalyst.

Polysaccharide	Catalyst	acid:polymer (w:w)	acid:catalyst (w:w)	T_{cure} [^{o}C]	t_{cure} [h]	Ref.
Chitosan	None	3:1, 1:3	N/a	110	6	[147]
Chitosan, cotton	SHP	n.g.	1:01	150 - 190	0.03	[142]
Hydroxyethyl cellulose, sodium carboxymethyl cellulose	None	1:0.01, 1:0.2	N/a	80	24	[133]
Alginate, chitosan blend	SHP	0.2:1, 1.2:1	1:0.5, 1:3	140 - 190	0.1 to 0.5	[138]
Chitosan, cotton	None	1:1	N/a	120 - 170	0.1	[135]
Starch	None	0.2:1	N/a	60	n.g.	[148]
Chitosan, wool	SHP	0.1:1	1:0.1	155	0.05	[143]
HPMC, chitosan	SHP	00.2:1	1:0.05	190	0.25	[5]
Starch	SHP	0.16:1	01:00.5	165	0.1	[6]
Starch	None	0.04:1	N/a	140	5	[141]
Starch	None	0.3:1	N/a	105 - 150	0.16	[149]
HPMC	SHP	0.15:1	01:00.5	190	0.25	[139]

n.g. - not given in respective references

2.3.5 Homogeneous (1 Step) vs. Heterogeneous (Multi Step) Crosslinking

A crosslinked film produced from a single solution containing both polymer and crosslinker is referred to as *homogeneous* crosslinking. The crosslinker is present in solution during the gelation and drying of the film, and may react spontaneously during these stages, or may be initiated by external stimuli (e.g. heat, UV) after the film has formed. Chitosan crosslinked by glutaraldehyde [9, 105, 150] and genipin [151] may be carried out homogeneously at room temperature. Another method of achieving crosslinking is by a multi-step approach referred to as *heterogeneous* crosslinking. For this method, a dried solvent cast chitosan film is neutralized to remove residual acid, and then the neutralized film is immersed in an aqueous solution containing the crosslinker, which is absorbed by the film. Epichlorohydrin [9, 152], glutaraldehyde [9, 118, 127], genipin [96], sulfuric acid [132], and various other dianhydride [129] crosslinked chitosan films can be prepared heterogeneously. This has also been applied for grafting and re-acetylation of chitosan into chitin with acetic anhydride and hexanoic anhydride [85]. The two methodologies are illustrated in Figure 2.12.

Glutaraldehyde and genipin can react with the neutralized chitosan film in solution at room temperature, whereas epichlorohydrin reacts at 40 °C [9]. Citric acid requires elevated temperatures to react with polysaccharides. Neutralization of chitosan film by NaOH, which is a necessary step for heterogeneous crosslinking, does not restrict the films from usage as food packaging, as NaOH is GRAS.

Homogeneous and heterogeneous crosslinking have different consequences on the reaction mechanism and overarching film microstructure. Gelation of a chitosan-glutaraldehyde solution occurs in several minutes [105, 127] as a consequence of crosslinking with the homogeneous method, but crosslinking could take up to 48 h [95, 127] to complete under heterogeneous conditions. Bond formation is also affected. Glutaraldehyde may react to form imines, or a combination of imine and Michael-type adducts, for heterogeneous *vs* homogeneous crosslinking, respectively [9]. Regardless of the procedure, however, substitution at the amine is preferred over the hydroxyl, as reported by acylation with acetic acid and hexanoic anhydride [85]. Heterogeneous crosslinking has been hypothesized to occur mostly at the film surface [9] and in the amorphous regions of the polymer matrix [118]. The crosslinking procedure can influence the degree of crystallinity [9, 118], and heterogeneous crosslinking with chitosan-glutaraldehyde does not reduce crystallinity to the extent that the homogeneous procedure does [9] compared to an uncrosslinked film.

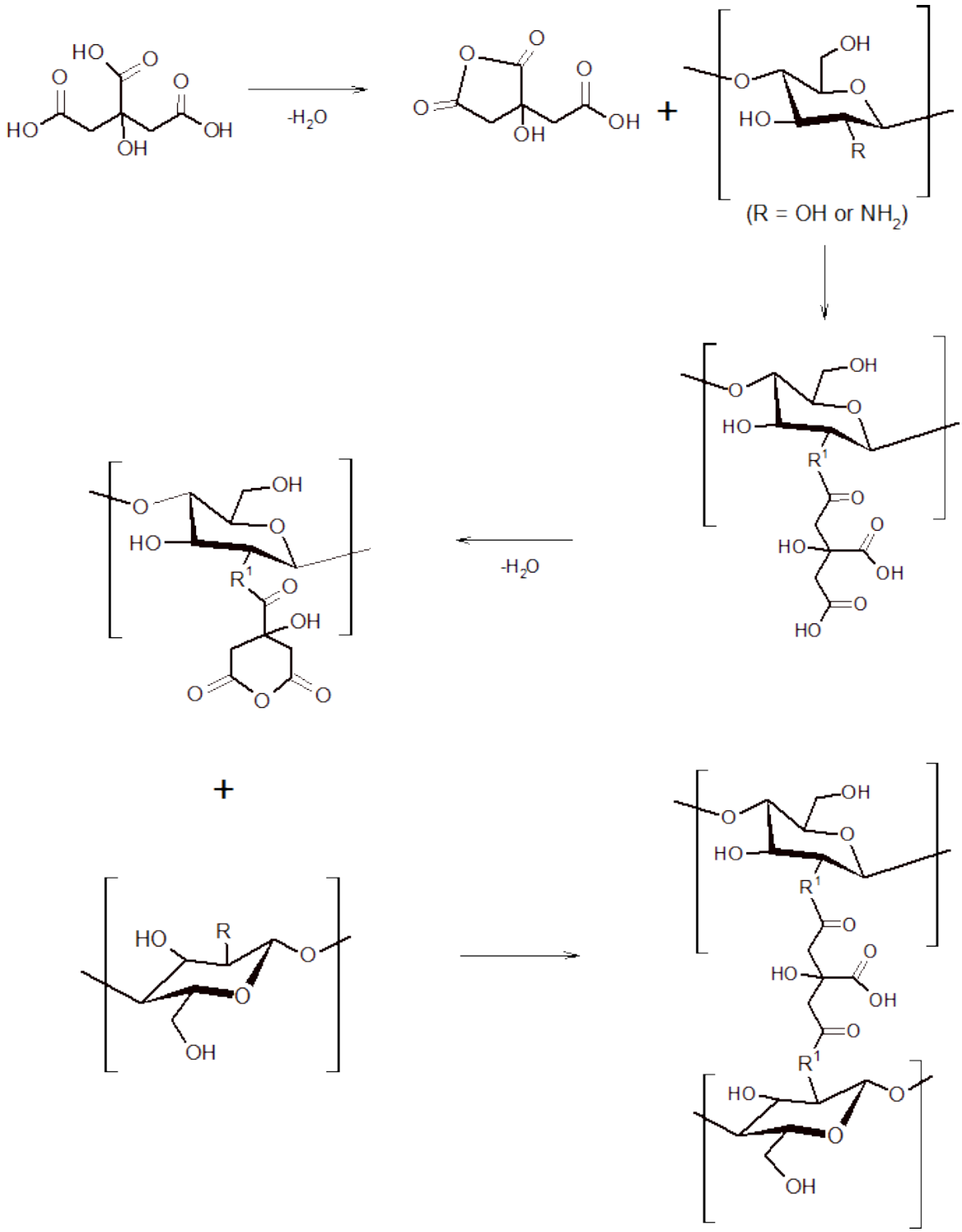

Figure 2.11: Theoretical crosslinking mechanism of citric acid with a polysaccharide, based on textile studies [144, 145]. R denotes either -OH or -NH_2. Citric acid undergoes conversion to a cyclic anhydride before reacting with the polysaccharide functional group. One water molecules is ejected per graft. Here, the terminal carboxylates of citric acid are assumed to be the more reactive constituents over the middle carboxylate.

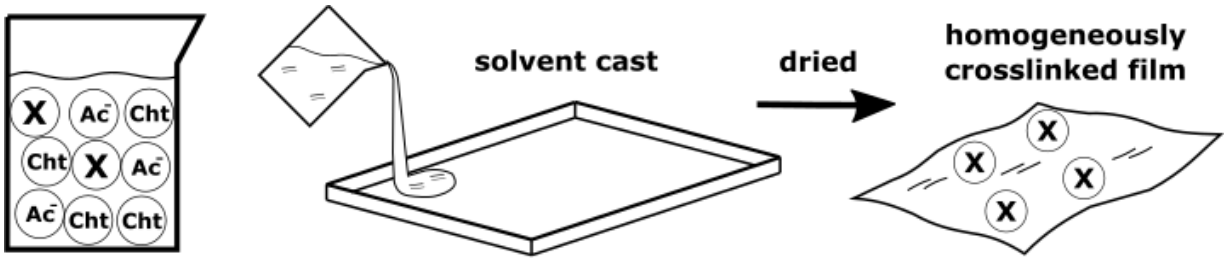

(A) Homogeneous crosslinking procedure

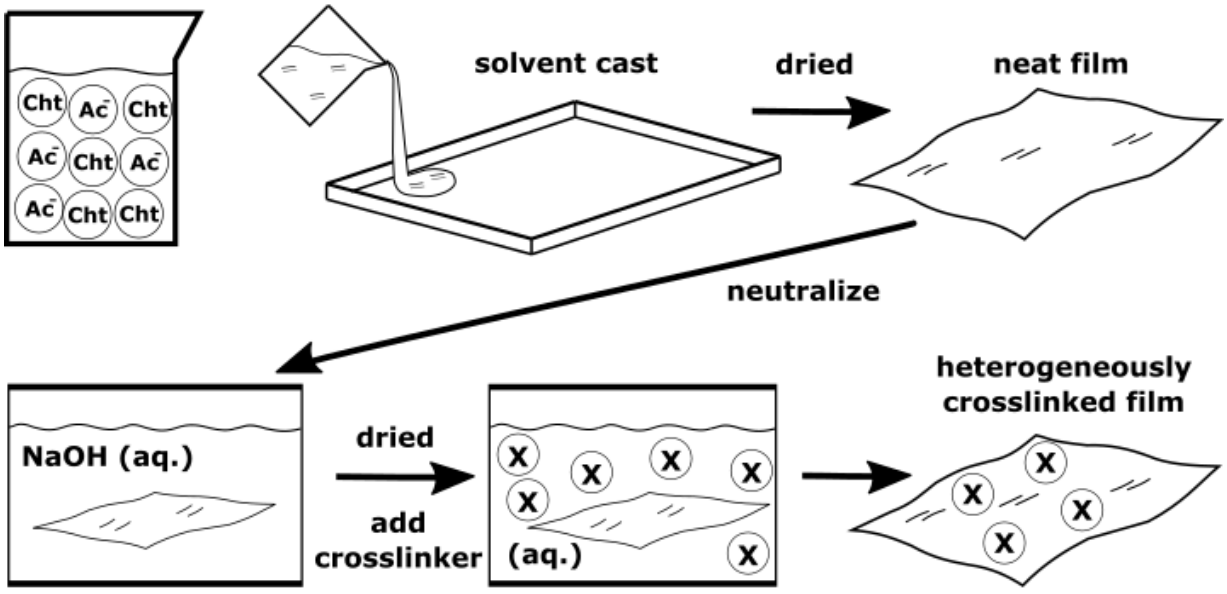

(B) Heterogeneous crosslinking procedure

Figure 2.12: Illustrations of the methodologies for producing (A) homogeneously and (B) heterogeneously crosslinked films. The text Cht, Ac^-, and X in the circles represent chitosan, acetate ions, and crosslinker, respectively.

Chapter 3

Experimental Techniques

3.1 Materials

Low molecular weight chitosan ($\overline{M}_{\mathrm{V}}$ 50 - 190 kDa, 20 - 300 cP, 1 % wt. in 1 % acetic acid solution at 25 °C, 75 - 85 % DD) was purchased from Sigma Aldrich (St. Louis, Missouri, USA). Acetic acid (> 99.7 %) (Sigma Aldrich) was used as the solvating agent in the solvent casting procedure for film formation. Citric acid (> 99.5 %) was obtained from Fisher Scientific (Fair Lawn, New Jersey, USA). The neutralizing agent, sodium hydroxide (> 95 %) was obtained from EMD Chemicals (Gibbstown, New Jersey, USA). Glutaraldehyde (Grade II, 25 % wt. aqueous solution) (Sigma Aldrich) served as a model crosslinker for DMA experiments. All reagents were used as received without modification. Ultra-pure water (resistivity > 16 MΩ·cm) was used to prepare the aqueous chitosan solutions for solvent casting, and to rinse neutralized films. The molecular and chemical properties of acetic acid, citric acid, and glutaraldehyde are given in Figure 3.1.

3.2 Film Preparation

3.2.1 Film Types

The following films were prepared: (i) neat films, (ii) neutralized films, (iii) heterogeneously crosslinked films with citric acid *without* heat treatment (denoted as CA), (iv) heterogeneously crosslinked films with citric acid *with* heat treatment (denoted as CA-HT), (v) homogeneously crosslinked films with GLU (denoted as GLU-HOM) of varying GLU concentration, and (vi) heterogeneously crosslinked films with GLU (denoted as GLU-HET) of varying GLU concentration. Chitosan-citrate films (vii) were also made for some characterization tests. Table 3.1 lists the film types, the crosslinking agent and content, and their corresponding code names.

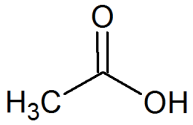

Acetic acid
M 60.05 g/mol, b.p. 118 °C,
ρ(25 °C) 1.05 g/mL, pKa 4.76

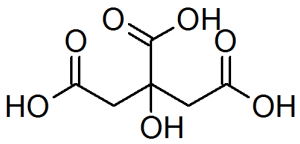

Citric acid
M 192.12 g/mol, m.p. 153 °C,
ρ(20 °C) 1.67 g/cm^3, pKa 3.09, 4.75, 5.41

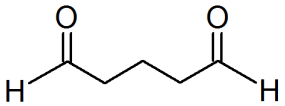

Glutaraldehyde
M 100.11 g/mol, b.p. 101 °C, ρ(20 °C) 1.06 g/cm^3, pKa 14.5

Figure 3.1: Chemical structures and properties of acetic acid, citric acid, and glutaraldehyde. M is molecular weight, b.p. is boiling point, m.p. is melting point and ρ is density.

3.2.2 Solvent Casting and Crosslinking

Neat Films

Neat chitosan films were prepared by casting 300 mL of 2 % (w/v) chitosan in 2 % (v/v) aqueous acetic acid filmogenic solutions. Solutions were stirred with a magnetic stirrer for approximately 1 - 2 h until chitosan dissolved. The solutions were filtered through cheesecloth to remove tiny undissolved chitosan bits and contaminants such as debris. Solutions were subsequently degassed using a vacuum aspirator to reduce the amount of dissolved gases. Dissolved gas bubbles in the dried films were observed using a light microscope, and are discussed in Appendix A.1.

The solutions were cast on glass trays of 16 × 30 cm, and were dried at ambient conditions in a fumehood. Temperature and relative humidity (RH) in the fumehood were monitored with a thermo-hygrometer (SMART^2, InterTAN Inc., Barrie, Ontario, Canada). Conditions ranged from 18 - 25 °C and 20 - 55 % RH, depending on the day and season; higher RH of 30 - 50 % during the spring and summer months and lower RH of 20 - 25 % during the winter. The films required approximately 48 to 60 h to completely dry and form. Drying was not carried out under controlled conditions in an environmental chamber due to the potential damage to any copper piping by corrosive acetic acid vapors.

A plasticizer was not used because the molecular weight of chitosan was sufficient in forming sturdy and flexible films. Moreover, if the plasticizer is small (e.g. glycerol), it will be washed out from the film by neutralization and rinsing. It is possible to incorporate glycerol into a neutralized film, by immersion in a solution of 20 % glycerol for 30 min [153, 154].

Table 3.1: Chitosan film types and assigned code names

Film	Code Name
Neat (also referred to as chitosan-acetate)	Neat
Neutralized (from neat film)	Neutralized
Homogeneously crosslinked with 3 % (w/w) glutaraldehyde	GLU-HOM-3
Homogeneously crosslinked with 6 % (w/w) glutaraldehyde	GLU-HOM-6
Homogeneously crosslinked with 12 % (w/w) glutaraldehyde	GLU-HOM-12
Heterogeneously crosslinked with 6 % (w/w) glutaraldehyde	GLU-HET-6
Heterogeneously crosslinked with 12 % (w/w) glutaraldehyde	GLU-HET-12
Heterogeneously prepared with 15 % (w/w) citric acid	CA
Heterogeneously prepared with 15 % (w/w) citric acid, heat treated	CA-HT
Chitosan-citrate (made as per neat film but with citric acid)	Chitosan-citrate

Neutralized Films

Neutralized films were prepared by treating dried neat films in 400 mL of 0.2 M NaOH for 30 min to remove residual acetic acid. The films were then thoroughly rinsed with ultra-pure water until the pH of the diluent reached that of water. Surface water was wiped off using Kim Wipes^{TM}. The wet neutralized films were sandwiched between a glass plate and wooden picture frame, and a heavy aluminum block was placed on top to maintain shape and dimensions and minimize shrinkage of the films as they dried. The neutralized films were dried in an environmental chamber (Sanyo MLR 351, Sanyo, now Panasonic, Japan) at 23 °C and 50 % RH for 24 h. The removal of acetic acid was confirmed by thermogravimetric analysis; see Section 6.3.1.

CA Films

Citric acid-containing films were prepared via the heterogeneous method. 200 mL citric acid aqueous solutions containing 15 % citric acid (wt. acid/wt. neutralized film) were prepared based on the weight of the dried neutralized films. The neutralized films were immersed in the citric acid solutions for 5 h at ambient conditions. Preliminary tests to determine an appropriate duration for immersion and citric acid concentration are described in Chapter 4. Surface water was wiped off of the wet citric acid-containing films, which were then dried between a glass plate and wooden picture frame, as was done with neutralized films, at 23 °C and 50 % RH for 24 h in an environmental chamber.

The dried citric acid-containing films were partitioned into two pieces. One piece was heat treated at 150 °C for 30 min, labelled CA-HT, to attempt to induce covalent crosslinking. These heat treatment conditions were selected according to the conditions

reported in the literature for chitosan films crosslinked with citric acid [5, 147], as discussed in Section 2.3.4, and by also considering that citric acid degrades after melting above 160 °C [133]. The other citric acid-containing film piece was not heat treated, and is labelled as a CA film.

Based on the DD value of the chitosan provided by the supplier (75 - 85 %) and molecular weights of glucosamine and *N*-acetyl glucosamine monomer units, the approximate ratio of [NH_2] from chitosan to [COOH] from citric acid could vary from 1.9 to 2.2; see Appendix A.5 for calculations. The postulated covalent crosslinking reaction between chitosan and citric acid expected by heat treating a CA film is given in Figure 3.2. Additionally, ionic bridging by citrate ions of chitosan chains when the film is not heat treated is depicted in Figure 3.2.

GLU Films

Films homogeneously crosslinked with GLU, labeled GLU-HOM, were prepared as per the procedure for neat films but with modification. A predetermined amount of GLU (3, 6, 12 % wt. of chitosan powder) was added drop-wise to the filmogenic solution while magnetically stirring it to maximize dispersion and solution homogeneity. As the crosslinking reactions occur spontaneously, the GLU was added slowly to prevent pre-maturely reacted clumps in solution. The reactions continued after casting and during the drying phase. The films required 24 to 36 h to completely form and dry.

Films heterogeneously crosslinked with GLU, labeled GLU-HET, were prepared by immersing dried neutralized films in 200 mL of GLU aqueous solutions of either 6 or 12 % GLU (wt. GLU/wt. film). The neutralized films were immersed for 24 h at ambient conditions where GLU absorbed into the film and then proceeded to crosslink with chitosan. (In a homogeneously crosslinked GLU film the reactions begin instantaneously, whereas with a heterogeneously crosslinked film a longer duration for crosslinking is required due to the slower reaction kinetics from the diffusion-limited step of GLU into the already formed matrix of the film [127].) Excess solution on the surface was wiped off the film, and the wet GLU-HET films were dried for 24 h at 23 °C and 50 % RH in an environmental chamber. Due to the brittleness of the water-saturated GLU-HET films, and a negligible amount of shrinkage during drying, the films were not clamped while drying as was done with the neutralized and CA films.

The molar ratio of reactive constituents, chitosan amine [NH_2] to GLU aldehyde groups [CHO] were estimated to be 8.1, 4.0, and 2.0 for 3, 6, 12 % wt. GLU and 85 % DD, respectively, and 7.0, 3.4, and 1.8 for 3, 6, 12 % wt. GLU and 75 % DD; see Appendix A.5 for calculations.

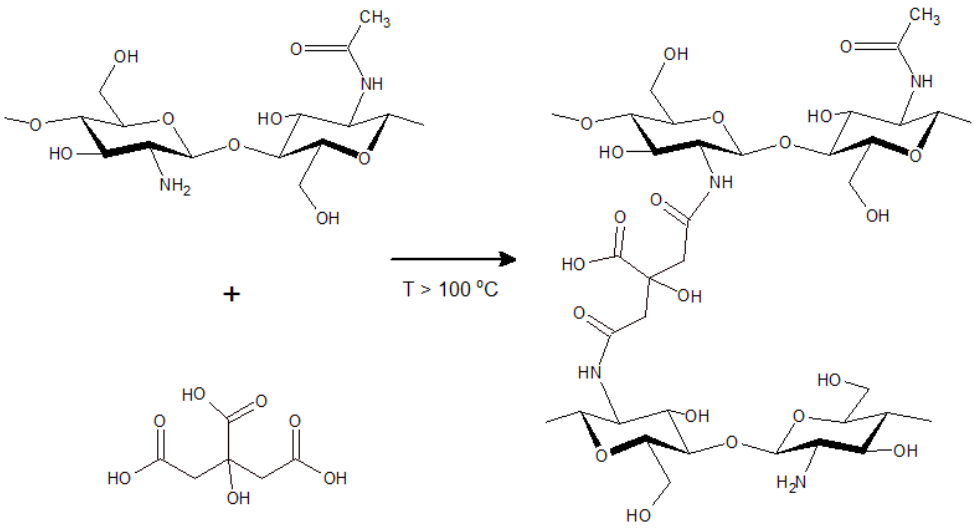

(A) Covalent crosslinking with heat treatment

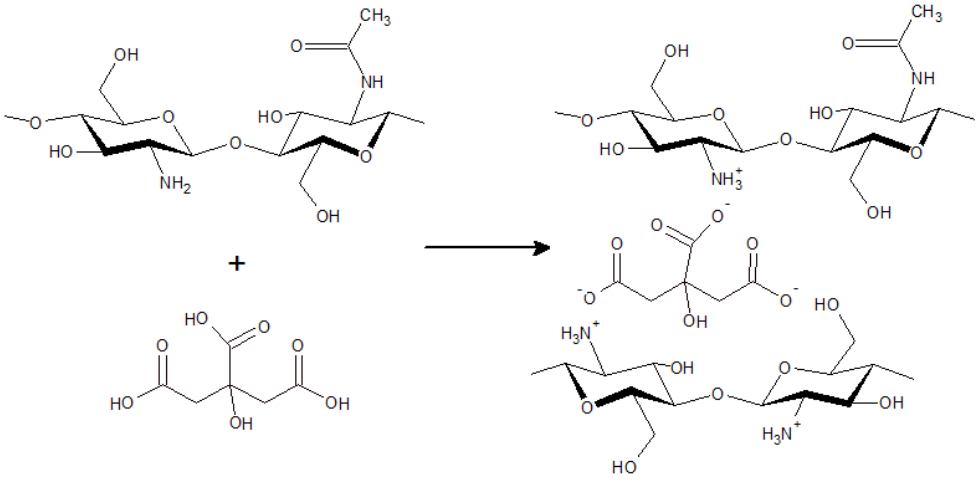

(B) Electrostatic interaction with no heat treatment

Figure 3.2: (A) Postulated thermally-induced covalent crosslinking of chitosan chains by citric acid and (B) ionic crosslinking between protonated chitosan amines by citrate ions without heat treatment.

Chitosan-Citrate Films

Chitosan-citrate films were prepared as per neat chitosan films, by casting 300 mL of 2 % (w/v) chitosan in 2 % (w/v) aqueous citric acid filmogenic solutions. Solutions were stirred until chitosan dissolved. The solutions were filtered and degassed. The solutions were cast on glass trays of 16 × 30 cm, and were dried at ambient conditions in a fume hood.

3.3 Dynamic Mechanical Analysis

3.3.1 Background

A viscoelastic material is one whose response to mechanical stimuli is neither that of a completely viscous fluid (90° phase lag, Newtonian fluid), nor of a perfectly elastic solid (zero phase lag, Hookian behavior). Polymers are inherently viscoelastic materials, and viscoelastic properties of polymers are sensitive to differences in crosslinking degree. To assess covalent crosslinking of the CA-HT films, the films were characterized by DMA. The films containing citric acid, both heat treated and non-heat treated, were compared with neat, neutralized, and GLU-containing films.

In DMA, the stress-strain behaviour is measured under sinusoidal conditions for small deformations, and tensile stress, σ, and strain, ϵ, are measured as:

$$\epsilon(t) = \epsilon_0 \sin(\omega t) \tag{3.1}$$

$$\sigma(t) = \sigma_0 \sin(\omega t + \delta) \tag{3.2}$$

where ω is angular frequency, t is lapsed time, δ is the phase angle, and ϵ_0 and σ_0 are maximum strain and stress, respectively. Stress and strain are related by tensile modulus, E, through Hooke's Law. When a material is deformed sinusoidally, the modulus is a complex value, E^*, comprised of a real (tensile storage modulus, E') and imaginary (tensile loss modulus, E'') component:

$$E^* = E' + iE'' \tag{3.3}$$

$$E' = (\sigma_0/\epsilon_0)\cos\delta \tag{3.4}$$

$$E'' = (\sigma_0/\epsilon_0)\sin\delta \tag{3.5}$$

The E' represents the energy recovered after deformation, and E'' is related to the energy lost during a cycle as heat from frictional losses. The E' and E'' are related by the causality principle which is described by the Kramers-Kronig relations [155]. Originally developed for optical dispersion, the Kramers-Kronig relations express causality of a property measured under dynamic conditions, including viscoelastic properties [156]. The real component of a property can be described by an integral that expresses the imaginary component [156], and the imaginary component can be approximated by a proportional derivative of the real component [157], as shown below.

$$E'(\omega) = E_\infty + \frac{2}{\pi}\int_0^\infty \frac{uE''(u)}{\omega^2 - u^2}du \tag{3.6}$$

$$E''(\omega) \approx \frac{\pi}{2}\left(\frac{dE'(u)}{d\ln u}\right)_{u=\omega} \tag{3.7}$$

where ω is angular frequency of the oscillating force, u is complex frequency, and E_∞ is the unrelaxed modulus, equivalent to $E^*(\omega \to \infty)$ or $E(t \to 0)$. Although experimental factors may cause the measured properties to deviate from the Kramers-Kronig relations [158], the fundamental causality premise remains. Any relaxation process observed in the plot of the real component within a frequency, time, or temperature-domain as a step-change is reflected by a peak in the imaginary plot in sync with the inflection point of the real component. The peak of the imaginary component can be amplified by taking the ratio with the real component to yield the dissipation factor,

$$\tan\delta = E''/E' \tag{3.8}$$

The $\tan\delta$ peak may be shifted to slightly higher temperatures than the E'' peak for temperature ramp measurements. The $\tan\delta$ is considered a technical parameter and its value is more important than E' and E'' for understanding relaxation processes. The general temperature-dependent viscoelastic behavior and phase transformations of polymers are graphically summarized in Figure 3.3.

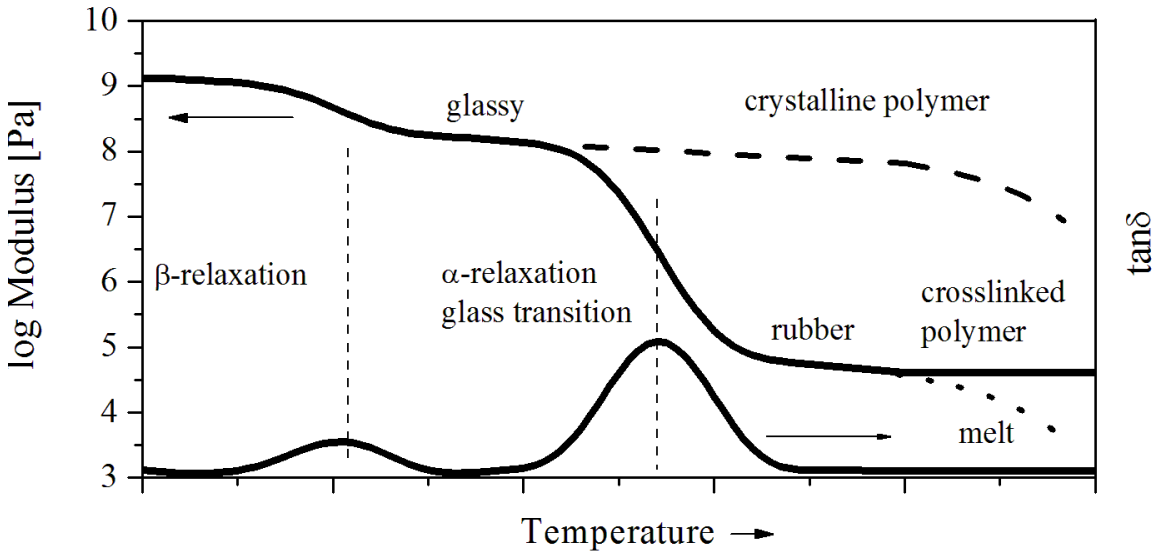

Figure 3.3: A depiction of the phase changes induced by heating a polymer through the glass transition as reflected in the storage modulus and $\tan\delta$.

3.3.2 Rubber Elasticity Theory

The storage modulus of a polymer is a reflection of chain mobility at the test temperature in response to a particular strain and frequency. The modulus above the glass transition temperature is proportional to the number of chemical crosslinks. Equation 3.9 relates mechanical properties to crosslinking density.

$$G = \nu RT \tag{3.9}$$

$$\nu = \rho/\overline{M_c} \tag{3.10}$$

G is the elastic shear modulus, ν is the crosslink density, ρ is the material density, $\overline{M_c}$ is the average molecular weight between crosslinks, and R and T are the ideal gas constant and temperature, respectively. To determine G experimentally, rheometry can be used under low frequency conditions where $G = \lim_{\omega \to 0} G'(\omega)$ and so G' must be considered independent of frequency and strain (in the linear viscoelastic region) to be applied [159]. The property G is related to Young's modulus:

$$G = E/2(1 + v) \tag{3.11}$$

where v is Poisson's ratio. When the material is assumed to be incompressible, Poisson's ratio is 0.5, and the relation condenses to,

$$G = E/3 \tag{3.12}$$

And by substituting Hooke's equation,

$$\epsilon = \sigma/(3\nu RT) \tag{3.13}$$

Crosslinking has several effects on viscoelastic properties [113]: (i) increase in rubbery modulus, (ii) increase in glass transition with sufficient increase in crosslink density, (iii) broadening of the transition region due to an increase in distribution of relaxation times and higher range of average molecular weight between crosslinks.

The capacity of a material to recover entirely after a large extension or deformation is the premise for rubber elasticity [160]. This can be exhibited by any polymer, granted under conditions of highly flexible polymeric chains connected into a network structure [161]. Crosslinking of chains prevents their permanent slippage during deformation. The fundamentals that describe elastic behaviour extend to polymers not classified as rubbers, namely swelled networks, semi-crystalline polymers, and linear amorphous polymers examined under melt or glassy conditions [161].

The elementary theories developed to model rubber elasticity assumed a network structure is comprised of freely jointed Gaussian chains. Intramolecular forces alone are responsible for chain configuration and elongation, while intermolecular effects are negligible and independent of deformation [162]. The crosslink junction positions were assumed to displace affinely with respect to macroscopic strain, and that junction fluctuations were suppressed, mainly by chain entanglements [160–162]. This is the affine model, (the mathematical definition of affine is constant proportion of distances, in this

case network junction positions, during stretching). Thus, the network deformation has an entirely entropic origin. The ideal gas law shares the same entropic and intramolecular derivation, hence the similar form as the expression of rubber elasticity in Equation 3.9 .

The phantom network model of James and Guth assumes that junctions fluctuate asymmetrically, and the *mean* positions of the junctions are affine, not the instantaneous positions during deformation. The fluctuations are strain-independent, and their mean positions are Gaussian [161]. The effects of junctions and chains on each other are negligible, as if the chains may move freely through each other. This reduces the local strain relative to the macroscopic strain [160], and the stress modulus is lower than that predicted by the affine model, because of the reduced strain experienced by the chains [160].

The affine and phantom models give the limits of the mobility of junctions within a network. The affine model is considered for more ideal situations, and more accurately describes the physical response of thermosets [163]. The two models are related by their assumption of intramolecular interaction along the chain contour [162], but diverge regarding the assumption of junction fluctuations and by the front factor in the elastic free energy expression. The elastic free energy of an isotropic network comprised of Gaussian end-to-end chain vectors, are described by the affine and phantom models [161]:

$$\Delta F_{\mathrm{el,aff}} = \frac{1}{2}\nu_{\mathrm{e}} k_{\mathrm{B}} T(\lambda_x^2 + \lambda_y^2 + \lambda_z^2 - 3) - \mu k_{\mathrm{B}} T \ln\left(\frac{V}{V_0}\right) \tag{3.14}$$

$$\Delta F_{\mathrm{el,ph}} = \frac{1}{2}\xi k_{\mathrm{B}} T(\lambda_x^2 + \lambda_y^2 + \lambda_z^2 - 3) \tag{3.15}$$

where λ is the principal extension ratio ($=L/L_0$) of the respective Cartesian direction, k_{B} is Boltzmann's constant, ν_{e} is the effective number of chains, μ is the number of junctions, ξ is the network cycle rank ($=\nu(1-2/\phi)$), where ϕ is crosslinking functionality), and V and V_0 are instantaneous network volume and volume of the reference or unswollen state, respectively. (The second term in Equation 3.14 can be neglected due to incompressibility, especially under non-crystallizable conditions.) The reference volume is based on the formation conditions of the network [162], and not the dried or solvent-free state. These free energy relations provide the basis for the expression of stress or other properties with various modes of deformation (i.e. tensile, compression, etc.). The modeled force is given by differentiating ΔF with respect to the work of deformation, $(\partial \Delta F_{\mathrm{el}}/\partial L)_{\mathrm{T,V}} = L_0^{-1}(\partial \Delta F_{\mathrm{el}}/\partial \lambda)_{\mathrm{T,V}}$.

$$\sigma_{\mathrm{aff}} = \frac{\nu_{\mathrm{e}} k_{\mathrm{B}} T}{L_0}(\alpha - \alpha^{-2}) \tag{3.16}$$

$$\sigma_{\mathrm{ph}} = \frac{\xi k_{\mathrm{B}} T}{L_0}(\alpha - \alpha^{-2}) \tag{3.17}$$

where α is the extension ratio, $\alpha = L/L_{i,V} = \lambda(V/V_0)^{-1/3}$ where $L_{i,V} = L_0(V/V_0)^{1/3}$ but since $V = V_0$ is assumed, α collapses to λ.

3.3.3 Experimental

The temperature-dependent E', E'', and tanδ of the films were measured by ramp experiments in tensile mode using a TA DMA Q800 instrument (TA Instruments, New Castle, Delaware, USA). ASTM D5206 (Standard Test Method for Plastics: Dynamic Mechanical Properties: In Tension) was referred to for general guidelines. The film specimens were heated at temperature ramp of 3 °C/min, at a fixed frequency of 1 Hz, and maximum strain of 0.15 % (constant). A 1 N preload force was applied during specimen gauge length measurements. Specimen dimensions were 5.5 ± 0.4 mm (width) $\times$ 10.0 ± 0.1 mm (gauge length) $\times$ 100 ± 20 µm (thickness). Preliminary tests were performed to determine the linear viscoelastic response region, to select an appropriate strain; see Appendix A.3. Neat, neutralized and CA-film specimens were tested in triplicate, each specimen cut from a bulk film. The GLU film specimens were tested in either single or duplicate measurements.

To observe the influence of absorbed water in the films on the viscoelastic properties, a new set of specimens were preheated prior to DMA testing. Preheating was conducted at 140 °C for 10 min in the DMA chamber, without applying strain. The preheated specimens were cooled down to room temperature, and then tested as per the previously outlined conditions. It is emphasized here that "*heat treatment*" is specific to thermal treatment of CA films for the purpose of covalent crosslinking, while "*preheating*" is applied to specimens heated prior to DMA tests. Those specimens not preheated are simply referred to as non-preheated.

The tanδ curves were deconvoluted to extract the peak width and center value using OriginPro 8s Peak Analyzer. The curves were fitted using a constant, horizontal baseline, whose value was specific to each plot and selected as the minimum tanδ value. The fit was assessed by a satisfactory visual overlap between experimental and fitted curves, and by the minimization of the chi-square metric. The peak center and full width at half maximum (FWHM) values were statistically evaluated using the Least Significant Difference method (significance level, $\alpha = 10$ %); see Chapter 5.

3.4 Water Vapor Permeability

3.4.1 Background

The diffusion rate of moisture across a film or membrane is an important property to control for coating or packaging applications and is often measured as the water vapor permeability (WVP). The WVP of a material is not an intrinsic property; it is merely a convenient expression of performance. Permeability is influenced by factors such as polymer microstructure [10, 164], polymer polarity [165], vapor pressure driving force [10, 166],

temperature and film thickness [10, 166]. The theoretical permeability coefficient, P, is governed by the relationship $P = D \times S$, where D and S are the diffusion and solubility coefficients, respectively, and P is membrane-structure dependent.

The solution-diffusion theory states that vapor or gas permeation through a dense material proceeds in three stages: adsorption and dissolution into the membrane, concentration-gradient driven diffusion, and desorption and evaporation on the low concentration side. The adsorption and desorption rates of the diffusing molecule are affected by the strength of hydrogen bonding or van der Waals forces which dictate the affinity of that gas or vapor compound to the membrane. The formulations of WVP and water vapor transmission rate are based on Fick's and Henry's laws [165], which are applicable to steady-state diffusion in isotropic and homogenous membranes. This is hardly the case with polysaccharide films, which are hydrophilic, because complications from polymer-moisture interaction [164] create non-ideal diffusion conditions. Modeling of the moisture sorption isotherms of hydrophilic materials is difficult [166] because of non-linearity and moisture-dependent diffusivity, but has been performed successfully with cellulose-derivatives [164]. Furthermore, irregularities in the film, such as pinholes, can drastically create a perception of a higher rate of diffusion. Nevertheless, WVP remains a standard measurement for polysaccharide edible films.

3.4.2 Experimental

The WVP of chitosan films was measured with the dry method following the E96 ASTM standard [167]. A 125 mL mason jar was filled with dried $CaCl_2$ (desiccant) up to 6 mm below the top of the jar. The specimens were sealed to the jar rim by an open jar lid. The seal was ensured to be air tight by placing Parafilm ®M strips on the edge of the jar, and by a flat rubber ring placed on top of the film. See Figure 3.4 for a schematic of the WVP apparatus. Two bulk films per film type were prepared, and three circular specimens of 6.1 cm ⌀ were tested per bulk film. The thickness of the specimens was determined by an average of six measurements using a digital micrometer (± 0.002 mm accuracy, Marathon Watch Company, Richmond Hill, Ontario, Canada). The sample cups were stored in an environmental chamber at 23 °C and 50 % RH as per the ASTM, and were weighed approximately every 24 h. The mass change was plotted against elapsed time, and water vapor transmission rate (WVTR) and WVP were calculated as follows:

$$WVTR = \frac{\Delta m}{\Delta t \cdot A} \tag{3.18}$$

where A is the test area (cup of mouth/exposed area of film) [m^2], $\Delta m/\Delta t$ is the rate of mass change due to transmission of water (linear portion of plot of mass, m *vs.* elapsed time, t) [g/s]. Assuming that the surfaces of the film are perfectly flat, and that diffusion

occurs normal to the surface, the *permeance* (Equation 3.19) takes into account the vapor pressure difference across the two surfaces,

$$Permeance = \frac{WVTR}{\Delta p} = \frac{WVTR}{S(RH_1 - RH_2)} \tag{3.19}$$

where Δp is vapor pressure difference across film [Pa], RH_1 and RH_2 are relative humidity at the source and vapor sink, respectively (expressed as a fraction), and S is saturation vapor pressure at test temperature [Pa]. WVP (Equation 3.20) is the permeance value normalized by the thickness of the film,

$$WVP = \frac{WVTR \cdot l}{\Delta p} = \frac{WVTR \cdot l}{S(RH_1 - RH_2)} \tag{3.20}$$

where l is film thickness [m]. The units for WVTR are [g/(m^2·s)] and for WVP are [g/(m·s·Pa)].

Section 13.3 of E96 states that the "calculation of permeability is optional and can be done only when the test specimen is homogeneous (not laminated) and not less than 1/2 in. (12.5 mm) thick" [167]. Despite this condition, many researchers still report a WVP value even though most edible films produced are on the μm scale.

Deviation in true driving force conditions and weight change are potentially caused by stagnant air between the film and desiccator, edge masking of the film and fluctuations in atmospheric pressure (buoyancy effects). These can skew the measured WVTR and WVP values. Buoyancy effects can be disregarded here, as they are mostly of concern for hydrophobic or high barrier materials. The other two effects are more applicable. Stagnant air (or still air) between the exposed bottom surface of the film and the content of the test cup (desiccant or water), gives some resistance to permeability. This is more concerning for highly permeable materials, especially hydrophilic compounds such as polysaccharides [168]. Formulas for these corrections can be found in E96 and were used in Section 6.3.2.

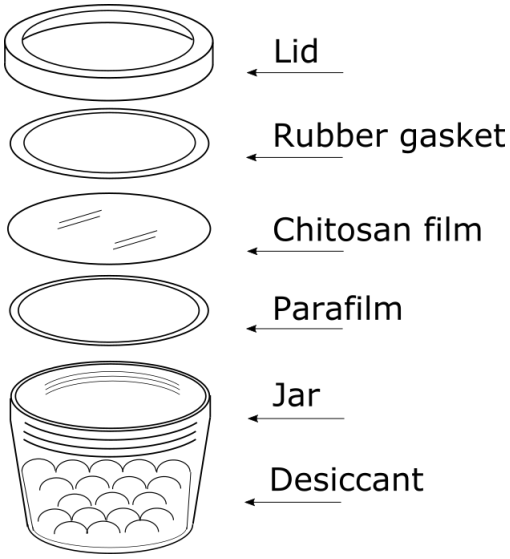

Figure 3.4: WVP test cup assembly.

3.5 Mechanical Properties

3.5.1 Background

Mechanical properties are correlated with microstructure, internal bonding mechanisms, and molecular orientation. Casting conditions of solvent cast films influence microstructure [169, 170], and slower evaporation [169] can result in higher crystallinity, which in turn increases film stiffness [169], tensile strength [170] and elastic modulus, especially in the rubbery state. Below the glass transition temperature, T_g, the effect of crystallinity is less influential, as evidenced by the insignificant variation in the measured tensile strength (TS), elongation-before-break (EBB) and elastic modulus of hydroxypropyl-starch films in the glassy [170] state. However, below T_g unorientated crystals can induce brittleness due to strains with amorphous segments [171].

Rubber elasticity theory states that the stress of a crosslinked material is proportional to density (which increases with crosslinking) and inversely proportional to the number-average molecular weight of polymer between crosslinks. Tensile strength of crosslinked materials increases at low concentrations of crosslinking agent, reaches a maximum, and then decreases with a further increase. EBB, on the other hand, decreases steadily with increasing crosslinker, as observed in Figure 2.9.

The thickness of test strips also affects measured mechanical properties. Plasticized starch films of 0.3 to 2.5 mm thickness displayed EBB values of $\sim$ 100 to 10 %, TS of 4.1 MPa to 1.5 MPa, and modulus from $\sim$ 100 MPa to 30 MPa [172]. In the case of TS and modulus, the values first increased and then decreased as the films became thicker.

3.5.2 Experimental

Tensile measurements on chitosan films were performed using an Instron 4465 (Instron, Norwood, Massachusetts, USA) by following the ASTM standard D882. An initial grip separation of 50 mm (flat grips) and crosshead speed of 50 mm/min were used. Test strips were cut to dimensions of 1.2 cm (width) × 11 cm (length). Specimens were cut from two bulk films per film type, with 8 specimens per bulk film. The thickness of the specimens was determined by an average of 4 measurements using a digital micrometer (± 0.002 mm accuracy, Marathon Watch Company, Richmond Hill, Ontario, Canada). The TS [MPa] and EBB [%], were calculated as per Equations 3.21 and 3.22:

$$TS = \frac{P}{A_0} \tag{3.21}$$

$$EBB = 100\% \times \frac{\Delta L}{L_0} \tag{3.22}$$

where A_0 is original minimum cross-sectional area in the break region [mm^2], P - peak load or load at failure [N], ΔL - elongation at rupture [mm], and L_0 - initial specimen gauge length [mm]. The elongation was measured as the Cauchy (engineering) strain.

3.6 Thermogravimetric Analysis

Thermogravimetric analysis (TGA) was performed using a TA Q500 instrument (TA Instruments, New Castle, Delaware, USA). Samples were heated on platinum pans at a constant rate of 10 ^{o}C/min from 30 to 550 ^{o}C, under a nitrogen purge (60 mL/ min to balance, 40 mL/min to sample). Sample sizes ranged from 2.5 to 5.5 mg. The differential curve of the TGA scans (DTGA) were obtained.

3.7 X-Ray Diffraction

3.7.1 Background

Elastic scattering of x-rays by parallel atomic planes from a long-range ordered (crystalline) material causes constructive interference and subsequent diffraction of the x-rays. The distance between these planes reveals crystallographic information such as grain orientation. The plane spacing is the normal vector from the crystal cell origin to the lattice plane that intersects the cell. Constructive interference occurs when the incident angle satisfies Bragg's law, Equation 3.23:

$$n\lambda = 2d\sin\theta \tag{3.23}$$

where n is a positive integer, λ is the incident light wavelength, d is the distance between parallel lattices and θ is the incident light scattering angle. The diffraction pattern produced is specific to the crystal structure responsible for the diffraction. Each peak appearing in the diffractogram corresponds to a different plane (denoted by hkl Miller indices) associated with the crystals present in the material. Broad scattering peaks result from amorphous domains which lack atomic order on the long range, and overlap with the more defined crystalline peaks.

The most common measuring arrangement for XRD is the Bragg-Brentano assembly. The x-ray source is located at an angle θ from the specimen, while the detector is positioned 2θ from the incident ray, as shown in Figure 3.5A. Commercial instruments are typically equipped with a tungsten filament (cathode) which emits electrons when heated, striking a copper anode which produces and emits $K\alpha$ x-ray waves. The rays are filtered to eliminate $K\beta$ and $K\alpha_2$ waves, isolating $K\alpha_1$ waves for diffraction. The diffracting beam is emitted into a photon-counting detector, and the signal is processed by converting electrical charge to a numerical value.

Signal to noise ratio can be lower for film specimens compared with powders, especially if the film is too thin and interference from the substrate is an issue with conventional XRD. Grazing incidence XRD (GIXRD) provides an alternative to obtain a stronger signal from the surface, at the expense of spatial resolution from deeper penetration. Here, the incident grazing angle, α_i, is kept constant while the detector position is varied by 2θ. The α_i is typically less than 1°, and must be greater than the critical angle for total reflection. The incident and detector geometries in GIXRD mode are shown in Figure 3.5B.

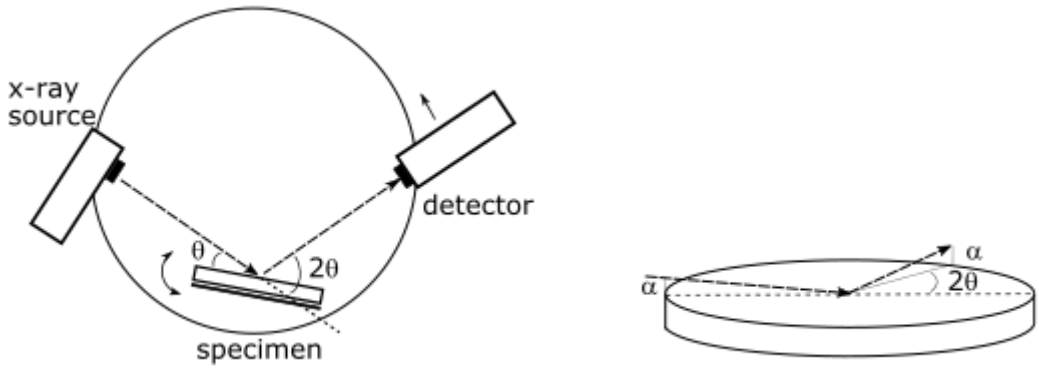

(A) Conventional $\theta/2\theta$ (B) Angles of GIXRD

Figure 3.5: Graphical depictions of (A) conventional Bragg-Brentano ($\theta/2\theta$) assembly and (B) associated angles of incident (α_i) and detection (2θ) from a GIXRD arrangement.

3.7.2 Experimental

Characterization of the crystalline structure of the chitosan films was performed using an X'Pert MRD-Pro instrument (Malvern Panalytical Ltd, Malvern, UK). The instrument was operated in line mode with an x-ray mirror to collimate the source, using a parallel plate collimator (0.27° spacing) prior to the detector. In GIXRD mode, α_i was set to 0.6°. Radiation source was CuKα_1 with a 1.54 Å wavelength, and was operated at power settings of 45 kV and 35 mA. The films were scanned over a 2θ range of 5 - 45°, with a scan step size of 0.1° and scan rate of 9 second/step at ambient conditions. For powder chitosan samples, X'Pert Powder instrument(Malvern Panalytical) was used and with the same parameters as the films.

The degree of crystallinity of the films and chitosan powder, CrI, was estimated from the diffractograms from the relative crystalline and amorphous portions of the curve, as per Equation 3.24:

$$\mathrm{CrI} = \frac{A_c}{A_c + A_a} \times 100\ \% \tag{3.24}$$

where A_c and A_a are the areas under the diffractogram corresponding to crystal and amorphous domains, respectively. Multiple methods of estimating CrI are compared and discussed in Appendix B.1, including a method based on peak height intensity. The methods based on integration vary with the choice of baseline, and the baseline selected for this study is highlighted in Appendix B.1.

3.8 Contact Angle

3.8.1 Background

Adhesion between two surfaces is generally driven by hydrogen and van der Waals forces, the latter consisting of Keesom, Debye, and London dispersion forces [173]. When a liquid is in contact with a smooth, homogeneous solid in equilibrium, the shape of its droplet is attributed to surface tension and gravity, and possibly other external forces. The contact angle is the tangent from the point of contact at the 3-phase boundary, as depicted in Figure 3.6A.

High adhesion causes high wetting ($\theta < 10^\circ$), while low surface energy (solid-vapor interface) and low interfacial tension (solid-liquid interface) creates high angles ($> 90^\circ$). The intermediate results in semi-wetting between ($10^\circ < \theta < 90^\circ$). A comparison of semi-wetting and low wetting cases is given in Figure 3.6B. Contact angles of liquid droplets on solids can be determined using a goniometer to observe the sessile drop profile. The

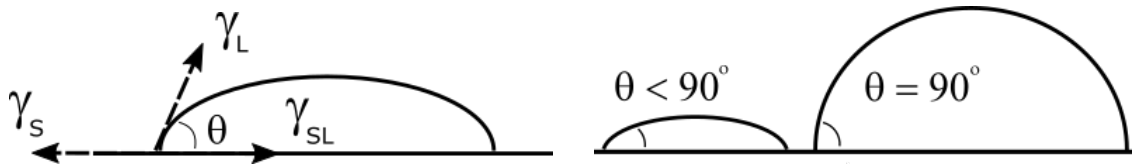

(A) (B)

Figure 3.6: (A) Contact angle, θ, between a liquid droplet and solid surface at the 3-phase boundary. The respective surface tensions, γ, are given by arrows. (B) Comparison of liquid droplets with low and high contact angles, corresponding to cases of semi-wetting and low wetting.

relation between the contact angle, θ, and surface tension, γ, (solid-liquid interface) on an ideal surface is described by Young's equation:

$$\gamma_{\mathrm{L}} \cdot \cos\theta = \gamma_{\mathrm{S}} - \gamma_{\mathrm{SL}} \tag{3.25}$$

where the subscripts L, S, and SL correspond to the liquid-vapor, solid-vapor, and solid-liquid interfacial tensions, respectively. Equation 3.25 assumes that the equilibrium pressure of adsorbed liquid vapor pressure on the solid is negligible.

As per molecular theory, polar and dispersive forces are the main contributing forces to a solid's surface energy. Polar forces include hydrogen bonding, dipole-dipole, and dipole-induced interactions, while non-polar forces are mainly van der Waals interactions. The relation between interfacial tension of a solid-liquid interface and its individual polar and dispersive forces is modeled by:

$$\gamma_{\mathrm{LS}} = \gamma_{\mathrm{S}} + \gamma_{\mathrm{L}} - 2\left(\gamma_{\mathrm{L}}^{\mathrm{D}}\gamma_{\mathrm{S}}^{\mathrm{D}}\right)^{1/2} - 2\left(\gamma_{\mathrm{L}}^{\mathrm{P}}\gamma_{\mathrm{S}}^{\mathrm{P}}\right)^{1/2} \tag{3.26}$$

where the subscripts L and S denote liquid and solid, respectively, and superscripts D and P denote dispersive and polar, respectively. The Fowke's and Owens/Wendt [173] models are quite adequate for estimating the surface tension of polar surfaces, especially polysaccharides. These two methods are for all intents and purposes mathematically identical but differ in experimental approach. The Owens/Wendt model combines Equations 3.25 and 3.26 to give the two parameter relationship shown in Equation 3.27, and is applied by measuring the contact angle of multiple polar liquids to estimate the surface energy of the solid, γ_{S}. The Fowke's version utilizes only two liquids, one polar, and one non-polar. Readers may consult the Krüss technical note [174] for background information on the different models to calculate total surface energy of polar and non-polar solids.

$$\gamma_{\mathrm{L}}\frac{(1+cos\theta)}{2(\gamma_{\mathrm{L}}^{\mathrm{D}})^{1/2}} = (\gamma_{\mathrm{S}}^{\mathrm{P}})^{1/2}\frac{(\gamma_{\mathrm{L}}^{\mathrm{P}})^{1/2}}{(\gamma_{\mathrm{L}}^{\mathrm{D}})^{1/2}} + (\gamma_{\mathrm{S}}^{\mathrm{D}})^{1/2} \tag{3.27}$$

The net surface energy of the solid is given by:

$$\gamma_{\mathrm{S}} = \gamma_{\mathrm{S}}^{\mathrm{P}} + \gamma_{\mathrm{S}}^{\mathrm{D}} \tag{3.28}$$

3.8.2 Experimental

The contact angles of deionized water (polar liquid) and hexadecane (non-polar liquid) (Sigma Aldrich, St. Louis, Missouri, USA) liquid droplets on the chitosan film surfaces were measured by the sessile drop method using a Krüss drop shape analyzer DSA 100 instrument (Krüss GmbH, Hamburg, Germany). The experiments were performed in static mode at room temperature. The droplet sizes were 15 µL for water, but were uncontrolled for hexadecane. The drop shapes were recorded and analyzed after initial deposit, and continued for 20 s after the initial drop. Both tray- (smooth) and air- (rough) sides of the film were tested on. DSA1 V1.9 software (Krüss GmbH) was used for imaging and droplet analysis. The contact angles were estimated using the tangent method 1 (conic section), polynomial (tangent method 2) and Young-Laplace fit methods, and were compared for best fit.

3.9 Moisture Sorption Isotherm

3.9.1 Background

The affinity of moisture to a material, especially in food or foodstuff, can be expressed with a moisture sorption isotherm, by determining the weight gain from moisture adsorption over a range of water activity values. Water activity, a_{w}, is approximately the ratio of partial vapor pressure from an aqueous solution within a closed system to the partial pressure from pure water at a fixed temperature, assuming a negligible fugacity coefficient of 1. It is also considered as the equilibrium relative humidity, or RH in air expressed as a fraction, as per Equation 3.29.

$$a_{\mathrm{w}} = \frac{p_{\mathrm{w}}}{p_{\mathrm{w}}^{0}} = \mathrm{RH}/100\% \tag{3.29}$$

The isotherms are influenced by a number of effects, such as the type of sorbent-water interactions and capillary effects [175]. One theory that adequately describes the moisture sorption isotherms of foodstuff or polysaccharide films is the statistical model of Guggenheim-Anderson-de Boer (GAB). The basis of the GAB model is the physical notion that the primary sorption layer of water vapor in contact with the sorbent is in a different energetic state than subsequently higher sorption layers. The GAB model is given as:

$$X = \frac{x_{\mathrm{m}} C_{\mathrm{G}} K_{\mathrm{G}} a_{\mathrm{w}}}{(1 - K_{\mathrm{G}} a_{\mathrm{w}})(1 - K_{\mathrm{G}} a_{\mathrm{w}} + C_{\mathrm{G}} K_{\mathrm{G}} a_{\mathrm{w}})} \tag{3.30}$$

where X is the percentage of moisture adsorbed by the sorbent as a function of a_{w}, x_{m} is the monolayer moisture value, C_{G} is the sorption monolayer constant, and K_{G} is the multilayer moisture sorption constant. C_{G} represents the chemical potential difference of the adsorbed water vapor molecules between the upper sorption layers and the monolayer, and K_{G} correlates the chemical potential difference between the water vapor molecules in the pure state with their state in upper sorption layers. The product of the energy constants, $C_{\mathrm{G}} \cdot K_{\mathrm{G}}$, describes the chemical potential difference of sorbed liquid molecules in the pure liquid state with their state in sorption monolayer. In the monolayer, the adsorbed water vapor molecules interact with the polar or ionic constituents of the substrate [175], contrasting with more direct higher hydrogen bonding and dipole interactions between subsequent layers of water vapor molecules.

The GAB model is based on the statistical theories of the Brunauer-Emmett-Teller (BET) and Langmuir models. The precursory BET model is limited in application to a_{w} of 0.05 to 0.45 [175, 176], while the GAB model sufficiently expresses isotherms over a large range, a_{w} 0.10 to 0.90 for a variety of foods and biopolymer materials. Additionally, the BET model tends to overestimate the energy constant and underestimate the monolayer value, x_{m} [176]. When K_{G} equals 1, Equation 3.30 condenses into the two-parameter BET model. Wang and Brennan [177] highlight other models available for isotherm absorption fitting that readers may consult. An illustration of multilayer adsorption postulated by the BET theory is given in Figure 3.7. A typical isotherm is also depicted in Figure 3.7, showing hysteresis from adsorption and desorption.

3.9.2 Experimental

The gravimetric technique was used to elucidate the moisture sorption isotherm of the chitosan films. The integral method was used, where by multiple samples were placed under different controlled RH conditions and the specimens' mass was measured periodically. (The differential method uses a single sample and progressively increases or decreases the environment settings [175].) Film specimen sizes of 3×3 cm^2 were prepared and were conditioned in a desiccator with Drierite$^{\mathrm{TM}}$ for 5 days until mass equilibrium was achieved. Neat film specimens mass lost $\sim$ 12 %, which accounts for 86 % of the estimated water content in a neat film, as estimated from TGA.

Saturated salt solutions of potassium acetate, magnesium chloride hexahydrate, sodium chloride, and potassium chloride were prepared to give a_{w} conditions of 0.23, 0.33, 0.78, and 0.85 at 23 °C, respectively. Solubility values are given in Table 3.2. Additionally, another set of specimens were exposed in the environmental chamber to give a fourth a_{w} of 0.5. The saturated salt solutions and specimens were kept in a desiccator and were separated

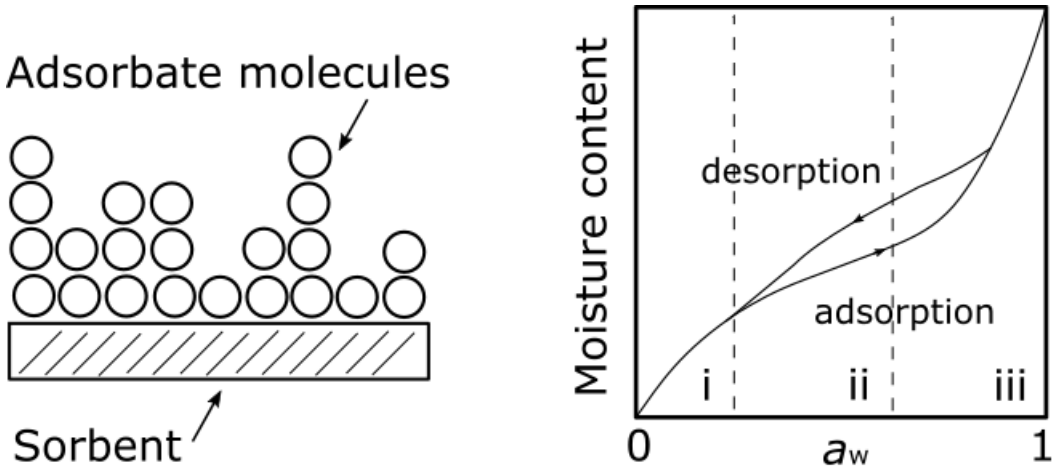

(A) (B)

Figure 3.7: (A) Multilayer adsorption of water vapor molecules as per the BET model, with a random distribution of the number of adsorbate molecules on the different interaction sites. (B) A typical isotherm showing hysteresis between adsorption and desorption of water vapor from the sorbent, showing different regions of sorbent-adsorbate interaction strengths: region (i) tightly bound water vapor molecules, region (ii) moderate bonding with water vapor molecules in small capillaries, and region (iii) loosely bound water molecules, held in large capillaries [175].

by a porous plate. The desiccators were ensured airtight with vacuum grease spread on the brims of the desiccator bowl that is in contact with the lids. The containers were stored in an environmental chamber at 23 °C. The RH in the containers was measured using a thermo-hygrometer (SMART^2, InterTAN Inc., Barrie, Ontario, Canada). The measured RH values were near the expected a_w value at 20 °C within ± 4 %, as listed in Table 3.2. Mass equilibrium of the specimens was complete when the difference between two consecutive recordings was less than 0.5 mg.

Table 3.2: Saturated salt solutions, estimated a_w and measured RH values

Salt	Solubility (g / 100 g H_2O)	a_w (20 °C)	RH (23 °C) (meas.)
CH_3CO_2K	256.0	0.23	22
$MgCl_2{\cdot}6H_2O$	167.0	0.33	36
NaCl	36.0	0.75	78
KCl	35.5	0.85	82

The parameters for the GAB model were estimated by transforming the GAB equation to a quadratic form, and then performing a least-square regression as outlined by Timmerman [176]; see Appendix A.7.

Chapter 4

Heterogeneous Crosslinking Methodology

4.1 Introduction

Preparation of a heterogeneously crosslinked chitosan film with citric acid consists of i) immersion of a neutralized film in an aqueous citric acid solution to introduce citric acid into the film matrix *via* absorption, followed by ii) heat treatment of the (air-dried) film to induce covalent crosslinking between the citric acid and chitosan amine groups. The experimental conditions for the film preparation were decided upon by adjusting parameters relevant to the procedure and observing the film response to solubility in a dilute acid solution as crosslinking affects polymer swelling [109] and dissolution. The conditions that were time efficient which resulted in low solubility were selected for the remainder of experiments throughout the study.

The conditions for the immersion of the film were citric acid concentration, and duration of immersion (ambient conditions), and the conditions for heat treatment were temperature and duration. The effects of citric acid concentration, and heat treatment temperature and duration on solubility in dilute acetic acid aqueous solution were taken as general indicators of changes in crosslinking degree. The use of a catalyst was excluded, as several bodies of work purport covalent crosslinking by heat treatment alone [8, 147, 149].

4.2 Experimental

4.2.1 Film Preparation

The preparation methods of neat, neutralized, and chitosan-citrate films, and heterogeneously crosslinked films without heat treatment (denoted as CA films) and with

heat treatment (CA-HT films) are described in Section 3.2. A list of the experimental parameters tested in order to select the final conditions for the preparation of CA and CA-HT films is given in Table 4.1.

Table 4.1: Experimental test conditions for heterogeneously prepared chitosan films with citric acid.

Condition	Parameters
Citric acid concentration	10, 15 % (w/w citric acid/dried neutralized film)
Immersion time	1, 3, 5, 12, 24 h (arbitrary)
Heat treatment	150 °C / 0.5 h, 110 °C / 6 h [147]

4.2.2 Solubility and Swelling

Film specimens of 1×1 cm were immersed in 15 mL of 1 % (v/v) acetic acid solution (pH 2.8) or deionized water at room temperature for 24 h. The residual specimens were rinsed, filtered (vacuum aspirator) and dried at room temperature. The specimens' mass was measured before and after immersion. Film solubility was calculated as:

$$\text{solubility} = \frac{m_\text{i} - m_\text{f}}{m_\text{i}} \times 100\% \tag{4.1}$$

where m_i and m_f are the initial and final dry specimen masses, respectively. Film swelling was estimated as:

$$\text{swelling} = \frac{m_\text{w} - m_\text{f}}{m_\text{f}} \times 100\% \tag{4.2}$$

where m_w is the wet specimen mass when removed from the solution after being rinsed and gently wiped to remove surface water.

4.3 Results and Discussion

4.3.1 Immersion Time

The mass increase of a dried film containing citric acid relative to a dried neutralized film should ideally be the mass of citric acid added to the solution. For these measurements a fixed citric acid concentration of 15 % (w/w) was used, since higher concentrations yield films that are brittle. The mass change was measured at immersion times of 1, 3, 5, 12 and 24 h, as shown in Table 4.2. An immersion time of 1 h led to a mass increase of 6 ± 3 %

and is insufficient since it is less than the required amount of 15 %. This requirement was achieved at 5 h with a 16 ± 3 % mass increase, and this duration was used for subsequent CA film preparations. By comparison, heterogeneous crosslinking with glutaraldehyde requires an immersion time of 24 to 48 h [127] to reach chemical equilibrium.

Table 4.2: Mass percent increase of dried neutralized film by citric acid uptake at different immersion times in aqueous citric acid solution. The concentration of citric acid was fixed at 15 % (w/w).

	Immersion duration [h]				
	1	3	5	12	24
Δm [%]	6 ± 3 [a]	12 ± 2 [b]	16 ± 3 [b]	15 ± 2 [b]	17

Number of replicates, $n = 3$ for 1 and 12 h, $n = 5$ for 5 h, and $n = 2$ for 3 h, and $n = 1$ for 24 h. The superscripted letters denote statistically different values (t-test, $\alpha = 0.05$).

4.3.2 Effects of Heat Treatment on Solubility and Swelling

The solubility of heterogeneously crosslinked films with 15 % citric acid, heat treated at 150 °C and without heat treatment were compared to one another, and also with neutralized and chitosan-citrate films. The dissolution and swelling values of specimens in H_2O and acetic acid are given in Table 4.3. Neutralized films showed less than 3 % soluble matter and swelling by 210 ± 20 % in deionized water. The CA and CA-HT were insoluble in deionized water, losing only ∼ 3 % and 1 % mass, respectively. This is not surprising given that the neutralized films did not dissolve in dilute aqueous citrate solution, demonstrating that the citric acid content in solution was below the 50 % protonation threshold [67, 69] that is necessary for chitosan dissolution in acidic media.

Table 4.3: The solubility and swelling of neutralized films, heat treated (HT) neutralized films, and CA and CA-HT films in deionized water and 1 % acetic acid solution (aq).

Film	Deionized H_2O		1 % acetic acid	
	Solubility [%]	Swelling [%]	Solubility [%]	Swelling [%]
Neutralized	2.6 ± 0.4 [a]	210 ± 20 [a]	100 [a]	N/a
Neutralized (HT)	-	-	100 [a]	N/a
CA	3.0 ± 0.4 [a]	140 ± 18 [b]	57 ± 6 [b]	595 ± 72 [a]
CA-HT	0.5 ± 0.3 [b]	139 ± 17 [b]	31 ± 6 [c]	5,100 ± 1,100 [b]
Chitosan-citrate	100 ± 0 [c]	N/a	100 [a]	N/a
Chitosan-citrate (HT)	-	-	22 ± 2 [d]	25 ± 2 [c]

Empty table entries (-) indicate no measurements were taken for those conditions. Number of replicates, $n = 3$ or 4 per film type. The superscripted letters denote statistically different values (t-test, $\alpha = 0.05$).

The soluble content of CA and CA-HT films in 1 % acetic acid was 57 ± 6 % and 31 ± 6 %, respectively. The lower solubility of CA-HT relative to CA specimens indicated that heat treatment induced a reaction between citric acid and chitosan amine groups. By comparison, heat treated neutralized films still completely dissolved in 1 % acetic acid. Therefore, the decrease in solubility with CA-HT compared to CA specimens was due to the combination of citric acid and heat treatment, as heat treatment had no effect on the solubility of the acid-free neutralized films. CA specimens swelled by 550 - 700 %, while CA-HT specimens retained water in excess of 3,000 % of the dry specimen weight. This large discrepancy in swelling between heat treated and non-heat treated specimens could be from hydrolysis of chitosan chains, thereby lowering the average polymer chain length. It is possible that the higher degree of substitution may have accelerated the hydrolysis rate. This hypothesis is borrowed from observations that the activation energy of hydrolysis is lower for adjacent acetylated chitosan units compared to two adjacent deacetylated units [178, 179].

Another possibility is that only one carboxylate per citric acid molecule grafted onto chitosan, forming a hybrid ionic-covalent crosslink as depicted in Figure 4.1. This dual ionic-covalent crosslink type was similarly proposed by Argüelles-Monal and Peniche-Covas [180], when they heat treated a chitosan-citrate film at 100 °C under vacuum for several hours. One mechanism that may possibly prevent further reactions, and therefore prevent the extension of grafting into crosslinking, is from the heat itself. High temperatures will increase polymer chain mobility, but conversely the chain and side group mobility will also be countered by a reduction in plasticization effects from moisture evaporation.

Chitosan-citrate films became less soluble in 1 % acetic acid with heat treatment, whereas they would otherwise completely dissolve. Their degree of swelling of 25 % was very low compared to CA and CA-HT specimens, which was likely from a reaction with the majority of amine groups. The ratio of moles of citric acid to glucosamine in a chitosan-citrate film is 1.0 - 1.2. The excess of citric acid molecules in this case makes grafting more likely than crosslinking.

Additional Comments on Solubility and Swelling

Fernández-de Castro et al. [181] report a soluble content of 57 % for neutralized chitosan films in distilled water, but these films were neutralized by spraying NaOH instead of the conventional immerse and rinse process outlined in Section 3.2.2. Unlike chitosan-salt films, neutralized chitosan films are insoluble in deionized water [182] and may swell between 65 to 250 % [182, 183]. A chitosan film in salt form with a monocarboxylic acid that has not been thermally treated is completely soluble in deionized water [184–186], owing to the protonated state of the film ($RCOO^- \cdots NH_3^+$). If the chitosan film is heat treated in order to obtain a completely dry basis of the specimens prior to solubility tests in deionized

water, this can render the measured solubility content [66, 186] to values below 22 %, because of inadvertent changes [186] to chitosan's side group chemistry and hydrophilicity due to amidization. The presence of a plasticizer in the chitosan film has also been shown to retard the total soluble content [186], from 100 % down to 24 % with 30 % glycerol.

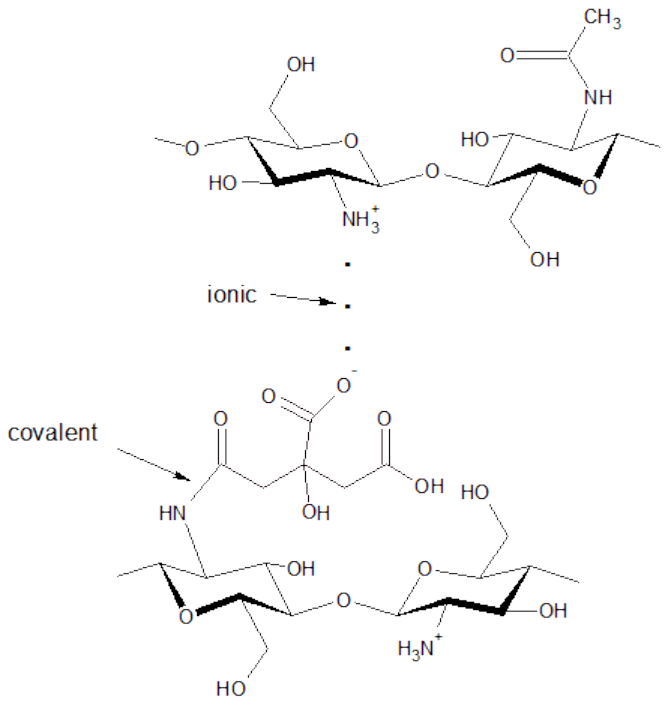

Figure 4.1: A possible scenario: grafting of citric acid onto chitosan and resulting in a hybrid ionic-covalent crosslink after heat treatment of a heterogeneously crosslinked film with citric acid.

4.3.3 Citric Acid Concentration and Heat Treatment Conditions

The results of the solubility study to assist with the conditions for heterogeneous crosslinking are shown in Table 4.4. The effect of citric acid concentration on the solubility of heat treated films was investigated. The solubility decreased from 52 ± 17 % for a film with 10 % citric acid to 26 ± 15 % with 15 % citric acid. Statistical analysis by paired comparisons to block the effect of film thickness was performed. The difference between the dissolution percentages was significant. Hence, the degree of citric acid in the heat treated films affects the degree of film solubility; the films are more soluble with lower citric acid content.

The difference in solubility between CA-HT films that were heat treated at 110 °C / 6 h and 150 °C / 0.5 h of 26 ± 15 % and 33 ± 9 % at a fixed concentration of 15 % citric acid was not statistically significant. The 110 °C / 6 h conditions were based on Cui et al. [147], which did not utilize a catalyst, yet claim that covalent crosslinking between

chitosan and citric acid still occurred. It should be clearly stated here that the conditions thus far tested in no way are being considered as an indicator that covalent crosslinking occurred. Remarks on the nature of the bonding between citric acid and chitosan are assessed using dynamic mechanical analysis (DMA) in the next chapter.

Given the conditions tested and presented, it was decided that a concentration of 15 % citric acid, an immersion time of 5 h in citric acid aqueous solution, and a heat treatment of 150 °C / 0.5 h would be efficient to prepare films for DMA experiments (Chapter 5).

Table 4.4: Effect of citric acid concentration, immersion time in solution, and heat treatment of films on film solubility in 1 % acetic acid solution.

Immersion time [h]	Citric acid conc. [wt. %]	Heat Treatment [°C] / [h]	Solubility [%]
5	10	150 / 0.5	52 ± 17
5	15	150 / 0.5	26 ± 15
5	15	150 / 0.5	26 ± 15
5	15	110 / 6	33 ± 9

Number of replicates, $n = 3$ for immersion time and heat treatment trials, $n = 5$ for citric acid concentration trials.

4.3.4 Film Characteristics

Changes to film mass, thickness, and dimensions from neutralization, citric acid addition, and heat treatment, are given in Table 4.5. As a consequence of neutralization, film surface area shrank by 16 ± 5 %, thickness decreased by 13 ± 8 %, and film mass was on average 21 % less than neat films. When the neutralized films were allowed to dry freely without clamping, the thickness of films increased by approximately 50 %, and the surface area decreased by approximately 50 % compared to neat films. For this reason, clamping was used. Citric acid also made the films slightly thicker, by 11 ± 2 % and 17 ± 9 % for 10 % and 15 % citric acid, respectively.

When the neutralized films were immersed in citric acid aqueous solutions, the films swelled and expanded from the protonation of NH_2 groups. Citric acid is a weak acid, and the electrostatic repulsion of NH_3^+ groups enables the chitosan chains to distance themselves. The films elongated by approximately 1 - 2 cm on each side of the film, relative to the dry neutralized film. In Chapter 5, chitosan films were heterogeneously crosslinked by glutaraldehyde (GLU). When the neutralized films were immersed in GLU aqueous solutions, the films swelled from water absorption, but did not expand, and the surface area dimensions did not change relative to dry neutralized films. GLU has a very high pKa, and is not a proton donor.

The neat chitosan films were transparent with a yellow offset. This yellow tinge was lessened upon neutralization. With heat treatment neat films darkened slightly and CA to a lesser extent, which is indicative of a chemical reaction, while neutralized films did not change color. Images of the films before and after heat treatment are shown in Figure 4.2. Heat treatment caused CA films to become brittle, which required a minimum of 72 h of conditioning at 23 °C/50 % RH to prevent cracking if bent or cut. Heat treatment of neat and neutralized films did not induce the same extent of brittleness (qualitative assessment) as it did with CA films. Films cast from citric acid are more brittle than those cast with acetic acid [66, 184]. This is a consequence of the solid state nature of citric acid at ambient conditions, and this has also been observed with other solid state acids such as malic acid [184].

Table 4.5: Changes to chitosan film thickness, l, mass, m, and surface area, A, with neutralization, citric acid addition, and heat treatment

Step	Δl [%]	Δm [%]	ΔA [%]
Neutralization (unclamped) compared to neat film	54 ± 2	-23 ± 1	-56 ± 1
Neutralization (clamped) compared to neat film	-13 ± 8	-21 ± 2	-16 ± 5
Citric acid addition, 10 % compared to neutralized film	11 ± 2	11 ± 1	-14 ± 6
Citric acid addition, 15 % compared to neutralized film	17 ± 9	16 ± 3	-14 ± 6
Heat treatment, 150 °C/0.5 h, 110 °C/6 h compared to non-heat treated CA film	∼ -5	-12 ± 3	∼ -5

Number of replicates, $n = 10$ for neat and neutralized films, $n = 6$ for CA films.

The density of the films, as calculated from volume and mass measurements, is given in Table 4.6. The density of the film increased after neutralization, as expected [187]. It increased further with the addition of citric acid since citric acid has a higher molecular weight than acetic acid, despite the increase in film thickness which would counter the mass gain to the density change.

4.4 Conclusion

Heat treatment induced a decrease in film solubility in dilute acid solution that reflects covalent reactions between citric acid and chitosan. The solubility of chitosan films in 1 % acetic acid solution were studied in order to select conditions for heterogeneous crosslinking

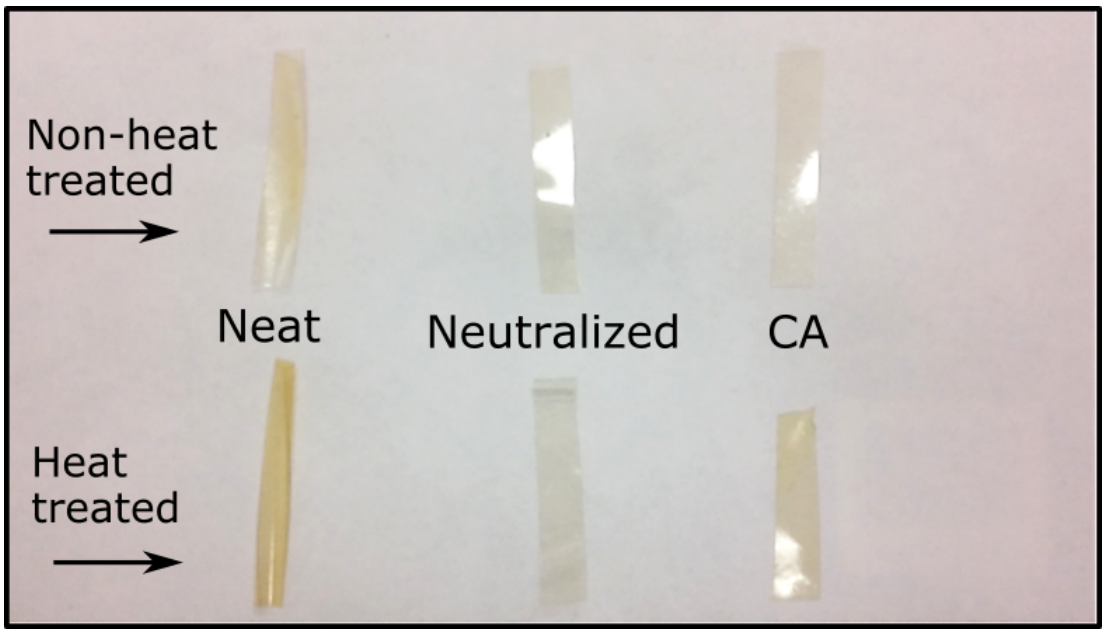

Figure 4.2: Photograph of neat, neutralized, and CA films, non-heat treated (above), and heat treated (below).

Table 4.6: Chitosan film densities.

Film Type	Density [g/cm^3]
Neat	1.50 ± 0.10 ^{a}
Neutralized	1.71 ± 0.13 ^{b}
CA	2.00 ± 0.22 ^{c}

The superscripted letters denote statistically different values, as determined by LSD comparison of means. Number of replicates, $n = 8$ for neat and neutralized films, $n = 5$ for CA films.

with citric acid. The effect of citric acid concentration and heat treatment conditions on solubility were investigated. The final conditions chosen for the CA and CA-HT film methodologies were 15 % citric acid, 5 h immersion time, and a heat treatment of 150 °C / 0.5 h. The conditions were subsequently used to prepare CA and CA-HT films for further film characterization.

Simple characteristics of the film were also observed including changes to film mass after neutralization and citric acid addition. The density of the films increased to 1.71 g/cm^3 with neutralization and to 2.00 g/cm^3 after addition of citric acid. Neat and CA films displayed darkening color change with heat treatment, signifying chemical reactions in the films, while neutralized films did not change color.

Chapter 5

Viscoelastic Properties of Crosslinked Films

5.1 Introduction

To test whether thermal treatment of chitosan films with citric acid (denoted as CA films) enabled covalent crosslinking, or if the crosslinking bonding type between chitosan and citric acid remained ionic, the viscoelastic properties of neat, neutralized, CA and heat treated CA films (referred to as CA-HT) were measured by dynamic mechanical analysis (DMA). Specifically, the study focuses on changes in storage modulus and the tanδ relaxation properties of heterogeneously-crosslinked CA films compared to neutralized and CA-HT films, as higher material stiffness and an increase in glass transition temperature, T_{g}, are correlated with an increase in crosslink density, as per the rubber elasticity theory (Section 3.3.2). To assist with the analysis, films crosslinked with a model crosslinker, glutaraldehyde (GLU), were also investigated, which were crosslinked homogeneously (GLU-HOM films) and heterogeneously (GLU-HET films). Additionally, since moisture in the films impacts mechanical properties, and because water content varies between film types, removal of absorbed water by preheating films prior to DMA was also performed.

A description of the changes in storage modulus, E', loss modulus, E'', and tanδ with temperature for each film type is given. Non-preheated film specimens are discussed first, followed by preheated films, and then the two are compared in Section 5.3.3. The GLU-crosslinked films are discussed separately in Section 5.3.5. A more detailed examination of the viscoelastic properties in the context of crosslinking and T_{g} is given in the Discussion (Section 5.4). Some of the work presented here has been published in *Processes*; *Processes* **2019**, 7(3), 157 [188].

5.2 Experimental

Experimental methodologies for film formation are given in Section 3.2.2. The DMA operation is outlined in Section 3.3.3. Film code names can be referred to in Table 3.1.

5.3 Results

5.3.1 General Trends of Non-Preheated Films

The plots of E', E'' and tanδ for replicate runs, n, of non-preheated neat, neutralized, CA-HT, and CA films are given in Figures 5.1 to 5.4, respectively. Each of these figures has been scaled differently to maximize curvature that may be observed for the respective film. More replicates were performed with neat films ($n = 6$) than the other films ($n = 3$ - 5) to obtain a visual representation of consistency of film production and DMA test results.

For neat films (Figure 5.1), the onset E' at 30 °C ranged from roughly 4,500 - 6,000 MPa. The E' then declined linearly to values of approximately 3,000 - 4,500 MPa at approximately 100 °C, and either entered a local minimum or a plateau. The E' declined a second time from approximately 120 - 140 °C to a local minimum near 160 - 170 °C at 1,250 - 2,500 MPa. It then increased to 2,000 - 2,500 MPa near 200 °C. The first and second declines in E' are due to polymer chain softening from an increase in internal energy with increasing temperature. The plateau or slight rise in E' near 100 °C after the initial incline shows reduced chain mobility due to the evaporation of absorbed water molecules which have a plasticizing effect on the film. The anti-plasticizing phenomena driving the second increase in E' above 160 °C is more nuanced and speculative in nature and will be discussed later on in this section.

The corresponding E'' for neat films began from 300 - 400 MPa at 30 °C, increased to a broad peak whose center is masked by a secondary peak of 425 - 475 MPa near 100 - 120 °C. The E'' then decreased to a local minimum from 375 - 450 MPa between 130 - 140 °C, and then increased to a maximum of 400 - 475 MPa near 150 - 160 °C. The corresponding tanδ increased from 0.05 at 30 °C to a broad peak near 100 °C merging with a secondary peak of 0.10 - 0.15 height at 100 - 120 °C, and reached a more pronounced peak maximum of 0.175 - 0.29 near 160 - 170 °C. The height and width characteristics of this relaxation peak seemingly can vary widely between different specimens from neat films prepared consistently with the same procedure. Structural and chemical heterogeneity within a chitosan film may be due to the broad molecular weight and DD properties of the chitosan causing density fluctuations, while heterogeneity between specimens from different films can be attributed to inconsistent drying temperature and relative humidity.

For neutralized films (Figure 5.2), E' decreased from 5,500 - 8,000 MPa at 30 °C to 5,000 - 6,000 MPa at 110 - 120 °C, plateaued until approximately 160 °C, and decreased to

4,000 - 5,000 MPa at 200 °C. Unlike neat films, E' did not increase at all above 160 °C, an important distinction that will be discussed further on. The corresponding E'' displayed but one distinct peak of 450 - 550 MPa between 80 - 90 °C. The corresponding tanδ increased from 0.055 - 0.60 at 30 °C to a broad maximum near 100 °C, plateaued to 0.075 - 0.08 near 140 - 160 °C or passed through a local minimum before increasing to an imperceptibly weak maximum near 180 °C. Thus, it appears that the prevalent tanδ peak between 160 and 180 °C in neat films becomes greatly diminished or non-existent with neutralization, as observed by Gartner et al. [189].

For CA-HT films (Figure 5.3), E' decreased linearly from 6,500 - 8,000 MPa at 30 °C to 3,500 - 5,000 MPa near 140 °C, plateaued to 180 °C, and decreased to 3,500 - 5,000 MPa at 200 °C. The corresponding E'' decreased from 400 - 600 MPa at 30 °C to 150 - 200 MPa at 200 °C, passing through several inflection points along the way. The corresponding tanδ increased from 0.05 - 0.08 at 30 °C to a broad peak of 0.07 - 0.09 height which seemingly was comprised of two merged peaks between 90 - 130 °C. The temperature-dependent viscoelastic behaviour of CA films (Figure 5.4) were both qualitatively and quantitatively similar with CA-HT films, and their description will be neglected to avoid redundancy. The E' of CA and CA-HT films increased/plateaued once during the temperature scan between 140 to 180 °C, compared to the two increasing/plateau segments at 100 - 140 °C and 160 - 200 °C for neat films.

The curves of the non-preheated films are graphed together for comparison in Figure 5.5, along with a GLU-HOM-6 film. (The results of the GLU-crosslinking study are given in Section 5.3.5.) Note that the scales of the sub-plots in Figure 5.5 have been made equal with the comparative plot of preheated films in Figure 5.10. The more pertinent information from the figures of the non-preheated specimens have been extracted and compiled into Table 5.1. This includes average tanδ peak height and center values, and E' values at 35 °C and 195 °C. These two temperature levels were chosen due to their proximity near ambient and onset of degradation conditions, respectively.

The tanδ peaks near 100 °C (low temperature) and 160 °C (high temperature) are designated as 'peak 1' and 'peak 2', respectively. For non-preheated neutralized films peak 2 is practically non-existent, but for intensive purposes, any maximum value in the 160 to 200 °C range is treated as one. The low temperature tanδ peak, peak 1, near 100 °C is the water-induced relaxation peak arising from the desorption and subsequent evaporation of water molecules [190]. The secondary peak which centers around 110 °C and overlaps with the water-induced peak is likely by consequence of residual acetic acid in the film, as it is absent from the scans of neutralized, CA and GLU-crosslinked films. It may be related to the σ-type conduction of acetate ions and protons observed in isochronal dielectric measurements [191] in the temperature range of -10 to 150 °C of neutralized and non-neutralized chitosan films. The nature of peak 2 is discussed in Section 5.4.2.

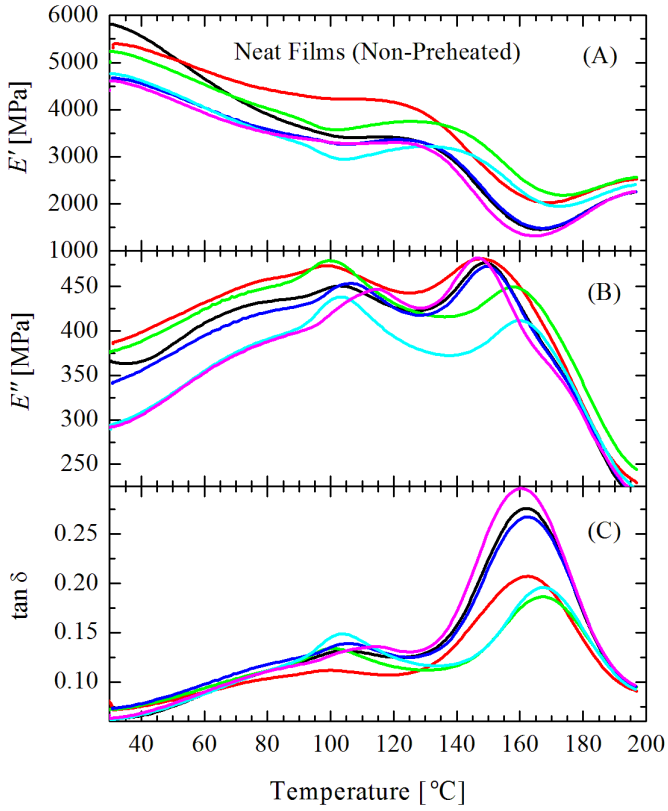

Figure 5.1: (A) E' plotted against temperature of neat chitosan films (6 replicates) and (B) corresponding E'' and (C) tanδ.

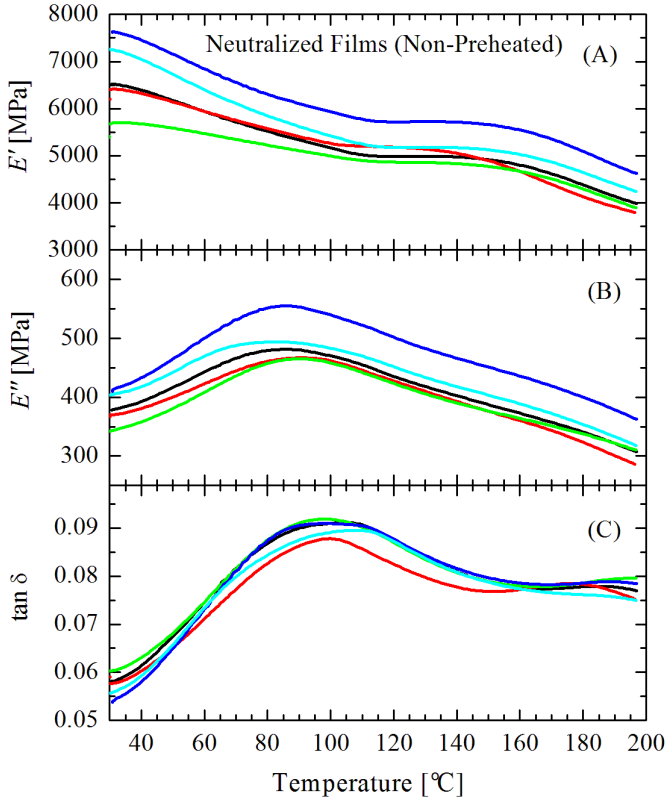

Figure 5.2: (A) E' plotted against temperature of neutralized chitosan films (5 replicates) and (B) corresponding E'' and (C) tanδ.

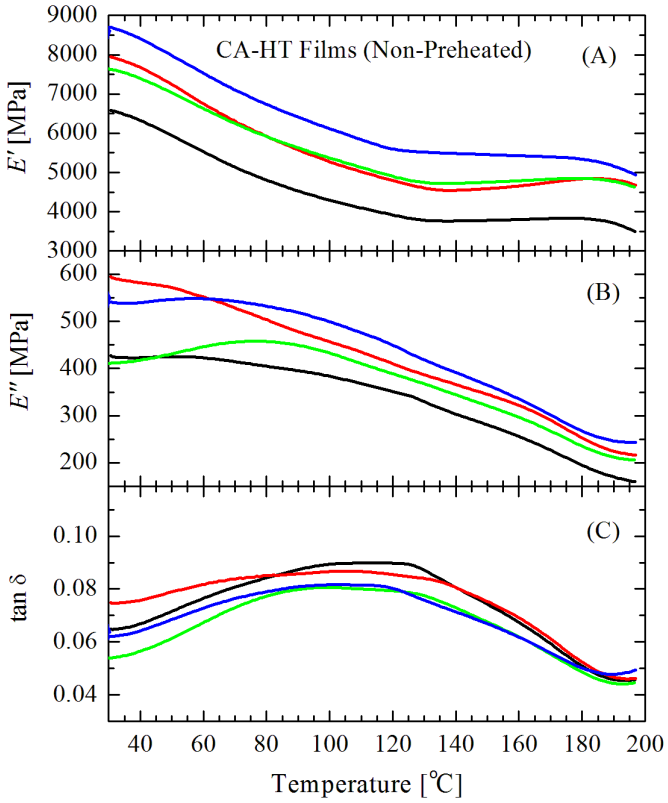

Figure 5.3: (A) E' plotted against temperature of CA-HT films (4 replicates) and (B) corresponding E'' and (C) tanδ.

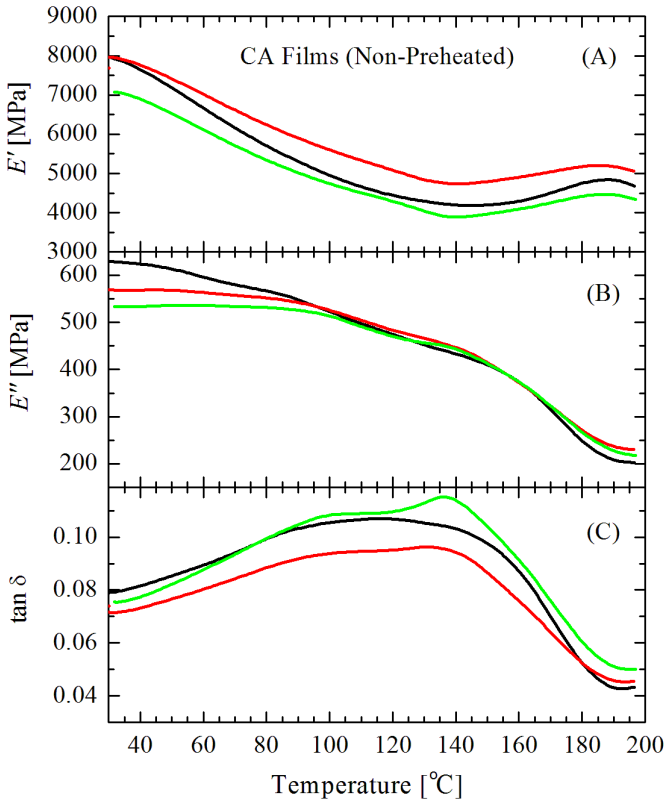

Figure 5.4: (A) E' plotted against temperature of CA films (3 replicates) and (B) corresponding E'' and (C) tanδ.

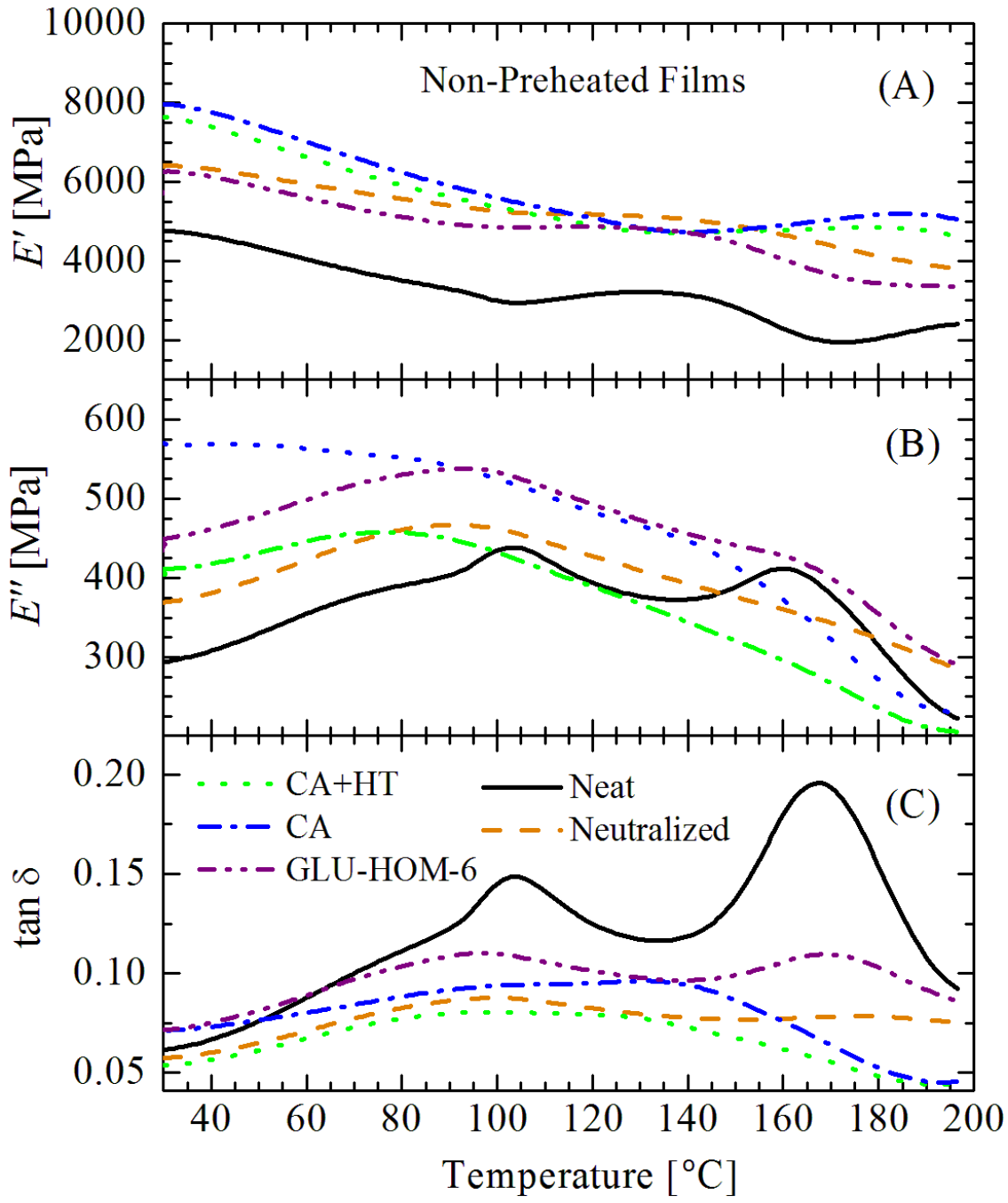

Figure 5.5: (A) E' plotted against temperature for one set of films (neat, neutralized, CA, CA-HT, and GLU-HOM-6) (non-preheated) and (B) corresponding E'' and (C) tanδ.

Table 5.1: The DMA E' and tanδ peak characteristics of non-preheated specimens (see Table 3.1 for film code names).

Film	Parameter	E' (35 °C) [MPa]	E' (195 °C) [MPa]	T (peak 1) [°C]	tanδ peak 1	T (peak 2) [°C]	tanδ peak 2
Neat	mean	5,071 [a]	2,382 [a]	102.0 [a]	0.129 [a]	164.8 [a]	0.216 [a]
	±	432	127	2.8	0.015	2.8	0.045
	COV* [%]	8.5	5.3	2.7	11.7	1.7	21.1
	n	6	6	6	6	6	6
Neutralized	mean	6,665 [b]	4,143 [b]	106.7 [a]	0.089 [b]	187.6 [b]	0.078 [b]
	±	728	334	12.9	0.003	9.8	0.001
	COV [%]	11.0	8.0	12.1	3.4	5.2	1.7
	n	5	5	5	5	4	5
CA-HT	mean	7,605 [c]	4,479 [b,c]	104.2 [a]	0.088 [b]	131.1 [c]	0.096 [c]
	±	871	635	4.6	0.005	N/a	N/a
	COV [%]	11.5	14.2	4.4	5.5	N/a	N/a
	n	4	4	4	4	1	1
CA	mean	7,588 [c]	4,727 [b,c]	106.9 [a]	0.099 [b]	130.2 [c]	0.097 [b,c]
	±	489	349	8.9	0.016	8.4	0.026
	COV [%]	6.4	7.4	8.3	16.4	6.5	26.3
	n	3	3	3	3	2	2
GLU-HOM-3	n = 1	5,123	2,475	106.5	0.156	165.7	0.201
GLU-HOM-6	n = 1	6,222	3,367	96.1	0.110	168.9	0.110
GLU-HOM-12	n = 1	5,882	3,160	97.3	0.090	167.0	0.091

*COV - Coefficient of Variation (= standard deviation / mean × 100 %)

The superscripted letters in a given column denote statistically different values, as determined by LSD comparison of means.

Comparison of neat and neutralized films yields noticeable differences. One of which is an increase of E' with temperature in neat films above 170 °C, but not with neutralized films. The increase signifies chain stiffening which is limited to several variables. At 170 °C the moisture has largely been removed, so it cannot be explained as evaporation of strongly-bound water molecules. Instead, this increase could be from moisture loss from a reaction, as acetylation with acetic acid is expected to occur at elevated temperatures (> 60 °C) [192]. This has been discussed and hypothesized in the works of Toffey and coworkers [193–195]. It could also correspond to acetic acid evaporation. While acetic acid is volatile at ambient conditions and has a boiling point of 118 °C, electrostatic and hydrogen bonding with chitosan may elevate its temperature range of evaporation. In thermogravimetric analysis (TGA) scans, a mass loss step is observed between 150 and 210 °C (Section 6.3.1), which may be from acetic acid evaporation or possibly from a reaction with acetic acid with water as a leaving group. Therefore, the increase in E' from 1,500 to 2,500 MPa after 170 °C in neat films is attributed to anti-plasticization associated with acetic acid in some capacity.

An increase in E' is similarly observed in CA films from 135 to 190 °C, and again is likely associated with the presence of the acid, either by evaporation of water molecules from a reaction between citric acid and chitosan, or by degradation of citric acid. A mass loss is also observed in the TGA scan of CA films between 160 and 275 °C (Section 6.3.1). Citric acid is likely dispersed throughout the film matrix, with perhaps some aggregation into small clusters of crystals on the film exterior. It is not self-evident whether citric acid will degrade and its derivatives evaporate out, as citric acid decomposes above its melting point of 160 °C, or if the citric acid molecules remain embedded in the film. Thus, in speculating whether the cause of anti-plasticization that is reflected in E' at higher temperatures in films containing an acid (acetic, citric, or other) is by a covalent reaction, or because of the evaporation of that acid, requires further investigation.

5.3.2 General Trends of Preheated Specimens

The plots of E', E'' and tanδ for preheated neat, neutralized, CA-HT, and CA film specimens are shown in Figures 5.6 to 5.9, respectively. Each of these figures has been scaled differently to maximize curvature that may be observed for the respective film. The E'(35 °C), E'(195 °C), and tanδ peak values extracted from the plots are given in Table 5.2. A comparison of the preheated films is given in Figure 5.10; note that the scales match those in Figure 5.5 for non-preheated specimens.

The E' for preheated neat chitosan films (Figure 5.6) decreased linearly from 7,500 - 9,000 MPa at 30 °C to a local minimum between 160 - 180 °C after passing through an inflection. It then increased to 2,000 - 3,000 at 200 °C. Two peaks appeared in the corresponding E'' curve, the first at 70 - 80 °C (350 - 475 MPa), and the second at 160 - 180 °C (300 - 400 MPa). Only one peak is evident in the tanδ plot at 165 - 180 °C with a height of 0.100 - 0.175. This peak height and width variability once more demonstrate the

structural and chemical heterogeneities that may exist within a film or between independent replicate films.

For preheated neutralized films (Figure 5.7), E' decreased continuously from 8,000 - 11,000 MPa at 30 °C to 4,000 - 5,000 MPa at 200 °C. Two peaks appeared in the E'' plots, at 100 - 110 °C (325 - 450 MPa) and at 160 - 180 °C (300 - 425 MPa), while in the corresponding tanδ plots the peaks appeared less pronounced. Unlike the non-preheated neutralized films, peak 2 in the preheated films is more pronounced and also elevated above the water-induced relaxation peak. This demonstrates a kind of masking effect by water.

The E' of preheated CA-HT films (Figure 5.8) decreased continuously from 8,500 - 10,000 MPa at 30 °C to 4,500 - 5,000 MPa at 200 °C. No increase in the average E'(195 °C) value compared to non-preheated CA-HT films was observed. In the corresponding loss modulus plots, E'' decreased continuously from 425 - 500 MPa at 30 °C to 225 - 250 MPa at 200 °C but passed through several inflection points. These inflections are more evident in the corresponding tanδ curves as peaks at 110 - 120 °C (0.05 - 0.055 height) and at 160 - 170 °C (0.05 - 0.055 height). Similar qualitative and quantitative trends were observed with CA films (Figure 5.9) as with CA-HT films. The brittleness of preheated CA and CA-HT samples prevented doing many replicate runs, as the specimens would sometimes break during the measurements at elevated temperatures, hence $n = 2$ - 3. No increase in E' above 135 °C for preheated CA and CA-HT specimens was observed, in contrast to their non-preheated counterparts. This demonstrates the influence of absorbed water during film conditioning prior to DMA testing on the increase in E' above 135 °C of non-preheated films.

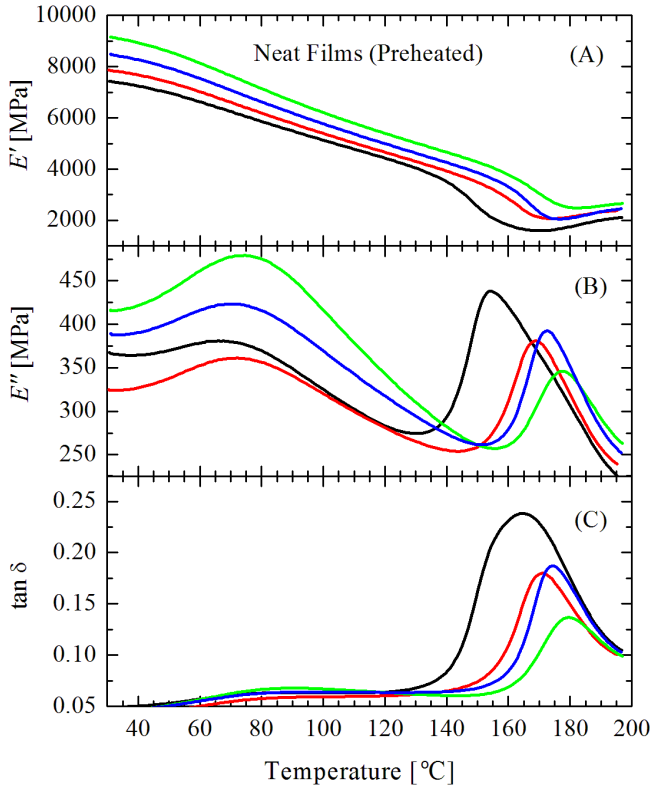

Figure 5.6: (A) E' plotted against temperature of preheated neat chitosan films (8 replicates) and (B) corresponding E'' and (C) tanδ.

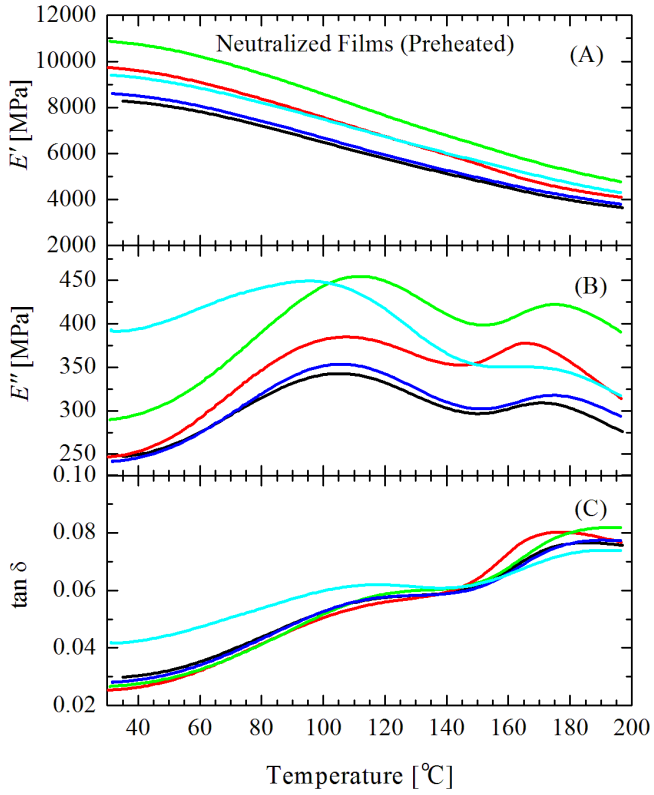

Figure 5.7: (A) E' plotted against temperature of preheated neutralized chitosan films (5 replicates) and (B) corresponding E'' and (C) tanδ.

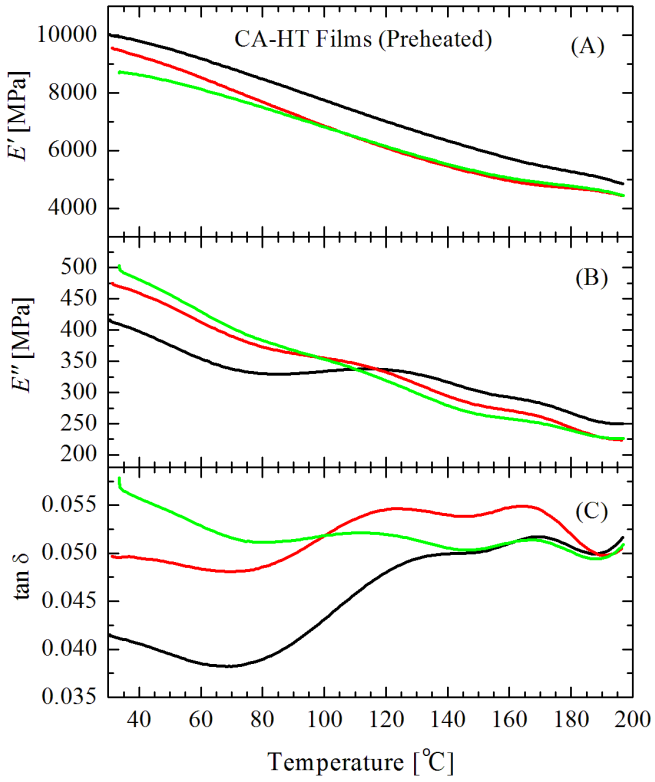

Figure 5.8: (A) E' plotted against temperature of preheated, CA-HT films (3 replicates) and (B) corresponding E'' and (C) tanδ.

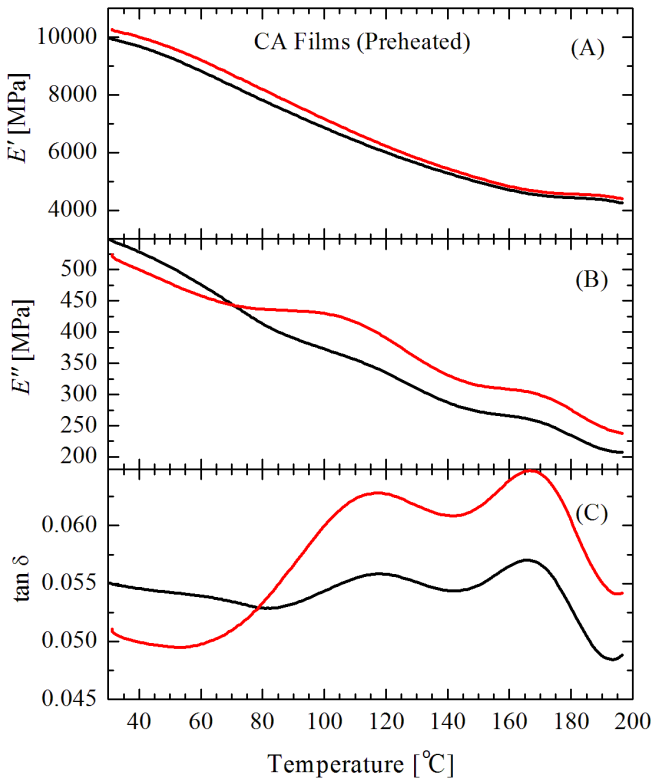

Figure 5.9: (A) E' plotted against temperature of preheated chitosan-CA films (2 replicates) and (B) corresponding E'' and (C) tanδ.

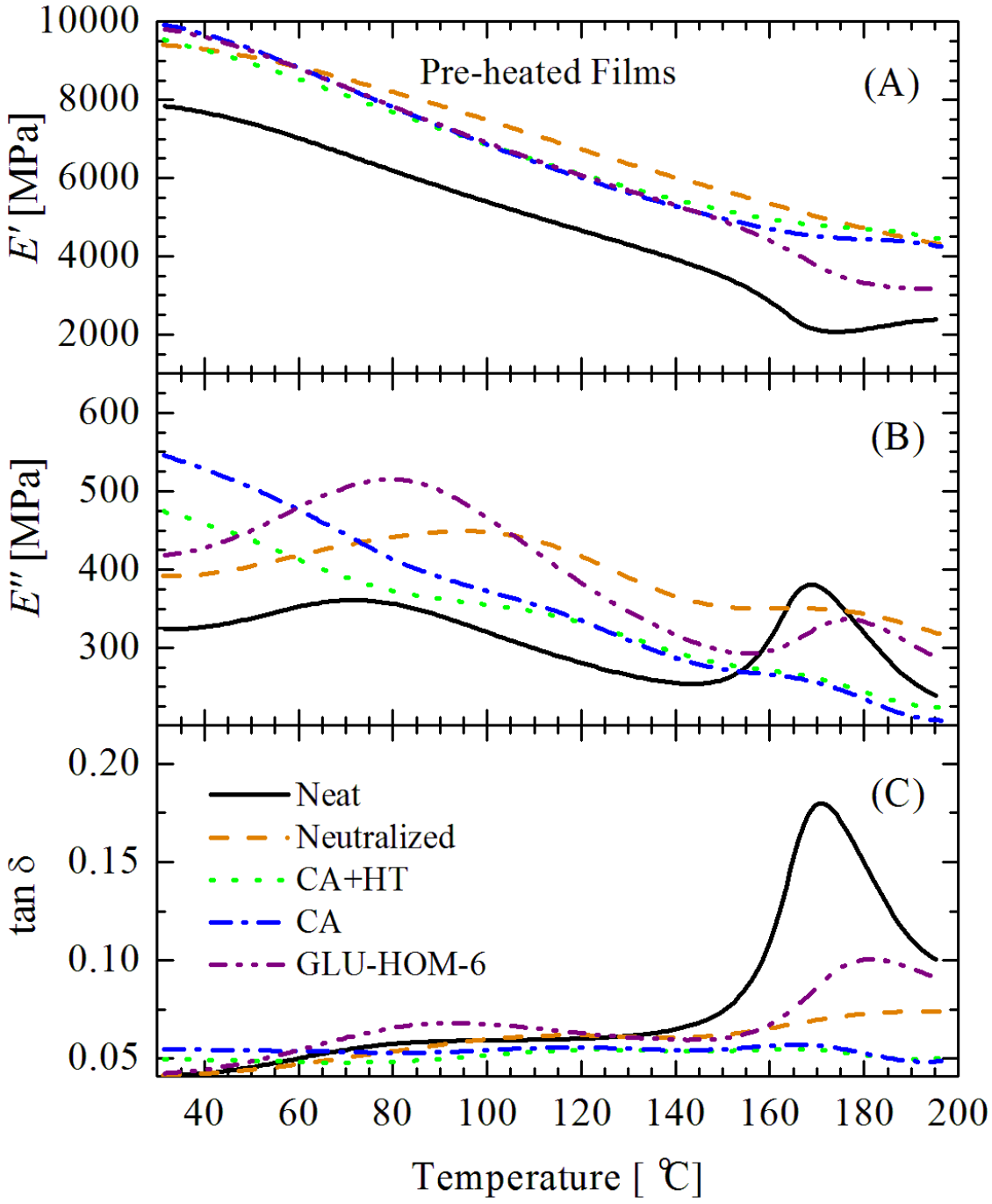

Figure 5.10: (A) E' plotted against temperature for one set of preheated films (neat, neutralized, CA, CA-HT, and GLU-HOM-6) and (B) corresponding E'' and (C) tanδ.

Table 5.2: The DMA E' and tanδ peak characteristics of preheated specimens (see Table 3.1 for film code names).

Film	Parameter	E' (35 °C) [MPa]	E' (195 °C) [MPa]	T (peak 1) [°C]	tanδ peak 1	T (peak 2) [°C]	tanδ peak 2
Neat	mean	7,826 [a]	2,289 [a]	N/a	N/a	169.3 [a]	0.213 [a]
	±	427	152	N/a	N/a	4.2	0.034
	COV* [%]	5.5	6.6	N/a	N/a	2.5	16.0
	n	4	4	0	0	4	4
Neutralized	mean	9,342 [b]	4,149 [b]	124.4 [a]	0.059 [b]	188.6 [b]	0.078 [b]
	±	1,001	445	4.1	0.002	4.9	0.003
	COV [%]	10.7	10.7	3.3	3.5	2.6	3.9
	n	5	5	5	5	5	5
CA-HT	mean	9,351 [b]	4,612 [b]	125.8 [a,b]	0.050 [b]	165.3 [a]	0.052 [c]
	±	609	244	10.0	0.004	3.2	0.004
	COV [%]	6.5	5.3	7.9	8.4	1.9	8.8
	n	3	3	3	3	3	3
CA	mean	9,982 [b]	4,348 [b]	117.8 [b]	0.059 [a,b]	166.5 [a]	0.061 [c]
	±	220	93	1.0	0.005	1.1	0.005
	COV [%]	2.2	2.1	0.8	8.3	0.7	9.0
	n	2	2	2	2	2	2
GLU-HOM-3	mean	9,119	2,749	97.3	0.060	175.3	0.167
	±	282.1	159.3	5.8	0.000	0.5	0.008
	n	2	2	2	2	2	2
GLU-HOM-6	n = 1	9,740	3,162	92.4	0.068	181.6	0.101
GLU-HOM-12	n = 1	9,412.6	3,584	77.9	0.067	191.8	0.080

*COV - Coefficient of Variation (= standard deviation / mean × 100 %)

The superscripted letters in a given column denote statistically different values, as determined by LSD comparison of means.

5.3.3 Comparison of Non-Preheated and Preheated Specimens

The effect of preheating the films at 140 °C for 10 min on viscoelastic properties, especially as the film approaches the glass transition, is now discussed. (The effect of heat treatment of CA films in the context of crosslinking is discussed in Section 5.4.1.) An example of the difference in viscoelastic response due to preheating for a neat film is given in Figure 5.11.

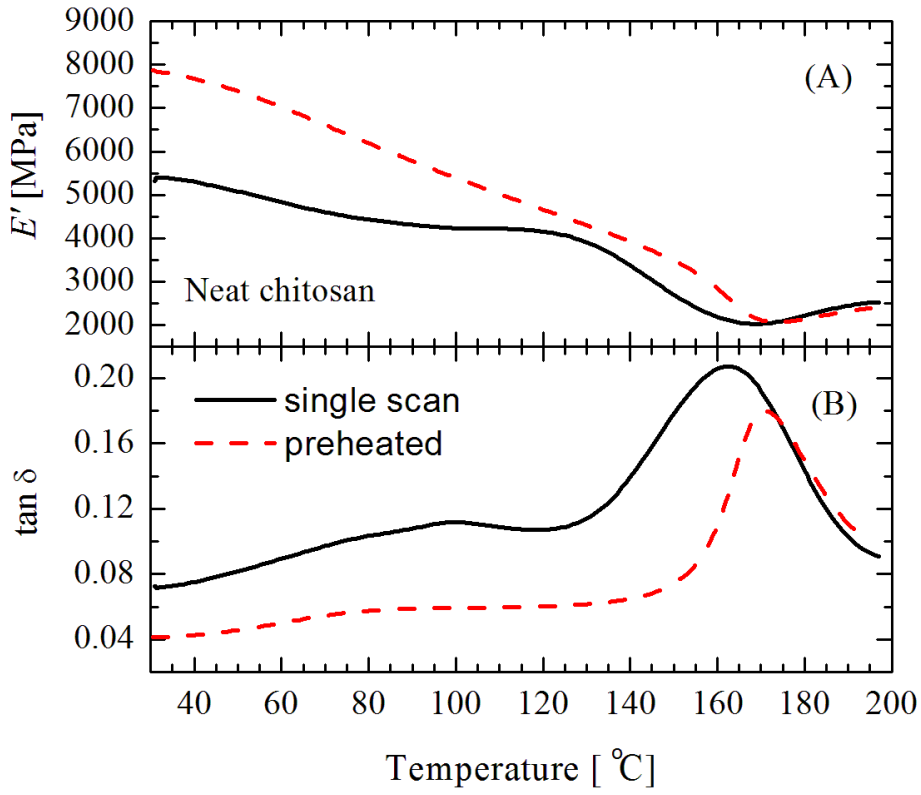

Figure 5.11: (A) E' plotted against temperature of a neat film for non-preheated (single scan) and preheated runs and (B) corresponding tanδ.

The E' values of preheated neat, neutralized, CA and CA-HT films at the onset were greater by roughly 2,000 MPa compared to non-preheated specimens (see Tables 5.1 and 5.2). The slope magnitude of $\Delta E'/\Delta T$ of preheated films was greater for the majority of the scan. Above approximately 170 °C the E' and tanδ curves of the preheated and non-preheated specimens overlapped as shown in Figure 5.11. The initial difference in E' at low temperatures followed by the overlap is due to a decreasing difference in water content with increasing temperature. This overlap at higher temperatures was observed for all film types produced here, and was also observed by Park and Ruckenstein [196] with their DMA scans of preheated and non-preheated methylcellulose films.

Supposing re-acetylation occurs to some degree by preheating neat specimens at 140 °C/10 min *via* nucleophilic attack of the amine onto the acid carbonyl group, the lack of difference in E' near 200 °C suggests that ultimately both preheated and non-preheated

specimens achieve the same final degree of deacetylation (DD) above 170 °C. Either that or differences in intramolecular and intermolecular bonding of a chitosan film with a higher DD compared to that of a lower one, is negligible at 200 °C. At ambient conditions, however, chitosan-acetate and neutralized chitosan films with a higher DD have shown increased tensile strength [9, 197, 198], and hence have higher chain stiffness. The Young's modulus, E, of dry [182] and wet chitosan films [199] were found to increase with increasing DD; E bears a closer relationship to E' than tensile strength. The dynamic shear modulus of gelatin-chitosan gels (3:1 w/w ratio) increased with increasing DD as well [200]. Therefore, any decrease in E' at 35 °C relative to a non-preheated film caused by a lower DD from re-acetylation of a heated chitosan-acetate film, is masked by a greater increase in E' from a lower moisture content. This might otherwise be observable if the preheated film is conditioned to absorb the same amount of water as a non-preheated film. In short, preheating shows little effect on E' in the approach towards the glass transition, and a non-preheated film will ultimately end up in the same chemical state as the preheated film when both are heated to the same temperature.

Preheating shifted the center of tanδ peak 2 for neat films from 164.8 ± 2.8 °C to 169.3 ± 4.2 °C (not significantly different; t-test, $\alpha = 0.05$). And while it is described as a shift because of the offset of the center, it is not a genuine shift. This is because the right sides of the peaks overlap. This demonstrates an incompleteness in the removal of, or reaction with, residual acetic acid. Preheating shifted the center of peak 2 for CA films to a higher temperature from an average of 130.2 to 166.5 °C. This demonstrates that for CA films and CA-HT films, the relaxation mechanism driving peak 2 is susceptible to plasticization effects from absorbed water. Therefore, tanδ peak 2 is affected by heat treatment, except with neutralized films where the center remains constant near 190 °C regardless of preheating.

5.3.4 Frequency Sweep

A frequency sweep was performed on non-preheated films (duplicate runs) from 0.1 to 10 Hz at 30 °C, as shown in Figure 5.12. At 1 Hz, the values of E', E'', and tanδ are within range with those from the temperature-ramp measurements at 35 °C; see Table 5.1. The lower dissipation factor of neutralized films compared to neat films over the measured frequency range show that acetic acid and water are responsible for a higher ratio of energetic losses to energy storage.

The tanδ of CA-HT specimens had a high experimental error, but nevertheless appeared stable from 1 to 10 Hz. The tanδ of CA-HT specimens cross over neat, neutralized and CA films below 0.3 Hz. Thus, the chain dynamics of CA-HT films at low frequencies show a reduced amount of frictional losses. No relaxation processes are evident at the measured temperature and frequency range, which would have been clear from a peak in the plots of E'' and tanδ against frequency.

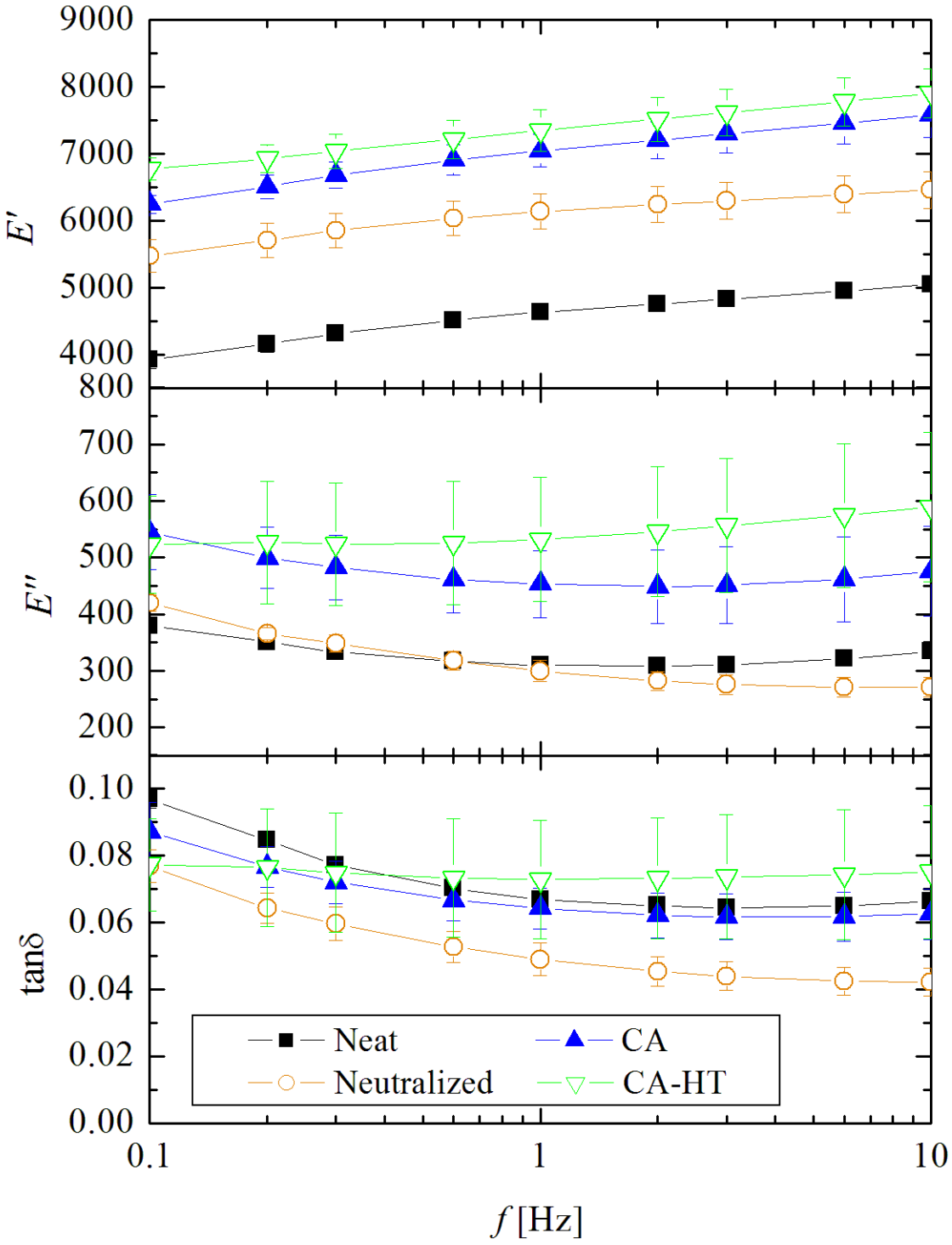

Figure 5.12: (A) E' plotted against frequency, f, (log-scale) of non-preheated neat, neutralized, CA and CA-HT films and corresponding (B) E'' and (C) tanδ. ($n = 2$ replicate runs.)

5.3.5 Homogeneously Crosslinked GLU Films

The temperature-ramp scans for non-preheated samples of films homogeneously-crosslinked with GLU are plotted in Figure 5.13, and the summarized data are given in Table 5.1. For the non-preheated specimens, the E', E'' and tanδ curves of the GLU-HOM-3 film qualitatively and quantitatively resembled that of a neat chitosan film, as if the degree of crosslinking was insufficient with a [NH_2]:[CHO] ratio of 8. Increasing GLU content from 3 to 6 % increased E' over the whole temperature range of the scan. The E' curves of the 6 and 12 % GLU samples greatly overlap, while the E'' curves are vertically displaced by roughly 77 MPa at most, indicating similar chain mobility and minor difference in crosslinking between those two samples. No replicates were performed to confirm this. Increasing GLU concentration from 3 to 12 % also decreased the tanδ peak heights of both peak 1 from 0.156 to 0.090, and peak 2 from 0.201 to 0.091.

The decrease in the magnitude of the water-induced relaxation peak of non-preheated samples with increasing GLU concentration is indicative of reduced H-bonding capacity as a result of amide or imide formation with GLU. While the magnitude of tanδ peak 2 decreased with increasing GLU content, the peak center remained nearly constant at 166 - 169 °C. The significance of this will be discussed in Section 5.4.2.

The temperature-dependent scans for preheated samples of films homogeneously-crosslinked with GLU are shown in Figure 5.14, and the data is summarized in Table 5.2. Similar qualitative shifts in E' and changes in the tanδ peaks occurred for preheated GLU-HOM films, as it did with the non-preheated forms. The magnitude of tanδ peak 2 decreased with increasing GLU content, and the peak center increased from 175 to 192 °C with 3 to 12 % GLU, respectively.

While a systematic increase in E'(195 °C) from 2,749 to 3,584 MPa with an increase in GLU concentration was observed for preheated films (but not statistically verified), this was not seen in the non-preheated GLU-HOM specimens. The lack of increase of E'(195 °C) between non-preheated GLU-HOM-6 and -12 films despite increasing aldehyde concentration may be related to the high stiffness of the polymer chain. Park et al. [196] hypothesized that the high rigidity of the polysaccharide backbone mitigates the indication of changes induced by covalent crosslinking to the net mobility of the polymer network. This is how they explained the insignificant changes to the glass transition peak in their DMA tanδ plots for methylcellulose-GLU crosslinked hydrogels, also tested under tensile mode.

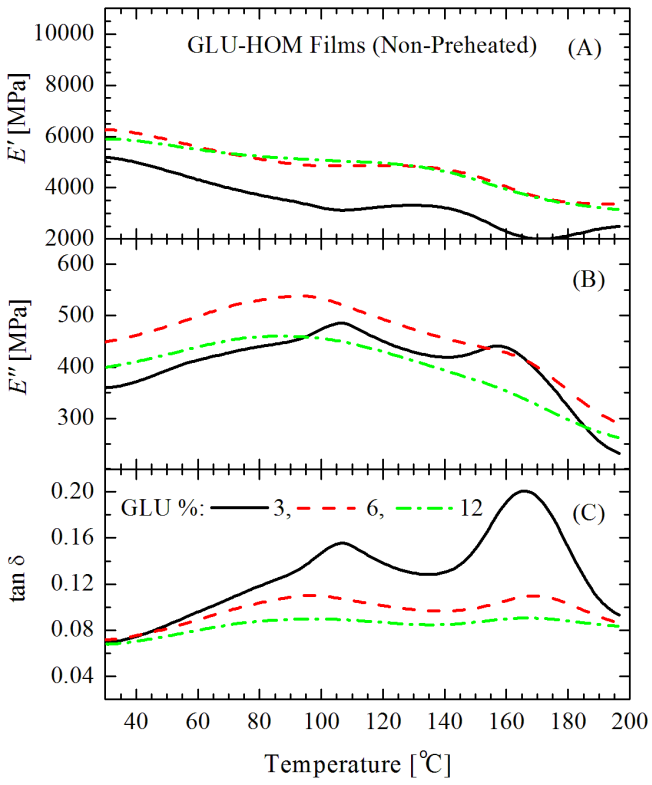

Figure 5.13: (A) E' plotted against temperature of homogeneously prepared GLU films at 3 different concentrations of GLU: 3, 6 and 12 % (wt. GLU / wt. chitosan) and (B) corresponding E'' and (C) tanδ. (no replicates)

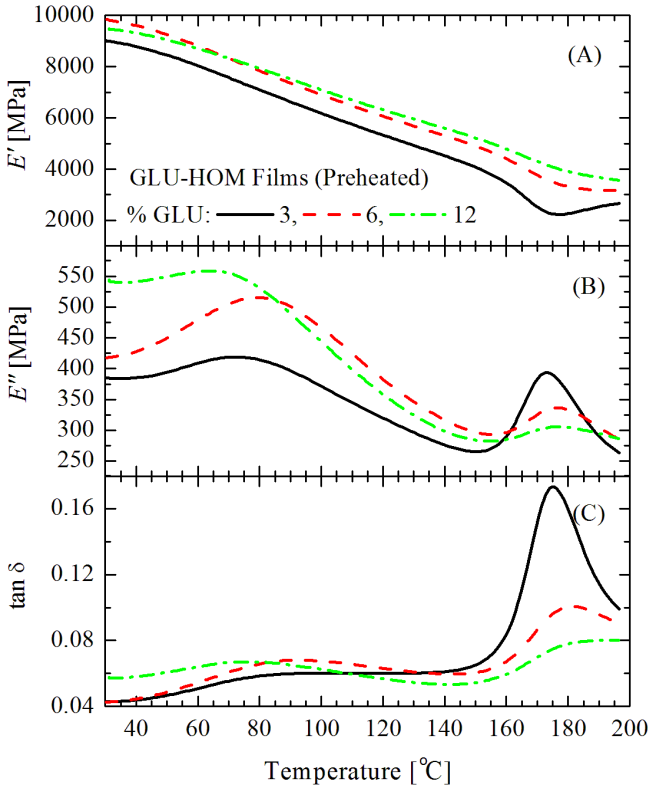

Figure 5.14: (A) E' plotted against temperature of homogeneously prepared preheated GLU films at 3 different concentrations of GLU: 3, 6 and 12 % (wt. GLU / wt. chitosan) and (B) corresponding E'' and (C) tanδ. (no replicates)

5.4 Discussion

5.4.1 Effect of Thermal Treatment on Viscoelastic Properties of Films, and Heat Treatment of CA Films

Since the films were heated by ramping in the DMA sample chamber, and CA-HT films were heated prior to DMA testing, it is important to discuss changes to the chemistry and chain structure following heat treatment and the subsequent effects on viscoelastic and mechanical properties on the chitosan films. One effect of heat treatment has been speculated to range from amidization of chitosan in films [184, 193, 194, 201] to intermolecular crosslinking of chitosan both in film [192, 201] and powder form [201, 202] between primary amines and carbonyl groups from *N*-acetyl units. Formation of these chemical bonds at elevated temperatures in the films have been deduced from infrared spectroscopy studies that reveal a decrease in protonated amine and carboxylate ion peaks [201] at approximately 1515/1615 and 1555 cm^{-1}, respectively [184], along with a simultaneous increase in the intensity of amide (-CONH-) (amide II; 1,560 cm^{-1}) [203] and amide-carbonyl (-N-C=O) (amide I; 1,650 cm^{-1}) [184, 192, 201, 203] bands.

Further evidence of amidization with the residual acid is manifested in reduced film solubility in water [203] and aqueous acid solutions [202, 203], because amine protonation is the driving mechanism of chitosan dissolution while secondary amides are unable to be protonated. Physical entanglements [192] have been proposed to explain the darkening color change when films are heated, but this seems unlikely because chain mobility is reduced with lower water content.

The effect of amidization on the mechanical properties of chitosan films is in general a decrease in tensile strength [42, 185, 197, 204] and Young's modulus [182] at ambient conditions. These references are not based on amidized chitosan films derived from thermal treatment but are instead from studies on the influence of DD on the physical properties of chitosan-acetate films. A lower DD is analogous with higher acetylation, since acetylation converts the primary amine to an amide. Zotkin et al. [201] estimated that the DD of a chitosan-acetate film can decrease by nearly 30 % (92 to 64 % DD) following heat treatment. Few papers cover the subject of mechanical properties of amidization of chitosan films by heat treatment, but one publication reported that heat treatment did not affect tensile strength of films crosslinked with (the bifunctional) adipic acid [102], likely due to the high standard deviation in their measurements.

The tensile modulus of a material is conceptually similar and analogous to viscoelastic storage modulus, and therefore information obtained from tensile measurements is extended to the discussion here. The lower tensile modulus properties expected for amidized chitosan films, extrapolated from observations for low DD chitosan films as mentioned in the preceding paragraph, are not appreciated in the DMA spectra. This is because at high temperatures, little to no difference was observed in the E' vs T curves between preheated and non-preheated neat films, as discussed in Section 5.3.3, both of

which have been amidized by 200 °C. In the neat films studied here, preheating at 140 °C for 10 min darkened the films slightly, which is a qualitative indicator of chemical reaction. By contrast, a color change of neutralized films was negligible; see Section 4.3.

Toffey and coworkers [193–195] have extensively studied the viscoelastic properties of acylated chitosan films under single cantilever bending mode. The films were acylated by formic, acetic, propionic and butyric acid by either isothermal heat treatment, or by ramp heating in the DMA. They observed a shift in their tanδ peaks to higher temperatures from approximately 60 to 150 °C with heating at progressively higher temperatures [193]. Their films, however, were cast with different conditions compared to this study: 1.4 % chitosan (w/v) in 10 % (v/v) acid solution versus 2 % chitosan in 2 % solution here. They ascribe the tanδ peak to the glass transition temperature. They also report [195] a decrease in T_g with increasing acid length, ∼180 °C for chitosan-formate to ∼160 °C for chitosan-butyrate films. The results with CA films here are in line with this trend of decreasing tanδ peak with larger sized acids, as tanδ peak 2 of CA films is near 130 °C, and citric acid is larger than butyric acid. Additionally, the time from 30 to 150 °C at 3 °C/min in the DMA scan is 40 min, so any reaction with citric acid in a CA film is likely to be at a lesser extent compared to CA-HT film heat treated at 150 °C for 30 min.

Attention is now turned to a heat-induced change in E' that signifies the chemical nature of the films. The E' increased by roughly 700 MPa in non-preheated and preheated chitosan-acetate films between 170 and 200 °C, and by roughly 500 MPa in non-preheated CA films between 145 and 185 °C. The E' did not increase between these temperatures with neutralized films. It did increase, however, with non-preheated and preheated GLU-HOM-3 films, but with none of the 6 and 12 % GLU-HOM films (Figures 5.13 and 5.14). Thus, this peculiar increase in E' is associated with the acids, as binding of acetate ions to the amines is diminished with films containing glutaraldehyde. Similar to the work here, Toffey and Glasser [193] observed an increase in E' with chitosan films at temperatures above 150 °C, which they interpret as an effect of further amidization reactions. The differential thermogravimetric analysis (DTGA) scans of neat chitosan film (Section 6.3.1 and in the literature [205, 206]) show a small shoulder peak on the low temperature side of the main decomposition peak, with an onset near 175 °C which is in a close range as the increase in E' of neat films. Differences in temperatures for the appearance of these events between the two analytical methods are probably from differences in rate of heating; 10 °C/min for TGA and <5 °C/min for DMA. Kinetically-driven phenomena are affected by the rate of temperature change (i.e. higher T_g with higher ramping rate). If this increase in E' above 150 °C is from acetylation reactions with acetic acid, as Toffey and Glasser [193] suggest, then the DTGA peak between 175 and 225 °C would be from water evaporation, because H_2O is a leaving group from the amidization reaction between an organic acid and amine (Figure 2.11). One way to verify this would be to analyze the emissions from a film under a coupled TGA-FTIR-GC apparatus, similar to the study by Corazzari et al. [207] on chitin and chitosan powder. Using TGA coupled with mass spectrometry, Quijada-Garrido et al. [205] showed that some of the emissions from a chitosan-acetate

film between approximately 175 and 225 °C include acetic acid, water, ammonia, and acetamide, amongst other compounds.

The reason for the increase in E' with increasing temperature can also be thought about in terms of the impact of chemical constituents. Since tensile modulus has been found to be higher with higher DD [182] at ambient conditions, by extrapolation E' would be expected to decrease with amidization, which contradicts the hypothesis that the increase in E' above 150 °C is a result of amidization. Additionally, it is unlikely from the scission of polymer chains, since a lower molecular weight would decrease E' [113, 160], especially at a temperature above a theoretical T_g; stress relaxation is generally independent of molecular weight [113] below T_g. Therefore, it is hypothesized that the increase in E' is more likely from chain stiffening due to acetic acid or *N*-acetyl evaporation out of the film. This can be extrapolated to CA and CA-HT films, where citric acid derivatives or *N*-citryl groups vaporize. Note that the DMA scans performed here were conducted under air atmosphere, whereas TGA was conducted under nitrogen, and the DMA scans of Toffey and coworkers [193–195] were conducted under nitrogen. However, the evaporation rate of water from chitosan films and decomposition rate of chitosan films under pure oxygen or pure nitrogen did not appear to differ much according to the TGA scans of Zawadzki and Kaczmarek [206] between 25 to 300 °C.

Crystallinity is an important factor in chain mobility, and therefore to E'. The literature on the effect of heating on the crystallinity of the chitosan films appears conflicting. Lim et al. [192] observed an increase in the 11° peak in the 2θ diffractogram, while other studies have shown a reduction of the intensity of this peak [203, 208], which corresponds to the tendon structure [51]. A decrease in the 11° peak is indicative of the diminution of hydrated crystals. In addition to changes with the tendon crystals, other studies have shown a concomitant emergence of the annealed crystals [203] at 15° [51, 52], that was previously absent until the films were thermally treated. (For powder chitosan, one study reports a transformation from the tendon to the annealed crystal structures [202].) In another study on films, no other XRD peaks emerged with heat treatment [208] indicating that films can lose their overall crystallinity [184] with heating. If the supposition of reduced crystallinity holds, the higher ratio of amorphous to crystalline regions would likely bolster the appearance of a glass transition in the films and cause it to shift to higher temperatures. A more amorphous material would also most likely yield a lower E'.

If there is such a reduction in crystallinity in preheated films or CA-HT films here, the changes in E'(195 °C) are likely negligible with respect to the error associated with experimentation, as E'(195 °C) of preheated and non-preheated specimens are not statistically different. Despite all potential changes to physico-chemical and structural properties from preheating or heat treatment that may affect viscoelastic properties, they are less likely to be detectable in the glassy state by the more pronounced effect of increased rigidity when absorbed water is evaporated out. In short, no effects from changes to crystal structure or crystallinity from heating were observed here.

To conclude, the kind of chemical, physico-chemical effects that one would expect to

be reflected in the plots of E' as a consequence of heating are regrettably insufficient to be detectable because the decrease in water content increases E' which masks effects by changes in chemistry and crystal structure.

5.4.2 Assessment of tanδ and Its Relation to Crosslinking and the Glass-Rubber Transition

In the literature, the high-temperature peak of the DMA tanδ curves of chitosan films is often attributed to the glass transition [58, 193, 209, 210], but objections and counter-arguments to this diagnosis [98, 189] have been put forward. If the tanδ peak 2 is a true expression of T_g, one would expect peak widening and a shift to higher temperatures as a consequence of crosslinking. Therefore, to evaluate the relaxation properties of the films further and to determine whether heat treatment of CA films yielded covalent crosslinking, peak deconvolution was performed on the tanδ curves to obtain an accurate peak center and to determine the full width at half maximum (FWHM) (units of temperature). (Note: Nielsen [113] points out that the tanδ maximum is close to, but is not actually the T_g point.) In fitting their DMA tanδ plots, Epure et al. [211] used a baseline of zero tanδ. Under this condition the material is considered perfectly elastic, i.e. $E'' = 0$, which is an invalid assumption for a viscoelastic material such as chitosan. Therefore, a zero baseline was not used here, but rather the minimum tanδ value of each plot was used as the baseline. Gaussian distribution of the peaks was assumed.

The tanδ peak deconvolution analysis is presented in Table 5.3. The peak 2 FWHM values of the neutralized films were higher (statistically significant) than those of the CA films for both preheated and single scans contrary to expectations of peak broadening with the addition of citric acid and the intended goal of covalent crosslinking. Furthermore, the FWHM values of CA and CA-HT films were not significantly different, which suggests that heat treatment possibly did not change all bonding between citric acid and chitosan from ionic to covalent, just as the lack of difference in E' values previously indicated in Section 5.3.1. By contrast, the peak width of preheated GLU-HOM films increased from 35 to 59 (°C) by increasing GLU concentration from 3 to 12 %, and peak 2 moved to higher temperatures, according to expectations of an increase in crosslink density.

The height of the tanδ peak 2 diminished from 0.213 ± 0.045 for neat to 0.078 ± 0.01 for neutralized films. The reason for this peak vanishing may be due to changes to the chemical nature of the films. Gartner et al. [189] speculated that the origins of this relaxation peak are from electrostatic, ionic interactions between the conjugate base of the solvating acid and the protonated amine. They compared the viscoelastic properties of neat and neutralized films made from acetic and hydrochloric acid using DMA, and a similar tanδ temperature-dependence of their chitosan acetate film was found with this study. Their ^{15}N CP-MAS NMR scans [189] provide supporting evidence for the electrostatic interactions by showing shifts in the peak correlated with the amine group of the HCl-prepared neutralized film to a position approximately that observed for the unprotonated chitosan powder, thus

Table 5.3: Peak deconvolution, fitting data for tanδ peak 2

Film Type	Preheat	Parameter	Baseline	Center [°C]	FWHM	Height
Neat	N	mean	0.068	166.0	36.5	0.130
		±	0.005	2.9	2.6	0.034
Neat	Y	mean	0.052	177.2	29.9	0.116
		±	0.008	6.5	4.4	0.047
Neutralized	N	mean	0.057	188.8	105.5	0.021
		±	0.002	12.2	29.1	0.002
Neutralized	Y	mean	0.029	188.5	67.9	0.048
		±	0.006	3.4	4.8	0.008
CA-HT	N	mean	0.046	137.6	56.8	0.013
		±	0.002	5.7	3.4	0.002
CA-HT	Y	mean	0.045	168.3	32.2	0.006
		±	0.006	4.1	7.6	0.004
CA	N	mean	0.046	146.2	44.7	0.024
		±	0.004	2.0	5.5	0.004
CA	Y	mean	0.045	173.3	44.1	0.012
		±	0.005	13.3	27.8	0.008

suggesting the conversion from -NH_3^+ back to -NH_2 [189] following treatment with NaOH. Thus, the reduction of the tanδ relaxation peak for neutralized chitosan films observed in this study makes this hypothesis plausible, and less likely to be the T_g.

Preheating the film prior to DMA analysis did not significantly change the tanδ peak 2 height or position for neat and neutralized films, as shown in Table 5.3. By contrast, Sakurai et al. [98] found that preheating their chitosan films at 180 °C caused the DMA tanδ peak at 150 °C (from non-preheated scans) to subside, and instead a new peak emerged at 205 °C which they speculated was closer to the true T_g, and thus argued that the peak at 150 °C was from a pseudo-stable state of the polymer chains. The removal of plasticization effects from water would increase T_g, but as this was not observed here for T (peak 2) of neat and neutralized films, this casts further doubt on the plausibility that peak 2 is the glass transition. Moreover, with preheating of neutralized specimens, peak 2 became more observable, indicating a partial masking effect caused by absorbed water and the water-induced relaxation peak.

Furthermore, the manner in which tanδ peak 2 of non-preheated GLU-HOM films changes with increasing GLU concentration, and therefore crosslinking density, is not conducive to typical changes observed with the long-range structural reordering of a polymer, as measured in dynamic mode. Instead of shifting to higher temperatures, the GLU-HOM tanδ peak 2 depresses with its center remaining constant. An illustration is given below in Figure 5.15 of the GLU-HOM tanδ peak 2 change with GLU concentration, and an example of an expected change in glass transition relaxation peak broadening with

increasing molecular weight between crosslinks $\overline{M_c}$.

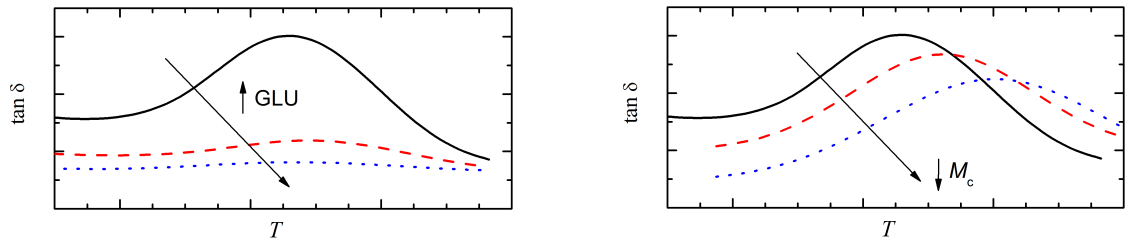

Figure 5.15: (A) GLU-HOM tanδ peak 2 and (B) sample illustration of the expected change in glass transition relaxation peak broadening with increasing molecular weight between crosslinks $\overline{M_c}$.

To further elucidate the nature of the tanδ peak 2, a film containing 15 % citric acid (w/w chitosan) was prepared in a manner congruent with homogeneously crosslinked films, by adding the citric acid to the 2 % acetic acid filmogenic solution. The DMA scan of this film is plotted in Figure 5.16. The similarity of the tanδ curves of the homogeneously (neat + 15 % citric acid) and heterogeneously prepared CA films sufficiently demonstrated that the shift of the peak 2 center from 167 to 142 °C by the incorporation of citric acid was independent of the film preparation method, as shown in Figure 5.16. This further supports the notion that the high-temperature peak is possibly from ionic effects, as citric acid will be in its conjugate form when it is directly included in the film-forming solution. Toffey and Glasser [195] demonstrated that the center of the high-temperature tanδ peak of chitosan-acylated films decreases to lower temperatures with increasing length of the monofunctional organic acid reacted with chitosan. These results are relevant here because the tanδ peak 2 of CA films here is situated at a lower temperature (130 °C) compared to neat films (165 °C) (see Table 5.1 and Figure 5.5), which supports the observations of Toffey and Glasser [195].

Despite this, while the tanδ peak 2 has been confirmed not to be analogous to a glass-transition that one would observe in calorimetric measurements, it may still be referred to as a type of glass transition. This is because the tanδ peak reveals structural relaxation, a dynamic, kinetic unfreezing at that time-scale within the temperature and frequency range of measurement. At the peak center, the structural relaxation time, τ ($=1/2\pi f$), is approximately 0.16 s, where f is frequency (1 Hz).

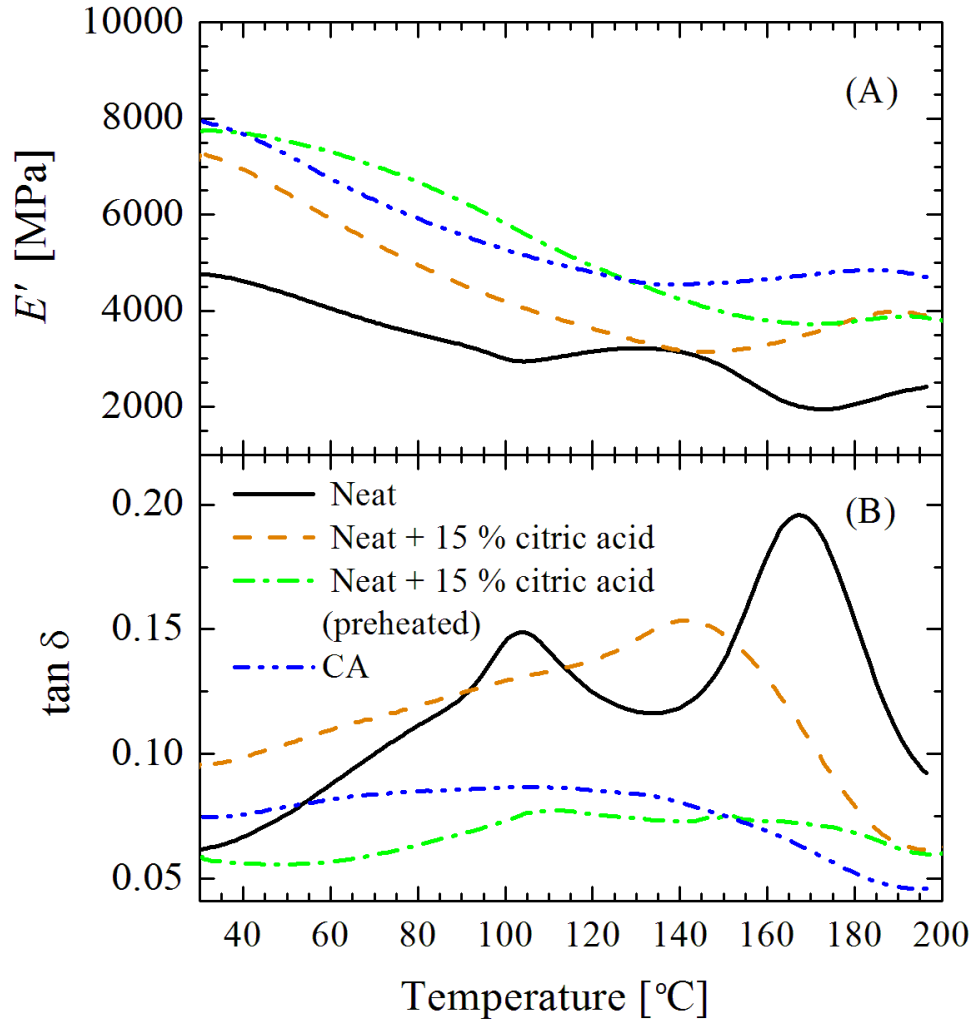

Figure 5.16: (A) E' plotted against temperature of neat film, and films containing 15 % citric acid, and CA film preheated runs and (B) corresponding tanδ.

5.4.3 Comparison of Homogeneous and Heterogeneous Crosslinking

In addition to HOM-GLU, heterogeneously prepared GLU films were also investigated. (DMA studies of heterogeneously crosslinked chitosan-glutaraldehyde films are seldom reported but are still available in the literature [95].) Figure 5.17 shows the DMA scans of GLU-HET-6 and GLU-HET-12 films. For these specimens, the maximum temperature of the scan was increased from 200 to 220 °C to test the temperature-DMA limits of the chitosan films. Despite being more brittle, the E' values of the GLU-HET crosslinked films were less than both the homogeneously prepared GLU and neutralized films within the majority of the temperature range recorded, as shown in Figure 5.17. This would suggest that producing films heterogeneously might have cleaved the polymer chains while

simultaneously crosslinking them, mostly at the exterior [9]. New bonds formed with glutaraldehyde may either be imines, or a combination of imine and Michael-type adducts, for heterogeneous *vs* homogeneous crosslinking, respectively [9]. The difference in bond formation and a majority of crosslinking at the exterior of the film might account for the extra brittleness exhibited by GLU-HET films.

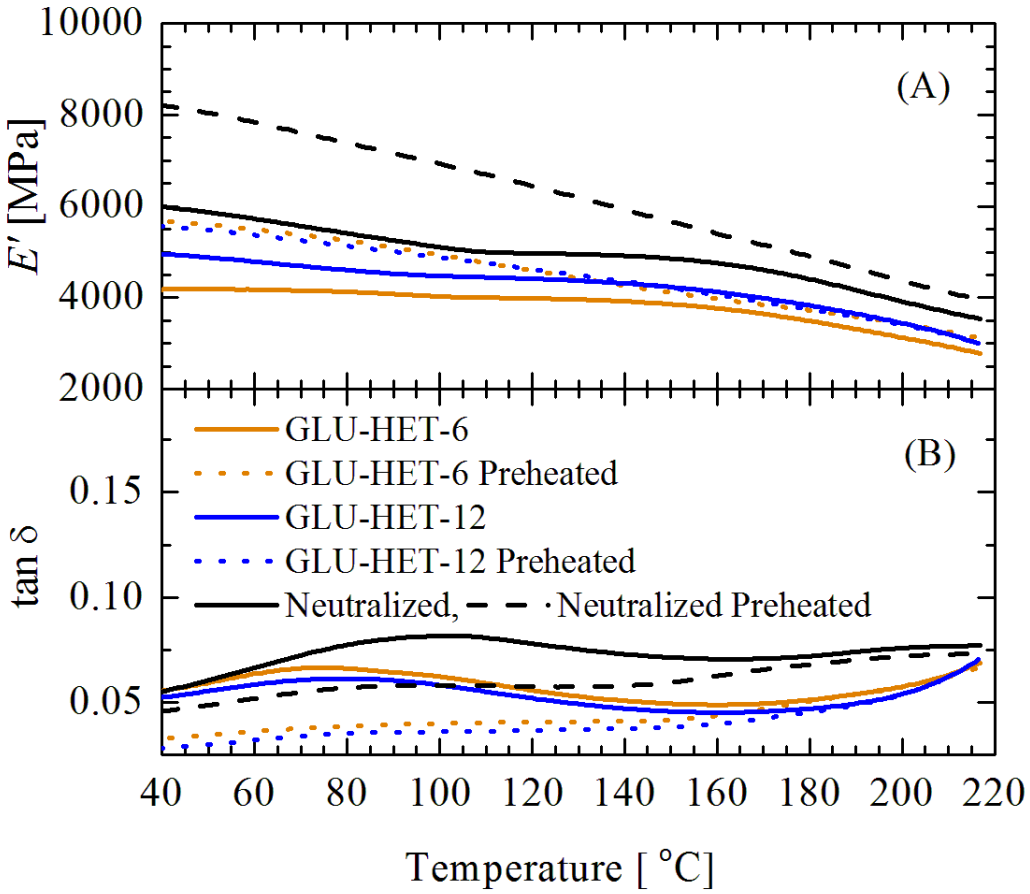

Figure 5.17: (A) E' plotted against temperature of GLU-HET and neutralized films and (B) corresponding tanδ.

The tanδ peak 2 was not visible for the GLU-HET films, but rather a new, broad peak with an onset near 170 °C began to emerge, whose center was out of the measured temperature range. This peak could be more representative of a glass-rubber transition which is speculated to exist within the degradation range, or at least some other relaxation process. The degradation of neutralized chitosan films typically begins near 200 °C and reaches a maximum degradation rate near 275 °C [212]. (For neutralized films, only a 2 % mass loss was found between 200 and 250 °C and the DTGA peak was at 314 °C.) It cannot be ruled out that the GLU-HET peak onset at 170 °C could be due to an earlier onset of degradation, as crosslinking with GLU [95] has been found to do. However, in the case of heterogeneously crosslinked chitosan membranes formed by electrospinning,

thermogravimetric analysis scans by Correia et al. [213] did not demonstrate differences between neutralized chitosan films and ethanol neutralized-heterogeneously crosslinked GLU membranes, showing that heterogeneous crosslinking with GLU does not necessarily lower the decomposition onset temperature.

5.4.4 Plasticized Films

In an attempt to shift the glass transition to a temperature lower than the degradation point, neutralized films were plasticized with glycerol. To achieve this, neutralized films were immersed in a 10 % (v/v) glycerol aqueous solution for 24 h. The weight gain of the film after drying in the environmental chamber was 27 %. The plasticized-neutralized film was then tested in the DMA by ramp heating as per the conditions outlined in Section 3.3.3. The DMA plot of this film is shown in Figure 5.18. The plot for a neat film is given in the figure for comparison.

For the neutralized film containing glycerol, a large and broad peak appears in the tanδ plot with a center near 182 °C and height of 0.20. The hysteresis of this peak was checked by preheating the film at 180 °C, and then subsequently scanned. The peak shifted to 212 °C and the height decreased to 0.13. Glycerol evaporation induced these changes. Although the boiling point of pure glycerol is 290 °C, the onset of its evaporation (according to TGA scans under nitrogen at 10 °C/min) is approximately 130 °C and loses approximately 20 % by 200 °C [214]. Therefore, a non-reversible liquid-induced relaxation is brought about from the evaporation of the plasticizing component from the film, as previously observed with water or acetic acid. In short, plasticization by glycerol is insufficient for observing the T_g. Instead, a higher molecular weight plasticizer with a higher evaporation point such as polyethylene glycol (PEG) may be more effective. The issue with using PEG, however, is that due to its size it may create phase boundaries which would also have to be investigated by other means, such as scanning electron microscopy.

5.5 Conclusion

The main conclusion from the viscoelastic study of chitosan films was that the E' and tanδ curves of CA and heat treated CA films (CA-HT) were not statistically different to state with confidence that heat treatment yielded covalent crosslinking of chitosan chains by citric acid. This does not rule out the possibility of covalent crosslinking entirely, but that DMA was unable to verify it. At high temperatures, E' was also not significantly different between CA, CA-HT and neutralized films which further added to the reasons for not assuming covalent crosslinking, even if citric acid covalently reacted to chitosan to some extent.

One important finding from this work is the additional support for rejecting the idea that the tanδ peak of 165 °C is the glass transition of chitosan-acetate films. This

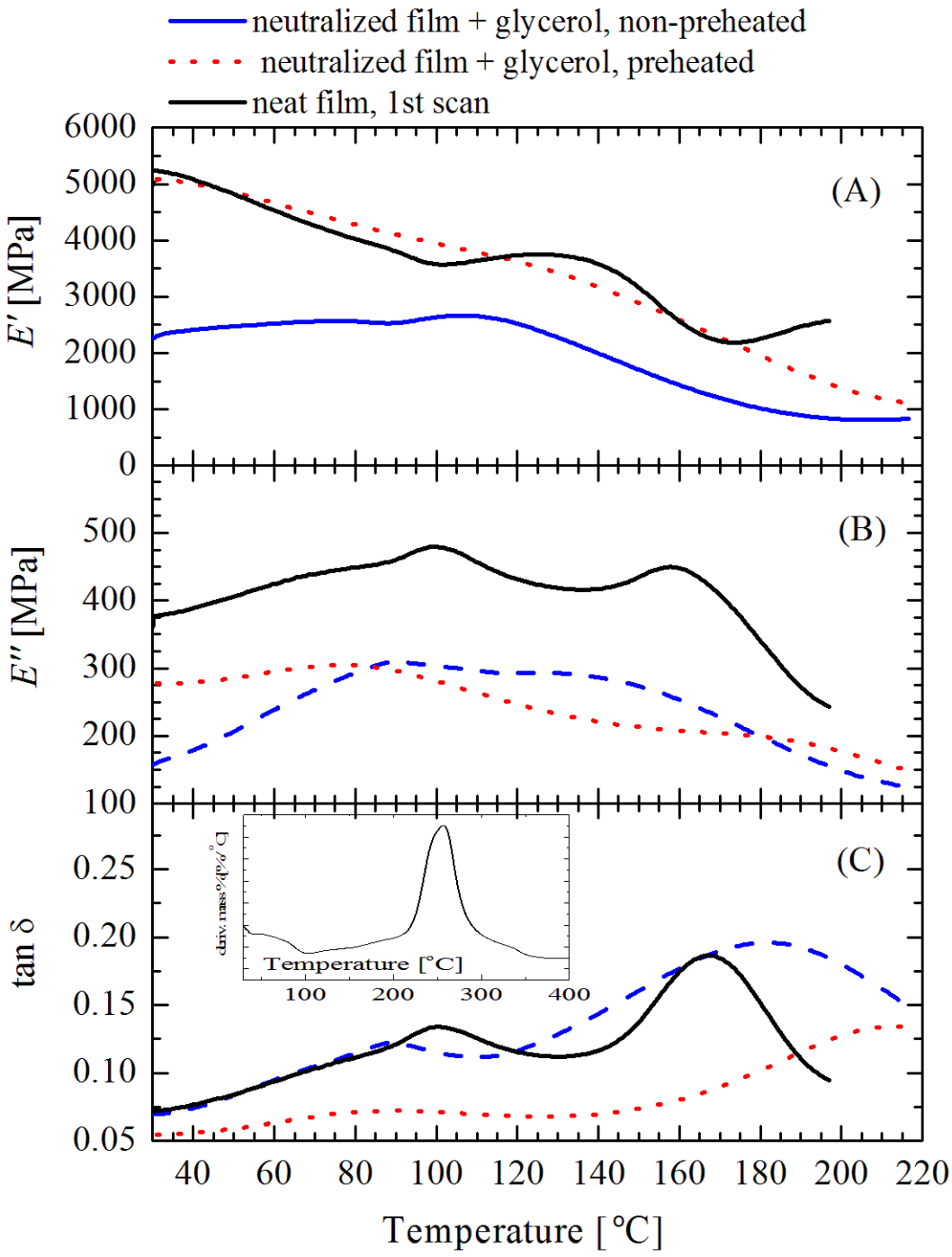

Figure 5.18: (A) E' plotted against temperature of neutralized film plasticized with glycerol and corresponding (B) E'' and (C) tanδ. The inset figure is the DTGA scan of the neutralized-plasticized film under nitrogen at 10 °C/min.

was demonstrated in several ways. The first was the disappearance of this peak with neutralization. The second was a re-emergence of this peak in the heterogeneously crosslinked CA films, both heat treated and non-heat treated, albeit at a lower temperature (130 °C). When the CA and CA-HT films were preheated the peak increased to 165 °C. The peak also shifted down from 165 °C for a neat film to 140 °C for a homogeneously crosslinked CA film, which contained 15 % (w/w) citric acid along with the 2 % (v/v) acetic acid. This showed a kind of plasticization effect by citric acid. In short, the tanδ that proceeds the water-induced relaxation peak is likely from ionic interactions between the acid and chitosan amine.

The study of films crosslinked with GLU-films also contributed to the understanding of the underlying phenomena of the structural relaxation near 165 °C. When the concentration of GLU was increased from 3 to 12 %, although the E' increased as expected for crosslinking, the tanδ peak 2 diminished. And while an upward shift, width broadening, and decrease in the tanδ peak height was expected with an increase in crosslinking degree, the extent of decrease in peak height was too great to be indicative of T_{g}. Therefore the changes to tanδ of crosslinked chitosan-GLU films was not conflated with changes to the glass transition because the imine bonds formed with GLU prevent ionic bonding with acetate ions, which would depress the tanδ associated with electrostatic interaction.

While elements of the viscoelastic study presented here have previously been reported in some capacity in the literature, this is the first time that they are presented in a combined and comprehensive manner. This includes the viscoelastic properties of chitosan films crosslinked with GLU, and heterogeneously crosslinked films.

For future considerations, the glass transition of chitosan films can be probed using the film preparation method of heterogeneous crosslinking. If the T_{g} is in the degradation range, it can be brought to lower temperatures by plasticization. A polyol plasticizer such as glycerol, however, has shown to be insufficient for this methodology since it is prone to evaporation. A higher molecular weight plasticizer, such as polyethylene glycol, may prove to be more useful.

Chapter 6

Mechanical and Moisture Barrier Properties of Ionically Crosslinked Films

6.1 Introduction

Mechanical and water vapor permeability (WVP) properties are essential for the characterization of packaging materials, and were studied here. The crystal structures of the films were analyzed with x-ray diffraction (XRD) to relate changes in the WVP and tensile strength (TS) with crystallinity after neutralization and citric acid absorption. Contact angle with water and hexadecane, as well as moisture sorption isotherms, were observed to further probe the hydrophilic nature of the films. Thermal stability and water content were assessed with thermogravimetric analysis (TGA).

Since the conclusion from the viscoelastic study in Chapter 5 was that covalent crosslinking between citric acid and chitosan could not be confirmed, the heterogeneously prepared films with citric acid (denoted as CA films) were not heat treated for any of the characterization experiments described in this chapter. This is the first characterization study of chitosan films ionically crosslinked with citric acid as prepared with the heterogeneous method, to the best of the author's knowledge. A portion of the work presented in this chapter has been submitted as an article to the *Journal of Applied Polymer Science*.

6.2 Experimental

Film formation methodologies are given in Section 3.2.2, and methodologies for WVP, tensile testing, TGA, XRD, contact angle, and moisture sorption measurements are outlined in Sections 3.4 to 3.9. The film types characterized were: neat, neutralized, and CA films. Films crosslinked with glutaraldehyde were not considered for this portion

of the study. The CA films were ionically crosslinked with 15 % (w/w) citric acid, and were not heat treated. For TGA tests, chitosan-citrate films were also analyzed, prepared as described in Section 3.2.2.

6.3 Results

6.3.1 Thermogravimetric Analysis

The TGA and derivative plots (DTGA) of neat, neutralized, and CA films, as well as powder chitosan, are shown in Figures 6.1A - 6.1C. The thermal profile of a chitosan-citrate film was also studied to compare with a CA film, shown in Figure 6.1D. The mass % plots of neat, neutralized, and CA films and chitosan powder exhibited two relative mass loss stages. Dehydration ranged between approximately 25 and 175 °C with losses of 14.0 % for neat films and 11.8 % for neutralized and CA films. Decomposition was more rapid, between approximately 225 and 375 °C, with losses of 35.6 % for neat film, 37.3 % for neutralized film, and 34.4 % for CA film. Their corresponding DTGA curves showed water evaporation from the films up to approximately 175 °C, and chitosan decomposition commenced around 250 °C.

The temperature of the maximum rate of degradation, $T_{\mathrm{d,p}}$, increased from 298 to 313 to 320 °C, for neat to neutralized to CA films, respectively. This demonstrated that heterogeneous crosslinking of chitosan films with citric acid can elevate decomposition temperature, and hence improve thermal stability. The temperatures associated with these events are listed in Table 6.1, including the mass loss values at specific temperatures. Additionally, the residual char mass at 425 °C was 38 % for powder, 42 % for the neat film, and 46 % for both neutralized and CA films.

Secondary mass loss events were observed with neat and CA films between approximately 175 to 275 °C, with losses of 5.2 and 6.8 % during these steps. For neat films, the center of this peak was masked by the onset of degradation. This peak was evidently affiliated with residual acid in neat films, due to its absence in the scans of chitosan powder and neutralized films. The peak diminished with film aging as acetic acid evaporates out of the film; see Appendix A.2. The peak re-emerged in CA films, and appeared to be comprised of two relatively small, overlapping peaks. The origin of these peaks may be from the evaporation of acetic acid or citric acid derivatives, as citric acid decomposes above 160 °C. It may also be evaporation of water molecules as a product of acylation between chitosan amine and acid carboxylate groups, as speculated by Toffey et al. [193, 194]. Acetylation reactions, however, might occur at lower temperatures [205], between 80 to 100 °C.

Another possibility may be the decomposition of side groups, namely *N*-acetyl or amine side groups in the form of acetamide or ammonia, respectively. Coupled scans of TGA and mass spectroscopy on a chitosan-acetate film by Quijada-Garrido et al. [205] detected

ammonia, acetic acid, water, and acetamide in the gas effluent between 125 to 225 °C. By comparison, DTGA scans of α-chitin show two decomposition stages [215, 216] overlapping each other from 200 to 400 °C. A coupled TGA-mass spectroscopy study [215] attributes the low temperature decomposition from 220 to 260 °C of α-chitin to acetamide removal. Chitin has an excess of *N*-acetyl groups compared with chitosan. Therefore, the mass loss from chitosan neat films on the low temperature side of the main pyrolysis DTGA peak could be due mainly to the scission of newly formed *N*-acetyl groups by consequence of heating, in addition to acetic acid and water evaporation. Since acetic acid is not present in neutralized films, new *N*-acetyl groups cannot be formed. This also demonstrates that citric acid likely reacts to some extent with chitosan in the CA film when heated to 175 °C. The mass loss from CA films from 175 to 275 °C is then possibly from the evaporation of a combination of *N*-citryl (citramide) groups, citrate derivatives, NH_3, and water.

Chitosan-citrate film had a more unique thermal profile than the other films, and is similar to that reported by Libio et al. [217]. Three stages of decline were observed from 25 to 175 °C, 175 - 300 °C, and above 300 °C. Part way through water evaporation, a series of peaks appeared merging together in the DTGA plot between 175 and 250 °C. A final peak appears at 370 °C. One hypothesis is that following the degradation of citric acid, the decomposition by-products catalyze the scission of chitosan chains, lowering its decomposition point. The DTGA peak at 370 °C could be from secondary decomposition reactions. The thermal behavior of the chitosan-citrate film compared with the CA film in that the 15 % of citric acid present in the heterogeneously crosslinked film did not lower $T_{\mathrm{d,p}}$, but rather increased it.

Table 6.1: Mass loss from TGA scans and corresponding peak centers from DTGA plots.

Film Type	T [°C] (DTGA peaks)				mass loss [%]					
	$T_{\mathrm{w,p}}$	$T_{\mathrm{w,f}}$	$T_{\mathrm{d,i}}$	$T_{\mathrm{d,p}}$	100 °C	150 °C	175 °C	200 °C	$T_{\mathrm{d,p}}$	425 °C
Neat	81.7	168.0	174.0	297.0	9.0	13.1	14.0	15.0	34.0	58.0
Neutralized	86.6	195.4	195.1	313.9	6.8	10.8	11.8	12.2	26.5	54.0
CA	85.0	184.0	264.0	320.0	6.1	11.4	11.9	13.1	34.0	54.0
Chitosan-citrate	125.5	N/a	(multiple)		1.6	5.8	10.0	18.1	N/a	60.5
Chitosan powder	53.8	135.7	200.0	289.5	8.4	9.1	9.3	9.4	28.6	60.0

Subscripts 'w' for water evaporation, 'd' for decomposition, 'i' for peak onset, 'f' for peak end point, and 'p' for peak center. Number of runs, $n = 1$ for all films.

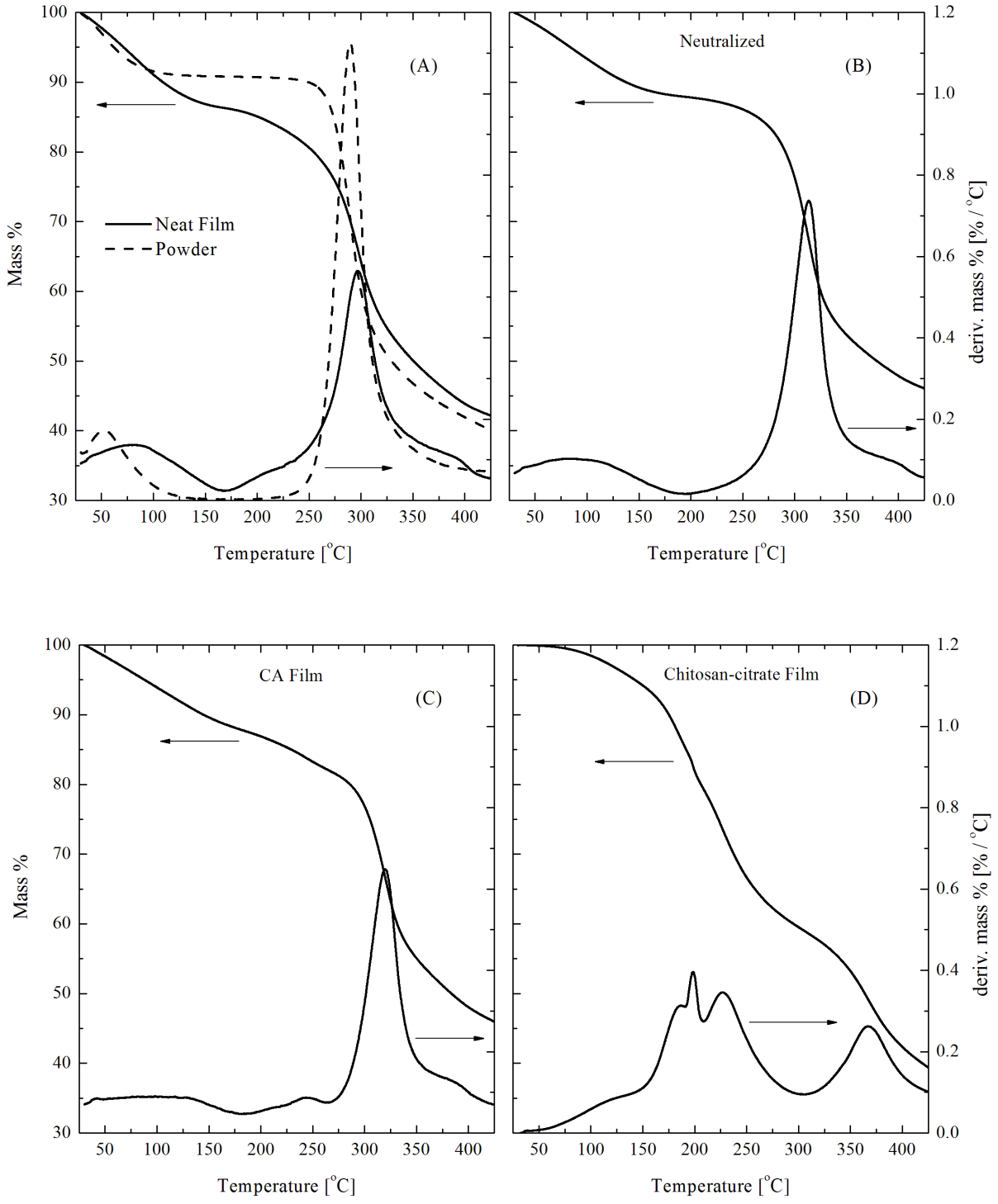

Figure 6.1: Mass percentage (left y-axis) and corresponding first-derivative (right y-axis) plotted against temperature for (A) neat film and chitosan powder, (B) neutralized, (C) CA and (D) chitosan-citrate films, heated at 10 °C/min under N_2.

6.3.2 Water Vapor Permeability

The WVP values of individual specimens and their corresponding specimen thickness values are given in Table 6.2. The plots of mass change from moisture transfer for the estimation of water vapor transmission rate (WVTR) are in Appendix A.4. The average WVP values of each film type are shown in Figure 6.2. The WVP increased from 5.06 $\pm$ 0.52 $\times$ 10^{-11} g/(m·s·Pa) for neat to 10.70 $\pm$ 1.34 $\times$ 10^{-11} g/(m·s·Pa) to neutralized films, and decreased to 7.38 $\pm$ 1.00 $\times$ 10^{-11} g/(m·s·Pa) with ionic crosslinking with citric acid. The WVP values are within range typical for chitosan/polysaccharide films [29, 218, 219], while the coefficient of variation (COV) values are slightly higher (10 - 13 % here versus literature [7, 218]). The difference of means was significant (Fisher's LSD test, $\alpha = 0.10$). An increase in WVP of chitosan films after neutralization has been reported by other studies, irrespective of neutralization method, either similar with the one used here [187, 220], or by spraying the film with NaOH [181].

Film thickness is an important factor to consider since it affects the WVP of hydrophilic materials (i.e. polysaccharides). While the WVP of hydrophobic thermoplastics are ideally independent of membrane thickness, the WVP of polysaccharide films typically have a linear, positive correlation with film thickness [166, 221]. This can be observed in Table 6.2, where the WVP values are arranged by increasing film thickness. A random block analysis ($\alpha = 0.05$) was performed to block thickness when comparing the means. The difference between means was significant, i.e. variations in thickness did not skew the comparison. The process of drying a wet neutralized film (Section 3.2.2) leads to neutralized films with a thickness on average 13 % less compared to the film prior to neutralization. In this case, however, if the thickness of neutralized films matched that of neat films, their WVP values would likely exceed 10.70 $\times$ 10^{-11} g/(m·s·Pa). Therefore, differences in the average thickness values of WVP specimens due to procedural differences of neat, neutralized and CA films did not influence the relative trends in WVP between the different film types. For additional observations on the effect of thickness on WVP (wider range), see Appendix A.4.

The WVP could be influenced by surface roughness of the films, as the surface characteristics depend on the drying conditions and casting tray material. Here, the air - exposed side of the films has a rougher contour than the one from the film - glass tray interface. Therefore, the orientation of the film specimen in the WVP test jar could skew the permeability measurement. However, no significant bias in WVP was found when this was tested; see Appendix A.4.

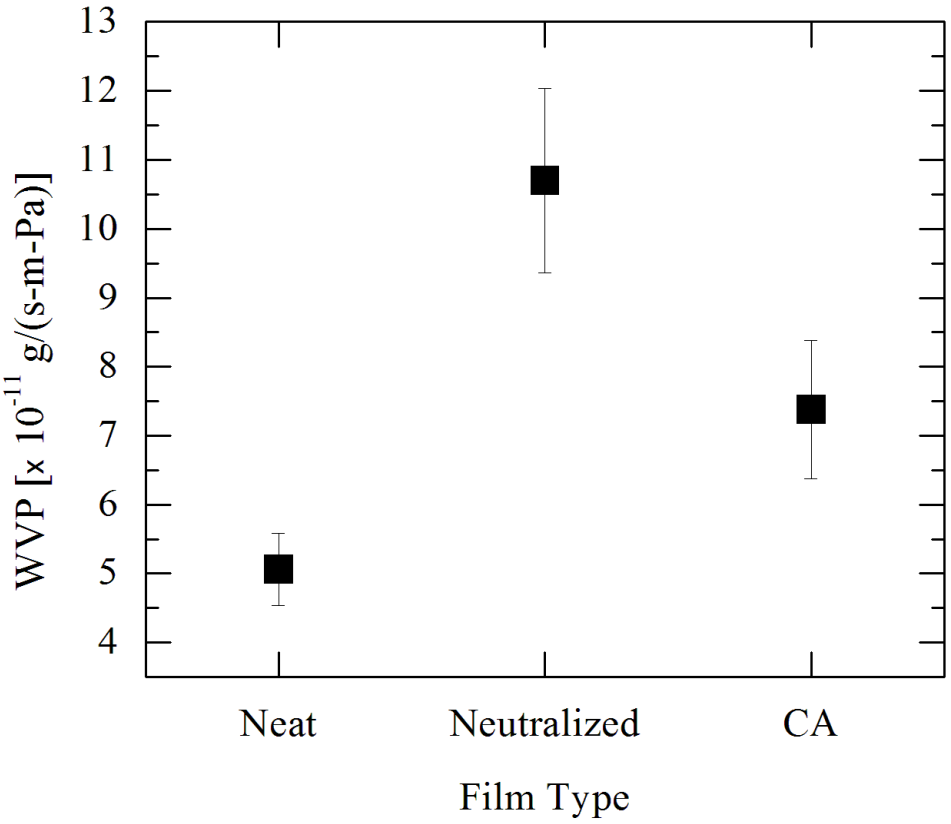

Figure 6.2: The average WVP values for each of the three types of film ($n = 6$, per film).

Table 6.2: WVP for neat, neutralized and CA films, with average specimen thickness, l.

Film Type	Sample	l [μm]	WVP $\times 10^{-11}$ [g/(s·m·Pa)]	Sample	l [μm]	WVP $\times 10^{-11}$ [g/(s·m·Pa)]
Neat	A1	75 ± 3	4.45	B1	91 ± 5	5.24
	A2	84 ± 7	4.68	B2	91 ± 11	5.26
	A3	94 ± 13	4.83	B3	100 ± 13	5.91
Neutralized	A1	66 ± 4	8.71	B1	70 ± 6	11.04
	A2	70 ± 1	9.92	B2	81 ± 9	11.87
	A3	88 ± 8	10.4	B3	98 ± 6	12.40
CA	A1	72 ± 19	6.47	B1	78 ± 11	6.80
	A2	84 ± 7	6.51	B2	91 ± 13	6.92
	A3	134 ± 14	8.72	B3	101 ± 19	8.35

'A' and 'B' denote bulk films. Data arranged by increasing specimen thickness per bulk film.

Another potential source of error could be stagnant air between the film surface and desiccant on the inside of the test cup, which can result in an underestimation of WVP. The stagnation causes resistance to moisture transport between the film and desiccant. This is more concerning for highly hydrophilic materials, such as polysaccharides and protein films, where permeability can be underestimated by as much as 65 % [168] when stagnation is unaccounted for. Two methods were used to estimate the effect of stagnant air, from ASTM E96 (Method 1) and by Krochta [222] and Gennadios et al. [168] (Method 2), which are outlined in Appendix A.4. The difference between the measured and corrected WVP values using Methods 1 and 2 are provided in Table 6.3.

Table 6.3: The percentage difference between measured, WVP_{mea}, and corrected, WVP_{cor}, permeability for still air resistance using ASTM E96 (Method 1) and literature methods [168, 222] (Method 2). The corresponding experimental COV of WVP is provided for comparison.

Film Type	ΔWVP (WVP_{cor} - WVP_{mea}) [%]		COV (WVP_{mea}) [%]
	Method 1	Method 2	
Neat	4.0 - 4.3	1.7 - 1.9	10.5
Neutralized	9.0 - 12.3	3.8 - 5.0	12.5
CA	4.7 - 6.7	2.1 - 2.9	13.6

$$\Delta WVP = (WVP_{cor} - WVP_{mea}) / WVP_{mea} \times 100\ \%$$

The effects of stagnant air are relatively small, at most 7 % for both CA and neat films, and 12 % for neutralized films, according to Method 1. The small difference between experimental and corrected values may be due to test conditions such as low difference in RH and small gap between film and desiccant (6 mm), as well as the notion that the theory was developed for the water test method but still applied to the desiccant method. Additionally, air circulation in the environmental test chamber reduces stagnant air *over* the test cup [168]. Considering that the differences here are less than the experimental error, indicated by COV in Table 6.3, the still air effects can be considered negligible. Gennadios et al. [168] consider differences less than 5 % to be insignificant.

6.3.3 Mechanical Properties

The stress (σ) - strain (ϵ) plots for the films are shown in Figure 6.3. Most specimens displayed mild necking and plastic flow in the plasticized region, while others displayed somewhat brittle and tough behavior by breaking shortly after yielding. Yield occurred between strains of roughly 3 and 6 %. The majority of specimens required less than 1 % elongation before displaying Hookean behavior, typical of thin polysaccharide films. Some stress-strain curves had to be corrected by a horizontal shift to the origin due to elongation

of the specimen before a load force was detected (i.e. $\sigma = 0$, while $\epsilon > 0$). Elastomeric behavior was not observed, not even with the ionically crosslinked CA films.

The average TS, EBB and Young's modulus values of the three film types are given in Table 6.4. The average TS increased from 60.1 MPa for neat films to 84.5 MPa for neutralized films. The heterogeneously crosslinked films with citric acid displayed a TS of 94.8 MPa. The average Young's modulus, E, increased with neutralization from 1.46 to 1.70 GPa, but did not differ significantly between neutralized and CA films. Additionally, EBB did not differ significantly between the three film types. Hence, the tensile strength increased with neutralization and ionic crosslinking of citric acid by 40 and 57 %, respectively, without compromising ductility, relative to chitosan-acetate films. The TS values are on the high end for chitosan films, but still within a typical range [38, 223], and the EBB and E values were also consistent with the literature [71, 224]. The large experimental error of the EBB may be an experimental artifact or may show that the structure of the films is highly heterogeneous.

The formation of ionic crosslinks is made possible by free water in the CA film matrix, which enables the formation and mobility of anionic and cationic species. The test conditions at ambient temperatures ensures that a sufficient water content is present in the films for the assumption of ionic crosslinking to be valid during testing.

Table 6.4: Tensile strength, elongation before break, and Young's modulus of neat, neutralized, and CA films, and the corresponding average specimen thickness.

Film Type	l [μm]	TS [MPa]	EBB [%]	E [GPa]
Neat	81 ± 11	60.2 ± 3.2 ^{a}	9.3 ± 1.5 ^{a}	1.47 ± 0.11 ^{a}
Neutralized	78 ± 12	85.2 ± 7.7 ^{b}	10.4 ± 2.7 ^{a}	1.76 ± 0.18 ^{b}
CA	94 ± 9	94.8 ± 7.2 ^{c}	10.2 ± 2.6 ^{a}	1.73 ± 0.21 ^{b}

Two means followed by the same letter indicates the values are not statistically different according to LSD test, $\alpha = 0.05$. $n_{\text{neat}} = 17$, $n_{\text{neutralized}} = 16$, $n_{\text{CA}} = 16$.

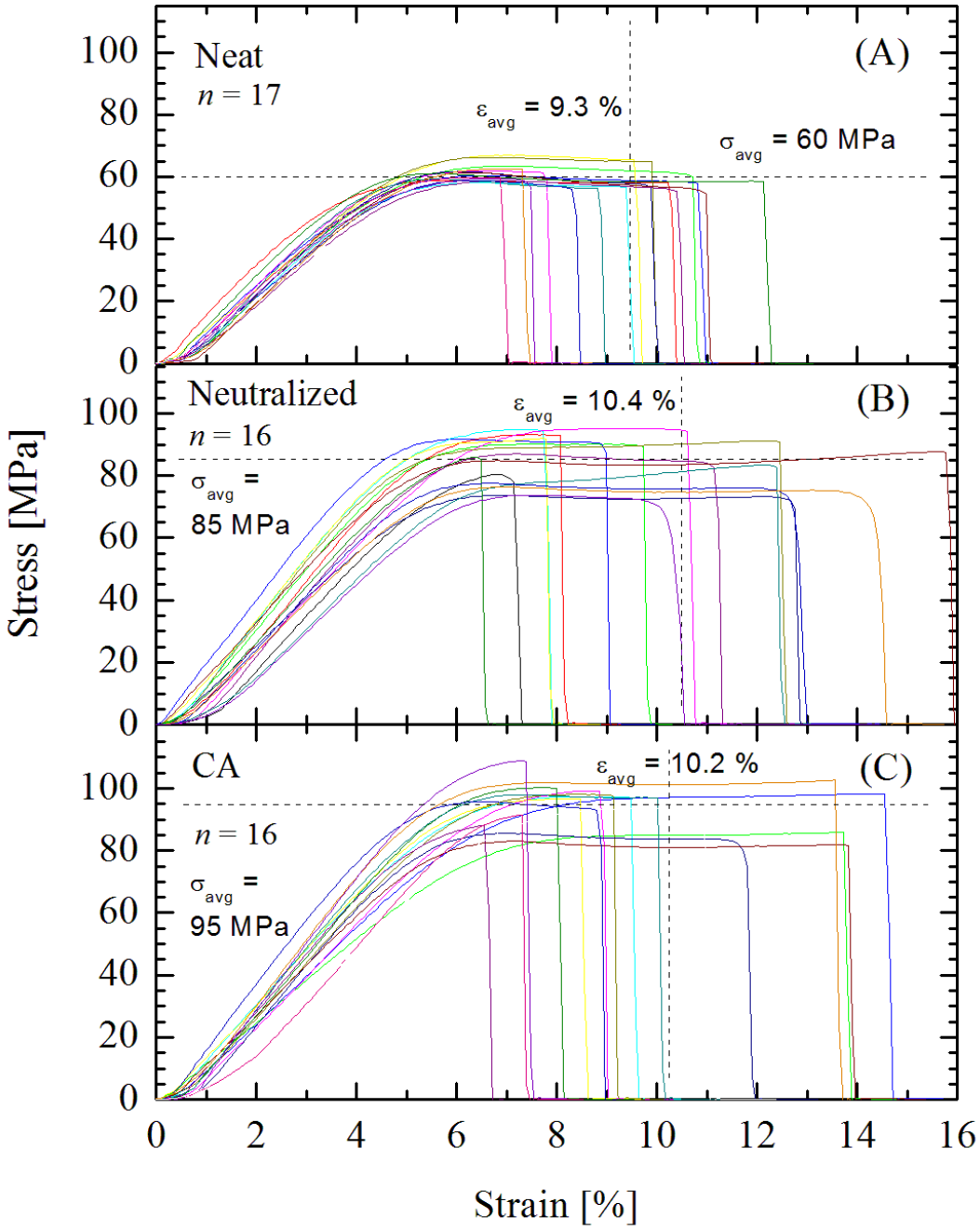

Figure 6.3: The stress, σ, plotted against strain, ϵ, for all (A) neat, (B), neutralized and CA film specimens. The average TS and EBB values are provided along with the number of tested specimens.

Neutralization lowers the water content relative to neat films, whose presence in the film matrix contribute to plasticization. Additionally, removal of water increases direct hydrogen bonding between polymer chains. The combined effects of reduced plasticization and increased inter- and intra-molecular hydrogen bonding are contributing factors in the improved TS and E. The EBB, however, would be expected to be lower, but the moderately high standard deviation for EBB calculations (COV = 16 - 25 %) may suggest true trends could be masked by either film inhomogeneities or experimental artefacts. If the comparisons are significant and no distinction can be made, then neutralization does not impact the elongation. The same argument can be made with the heterogeneous addition of citric acid.

Neat films of chitosan-acetate have been found to have a higher TS than neat chitosan-citrate films (e.g. 42 *vs* 26 MPa [66], or 69 *vs* 7 MPa [29], respectively). Here, TS increased with ionic crosslinking with citric acid. Both homogeneous and heterogeneous chitosan-citrate films will be ionically crosslinked by citric acid, but the heterogeneous method demonstrates that lower concentrations of citric acid can increase TS without compromising ductility. Qualitative assessment by bending the CA films suggests they are more brittle than the other two films, however, flexural tests were not performed here to make a quantitative statement.

Thickness is also considered, as neutralization resulted in a lower thickness and CA increased thickness relative to neat films, as discussed in Sections 4.3 and 6.3.2. Jansson and Thuvander [172] demonstrated with plasticized starch that thinner films display a higher Young's modulus. This effect is more significant, however, with differences in thickness on the mm-range. Therefore, the 16 μm difference in thickness between the neutralized and CA films (Table 6.4) is unlikely to underestimate the mechanical properties with equal thicknesses.

6.3.4 X-Ray Diffraction

The diffractograms of the 3 film types are shown in Figure 6.4, while the replicate diffractograms are shown in Figures B.5A - B.5C in Appendix B.2. The diffuse background scatter of all three film types were similar with one another, as the curves tended to converge below 7° and above 30° 2θ. Neat films displayed peaks at approximately 9.3°, 13.3°, and 19.9°, and are labelled peaks 1, 2 and 3, respectively. The 9.3° and 13.3° peaks correspond to hydrated and anhydrous crystal structures [52] that are associated with the 'Type II' crystal form (Section 2.2.2), which is characteristic of chitosan-monocarboxylic acid salts [50]. Peak 2 appeared at different 2θ angles, 12.8° or 14.9°, depending on the replicate film. This indicated heterogeneities within the same film, captured from different sampling spots that have differences in d-spacing and cell size. Peak 3 is asymmetrical as it is composed of two peaks closely merged together, as also observed elsewhere [55].

The neutralized films displayed crystallographic characteristics of tendon chitosan (Section 2.2.2), with peaks near 10° and 20°. Peak 1 shifted from 9.3° to 10.3° after

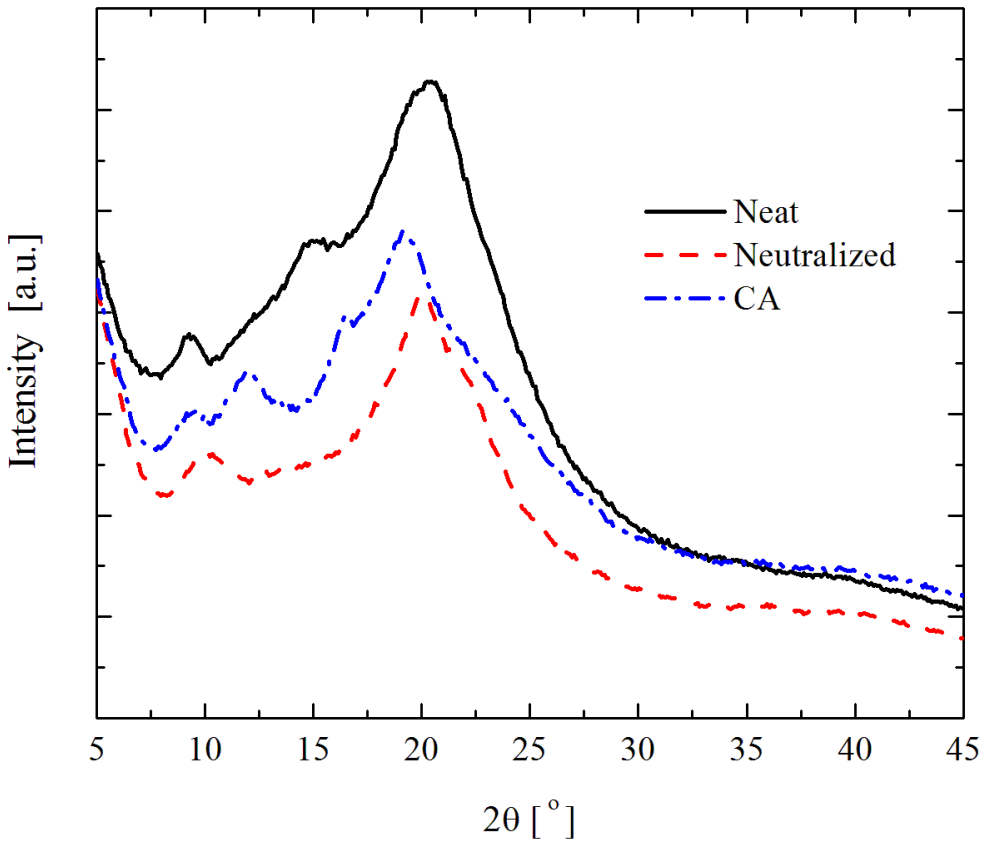

Figure 6.4: Diffractograms of neat, neutralized, and CA films.

neutralization. This resulted in a change of d-spacing from 9.6 to 8.6 Å, indicating smaller, more dense crystals. The diffractograms of neat and neutralized chitosan film were consistent with diffraction studies of Ogawa et al. [52].

After the addition of citric acid, the peak at 10.1° (in the diffractogram of the neutralized film) shifted back to 9.5°. Additionally, two peaks emerged at 11.8° and 16.5° for the CA films. The peak at 12.6° is likely due to a re-emergence of anhydrous crystals within the Type II structure, but with a larger d-spacing compared to neat films. The new peak at 16.5°, labelled peak 4, is speculated to be from citric acid crystals that remained adsorbed on the film surface, or from a slightly different mixed hydrated-anhydrous chitosan crystal structure that is occasionally observed with some as-cast chitosan-acetate films [225–228]. Pure citric acid diffracts at 18.1° (d = 4.88 Å) (Appendix B). The 16.5° peak in CA films might correspond to distorted 18.1° crystals whose d-spacing has increased to 5.37 Å. Alternatively, it may also be due to a more complex mixture of hydrated and non-hydrated crystal structures. Probing the distribution and arrangement of citric acid molecules along the thickness direction of the film can be done with scanning electron microscopy by imaging the film cross section. This would complement the XRD studies to achieve a better understanding of the origins of the 16.5° peak in CA films.

Diffusion of citric acid into the fully formed film matrix is limited due to the nature

of the film-forming procedure. Studies on chitosan films heterogeneously crosslinked with glutaraldehyde and epichlorohydrin speculated that crosslinking partially occurs at the surface [9]. This also appeared to be the case with citric acid which has a molecular size approximately 20 % greater than glutaraldehyde, as estimated from the compounds' densities and bond lengths. One significant difference, however, is that the protonation of chitosan by the dissociated citric acid (pKa = 3.09, 4.75, 5.41) caused the neutralized films to swell and expand by approximately 1 cm on each side when they were immersed in the citric acid aqueous solutions. This indicated some electrostatic repulsion of chitosan chains and a plausible penetration of some citrate ions into the films. By contrast, neutralized chitosan films became swollen but did not expand in glutaraldehyde solutions, as observed for heterogeneously crosslinked chitosan-glutaraldehyde films prepared for the viscoelastic study in Chapter 5.

The 2θ diffractogram peaks, d-spacing values (Equation 3.23), and the crystallinity, CrI, of the films are given in Table 6.5. The average CrI increased from neat to neutralized, 19.3 to 26.2 %, respectively. The increase in crystallinity with neutralization agrees with previous studies [227, 229]. The CrI of CA films, 20.4 %, decreased relative to neutralized films but was not significant relative to neat films. This is likely from counter-balancing effects from citric acid. Citric acid is expected to increase the amorphous character of the film when the heterogeneous crosslinking method is used. This assumption is based on the diffractograms of solvent cast chitosan-citrate films that show a more amorphous structure compared to a chitosan-acetate film [184]; see Appendix B.2 for diffractogram of chitosan-citrate. If there are residual citric acid molecules on the film exterior that have agglomerated into small crystalline clusters, this would not actually contribute to the crystallinity of the film. Peak 4 comprises less than 11 % to the overall crystallinity of CA films, and when subtracted, CrI of CA films would be 18.6 ± 2.0 %.

Table 6.5: Diffractogram peaks, d-spacing values, and film crystallinity.

Film Type	2θ peaks					CrI
	param.	peak 1	peak 2	peak 3	peak 4	[%]
Neat	2θ [°]	9.26 ± 0.10	13.34 ± 1.39	19.86 ± 0.44	N/a	19.3
	d [Å]	9.54 ± 0.10	6.68 ± 0.66	4.47 ± 0.10	N/a	± 2.4
Neutralized	2θ [°]	10.32 ± 0.42	N/a	20.15 ± 0.23	N/a	26.2
	d [Å]	8.57 ± 0.34	N/a	4.40 ± 0.05	N/a	± 2.2
CA	2θ [°]	9.48 ± 0.27	12.60 ± 1.25	19.42 ± 0.62	16.57 ± 0.26	20.4
	d [Å]	9.32 ± 0.26	7.06 ± 0.66	4.57 ± 0.14	5.34 ± 0.08	± 2.1

6.3.5 Contact Angle

The average contact angle of water droplets increased from 72.5° for neat films to 77.6° for neutralized films, but did not change with CA films at 78.1°. The relatively high contact angles with water demonstrate chitosan's non-polar surface characteristics, despite being a hydrophilic material. The change in water contact angle over a duration of 20 s showed that the droplets on neat films decreased by an average of 8.8°, while no discernible change in water contact angle on neutralized and CA films was observed. Thus, the water droplets are more stable on neutralized and CA films. The contact angles with hexadecane decreased from 35.0° for neat film to 27.3° for CA film, demonstrating increasing dispersive characteristics. This supports the results of the water droplet measurements. Contact angles with water and hexadecane are given in Table 6.6. In estimating the contact angles, the tangent method 1 (conic section) fit the water droplets more accurately and consistently, while the Young-Laplace method fit the hexadecane droplets best. See Figure 6.5 for contact angle images with corresponding fitted curves. No significant difference in contact angle was observed between the air-surface and tray-surface sides of the films.

The dispersive forces of the surface tension of the films, as calculated by Fowke's method (outlined in Section 3.8), increased from 22.8 mJ/m^2 of neat films to approximately 24 mJ/m^2 for neutralized and CA films. The polar components of the surface tension decreased from 12.3 mJ/m^2 for neat films to 9.0 mJ/m^2 with neutralization and to 8.5 mJ/m^2 with citric acid addition. This demonstrated the strong contribution of the residual acid on the polar component and ultimately higher surface energy of neat films.

In a study on chitosan film composites with long chain fatty acids cast with formic acid, Wong et al. [75] report a general decrease in total film surface energy as the acid chain length increases. The surface energy, γ_S, of chitosan-fatty acid films decreased from 28.9 to 21.2 mJ/m^2, for films containing an undisclosed amount of lauric acid ($C_{12}H_{24}O_2$) to stearic acid ($C_{18}H_{36}O_2$) [75], respectively. Their neat chitosan-formate film yielded a γ_S of 24.8 mJ/m^2. Increasing fatty acid length was considered to shield the polar constituents of chitosan as a result of poor chitosan-fatty acid interaction and therefore decrease γ^D and overall surface energy. Based on SEM images lauric acid was better dispersed in the chitosan polymer matrix relative to the other fatty acids, which may explain the increased γ^D, γ^P and γ_S over the chitosan-formate film.

It should be noted that due to the instability of a water droplet on the chitosan film, the measured angle may not be the true angle. Therefore, the estimated surface energy could be erroneous or biased. An alternative approach would be to use multiple liquids that are more stable on the film surface. This can be verified by observing the angles of these liquids on the surface for extended durations (> 20 s). The surface energy can be re-estimated using these liquids. However, comparing the surface energy values of two different materials is only appropriate if the procedures and liquids used are identical [174].

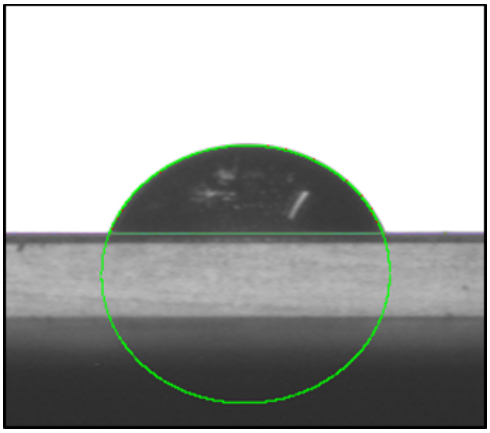

(A) Water on neat film

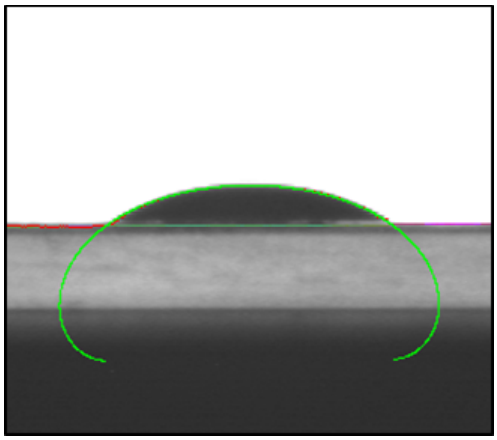

(B) Hexadecane on neat film

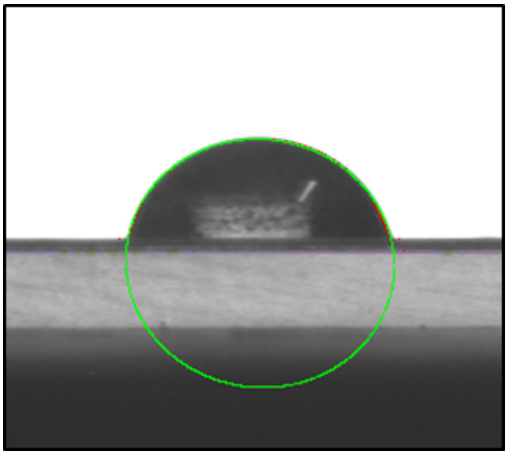

(C) Water on neutralized film

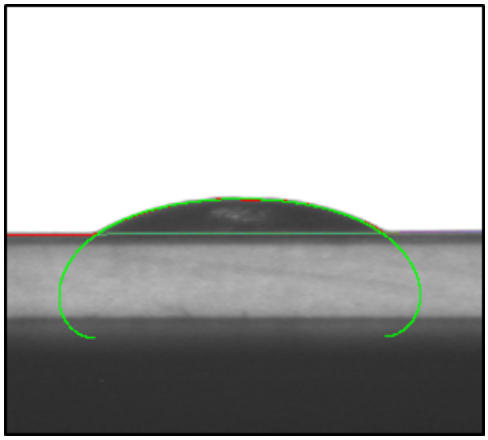

(D) Hexadecane on neutralized film

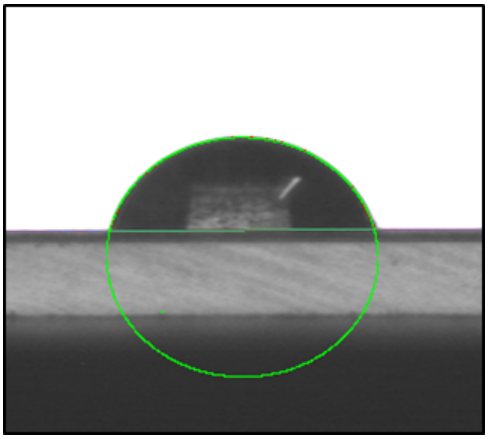

(E) Water on CA film

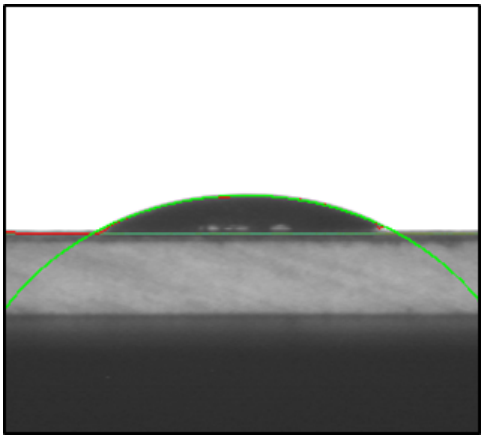

(F) Hexadecane on CA film

Figure 6.5: Contact angle droplets on the films, upon immediate contact ($t = 0$ s): (A) water on neat, (B) hexadecane on neat, (C) water on neutralized, (D) hexadecane on neutralized, (E) water on CA film, and (F) hexadecane on CA film. The angles with water were estimated with the tangent 1 method, and Young-Laplace method with hexadecane droplets.

Table 6.6: Contact angles of water and hexadecane droplets on chitosan films. Surface tensions and energy calculated from Fowke's method.

Film Type	Contact ∠ (H_2O) [°]	Δ ∠ (H_2O) ($\Delta t = 20$ s) [°]	Contact ∠ ($C_{16}H_{34}$) [°]	γ_S^P [mJ/m^2]	γ_S^D [mJ/m^2]	γ_S [mJ/m^2]
Neat	72.5 ± 3.2 [a]	8.8 ± 1.4 [a]	35.0 ± 4.4 [a]	12.3	22.8	35.1
Neutralized	77.6 ± 3.7 [b]	2.4 ± 2.5 [b]	30.8 ± 3.1 [a,b]	9.0	23.8	32.8
CA	78.1 ± 2.7 [b]	1.3 ± 0.6 [b]	27.3 ± 1.7 [b]	8.5	24.5	33.0

Subscript 's' denotes solid phase, superscripts denote 'p' for polar and 'd' for dispersive components. $n = 18$ for neat, 14 for neutralized, and 17 for CA films. The superscripted letters in a given column denote statistically different values, as determined by LSD comparison of means ($\alpha = 0.05$).

6.4 Discussion

The effects of crystallinity and crystal structure on the tensile, viscoelastic, and WVP properties are now discussed. The films are also compared on the basis of hydrophilicity and affinity to moisture or water.

6.4.1 Mechanical Properties in Relation to Crystallinity

Chitosan-salt films of Type II (i.e. chitosan-acetate) are comprised of a relaxed 2-fold helix chain structure, where the repeating period (fibre axis) is nearly 4 times longer than the extended 2-fold helix structure of tendon chitosan [50], as shown in Figures 2.3 and 2.5. The chitosan units in the Type II form are elongated beyond the typical lengths of a tendon chitosan, and have a lower number of glucosamine units per angstrom along the long-chain axis (0.196 unit/Å) than the tendon form (0.290 unit/Å), as estimated from the models of the structures presented by Ogawa et al. [50]. Upon removal of acetic acid from the chitosan-acetate film by neutralization, the crystal structure reverts back to an extended 2-fold structure, and the chain structure is secured by intramolecular O3$\cdots$O5 hydrogen bonds [230], whereas the strength of these bonds in the Type II form are partially weakened. And while the energies of secondary bonds, such as hydrogen bonds, are no more than 5 % of the intramolecular covalent bonds in a polymer chain [231], intramolecular forces contribute the most to a polymer's tensile strength. Such intra-chain hydrogen bonds of polysaccharides are an important factor in chain stability and stiffness [232]. Thus, these O3$\cdots$O5 intramolecular bonds may contribute to a small extent to the increased TS observed in neutralized films relative to neat films.

The increase in TS with neutralization compared to neat films is also in part caused by diminished plasticization effects from the reduced water content. The water content of neutralized films is 2 - 3 % lower than neat films, as determined by TGA scans shown in Figure 6.1, which confirms the value reported by Gartner et al. [189]. The

extent of plasticization attributed to residual acid in the films is seldom discussed in the literature. Caner, Vergano and Wiles [233] studied chitosan-acetate, -formate, -propionate, and -lactate films prepared with 1 and 7.5 % acid solutions, and their results indicate that, with the exception of chitosan-lactate films, acid concentration was inconsequential to the mechanical properties. Chen et al. [226] similarly failed to observe a significant difference in tensile properties between chitosan films cast with either 0.2 and 1 M acetic acid. Thus, it appears that acetate ions do not act as plasticizers in chitosan-acetate films, unlike water molecules. This may be related to the final concentration of residual acid in the film and a limited number of bonding sites for the acid molecules. Zotkin et al. [201] estimated that regardless of casting with monocarboxylic acids of either acetic, formic or propionic acid, the final ratio of acid to chitosan monomer in the film was nearly constant, 1.1 - 1.2 (mol/mol), showing that despite differences in volatility, a balance of carboxylate to amine is maintained. Ogawa et al. [50] hypothesize that the acids are not actually present in the Type II crystals but rather in the amorphous domains.

Ionic crosslinking can improve mechanical strength, as demonstrated by chitosan-alginate ionic complexes [234]. Marques et al. [132], however, reported a decrease in TS and increase in E with neutralized chitosan films that were ionically crosslinked with sulfuric acid under both homogeneous and heterogeneous preparation methods. Marques et al. [132] neutralized films after homogeneous crosslinking, which would hypothetically remove the sulfuric acid.

In this study, the ionic bonding from citric acid contributed to the increased TS from 85 to 95 MPa. The elastic modulus at room temperature however, was uninfluenced by ionic crosslinking. This was not similarly reflected in dynamic mechanical analysis (DMA) measurements, where the average dynamic storage modulus, E', at 30 °C of neutralized and CA films were significantly different, 6,665 and 7,588 MPa, respectively. Although E and E' may not be directly comparable, they do represent the same property under different conditions. Thus, under dynamic conditions and very small strain (< 0.15 %), CA films may demonstrate a greater capacity to store mechanical energy upon elongation of chains, but this same trait is not exhibited under non-dynamic treatment for larger strains (>1 %). There may also be an issue with low sampling degree and high experimental error, whereby the true E of CA films is larger than that of neutralized films, or conversely, E'(30 °C) of CA films is not significantly different with that of neutralized films. Neutralized and CA films have a similar degree of water content, ∼11 %, but their hydrogen bonding network and differences in crystal structure also account for their different mechanical characteristics. One would expect neutralized films to have a higher TS than CA films because of their higher CrI (26 *vs* 20 %), and more dense crystal structure. However, based on the higher TS and E'(30 °C) of CA than neutralized films, and comparable E values, ionic crosslinking with citric acid has a greater, and positive impact on the mechanical properties.

6.4.2 Film Hydrophilicity and WVP in Relation to Crystallinity

The hydrophilic character of the chitosan films as it relates to WVP contrasts with that observed with contact angle measurements. The relative shift of water contact angle on chitosan films before and after neutralization as reported in literature, is conflicting [187, 227]. One might expect a higher water contact angle for a material that exhibits a lower WVP, as presented by Oliveira et al. [187]. The observations here are more aligned with Chang et al. [227]. The neutralized films here are seemingly less hydrophilic due to higher contact angle (77.6° *vs* 72.5°), but more hydrophilic due to higher WVP compared to neat films (10.70 *vs* 5.06 $\times$ 10^{-11} g/m·s·Pa). To better understand this seemingly contradictory behavior between WVP and contact angle, insomuch as designating which film is more hydrophilic than the other, the fundamentals that govern WVP and surface tension are briefly described.

The permeation of a gas through a penetrable film occurs in several steps: (i) adsorption of the gas molecules on the surface followed by dissolution into the material, (ii) concentration gradient-driven diffusion across the film, and (iii) desorption of the gas on the low concentration side. While it appears that a neat film is more hydrophilic based on its interaction with bulk H_2O in the liquid phase from contact angle measurements, neat films are more restrictive to water vapor according to their WVP.

The main physico-chemical factors that influence WVP (neglecting the effect of test conditions) include crystallinity and density, and secondary factors such as water content have been identified. Neutralized films are more dense (Table 4.6 and [187]) and slightly more crystalline (Table 6.5 and [227, 229]). Permeability has an inverse relationship with crystallinity [235]. The work of Lasoski and Cobbs [236] on polyethylene, polyethylene terephthalate and nylon films showed that a linear relationship could be drawn between WVP and the square value of the volume fraction of the amorphous phase, concluding that diffusion occurs mostly in the amorphous regions of a membrane.

Additionally, the WVTR is also influenced by initial water content in the film, which is higher in neat films. Debeaufort, Voilley, and Meares [237] showed that as the initial water content ($m_{H_2O}/m_{dryfilm}$) in methylcarboxycellulose films increased, steady-state WVTR increased too. The steady-state water content, however, remained constant [237] regardless of initial concentration, for fixed vapor pressure, temperature and film thickness.

Therefore, all reasoning up to this point would lead to the assumption that the WVP of neat films should be greater compared to neutralized films due to lower crystallinity (32 *vs* 48 %), lower density (1.5 *vs* 1.7 g/cm^3), and higher initial water content (13 *vs* 11 %). What would make neat chitosan film more restrictive to water vapor permeability compared to neutralized films? The difference is the presence of acetate ions in the film, something lacking from neutralized chitosan films and methylcarboxycellulose films. Thus, acetate ions influence hydrogen bonding network in such a capacity as to restrict the diffusion of water molecules through the film.

If the neutralization process induced changes to surface roughness, this may also account

for the seeming discrepancy between WVP and contact angle measurements. That is, if it resulted in a smoother surface, while maintaining other factors, a higher contact angle is a reasonable observation. For silica-loaded plasticized chitosan films [187], neutralized films exhibited a rougher surface with more pronounced silica particles, and also exhibited lower water contact angles compared to non-neutralized films.

Another factor for consideration is the net polarity of the surface. For chitosan-poly(vinyl alcohol) (PVA) blend films, water contact angle decreased with an increase in PVA [238]. A corresponding chemical analysis by electron spectroscopy of the surface revealed an increase in polar, hydrophilic O-C=O groups on the surface as a result of increasing PVA content. Returning to the chitosan films here, residual acetate ions would contribute to the presence of carbonyl groups, possibly at the film exterior. These carbonyl groups could possibly explain the lower contact angle compared to neutralized films by virtue of enhanced polarity. By this reasoning, however, one might therefore expect a decrease in contact angle upon heterogeneous addition of citric acid, as citric acid is comprised of three carboxylic groups, and acetic acid only one. Furthermore, reintroducing an acid into the film, in this case citric acid, and thus altering the hydrogen bonding network of the polymer matrix, has shown to increase the barrier against moisture permeability by lowering WVP relative to the neutralized film.

To further relate the observations from WVP and contact angle measurements, the moisture sorption isotherms of the films was produced, as shown in Figure 6.6. At water activities, a_{w}, less than 0.5 the amount of moisture absorbed by the neat films was less than that of neutralized and CA films, and the moisture gain by CA films was less than neutralized films, in agreement with WVP measurements performed at 50 % RH. This further demonstrated that the presence of acetic acid or citric acid inhibits uptake of water vapor. Above 75 % a_{w}, neat films become more moisture absorbent. The parameters estimates from the GAB model (Section 3.9) are listed in Table 6.7, and are within range reported in the literature [228, 239]. In contrast to the sorption isotherms of chitosan-formate and neutralized chitosan-formate films by Sakurai et al. [240], their monolayer sorption constant decreased with neutralization (as per the BET model), suggesting higher moisture affinity, whereas it increased here from 0.0496 to 0.715. Moreover, interpretation of x_{m} here is questionable because the model fit has not been performed with a low enough a_{w}. More empirical data points along a wider a_{w} range may be needed for more accurate parameter estimates.

Table 6.7: Parameter estimates from the GAB model.

Film Type	x_{m}	C_{G}	K_{G}
Neat	0.0496	51.9	0.889
Neutralized	0.0715	78.3	0.778
CA	0.0687	112.9	0.687

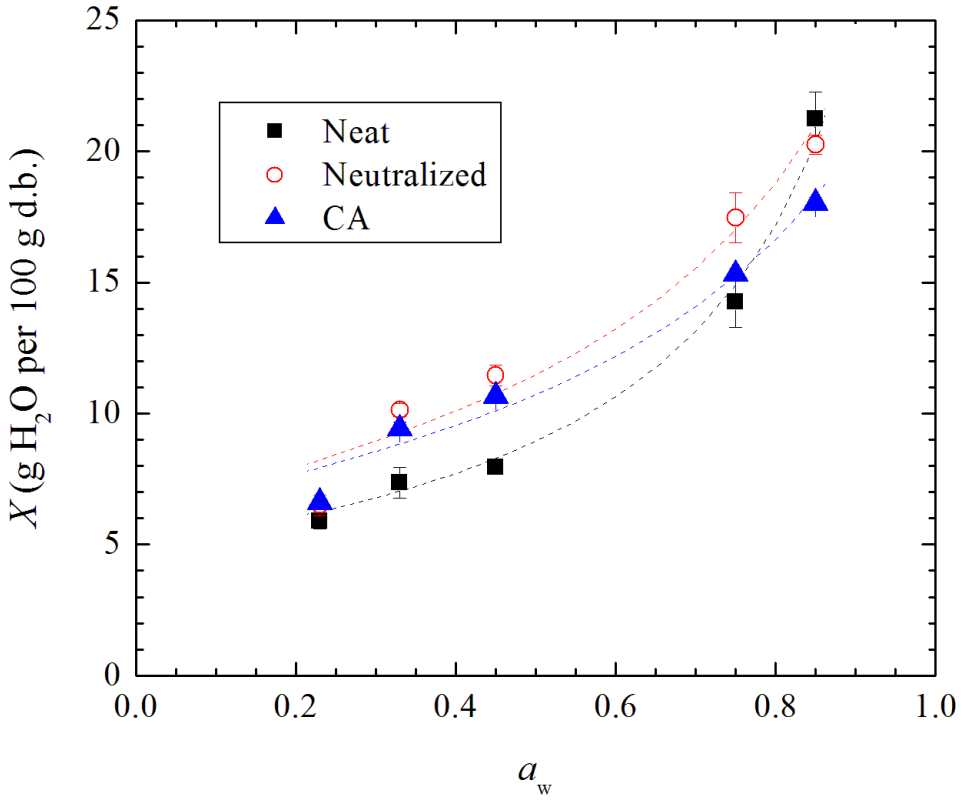

Figure 6.6: Moisture sorption isotherm for neat, neutralized and CA film; percentage of moisture absorbed X, plotted against water activity, a_w. Dashed lines correspond to GAB model fitting. Measurements were performed in triplicate.

6.5 Conclusions

The mechanical and moisture barrier properties of neat films, neutralized films, and chitosan films heterogeneously crosslinked with 15 % citric acid were characterized. Ultimately, the results indicate that the heterogeneous crosslinking method with citric acid could improve some properties, compared to both neutralized and neat films. The tensile strength increased from 84.5 MPa of neutralized films to 94.8 MPa of CA films, while maintaining ductility. Thermal stability also increased as a consequence of ionic crosslinking by citric acid, as indicated from the temperature of maximum rate of decomposition from DTGA scans. Despite neat films displaying the lowest WVP, they had the lowest degree of crystallinity, 19.3 %, lowest water contact angle, 72°, and highest water content, 14 %, contrary to expectations of how these factors influence WVP. When citric acid was added to the neutralized film, WVP decreased from 10.7 to 7.38 $\times$ 10^{-11} g/(m·s·Pa). This demonstrated how the barrier against moisture is affected by the presence of an acid embedded in the film matrix. This was similarly reflected in the moisture sorption isotherms, whereby films previously dried in a desiccator showed lower

moisture uptake if they contained either citric or acetic acid. The presence of acetic acid in neat films also demonstrated high surface hydrophilicity and unstable water droplets, compared to neutralized and CA films. The films with citric acid displayed a similar water content, 12 %, and water contact angle, 78°, with neutralized films. The XRD scans of CA films showed potential evidence of some citric acid on the surface of the film, indicating that the selected heterogeneous step conditions may be insufficient for adequate dispersion of citric acid into the film. In short, heterogeneous crosslinking with citric acid, even if the bonding mechanism is ionic, offers the potential for enhanced physicochemical properties, but the film preparation method and other important factors, such as concentration, must be optimized.

Chapter 7

Conclusions, Contributions, and Recommendations

7.1 Summary

Crosslinking is an effective method in improving mechanical strength and moisture barrier properties of chitosan films. For food and packaging applications, a natural crosslinking agent such as citric acid can be advantageous. The heterogeneous crosslinking method was applied here to observe how the physico-chemical properties fare with citric acid in comparison to neat (chitosan-acetate) and neutralized (acetate-free) chitosan films.

Heat treatment was expected to convert the bonding between citric acid and chitosan amine groups from ionic to covalent bonds. A preliminary study (Chapter 4) on the solubility and swelling of heterogeneously crosslinked chitosan films with citric acid showed that heat treatment improved the films' resistance to dissolution in dilute acetic acid solution, indicating some degree of amidization of chitosan. This was insufficient for commenting on the extent of reaction being either grafting, i.e. one covalent bond per citrate molecule, or covalent crosslinking, two covalent bonds bridging two chitosan chains.

A detailed study of the viscoelastic properties (Chapter 5) of chitosan films using dynamic mechanical analysis (DMA) was conducted to assess the extent of covalent crosslinking of films containing 15 % citric acid, with heat treatment (denoted as CA-HT films) and without heat treatment (denoted as CA films). A comparison was also made with neat films, neutralized films, and homogeneously and heterogeneously crosslinked films with a model crosslinker, glutaraldehyde (GLU). An increase in GLU concentration from 3 to 12 % in homogeneously crosslinked films (GLU-HOM) caused the dynamic storage modulus, E', to increase relative to neat films from chain stiffening by consequence of crosslinking. Additionally, covalent crosslinking with GLU at the amine reduced the hydrogen bonding capacity which further contributed to the increase in E' from reduced plasticization.

The changes in E' that are indicative of covalent crosslinking were not reflected in the

films containing citric acid. The difference in E'(195 °C) between neutralized, CA and CA-HT films was not significant. Therefore, the effect of heat treatment on the total conversion from ionic crosslinking to covalent crosslinking between citric acid and chitosan was not assumed.

An analysis of the tanδ relaxation peak near 170 °C for neat films suggested that this peak is not from structural relaxation in the usual sense of long-range chain restructuring to a rubbery-state that is commonly observed by calorimetry. Several observations led to this conclusion: i) Absence of the peak in neutralized films. ii) The CA and CA-HT films exhibited a small tanδ peak at 130 °C which increased to 170 °C after preheating. This was also observed for non-heat treated chitosan films prepared with 15 % citric acid in an acetic acid solution. iii) This peak diminished with an increase in GLU concentration in GLU-HOM films. Therefore, the conclusion was that this high temperature tanδ peak is more likely from electrostatic interactions between acetate ions and protonated amines, as previously speculated by others [189]. This form of structural relaxation was not useful for commenting on covalent crosslinking.

The mechanical, water vapor barrier, crystallinity, and thermal properties of ionically crosslinked CA films were characterized and compared with neat and neutralized films (Chapter 6). The tensile strength (TS) increased from 60 to 85 MPa with neutralization due to reduced plasticization from a reduced water content, and from an increase in crystallinity relative to neat films. The TS further increased to 95 MPa with citric acid from ionic crosslinking. The water vapor permeability (WVP) increased from 5.06 to 10.7 $\times$ 10^{-11} g/(m·s·Pa) with neutralization but decreased to 7.38 $\times$ 10^{-11} g/(m·s·Pa) when citric acid was incorporated into the films. Clearly, films containing electrostatically bound acid ions, either acetic or citric acid, have a positive effect on resistance to moisture diffusion. The water contact angle, however, was lowest for neat films, 72^{o} and highest for neutralized/CA films, 78^{o}, showing that the surface characteristics were different with respect to the concept of hydrophilicity when compared to WVP. This was explained by acetic acid's contribution to the polar characteristics at the film surface. Moisture sorption isotherms of the three film types showed that from water activities of 0.33 to 0.75 films containing either acetic or citric acid absorbed less water per dry film mass compared to neutralized films, in agreement with the trend of WVP measurements. CA films also had higher thermal stability than neutralized films, as per thermogravimetric analysis (TGA).

To summarize, heterogeneous crosslinking of chitosan films with citric acid was characterized for the first time. An overall improvement in mechanical and water vapor barrier properties was observed. The structural relaxation of chitosan films observed with DMA was thoroughly examined. With respect to the target application, it can be said based on the physical properties, that CA films have met the objective of enhanced mechanical and water vapor barrier properties, as well as thermal stability. These improvements can be seen by comparison with either neat or neutralized films depending on the property. Neat or neutralized films can be both considered as a reference. Despite the improvement, the overall properties are still poor in comparison to thermoplastics.

Additionally, the issue of large scale production or scalability has not been addressed. Other important factors should also be considered from an application and commercial aspect, such as long-term storage, heat-sealability of films containing citric acid, and migration of citric acid from the film.

7.2 Contributions to the Research Field

A portion of the viscoelastic study in Chapter 5 has been published in *Processes*; *Processes* **2019**, 7(3), 157. A manuscript based on the characterization study in Chapter 6 has been submitted to the *Journal of Applied Polymer Science*. A review article on chitosan edible films is currently in progress. The content of the review paper will cover topics such as the effects of heat treatment and neutralization on film physico-chemical properties, and emerging studies on thermo-formed chitosan and thermoplastic/chitosan films.

The application of the heterogeneous crosslinking method of chitosan has been applied with citric acid for the first time, to the best of the author's knowledge. The major implication of this work is that proper application of film crosslinking and a comprehensive understanding of the thermomechanical properties of chitosan films remains to be fully developed. While some of the DMA measurements performed here have previously been made available in the literature to some extent, this is the first study that comprehensively compares changes to mechanical storage modulus of neutralized films, heterogeneously and homogeneously crosslinked films, especially films crosslinked with GLU. And while there are studies that compare the heterogeneous and homogeneous crosslinking of chitosan [9, 96, 132], their focus is not on food packaging.

The effect of citric acid on film properties in a smaller concentration than would normally be used for a chitosan-citrate film was tested. This approach allows researchers to better understand how chitosan responds to incremental, controlled changes of organic acid concentration. While heterogeneous crosslinking is not uncommon for industrial applications of chitosan, it is less often applied to food applications. Therefore, the effects of the crosslinker can be studied in insolation, without interference of acetic acid. Heterogeneous crosslinking with other kinds of safe, natural crosslinkers can be tested. And lastly, this work also provides confirmatory results to some of the physical properties of chitosan films measured by previous researchers.

7.3 Recommendations for Future Work

The results obtained from the characterization of neat, neutralized and CA films present the following research questions and consideration for further investigation:

Coupled Spectroscopy-Thermal Characterization of Heterogeneously Crosslinked Film with Citric Acid

TGA coupled with either mass spectroscopy or infrared spectroscopy would assist in addressing the question of what is the most dominant compound(s) released from a CA film prior to decomposition. The differential TGA scans of CA films showed a mass loss between 175 and 225 °C, which has been speculated to be due to either cleavage of N-citryl groups that reacted on the amine, a release of water from a reaction with citric acid, or the evaporation of citric acid derivatives or a combination of all of these (Section 6.3.1).

Barrier Against O_2, CO_2, and Ethylene gas

Citric acid improves the barrier properties against water vapor diffusion. But what effect does it have on the permeability of O_2, CO_2, and ethylene gas?

Investigation of the Glass Transition of Plasticized Chitosan Films using DMA

Since the structural relaxation above 130 °C observed in the DMA tanδ plots of neat and CA films is associated with the interaction with acetic or citric acid, respectively, can structural relaxation of the glass - rubber transition type be observed? Plasticization of the film could shift the glass transition temperature, T_g, to a temperature below 200 °C. If the film is cast with a plasticizer in the film-forming solution, the T_g could potentially overlap with the acid-induced tanδ relaxation peak near 170 °C. To avoid this, the film tested could be prepared as per the heterogeneous crosslinking method but with a plasticizer.

Property Optimization

An optimization study using response surface plots and a Design of Experiments could help find a combination of CA film preparation variables that yield high mechanical and gas barrier properties. Such parameters include citric acid concentration, plasticizer content, catalyst concentration, cure temperature and cure time.

Anti-Microbial and Anti-Bacterial Properties of CA films

One theory attributes chitosan's anti-microbial and anti-bacterial properties to the protonated amines. Neutralization therefore reduces these activities, so re-introducing citric acid would theoretically re-initiate them. What effect does citric acid have on the microbe inhibition and free-radical scavenging properties of chitosan? Scavenging activity of hydrogen peroxide using UV absorbance measurements could be performed.

Migration of Citric Acid from the Film

For films ionically crosslinked with citric acid, there is susceptibility of citric acid diffusing from the film. This has implications for commercial and end market use. The kinetics of diffusion can be estimated from immersion in buffer solutions [241].

Crosslinking Chitosan with an Enzyme

One route for potential crosslinking of chitosan may be with an enzyme, specifically transglutaminase. The literature seems to suggest that transglutaminase crosslinks only the protein in a protein-chitosan blended film [78]. Transglutaminase catalyzes the isopeptide bond (-(C=O)NH-) of glutamine with the primary amine of lysine. Chitosan contains both kinds of bonds through the acetylated amine, and primary amine side groups, respectively. Tryosinase is another option.

Letter of Copyright Permission

- License agreements for Figures 2.3 and 2.4.

Copyright Clearance Center RightsLink®

Home | Account Info | Help

ACS Publications Most Trusted. Most Cited. Most Read.

Title: Molecular and Crystal Structure of Hydrated Chitosan
Author: Kenji Okuyama, Keiichi Noguchi, Takashi Miyazawa, et al
Publication: Macromolecules
Publisher: American Chemical Society
Date: Sep 1, 1997
Copyright © 1997, American Chemical Society

Logged in as: Joseph Khouri
Account #:
LOGOUT

PERMISSION/LICENSE IS GRANTED FOR YOUR ORDER AT NO CHARGE

This type of permission/license, instead of the standard Terms & Conditions, is sent to you because no fee is being charged for your order. Please note the following:

- Permission is granted for your request in both print and electronic formats, and translations.
- If figures and/or tables were requested, they may be adapted or used in part.
- Please print this page for your records and send a copy of it to your publisher/graduate school.

ACS Publications Most Trusted. Most Cited. Most Read.

Title: Molecular and crystal structure of the anhydrous form of chitosan
Author: Toshifumi Yui, Kiyohisa Imada, Kenji Okuyama, et al
Publication: Macromolecules
Publisher: American Chemical Society
Date: Dec 1, 1994
Copyright © 1994, American Chemical Society

Logged in as: Joseph Khouri
Account #:
LOGOUT

PERMISSION/LICENSE IS GRANTED FOR YOUR ORDER AT NO CHARGE

This type of permission/license, instead of the standard Terms & Conditions, is sent to you because no fee is being charged for your order. Please note the following:

- Permission is granted for your request in both print and electronic formats, and translations.
- If figures and/or tables were requested, they may be adapted or used in part.
- Please print this page for your records and send a copy of it to your publisher/graduate school.

• License agreement for Figure 2.5A: "This Agreement between Mr. Joseph Khouri ("You") and Elsevier ("Elsevier") consists of your license details and the terms and conditions provided by Elsevier and Copyright Clearance Center."

License Number 4566601323082
License date Apr 12, 2019
Licensed Content Publisher Elsevier
Licensed Content Publication International Journal of Biological Macromolecules
Licensed Content Title Three D structures of chitosan
Licensed Content Author Kozo Ogawa,Toshifumi Yui,Kenji Okuyama
Licensed Content Date Apr 1, 2004
Licensed Content Volume 34, Licensed Content Issue 1-2
Licensed Content Pages 8, Start Page 1, End Page 8
Type of Use reuse in a thesis/dissertation
Intended publisher of new work other
Portion figures/tables/illustrations
Number of figures/tables/illustrations 1
Format both print and electronic
Are you the author of this Elsevier article? No
Will you be translating? No
Original figure numbers 5

• Additional license agreement for Figure 2.5A; Figure from [50] originally printed in [230]: "This Agreement between Mr. Joseph Khouri ("You") and Elsevier ("Elsevier") consists of your license details and the terms and conditions provided by Elsevier and Copyright Clearance Center."

License Number 4566610422694
License date Apr 12, 2019
Licensed Content Publisher Elsevier
Licensed Content Publication Carbohydrate Polymers
Licensed Content Title Structural diversity of chitosan and its complexes
Licensed Content Author K. Okuyama,K. Noguchi,M. Kanenari,T. Egawa,K. Osawa
Licensed Content Date Mar 1, 2000
Licensed Content Volume 41, Licensed Content Issue 3
Licensed Content Pages 11, Start Page 237, End Page 247
Type of Use reuse in a thesis/dissertation
Intended publisher of new work other
Portion figures/tables/illustrations
Number of figures/tables/illustrations 1
Format both print and electronic
Are you the author of this Elsevier article? No
Will you be translating? No; Original figure numbers 10

• License agreement for Figure 2.5B.

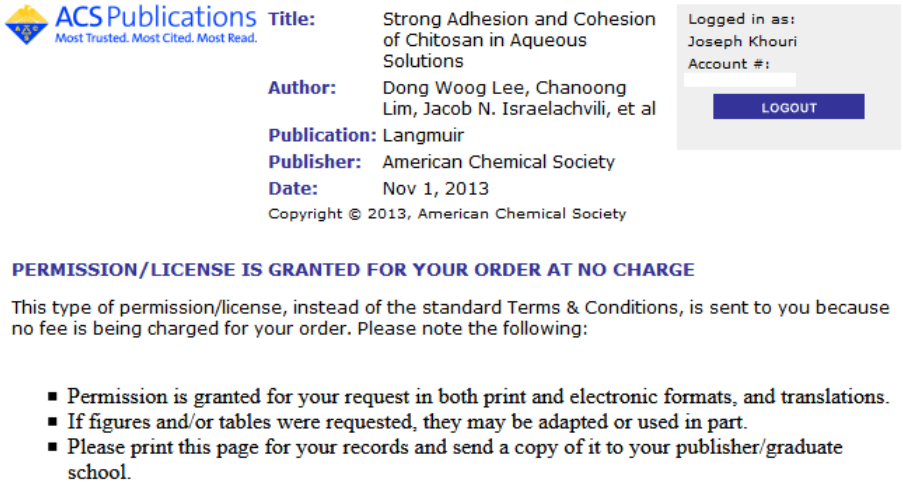

• License agreement for Figure 2.8: "This Agreement between Mr. Joseph Khouri ("You") and Elsevier ("Elsevier") consists of your license details and the terms and conditions provided by Elsevier and Copyright Clearance Center."

License Number 4566610874224
License date Apr 12, 2019
Licensed Content Publisher Elsevier
Licensed Content Publication Food Chemistry
Licensed Content Title Citric acid cross-linking of starch films
Licensed Content Author Narendra Reddy,Yiqi Yang
Licensed Content Date Feb 1, 2010
Licensed Content Volume 118, Licensed Content Issue 3
Licensed Content Pages 10, Start Page 702, End Page 711
Original figure numbers 4

• License agreements for Figure 2.9.

• License agreement for Figure 2.10: "This Agreement between Mr. Joseph Khouri ("You") and Elsevier ("Elsevier") consists of your license details and the terms and conditions provided by Elsevier and Copyright Clearance Center."

License Number 4566620240442
License date Apr 12, 2019
Licensed Content Publisher Elsevier
Licensed Content Publication Thermochimica Acta
Licensed Content Title Crosslink density dependence of polymer degradation kinetics
Licensed Content Author Vadim V. Krongauz

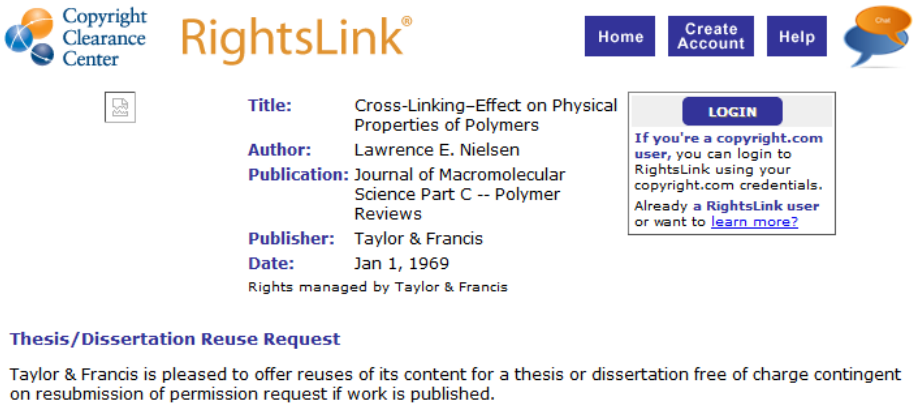

Licensed Content Date May 20, 2010
Licensed Content Volume 503, Licensed Content Issue n/a
Licensed Content Pages 15, Start Page 70, End Page 84
Original figure numbers 1

- License agreements for Figure A.7.

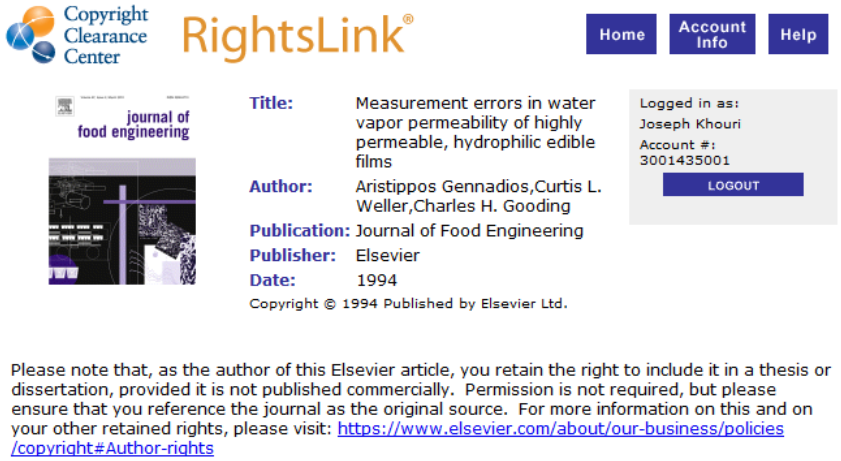

- Acknowledgement for using images from Noun Project: Icon Id: 197630 (K. Tezak) and 1156440 (M.G. Brown) used for Figure 2.1.

References

[1] D. Raafat and H.G. Sahl. Chitosan and its antimicrobial potential - a critical literature survey. *Microbial Biotechnology*, 2:186 – 201, 2009.

[2] M. Lacroix. Mechanical and permeability properties of edible films and coatings for food and pharmaceutical applications. In M. Embuscado and K.C. Huber, editors, *Edible Films and Coatings for Food Applications*, chapter 13, pages 347 – 366. Springer, New York, 2009.

[3] M. Pereda, G. Amica, and N.E. Marcovich. Development and characterization of edible chitosan/olive oil emulsion films. *Carbohydrate Polymers*, 87:1318 – 1325, 2012.

[4] B. Layek and J. Singh. N-hexanoyl, n-octanoyl and n-decanoyl chitosans: Binding affinity, cell uptake and transfection. *Carbohydrate Polymers*, 89:403 – 410, 2012.

[5] H. Möller, S. Grelier, P. Pardon, and V. Coma. Antimicrobial and physicochemical properties of chitosan-hpmc-based films. *Journal of Agricultural and Food Chemistry*, 52:6585 – 6591, 2004.

[6] N. Reddy and Y. Yang. Citric acid cross-linking of starch films. *Food Chemistry*, 118:702 – 711, 2010.

[7] S. Rivero, M.A. García, and A. Pinotti. Crosslinking capacity of tannic acid in plasticized chitosan films. *Carbohydrate Polymers*, 82:270 – 276, 2010.

[8] R. Priyadarshi, S. Singh, B. Kumar, and Y.S. Negi. Chitosan film incorporated with citric acid and glycerol as an active packaging material for extension of green chilli shelf life. *Carbohydrate Polymers*, 195:329 – 338, 2018.

[9] Y. Wan, K.A.M. Creber, B. Peppley, and V.T. Bui. Ionic conductivity and related properties of crosslinked chitosan membranes. *Journal of Applied Polymer Science*, 89:306 – 317, 2003.

[10] A. Pavlath and W. Orts. Edible films and coatings. In M. Embuscado and K. Huber, editors, *Edible Films and Coatings for Food Applications*, chapter 1. Springer, New York, 2009.

[11] H. Wang, J. Qian, and F. Ding. Emerging chitosan-based films for food packaging applications. *Journal of Agricultural and Food Chemistry*, 66:395 – 413, 2018.

[12] R. Soliva-Fortuny, M.A. Rojas-Grau, and O. Martin-Belloso. Polysaccharide coatings. In Baldwin E.A., R. Hagenmaier, and H. Bai, editors, *Edible Coatings and Films to Improve Food Quality*, pages 103 – 136. CRC Press - Taylor Francis Group, Boca Raton, 2nd edition, 2012.

[13] J.M. Rossman. Commercial manufacture of edible films. In M. Embuscado and K. Huber, editors, *Edible Films and Coatings for Food Applications*, chapter 14. Springer, New York, 2009.

[14] BioMass Packaging. Biomass packaging. Retrieved from `http://www.biomasspackaging.com/`, 2017.

[15] A. Jiménez, M.J. Fabra, P. Talens, and A. Chiralt. Edible and biodegradable starch films: A review. *Food Bioprocess Technology*, 5:2058 – 2076, 2012.

[16] G.L. Robertson. *Food Packaging - Principles and Practice*. CRC Press - Taylor Francis Group, Boca Raton, third edition, 2013.

[17] M.A. Repka, K. Gutta, S. Prodduturi, M. Munjal, and S.P. Stodghill. Characterization of cellulosic hot-melt extruded films containing lidocaine. *European Journal of Pharmaceutics and Biopharmaceutics*, 59:189 – 196, 2005.

[18] Q. Meng, M.C. Heuzey, and P.J. Carreau. Hierarchical structure and physicochemical properties of plasticized chitosan. *Biomacromolecules*, 15:1216 – 1224, 2014.

[19] M. Matet, M.C. Heuzey, E. Pollet, A. Ajji, and L. Avérous. Innovative thermoplastic chitosan obtained by thermo-mechanical mixing with polyol plasticizers. *Carbohydrate Polymers*, 95:241 – 251, 2013.

[20] M. Matet, M.C. Heuzey, A. Ajji, and P. Sarazin. Plasticized chitosan/polyolefin films produced by extrusion. *Carbohydrate Polymers*, 117:177 – 184, 2015.

[21] V.M. Correlo, L.F. Boesel, M. Bhattacharya, J.F. Mano, N.M. Neves, and R.L. Reis. Properties of melt processed chitosan and aliphatic polyester blends. *Materials Science and Engineering A*, 403:57 – 68, 2005.

[22] S. Jeung and M. Mishra. Hot melt reactive extrusion of chitosan with poly(acrylic acid). *International Journal of Polymeric Materials*, 60:102 – 113, 2010.

[23] I. Arvanitoyannis and C.G. Biliaderis. Physical properties of polyol-plasticized edible blends made of methyl cellulose and soluble starch. *Carbohydrate Polymers*, 38:47 – 58, 1999.

[24] M.J. Bof, V.C. Bordagaray, D.E. Locaso, and M.A. García. Chitosan molecular weight effect on starch-composite film properties. *Food Hydrocolloids*, 51:281 – 294, 2015.

[25] T. Bourtoom and M. Chinnan. Preparation and properties of rice starch - chitosan blend biodegradable film. *LWT - Food Science and Technology*, 41:1633 – 1641, 2008.

[26] M.A. Garcia, A. Pinotti, and N.E. Zaritzsky. Physicochemical, water vapor barrier and mechanical properties of corn starch and chitosan composite films. *Starch/Stärke*, 58:453 – 463, 2006.

[27] B. Ghanbarzadeh, H. Almasi, and A.A. Entezami. Physical properties of edible modified starch/carboxymethyl cellulose films. *Innovative Food Science and Emerging Technologies*, 11:697 – 702, 2010.

[28] B.L. Butler, P.J. Vergano, R.F. Testin, J.M. Bunn, and J.L. Wiles. Mechanical and barrier properties of edible chitosan films as affected by composition and storage. *Journal of Food Science*, 61:953 – 956, 1996.

[29] S.Y. Park, K.S. Marsh, and J.W. Rhim. Characteristics of different molecular weight chitosan films affected by the type of organic solvents. *Journal of Food Science*, 67: 194 – 197, 2002.

[30] J.L. Chen and Y. Zhao. Effect of molecular weight, acid, and plasticizer on the physicochemical and antibacterial properties of β-chitosan based films. *Journal of Food Science*, 77:127 – 136, 2012.

[31] S. Guilbert, N. Gontard, and L.G.M. Gorris. Prolongation of the shelf-life of perishable food products using biodegradable films and coatings. *LWT - Food Science and Technology*, 29:10 – 17, 1996.

[32] H.J. Park, C.L. Weller, P.J. Vergano, and R.F. Testin. Permeability and mechanical properties of cellulose-based edible films. *Journal of Food Science*, 58:1361 – 1364, 1993.

[33] J.S. Park, J.W. Park, and E. Ruckenstein. Thermal and dynamic mechanical analysis of pva/mc blend hydrogels. *Polymer*, 42:4271 – 4280, 2001.

[34] S. Rimdusit, S. Jingjid, S. Damrongsakkul, S. Tiptipakorn, and T. Takeichi. Biodegradability and property characterizations of methyl cellulose: Effect of nanocompositing and chemical crosslinking. *Carbohydrate Polymers*, 72:444 – 455, 2008.

[35] K.S. Miller and J.M. Krochta. Oxygen and aroma barrier properties of edible films. *Trends in Food Science and Technology*, 8:228 – 237, 1997.

[36] I. Sebti, E. Chollet, P. Degraeve, C. Noel, and E. Peyrol. Water sensitivity, antimicrobial, and physicochemical analyses of edible films based on hpmc and/or chitosan. *Journal of Agricultural and Food Chemistry*, 55:693 – 699, 2007.

[37] R.A.A. Muzzarelli. *Chitin*. Pergamon Press Ltd, Toronto, Ontario, 1977.

[38] H.S. Blair, J. Guthrie, T.K. Law, and P. Turkington. Chitosan and modified chitosan membranes: I. preparation and characterisation. *Journal of Applied Polymer Science*, 33:641 – 656, 1987.

[39] E.S. Abdou, K.S.A. Nagy, and M.Z. Elsabee. Extraction and characterization of chitin and chitosan from local sources. *Bioresource Technology*, 99:1359, 2008.

[40] S. Hajji, I. Younes, O. Ghorbel-Bellaaj, R. Hajji, M. Rinaudo, M. Nasri, and K. Jellouli. Structural differences between chitin and chitosan extracted from three different marine sources. *International Journal of Biological Macromolecules*, 65:298 – 306, 2014.

[41] A. Aljawish, I. Chevalot, J. Jasniewski, and J. Scher. Enzymatic synthesis of chitosan derivatives and their potential applications. *Journal of Molecular Catalysis B: Enzymatic*, 112:25 – 39, 2015.

[42] S. Mima, M. Miya, R. Iwamoto, and Y. Susumu. Highly deacetylated chitosan and its properties. *Journal of Applied Polymer Science*, 28:1909 – 1917, 1983.

[43] M. Rhazi, J. Desbieres, A. Alagui, and P. Vottero. Investigation of different natural sources of chitin: Influence of the source and deacetylation process on the physicochemical characteristics of chitosan. *Polymer International*, 49:337 – 344, 2000.

[44] Sigma Aldrich. Chitosan - high molecular weight. Retrieved from `https://www.sigmaaldrich.com/catalog/product/aldrich/419419?lang=en&region=CA`, No Date Given.

[45] W. Maniukiewicz. X-ray diffraction studies of chitin, chitosan, and their derivatives. In S.K. Kim, editor, *Chitin, Chitosan, Oligosaccharides and Their Derivatives: Biological Activities and Applications*, chapter 8, pages 83 – 94. CRC Press, Boca Raton, FL, 2011.

[46] K. Kurita, K. Tomita, T. Tada, S. Ishii, S.I. Nishimura, and K. Shimoda. Squid chitin as a potential alternative chitin source: Deacetylation behaviour and characteristic properties. *Journal of Polymer Science: Part A: Polymer Chemistry*, 31:485 – 491, 1993.

[47] R. Minke and J. Blackwell. The structure of α-chitin. *Journal of Molecular Biology*, 120:167 – 181, 1978.

[48] M. Rinaudo. Chitin and chitosan: Properties and applications. *Progress in Polymer Science*, 31:603 – 632, 2006.

[49] K. Okuyama, K. Noguchi, T. Miyazawa, T. Yui, and K. Ogawa. Molecular and crystal structure of hydrated chitosan. *Macromolecules*, 30:5849 – 5855, 1997.

[50] K. Ogawa, T. Yui, and K. Okuyama. Three d structures of chitosan. *International Journal of Biological Macromolecules*, 34:1 – 8, 2004.

[51] K. Ogawa. Effect of heating an aqueous suspension of chitosan on the crystallinity and polymorphs. *Agricultural Biology and Chemistry*, 55:2375 – 2379, 1991.

[52] K. Ogawa, T. Yui, and M. Miya. Dependence on the preparation procedure of the polymorphism and crystallinity of chitosan membranes. *Bioscience, Biotechnology and Biochemistry*, 56:858 – 862, 1992.

[53] A. Yamamoto, J. Kawada, T. Yui, and K. Ogawa. Conformational behaviour of chitosan in the acetate salt: an x-ray study. *Bioscience, Biotechnology, and Biochemistry*, 61:1230 – 1232, 1997.

[54] S. Demarger-Andre and A. Domard. Chitosan carboxylic acid salts in solution and in the solid state. *Carbohydrate Polymers*, 23:211 – 219, 1994.

[55] M. Jaworska, K. Sakurai, P. Gaudon, and E. Guibal. Influence of chitosan characteristics on polymer properties. i: Crystallographic properties. *Polymer International*, 52:198 – 205, 2003.

[56] B. Focher and P.L. Beltrame. Alkaline n-deacetylation of chitin enhanced by flash treatments: Reaction kinetics and structure modifications. *Carbohydrate Polymers*, 12:405 – 418, 1990.

[57] K. Ziani, J. Oses, V. Coma, and J. I. Maté. Effect of the presence of glycerol and tween 20 on the chemical and physical properties of films based on chitosan with different degree of deacetylation. *LWT - Food Science and Technology*, 41:2159 – 2165, 2008.

[58] W. Thakhiew, S. Devahastin, and S. Soponronnarit. Physical and mechanical properties of chitosan films as affected by drying methods and addition of antimicrobial agent. *Journal of Food Engineering*, 119:140 – 149, 2013.

[59] S. Prateepchanachai, W. Thakhiew, S. Devahastin, and S. Soponronnarit. Mechanical properties improvement of chitosan films via the use of plasticizer, charge modifying agent and film solution homogenization. *Carbohydrate Polymers*, 174:253 – 261, 2017.

[60] T. Yui, K. Imada, K. Okuyama, Y. Obata, K. Suzuki, and K. Ogawa. Molecular and crystal structure of the anhydrous form of chitosan. *Macromolecules*, 27:7601 – 7605, 1994.

[61] D.W. Lee, C. Lim, J.N. Israelachvili, and D.S. Hwang. Strong adhesion and cohesion of chitosan in aqueous solutions. *Langmuir*, 29:14222 – 14229, 2013.

[62] Z. Zong, Y. Kimura, M. Takahashi, and H. Yamane. Characterization of chemical and solid state structures of acylated chitosans. *Polymer*, 41:899 – 906, 2000.

[63] S.I. Nishimura, K. Kohgo, O. Kurita, and H. Kuzuhara. Chemospecific manipulations of a rigid polysaccharide: Syntheses of novel chitosan derivatives with excellent solubility in common organic solvents by regioselective chemical modifications. *Macromolecules*, 24:4745 – 4748, 1991.

[64] H. Sashiwa, Y. Shigemasa, and R. Roy. Homogeneous n, o-acylation of chitosan in dimethyl sulfoxide with cyclic acid anhydrides. *Chemistry Letters*, 29:1186 – 1187, 2000.

[65] V.K. Mourya and N.N. Inamdar. Chitosan-modifications and applications: Opportunities galore. *Reactive and Functional Polymers*, 68:1013 – 1051, 2008.

[66] J.W. Rhim, C.L. Weller, and K.S. Ham. Characteristics of chitosan films as affected by the type of solvent acid. *Food Science and Biotechnology*, 7:263 – 268, 1998.

[67] M. Rinaudo, G. Pavlov, and J. Desbrières. Influence of acetic acid concentration on the solubilization of chitosan. *Polymer*, 40:7029 – 7032, 1999.

[68] C.K.S. Pillai, W. Paul, and C.P. Sharma. Chitin and chitosan polymers: Chemistry, solubility, and fibre formation. *Progress in Polymer Science*, 34:641 – 678, 2009.

[69] M. Rinaudo, G. Pavlov, and J. Desbrières. Solubilization of chitosan in strong acid medium. *International Journal of Polymer Analytical Characterization*, 5:267 – 276, 1999.

[70] K. Kurita, M. Kamiya, and S-I. Nishimura. Solubilization of a rigid polysaccharide: Controlled partial n-acetylation of chitosan to develop solubility. *Carbohydrate Polymers*, 16:83 – 92, 1991.

[71] A. Bégin and M.R. Van Calsteren. Antimicrobial films produced from chitosan. *International Journal of Biological Macromolecules*, 26:63 – 67, 1999.

[72] C.A. Kienzle-Sterzer, D. Rodriquez-Sanchez, and C. Rha. Mechanical properties of chitosan films: Effect of solvent acid. *Die Makromolekulare Chemie*, 183:1353 – 1359, 1982.

[73] K.M. Kim, J.H. Son, S.K. Kim, C.L. Weller, and M.A. Hanna. Properties of chitosan films as a function of ph and solvent type. *Journal of Food Science*, 71:119 – 124, 2006.

[74] P.C. Srinivasa, M.N. Ramesh, and R.N. Tharanathan. Effect of plasticizers and fatty acids on mechanical and permeability characteristics of chitosan films. *Food Hydrocolloids*, 21:1113 – 1122, 2007.

[75] D.W.S. Wong, F.A. Gastineau, K.S. Gregorski, S.J. Tillin, and A.E. Pavlath. Chitosan-lipid films: Microstructure and surface energy. *Journal of Agricultural and Food Chemistry*, 40:540 – 544, 1992.

[76] C.M.P. Yoshida, E.N.J. Oliveira, and T.T. Franco. Chitosan tailor-made films: The effects of additives on barrier and mechanical properties. *Packaging Technology and Science*, 22:161 – 170, 2009.

[77] P. Di Pierro, B. Chico, R. Villalonga, L. Mariniello, A.E. Damiao, P. Masi, and R. Porta. Chitosan-whey protein edible films produced in the absence or presence of transglutaminase: Analysis of their mechanical and barrier properties. *Biomacromolecules*, 7:744 – 749, 2006.

[78] P. Di Pierro, B. Chico, L. Villalonga, R. Mariniello, P. Masi, and R. Porta. Transglutaminase-catalyzed preparation of chitosan-ovalbumin films. *Enzyme and Microbial Technology*, 40:437 – 441, 2007.

[79] Y.S. Cho, S.W. Kim, C.B. Ahn, and J.Y. Je. Preparation, characterization and antioxidant properties of gallic acid - grafted - chitosans. *Carbohydrate Polymers*, 83:1617 – 1622, 2011.

[80] S.B. Schreiber, J.J. Bozell, D.G. Hayes, and S. Zivanovic. Introduction of primary antioxidant activity to chitosan for application as a multifunctional food packaging material. *Food Hydrocolloids*, 33:207 – 214, 2013.

[81] L. Itzincab-Mejía, A. López-Luna, M. Gimeno, K. Shirai, and E. Barzana. Enzymatic grafting of gallate ester onto chitosan: Evaluation of antioxidant and antibacterial activities. *International Journal of Food Science and Technology*, 48:2034 – 2041, 2013.

[82] C. Wu, J.T. Tian, S. Li, T. Wu, Y. Hu, S. Chen, T. Sugawara, and X. Ye. Structural properties of films and rheology of film-forming solutions of chitosan gallate for food packaging. *Carbohydrate Polymers*, 146:10 – 19, 2016.

[83] N. Bordenave, S. Grelier, and V. Coma. Hydrophobization and antimicrobial activity of chitosan and paper-based packaging material. *Biomacromolecules*, 11:88 – 96, 2010.

[84] C.G. Liu, X.G. Chen, and H.J. Park. Self-assembled nanoparticles based on linoleic-acid modified chitosan: Stability and adsorption of trypsin. *Carbohydrate Polymers*, 62:293 – 298, 2005.

[85] J. Xu, S.P. McCarthy, and R. A. Gross. Chitosan film acylation and effects on biodegradability. *Macromolecules*, 29:3436 – 3440, 1996.

[86] S. Hirano, Y. Ohe, and H. Ono. Selective *n*-acylation of chitosan. *Carbohydrate Research*, 47:315 – 320, 1976.

[87] S. Dimida, C. Demitri, V.M. De Benedictis, F. Scalera, F. Gervaso, and A. Sannino. Genipin-cross-linked chitosan-based hydrogels: Reaction kinetics and structure-related characteristics. *Journal of Applied Polymer Science*, 132:42256, 2015.

[88] L. Félix, J. Hernández, W. Argüelles-Monal, and F.M. Goycoolea. Kinetics of gelation and thermal sensitivity of *n*-isobutyryl chitosan hydrogels. *Biomacromolecules*, 6: 2408 – 2415, 2005.

[89] A. Pawlak and M. Mucha. Thermogravimetric and ftir studies of chitosan blends. *Thermochimica Acta*, 396:153 – 166, 2003.

[90] D. de Britto and S.P. Campana-Filho. Kinetics of the thermal degradation of chitosan. *Thermochimica Acta*, 465:73 – 82, 2007.

[91] P.J. Flory. *Principles of Polymer Chemistry*. Cornell University Press, Ithica, New York, 1953.

[92] J.D. Ferry. *Viscoelastic Properties of Polymers*. John Wiley and Sons, USA, 1980.

[93] J. Berger, M. Reist, J.M. Mayer, O. Felt, N.A. Peppas, and R. Gurny. Structure and interactions in covalently and ionically crosslinked chitosan hydrogels for biomedical applications. *European Journal of Pharmaceutics and Biopharmaceutics*, 57:19 – 34, 2004.

[94] L.E. Nielsen. Cross-linking-effect on physical properties of polymers. *Journal of Macromolecular Science, Part C*, 3:69 – 103, 1969.

[95] C.G.T. Neto, J.A. Giacometti, A.E. Job, F.C. Ferreira, J.L.C. Fonseca, and M.R. Pereira. Thermal analysis of chitosan based networks. *Carbohydrate Polymers*, pages 97 – 103, 2005.

[96] C. Pandis, S. Madeira, J. Matos, A. Kyritsis, J.F. Mano, and J.L.G. Ribelles. Chitosan-silica hybrid porous membranes. *Materials Science and Engineering C*, 42:553 – 561, 2014.

[97] G. Sartor, E. Mayer, and G.P. Johari. Calorimetric studies of the kinetic unfreezing of molecular motions in hydrated lysozyme, hemoglobin, and myoglobin. *Biophysical Journal*, 66:249 – 258, 1994.

[98] K. Sakurai, T. Maegawa, and T. Takahashi. Glass transition temperature of chitosan and miscibility of chitosan/poly(n-vinyl pyrrolidone) blends. *Polymer*, 41:7051 – 7056, 2000.

[99] Y. Dong, Y. Ruan, H. Wang, Y. Zhao, and D. Bi. Studies on glass transition temperature of chitosan with four techniques. *Journal of Applied Polymer Science*, 93:1553 – 1558, 2004.

[100] S. Höhne, R. Frenzel, A. Heppe, and F. Simon. Hydrophobic chitosan microparticles: Heterogeneous phase reaction with hydrophobic carbonyl reagents. *Biomacromolecules*, 8:2051 – 2058, 2007.

[101] J.V. Azevedo, J.F. Mano, and N.M. Alves. Development of new poly(ϵ-caprolactone)/chitosan films. *Polymer International*, 62:1425 – 1432, 2013.

[102] M. Cai, J. Gong, J. Cao, Y. Chen, and X. Luo. In situ chemically crosslinked chitosan membrane by adipic acid. *Journal of Applied Polymer Science*, 128:3308 – 3314, 2013.

[103] Y. Feng and W. Xia. Preparation, characterization and antibacterial activity of water-soluble o-fumaryl-chitosan. *Carbohydrate Polymers*, 83:1169 – 1173, 2011.

[104] J. Coates. Interpretation of infrared spectra, a practical approach. In R.A. Meyers, editor, *Encyclopedia of Analytical Chemistry*, pages 10815 – 10837. John Wiley Sons Ltd., Chichester, 2000.

[105] D.Y. Pratt, L.D. Wilson, and J.A. Kozinski. Preparation and sorption studies of glutaraldehyde cross-linked chitosan copolymers. *Journal of Colloid and Interface Science*, 395:205 – 211, 2013.

[106] E.A. Ryan and A.M. Kropinski. Separation of amino sugars and related compounds by two-dimensional thin-layer chromatography. *Journal of Chromatography*, 195:127 – 132, 1980.

[107] S. Prochazkova, K.M. Vårum, and K. Østgaard. Quantitative determination of chitosans by ninhydrin. *Carbohydrate Polymers*, 38:115 – 122, 1999.

[108] M. Friedman. Applications of the ninhydrin reaction for analysis of amino acids, peptides, and proteins to agricultural and biomedical sciences. *Journal of Agricultural and Food Chemistry*, 52:385 – 406, 2004.

[109] F. Ganji, S.V. Farahani, and E.V. Farahani. Theoretical description of hydrogel swelling: A review. *Iranian Polymer Journal*, 19:375 – 398, 2010.

[110] X.Z. Shu and K.J. Zhu. Controlled drug release properties of ionically cross-linked chitosan beads: The influence of anion structure. *International Journal of Pharmaceutics*, 233:217 – 225, 2002.

[111] J. Vincent. *Structural Biomaterials*. Princeton University Press, New Jersey, third edition, 2012.

[112] V.V. Krongauz. Diffusion in polymers dependence on crosslink density. *Journal of Thermal Analysis and Calorimetry*, 102:435 – 445, 2010.

[113] L.E. Nielsen and R.F. Landel. *Mechanical Properties of Polymers and Composites*. Marcel Dekker, Inc., New York, second edition, 1994.

[114] G. Galietta, L. di Gioia, S. Guilbert, and B. Cuq. Mechanical and thermomechanical properties of films based on whey proteins as affected by plasticizer and crosslinking agents. *Journal of Dairy Science*, 81:3123 – 3130, 1998.

[115] D. Demirgöz, C. Elvira, J.F. Mano, A.M. Cunha, E. Piskin, and R.L. Reis. Chemical modification of starch based biodegradable polymeric blends: Effects on water uptake, degradation behaviour and mechanical properties. *Polymer Degradation and Stability*, 70:161 – 170, 2000.

[116] S.S. Silva, S.G. Caridade, J.F. Mano, and R.L. Reis. Effect of crosslinking in chitosan/aloe vera-based membranes for biomedical applications. *Carbohydrate Polymers*, 98:581 – 588, 2013.

[117] J.R. Mitchell. The rheology of gels. *Journal of Texture Studies*, 11:315 – 337, 1980.

[118] C. Tual, E. Espuche, M. Escoubes, and A. Domard. Transport properties of chitosan membranes: Influence of crosslinking. *Journal of Polymer Science: Part B: Polymer Physics*, 38:1521 – 1529, 2000.

[119] S. Beil, A. Schamberger, W. Naumann, S. Machill, and K.J. van Pée. Determination of the degree of *n*-acetylation (da) of chitin and chitosan in the presence of water by first derivative atr ftir spectropscopy. *Carbohydrate Polymers*, 87:117 – 122, 2012.

[120] M.L. Duarte, M.C. Ferreira, M.R. Marvão, and J. Rocha. An optimised method to determine the degree of acetylation of chitin and chitosan by ftir spectroscopy. *International Journal of Biological Macromolecules*, 31:1 – 8, 2002.

[121] G. Hollinger, L. Kuniak, and R.H. Marchessault. Thermodynamic aspects of the gelationization and swelling of crosslinked starch. *Biopolymers*, 13:879 – 890, 1974.

[122] I. Kolodziejska and B. Piotrowska. The water vapour permeability, mechanical properties and solubility of fish gelatin-chitosan films modified with transglutaminase or 1-ethyl-3-(3-dimethylaminopropyl) carbodiimide (edc) and plasticized with glycerol. *Food Chemistry*, 103:295 – 300, 2007.

[123] R.A.A. Muzzarelli. Genipin-crosslinked chitosan hydrogels as biomedical and pharmaceutical aids. *Carbohydrate Polymers*, 77:1 – 9, 2009.

[124] J. Xu, S. Strandman, J.X.X. Zhu, J. Barralet, and M. Cerruti. Genipin-crosslinked catechol-chitosan mucoadhesive hydrogels for buccal drug delivery. *Biomaterials*, 37: 395 – 404, 2015.

[125] A.A. Aldana, R. Toselli, M.C. Strumia, and M. Martinelli. Chitosan films modified selectively on one side with dendritic molecules. *Journal of Materials Chemistry*, 22: 22670 – 22677, 2012.

[126] F.L. Mi, C.T. Huang, H.F. Liang, M.C. Chen, Y.L. Chiu, C.H. Chen, and H.W. Sung. Physicochemical, antimicrobial, and cytotoxic characteristics of a chitosan film cross-linked by a naturally occurring cross-linking agent, aglycone geniposidic acid. *Journal of Agricultural Chemistry*, 54:3290 – 3296, 2006.

[127] T.Y. Hsien and G.L. Rorrer. Heterogeneous cross-linking of chitosan gel beads: Kinetics, modeling, and influence on cadmium ion adsorption capacity. *Industrial and Engineering Chemistry Research*, 36:3631 – 3638, 1997.

[128] Q. Yang, F. Dou, B. Liang, and Q. Shen. Studies of cross-linking reaction on chitosan fiber with glyoxal. *Carbohydrate Polymers*, 59:205 – 210, 2005.

[129] I. Kavianinia, P.G. Plieger, N.G. Kandile, and D.R.K. Harding. Preparation and characterization of chitosan films, crosslinked with symmetric aromatic dianhydrides to achieve enhanced thermal properties. *Polymer International*, 64:556 – 562, 2015.

[130] W.S.W. Ngah, L.C. Teong, and M.A.K.M. Hanafiah. Adsorption of dyes and heavy metal ions by chitosan composites: A review. *Carbohydrate Polymers*, 83:1446 – 1456, 2011.

[131] W.S.W. Ngah, M.A.K.M. Hanafiah, and S.S. Yong. Adsorption of humic acid from aqueous solutions on crosslinked chitosan-epichlorohydrin beads: Kinetics and isotherm studies. *Colloids and Surfaces B: Biointerfaces*, 65:18 – 24, 2008.

[132] J.S. Marques, J.A.O.D. Chagas, J.L.C. Fonseca, and M.R. Pereira. Comparing homogeneous and heterogeneous routes for ionic crosslinking of chitosan membranes. *Reactive and Functional Polymers*, 103:156 – 161, 2016.

[133] C. Demitri, R. Del Sole, F. Scalera, A. Sannino, G. Vasapollo, A. Maffezzoli, L. Ambrosio, and L. Nicolais. Novel superabsorbent cellulose-based hydrogels crosslinked with citric acid. *Journal of Applied Polymer Science*, 110:2453 – 2460, 2008.

[134] X.Z. Shu, K.J. Zhu, and W. Song. Novel ph-sensitive citrate cross-linked chitosan film for drug controlled release. *International Journal of Pharmaceutics*, 212:19 – 28, 2001.

[135] S.M. Gawish, S.M. Abo El-Ola, A.M. Ramadan, and A.A. Abou El-Kheir. Citric acid used as a crosslinking agent for the grafting of chitosan onto woolen fabric. *Journal of Applied Polymer Science*, 123:3345 – 3353, 2012.

[136] T. Furuike, D. Komoto, H. Hashimoto, and H. Tamura. Preparation of chitosan hydrogel and its solubility in organic acids. *International Journal of Biological Macromolecules*, 104:1620 – 1625, 2017.

[137] S. Kim, M.E. Nimni, Z. Yang, and B. Han. Chitosan/gelatin-based films crosslinked by proanthocyanidin. *Journal of Biomedical Materials Research Part B: Applied Biomaterials*, 75B:442 – 450, 2005.

[138] H.M. Fahmy and M.M.G. Fouda. Crosslinking of alginic acid/chitosan matrices using polycarboxylic acids and their utilization for sodium diclofenac release. *Carbohydrate Polymers*, 73:606 – 611, 2008.

[139] V. Coma, I. Sebti, P. Pardon, F.H. Pichavant, and A. Deschamps. Film properties from crosslinking of cellulosic derivatives with a polyfunctional carboxylic acid. *Carbohydrate Polymers*, 51:265 – 271, 2003.

[140] N. Reddy, Q. Jiang, and Y. Yang. Preparation and properties of peanut protein films crosslinked with citric acid. *Industrial Crops and Products*, 39:26 – 30, 2012.

[141] B. Wepner, E. Berghofer, E. Miesenberger, K. Tiefenbacher, and P.N.K. Ng. Citrate starch-application as resistant starch in different food systems. *Starch/Stärke*, 51: 354 – 361, 1999.

[142] Y.S. Chung, Lee K.K., and J.W. Kim. Durable press and antimicrobial finishing of cotton fabrics with a citric acid and chitosan treatment. *Textile Research Journal*, 68:772 – 775, 1998.

[143] S.H. Hsieh, F.R. Zhang, and H.S. Li. Anti-ultraviolet and physical properties of woolen fabrics cured with citric acid and tio_2/chitosan. *Journal of Applied Polymer Science*, 100:4311 – 4319, 2006.

[144] B. Martel, M. Weltrowski, D. Ruffin, and M. Morcellet. Polycarboxylic acids as crosslinking agents for grafting cyclodextrins onto cotton and wool fabrics: Study of the process parameters. *Journal of Applied Polymer Science*, 83:1449 – 1456, 2002.

[145] C.M. Welch and B.A.K. Andrews. Ester crosslinks: A route to high performance nonformaldehyde finishing of cotton. *Textile Chemist and Colorist*, 21:13 – 17, 1989.

[146] X. Gu and C.Q. Yang. Ftir spectroscopy of the formation of cyclic anhydride intermediates of polycarboxylic acids catalyzed by sodium hypophosphite. *Textile Research Journal*, 70:64 – 70, 2000.

[147] Z. Cui, E.S. Beach, and P.T. Anastas. Modification of chitosan films with environmentally benign reagents for increased water resistance. *Green Chemistry Letters and Reviews*, 4:35 – 40, 2011.

[148] B. Ghanbarzadeh, H. Almasi, and A.A. Entezami. Improving the barrier and mechanical properties of corn starch-based edible films: Effect of citric acid and carboxymethyl cellulose. *Industrial Crops and Products*, 33:229 – 235, 2011.

[149] E. Olsson, M.S. Hedenqvist, C. Johansson, and L. Järnström. Influence of citric acid and curing on moisture sorption, diffusion and permeability of starch films. *Carbohydrate Polymers*, 94:765 – 772, 2013.

[150] G.A.F. Roberts and K.E. Taylor. The formation of gels by reaction of chitosan with glutaraldehyde. *Makromolekulare Chemie*, 190:951 – 960, 1989.

[151] M.F. Butler, Y.F. Ng, and P.D.A. Pudney. Mechanism and kinetics of the crosslinking reaction between biopolymers containing primary amine groups and genipin. *Journal of Polymer Science: Part A: Polymer Chemistry*, 41:3941 – 3953, 2003.

[152] Y.C. Wei, M. Hudson, J.M. Mayer, and D.L. Kaplan. The crosslinking of chitosan fibers. *Journal of Polymer Science: Part A: Polymer Chemistry*, 30:2187 – 2193, 1992.

[153] Y. Zhong, J. Li, Y. Gong, N. Zhao, and X. Zhang. Feasability of using chitosan in nerve repair. *Tsinghua Science and Technology*, 5:432 – 435, 2000.

[154] D.E.S. Santos, C.G.T. Neto, J.L.C. Fonseca, and M.R. Pereira. Chitosan macroporous asymmetric membranes - preparation, characterization and transport drugs. *Journal of Membrane Science*, 325:362 – 370, 2008.

[155] H.A. Kramers. Diffusion of light by atoms. *Atti del Congresso Internationale dei Fisici, Como*, 2:545 – 557, 1927.

[156] L. Rouleau, J.F. Deü, A. Legay, and F. Le Lay. Application of kramers-kronig relations to time-temperature superposition for viscoelastic materials. *Mechanics for Materials*, 65:66 – 75, 2013.

[157] H.C. Booij and G.P.J Thoone. Generalization of kramers-kronig transforms and some approximations of relations between viscoelastic quantities. *Rheologica Acta*, 21:15 – 24, 1982.

[158] G.P. Johari. Electrode-spacer and other effects on the validity of the kramers-kronig relations and the fittings to the permittivity and electrical modulus spectra. *Thermochimica Acta*, 547:47 – 52, 2012.

[159] A.M. Kloxin, C.J. Kloxin, C.N. Bowman, and K.S. Anseth. Mechanical properties of cellularly responsive hydrogels and their experimental determination. *Advanced Materials*, 22:3484 – 3494, 2010.

[160] J.E. Mark. The rubber elastic state. In J.E. Mark, editor, *Physical Properties of Polymers*, chapter 1, pages 1 – 70. Cambridge University Press, Cambridge, United Kingdom, third edition, 2004.

[161] P.J. Flory. Molecular theory of rubber elasticity. *Polymer Journal*, 17:1 – 12, 1985.

[162] B. Erman and M. James. *Structures and Properties of Rubberlike Networks*. Oxford University Press, New York, New York, first edition, 1997.

[163] A. Rogalsky. *Development of an Injectable Hybrid-Hydrogel using Oxidised-Alginate and N-Succinyl-Chitosan*. PhD thesis, University of Waterloo, 2016.

[164] A.H. Bedane, M. Eic, M. Farmahini-Farahani, and H. Xiao. Water vapor transport properties of regenerated cellulose and nanofibrillated cellulose films. *Journal of Membrane Science*, 493:46 – 57, 2015.

[165] F. Debeaufort, M. Martin-Polo, and A. Voilley. Polarity homogeniety and structure affect water vapor permeability of model edible films. *Journal of Food Science*, 58: 426 – 429, 1993.

[166] T.B. McHugh, R. Avena-Bustillos, and J.M. Krochta. Hydrophilic edible films: Modified procedure for water vapor permeability and explanation of thickness effects. *Journal of Food Science*, 58:899 – 903, 1993.

[167] ASTM International. E96/e96m - 15: Standard test methods for water vapor transmission of materials, 2015.

[168] A. Gennadios, C.L. Weller, and C.H. Gooding. Measurement errors in water vapor permeability of highly permeable, hydrophilic edible films. *Journal of Food Engineering*, 21:395 – 409, 1994.

[169] T. Janjarasskul and J.M. Krochta. Edible packaging materials. *Annual Review of Food Science and Technology*, 1:415 – 448, 2010.

[170] D. Lafargue, B. Pontoire, A. Buléon, J.L. Doublier, and D. Lourdin. Structure and mechanical properties of hydroxypropylated starch films. *Biomacromolecules*, 8:3950 – 3958, 2007.

[171] L.E. Nielsen. *Mechanical Properties of Polymers and Composites*, volume 2. Marcel Dekker, Inc., New York, 1974.

[172] A. Jansson and F. Thuvander. Influence of thickness on the mechanical properties for starch films. *Carbohydrate Polymers*, 56:499 – 503, 2004.

[173] D. Owens and R. Wendt. Estimation of the surface free energy of polymers. *Journal of Applied Polymer Science*, 13:1741 – 1747, 1969.

[174] Krüss. Models for surface free energy calculation - technical note 306. Retrieved from `https://www.kruss-scientific.com/fileadmin/user_upload/website/literature/kruss-tn306-en.pdf`, 1999.

[175] S. Sahin and S.G Sumnu. *Physical Properties of Foods*. Springer Science+Business Media, New York, USA, 2006.

[176] E.O. Timmerman, J. Chirife, and H.A. Iglesias. Water sorption isotherms of foods and foodstuffs: Bet or gab parameters? *Journal of Food Engineering*, 48:19 – 31, 2001.

[177] N. Wang and J.G. Brennan. Moisture sorption isotherm characteristics of potatoes at four temperatures. *Journal of Food Engineering*, 14:269 – 287, 1991.

[178] K.M. Vårum, M.H. Ottøy, and O. Smidsrød. Acid hydrolysis of chitosans. *Carbohydrate Polymers*, 46:89 – 98, 2001.

[179] A.V. Il'ina and V.P. Varlamov. Hydrolysis of chitosan in lactic acid. *Applied Biochemistry and Microbiology*, 40:300 – 303, 2004.

[180] W. Argüelles-Monal and C. Peniche-Covas. Preparation of a novel polyampholyte from chitosan and citric acid. *Makromolekulare Chemie, Rapid Communications*, 14: 735 – 740, 1993.

[181] L. Fernández-de Castro, M. Mengíbar, A. Sánchez, L. Arroya, M.C. Villarán, E.D. de Apodaca, and A. Heras. Films of chitosan and chitosan-oligosaccharide neutralized and thermally treated: Effects on its antibacterial and other activities. *LWT - Food Science and Technology*, 73:368 – 374, 2016.

[182] E.A. Takara, J. Marchese, and N.A. Ochoa. Naoh treatment of chitosan films: Impact on macromolecular structure and film properties. *Carbohydrate Polymers*, 132:25 – 30, 2015.

[183] F.A. Corsello, P.A. Bolla, P.S. Anbinder, M.A. Serradell, J.I. Amalvy, and P.J. Peruzzo. Morphology and properties of neutralized chitosan-cellulose nanocrystals biocomposite films. *Carbohydrate Polymers*, 156:452 – 459, 2017.

[184] G.C. Ritthidej, T. Phaechamud, and T. Koizumi. Moist heat treatment on physicochemical change of chitosan salt films. *International Journal of Pharmaceutics*, 232:11 – 22, 2002.

[185] J. Nunthanid, S. Puttipipatkhacorn, K. Yamamoto, and G.E. Peck. Physical properties and molecular behaviour of chitosan films. *Drug Development and Industrial Pharmacy*, 27:143 – 157, 2001.

[186] I. Leceta, P. Guerrero, and K. de la Caba. Functional properties of chitosan-based films. *Carbohydrate Polymers*, 93:339 – 346, 2013.

[187] F.C. Oliveira, A. Barros-Timmons, and J. Lopes-da Silva. Preparation and characterization of chitosan/sio_2 composite films. *Journal of Nanoscience and Nanotechnology*, 10:2816 – 2825, 2010.

[188] J. Khouri, A. Penlidis, and C. Moresoli. Viscoelastic properties of crosslinked chitosan films. *Processes*, 7:157, 2019.

[189] C. Gartner, B.L. López, L. Sierra, R. Graf, H.W. Spiess, and M. Gaborieau. Interplay between structure and dynamics in chitosan films investigated with solid-state nmr, dynamic mechanical analysis, and x-ray diffraction. *Biomacromolecules*, 12:1380 – 1386, 2011.

[190] M. Pizzoli, G. Ceccorulli, and M. Scandola. Molecular motions of chitosan in the solid state. *Carbohydrate Research*, 222:205 – 213, 1991.

[191] M.T. Viciosa, M. Dionisio, R.M. Silva, R.L. Reis, and J.F. Mano. Molecular motions in chitosan studied by dielectric relaxation spectroscopy. *Biomacromolecules*, 5:2073 – 2078, 2004.

[192] L.Y. Lim and L.S.C. Wan. Heat treatment of chitosan films. *Drug Development and Industrial Pharmacy*, 21:839 – 846, 1995.

[193] A. Toffey, G. Samaranayake, C.E. Frazier, and W.G. Glasser. Chitin derivatives. i. kinetics of the heat-induced conversion of chitosan to chitin. *Journal of Applied Polymer Science*, 60:75 – 85, 1996.

[194] A. Toffey and W.G. Glasser. Chitin derivatives. ii. time-temperature-transformation cure diagrams of the chitosan amidization process. *Journal of Applied Polymer Science*, 73:1879 – 1889, 1999.

[195] A. Toffey and W.G. Glasser. Chitin derivatives. iii. formation of amidized homologs of chitosan. *Cellulose*, 8:35 – 47, 2001.

[196] J.S. Park and E. Ruckenstein. Viscoelastic properties of plasticized methylcellulose crosslinked methylcellulose. *Carbohydrate Polymers*, 46:373 – 381, 2001.

[197] H.T. Chiu, R.L. Chen, P.Y. Wu, T.Y. Chiang, and S.C. Chen. A study on the effects of the degree of deacetylation of chitosan films on physical and antibacterial properties. *Polymer-Plastics Technology and Engineering*, 46:1121 – 1127, 2007.

[198] J.A.P. da Silva and C.A.N.S. Santos. Linear viscoelastic behaviour of chitosan films as influenced by changes in biopolymer structure. *Journal of Polymer Science Part B Polymer Physics*, 45:1907 – 1915, 2007.

[199] W. Cao, D. Jing, J. Li, Y. Gong, N. Zhao, and X. Zhang. Effects of the degree of deacetylation on the physicochemical properties and schwann cell affinity of chitosan films. *Journal of Biomaterials Applications*, 20:157 – 177, 2005.

[200] Z. Liu, X. Ge, Y. Lu, S. Dong, Y. Zhao, and M. Zeng. Effects of chitosan molecular weight and degree of deacetylation on the properties of gelatine-based films. *Food Hydrocolloids*, 26:311 – 317, 2012.

[201] M.A. Zotkin, G.A. Vikhoreva, T.V. Smotrina, and M.A. Derbenev. Thermal modification and study of the structure of chitosan films. *Fibre Chemistry*, 36:16 – 20, 2004.

[202] L.Y. Lim, E. Khor, and C.E. Ling. Effects of dry heat and saturated steam on the physical properties of chitosan. *Journal of Biomedical Materials Research*, 48:111 – 116, 1999.

[203] S. Rivero, M.A. García, and A. Pinotti. Heat treatment to modify the structural and physical properties of chitosan-based films. *Journal of Agricultural and Food Chemistry*, 60:492 – 499, 2012.

[204] R.H. Chen, J.H. Lin, and M.H. Yang. Relationships between the chain flexibilities of chitosan molecules and the physical properties of their casted films. *Carbohydrate Polymers*, 24:41 – 46, 1994.

[205] I. Quijada-Garrido, V. Iglesias-González, J.M. Mazón-Arechederra, and J.M. Barrales-Rienda. The role played by the interactions of small molecules with chitosan and their transition temperature. glass-forming liquids: 1,2,3-propantriol (glycerol). *Carbohydrate Polymers*, 68:173 – 186, 2007.

[206] J. Zawadzki and H. Kaczmarek. Thermal treatment of chitosan in various conditions. *Carbohydrate Polymers*, 80:394 – 400, 2010.

[207] I. Corazzari, R. Nistrico, F. Turci, M.G. Faga, F. Franzoso, S. Tabasso, and G. Magnacca. Advanced physico-chemical characterization of chitosan by means of tga coupled on-line with ftir and gcms: Thermal degradation and water adsorption capacity. *Polymer Degradation and Stability*, 112:1 – 9, 2015.

[208] V. Rubentheren, T.A. Ward, C.Y. Chee, P. Nair, E. Salami, and C. Fearday. Effects of heat treatment on chitosan nanocomposite film reinforced with nanocrystalline cellulose and tannic acid. *Carbohydrate Polymers*, 140:202 – 208, 2016.

[209] S. Rivero, L. Damonte, M.A. García, and A. Pinotti. An insight into the role of glycerol in chitosan films. *Food Biophysics*, 11:117 – 127, 2016.

[210] M. Mucha and A. Pawlak. Thermal analysis of chitosan and its blends. *Thermochimica Acta*, 427:69 – 76, 2005.

[211] V. Epure, M. Griffon, E. Pollet, and L. Averous. Structure and properties of glycerol-plasticized chitosan obtained by mechanical kneading. *Carbohydrate Polymers*, 83:947 – 952, 2011.

[212] L.S. Casey and L.D. Wilson. Investigation of chitosan-pva composite films and their adsorption properties. *Journal of Geoscience and Environment Protection*, 3:78 – 84, 2015.

[213] D.M. Correia, M.A. Gámiz-González, G. Botelho, A. Vidaurre, J.L. Gomez Ribelles, Lanceros-Mendez, and V. Sencadas. Effect of neutralization and cross-linking on the thermal degradation of chitosan electrospun membranes. *Journal of Thermal Analysis and Calorimetry*, 117:123 – 130, 2014.

[214] J.L.A Cousineau. Production and characterization of wheat gluten films. Master's thesis, University of Waterloo, 2012.

[215] P. Köll, G. Borchers, and J.O. Metzger. Thermal degradation of chitin and cellulose. *Journal of Analytical and Applied Pyrolysis*, 1991:119 – 129, 1991.

[216] M. Jang, B. Kong, Y. Jeong, C. Lee, and J. Nah. Physicochemical characterization of α-chitin, β-chitin, and γ-chitin separated from natural resources. *Journal of Applied Polymer Science: Part A: Polymer Chemistry*, 42:3423 – 3432, 2004.

[217] I.C. Libio, R. Demori, M.I.Z. Ferrão, Lionzo, and N.P. da Silveira. Film based on neutralized chitosan citrate as innovative composition for cosmetic application. *Materials Science and Engineering C*, 67:115 – 124, 2016.

[218] M. Liu, Y. Zhou, Y. Zhang, C. Yu, and S. Cao. Physicochemical, mechanical and thermal properties of chitosan films with and without sorbitol. *International Journal of Biological Macromolecules*, 70:340 – 346, 2014.

[219] R.Y. Aguirre-Loredo, A.I. Rodríguez-Hernández, E. Morales-Sánchez, C.A. Gómez-Aldapa, and G. Velazquez. Effect of equilibrium moisture content on barrier, mechanical and thermal properties of chitosan films. *Food Chemistry*, 196:560 – 566, 2016.

[220] M.G.N. Campos, L.H.I. Mei, and A.R. Santos. Sorbitol-plasticized and neutralized chitosan membranes as skin substitutes. *Materials Research*, 18:781 – 790, 2015.

[221] M.A. Bertuzzi, E.F. Castro Vidaurre, M. Armada, and J.C. Gottifredi. Water vapor permeability of edible starch based films. *Journal of Food Engineering*, 80:972 – 978, 2007.

[222] J.M. Krochta. Control of mass transfer in foods with edible coatings and films. In R.P. Singh and M.A. Wirakartakasumah, editors, *Advances in Food Engineering*, pages 517 – 538. CRC Press, Boca Raton, FL, USA, 1992.

[223] A. Lazaridou and C.G. Biliaderis. Thermoplastic properties of chitosan, chitosan-starch and chitosan-pullulan films near the glass transition. *Carbohydrate Polymers*, 48:179 – 190, 2002.

[224] I. Arvanitoyannis, A. Nakayama, and S-I. Aiba. Chitosan and gelatin based edible films: State diagrams, mechanical and permeation properties. *Carbohydrate Polymers*, 37:371 – 382, 1998.

[225] K. Sakurai, A. Minami, and T. Takahashi. Crystal structure of chitosan. i. unit cell parameters. *Sen'i Gakkaishi*, 40:246 – 253, 1984.

[226] F. Chen, M. Gällstedt, R.T. Olsson, U.W. Gedde, and M.S. Hedenqvist. Unusual effects of monocarboxylic acids on the structure and on the transport and mechanical properties of chitosan films. *Carbohydrate Polymers*, 132:419 – 429, 2015.

[227] W. Chang, F. Liu, H.R. Sharif, Z. Huang, H.D. Goff, and F. Zhong. Preparation of chitosan films by neutralization for improving their preservation effects on chilled meat. *Food Hydrocolloids*, 90:50 – 61, 2019.

[228] I. Leceta, P. Arana, P. Guerrero, and K. de la Caba. Structure-moisture sorption relation in chitosan thin films. *Materials Letters*, 128:125 – 127, 2014.

[229] J.A. Ratto, C.C. Chen, and R.B. Blumstein. Phase behaviour study of chitosan/polyamide blends. *Journal of Applied Polymer Science*, 59:1451 – 1461, 1996.

[230] K. Okuyama, K. Noguchi, M. Kanenari, T. Egawa, K. Osawa, and K. Ogawa. Structural diversity of chitosan and its complexes. *Carbohydrate Polymers*, 41:237 – 247, 2000.

[231] B. Crist. The ultimate strength and stiffness of polymers. *Annual Review of Materials Science*, 25:295 – 323, 1995.

[232] R.J. Moon, A. Martini, J. Nairn, J. Simonsen, and J. Youngblood. Cellulose nanomaterials review: Structure properties and nanocomposites. *Chemical Society Reviews*, 40:3941 – 3994, 2011.

[233] C. Caner, P.J. Vergano, and J.L. Wiles. Chitosan film mechanical and permeation properties as affected by acid, plasticizer, and storage. *Journal of Food Science*, 63: 1049 – 1053, 1998.

[234] B. Smitha, S. Sridhar, and A.A. Khan. Chitosan-sodium alginate polyion complexes as fuel cell membranes. *European Polymer Journal*, 41:1859 – 1866, 2005.

[235] P.M. Doty, W.H. Aiken, and H. Mark. Temperature dependence of water vapor permeability. *Industrial and Engineering Chemistry*, 38:788 – 791, 1946.

[236] S.W. Lasoski and W.H. Cobbs. Moisture permeability of polymers. i. role of crystallinity and orientation. *Journal of Polymer Science*, 36:21 – 33, 1959.

[237] F. Debeaufort, A. Voilley, and P. Meares. Water vapor permeability and diffusivities through methylcellulose edible films. *Journal of Membrane Science*, 91:125 – 133, 1994.

[238] Y. Nakano, Y. Bin, M. Bando, T. Nakashima, T. Okuna, H. Kurosu, and M. Matsuo. Structure and mechanical properties of chitosan. *Macromolecular Symposia*, 258:63 – 81, 2007.

[239] S. Volpe, S. Cavella, P. Masi, and E. Torrieri. Effect of solid concentration on structure and properties of chitosan-caseinate blend films. *Food Packaging and Shelf Life*, 13:76 – 84, 201.

[240] K. Sakurai, M. Takugi, and T. Takahashi. Sorption of water vapor by chitosan membranes. *Sen'i Gakkaishi*, 40:425 – 430, 1984.

[241] B. Ouattara, R.E. Simard, G. Piette, A. Bégin, and R.A. Holley. Diffusion of acetic and propionic acids from chitosan-based antimicrobial packaging films. *Journal of Food Science*, 65:768 – 773, 2000.

[242] TA-Instruments. Thermal solutions: Determination of the linear viscoelastic region of a polymer using a strain sweep on the dma 2980. Retrieved from `http://http://www.tainstruments.com/pdf/literature/TS61.pdf`, No Date Given.

[243] TA-Instruments. Rheology solutions: Determining the linear viscoelastic region in polymers. Retrieved from `http://www.tainstruments.com/pdf/literature/RS23.pdf`, No Date Given.

[244] W. Ruland. X-ray determination of crystallinity and diffuse disorder scattering. *Acta Crystallophica*, 14:1180 – 1185, 1961.

[245] S. Park, J.O. Baker, M.E. Himmel, P.A. Parilla, and D.K. Johnson. Cellulose crystallinity index: Measurement techniques and their impact on interpreting cellulase performance. *Biotechnology for Biofuels*, 3:1 – 10, 2010.

[246] M.Y. Ioelovich and G.P. Veveris. Determination of cellulose crystallinity by x-ray diffraction method. *Journal of Wood Chemistry*, 5:72 – 80, 1987.

[247] S. Nara and T. Komiya. Studies on the relationship between water-saturated state and crystallinity by the diffraction method for moistened potato starch. *Starch/Stärke*, 35:407 – 410, 1983.

[248] P.C. Srinivasa, M.N. Ramesh, K.R. Kumar, and R.N. Tharanathan. Properties of chitosan films prepared under different drying conditions. *Journal of Food Engineering*, 63:79 – 85, 2004.

Appendix A

Additional Experimental Data

A.1 Dissolved Gases

Degassing method and drying environment of the filmogenic solutions impacts the extent of retained gases in the dried films, which impact the physical properties. Entrapped gases were photographed by a light microscope. A Nikon Eclipse MA200 light microscope (Nikon Corp., Japan) and NIS-Elements Documentation software (5× viewing magnitude). Figure A.1 shows images of un-degassed and degassed neat films dried in an environmental chamber and fume hood. The images were analyzed using MATLAB's *imfindcircles* function in the 'image processing toolbox' to determine bubble diameter and number of bubbles per unit area. Average bubble diameter was 24 to 29 ± 5 μm, irrespective of degassing, and diameter ranged from 10 to 52 μm. Films dried in the fume hood yielded the lowest concentration of bubbles. Films dried in the fume hood had an average bubble count less than 1 bubbles/mm^2, and those dried in the chamber averaged between 1.5 and 6.2 bubbles/mm^2. Degassing using a vacuum aspirator followed by drying in a fume hood can be as effective if not more than drying in a vacuum oven or degassing with a centrifuge.

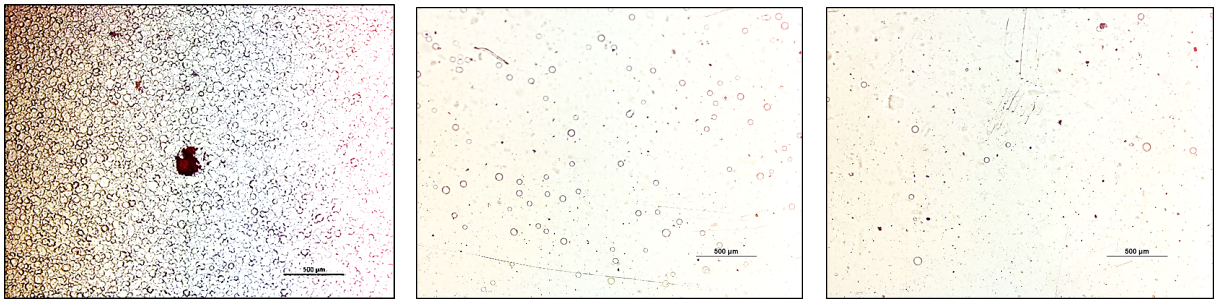

(A) No degas (B) Degassed, chamber dried (C) Degassed, fume hood

Figure A.1: Microscope images (with a 500 μm scale bar) of (A) an un-degassed neat film dried in an environmental chamber, (B) a degassed film dried in an environmental chamber and (C) a degassed film dried in a fume hood.

A.2 TGA

The second loss event between 150 and 200 °C in a DTGA scan of a neat film is related to residual acetic acid. A comparison of film specimens conditioned for different durations was performed. See Figure A.2. After aging for 7 days the peak magnitude diminished slightly, due to partial evaporation of acetic acid molecules out of the film. At 200 °C, the difference in mass loss between the two films is ~ 3 %. This lower mass loss is entirely from lower acetic acid content acid as the water evaporation trajectory remains unchanged.

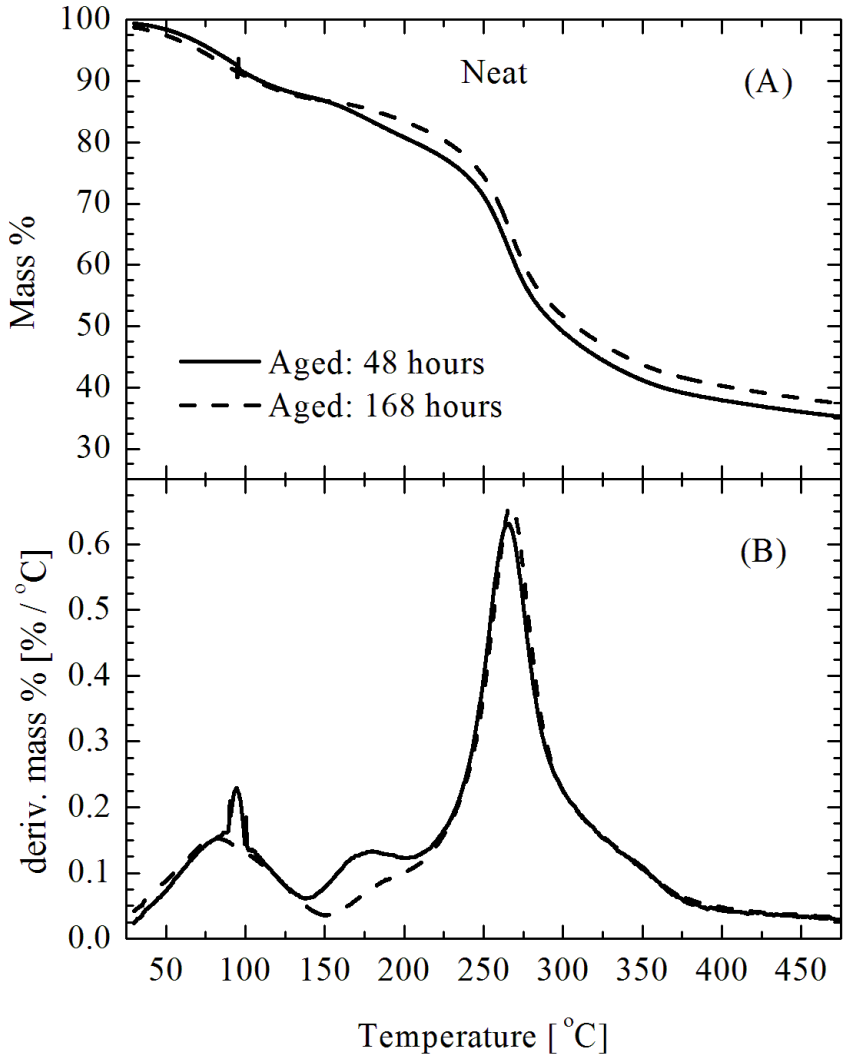

Figure A.2: (A) Mass percentage plotted against temperature and (B) corresponding first derivative for two neat film specimens, one conditioned for 48 h, and the other for 168 h (7 days).

A.3 Linear Viscoelastic Region of Chitosan Films

The range of elongation in which storage modulus is independent of the strain is the Linear Viscoelastic Region (LVR). Determining the LVR of the films at the onset temperature assists in selecting an appropriate strain for the set of DMA experiments on the films.

To determine the LVR, the chitosan films were equilibrated at 30 °C and held isothermally for 5 min. An amplitude sweep was performed under the 'Multi-Strain' mode, from 5 to 30 µm in step-wise increments of 1 µm. The films tested included neat, neutralized, CA film, and a polyethylene terephthalate (PETE) film. The film thickness was approximately 100 µm for the chitosan films, and 230 µm for the PETE film. The plots of the E' (log-scale) against strain are shown in Figure A.3A.

The storage modulus of the PETE film is fairly constant over the range of tested strain values. The E' of the neat, neutralized, and CA chitosan films increased significantly and began to plateau above 0.10 % strain. A 5 % depression from the initial maximum E' value is defined as the LVR [242, 243]. Using this requirement and the plateau value from the curves in Figure A.3, the LVRs for neat, neutralized and CA films were estimated to be above 0.10, 0.11 and 0.06 % respectively. The chitosan films were additionally preheated at 150 °C for 10 min and then tested to see the effect of moisture on the viscoelastic behavior; those plots are given in Figure A.3B.

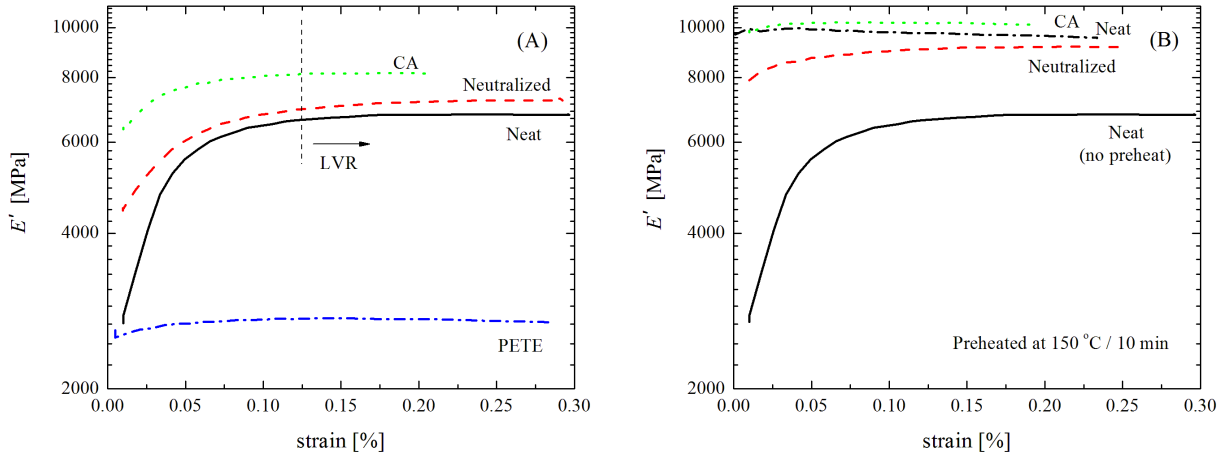

Figure A.3: The storage modulus, E', (log-scale) at increasing strain values for (A) neat, neutralized, CA and PETE films and (B) neat, neutralized, and CA films previously heated at 150 °C for 10 min to reduce film moisture content. Films were strained at a fixed frequency of 1 Hz and constant temperature of 30 °C.

The large increase in E' at low strain values is in contrast to the behavior of many polymers which show a decline with increasing elongation. To test whether this increase in E' was characteristic of chitosan, or due to the strain value, or due to the evaporation

of moisture from the film during the experiment, which would yield a stiffer material from reduced plasticization, a dynamic stress relaxation experiment was performed. The samples were tested at 30 °C for 30 to 60 min. Chitosan films were tested at two strain values, 0.05 and 0.15 %, and a third for a preheated specimen to see moisture effects. These were compared with a PETE film, as show in Figure A.4. The curves in Figure A.4 demonstrate that the increase in E' with time is independent of strain value, it is attributable to moisture evaporating out of the films. Preheating films yields a wider LVR.

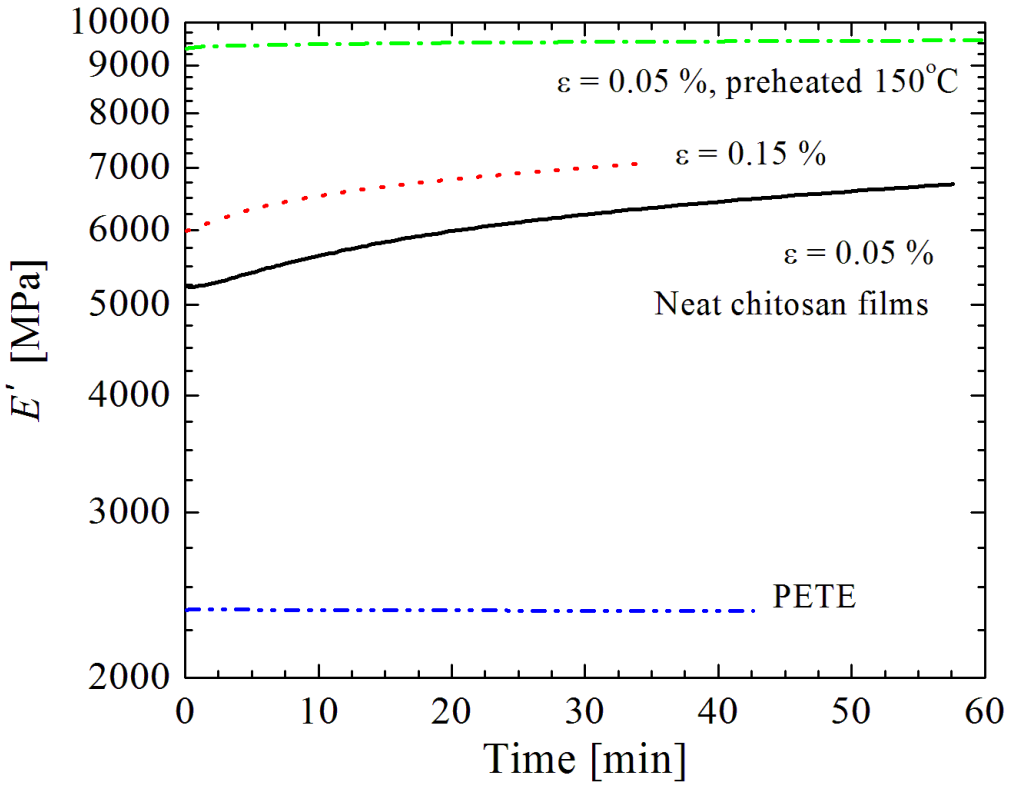

Figure A.4: The storage modulus, E', (log-scale) of stress relaxation tests for neat chitosan films strained at 0.05 and 0.15 %, and a PETE film strained at 0.05 %. A chitosan film was also preheated at 150 °C for 10 min and strained at 0.05 %.

A.4 Water Vapor Permeability Data

A.4.1 Plots for Water Vapor Transmission Rate

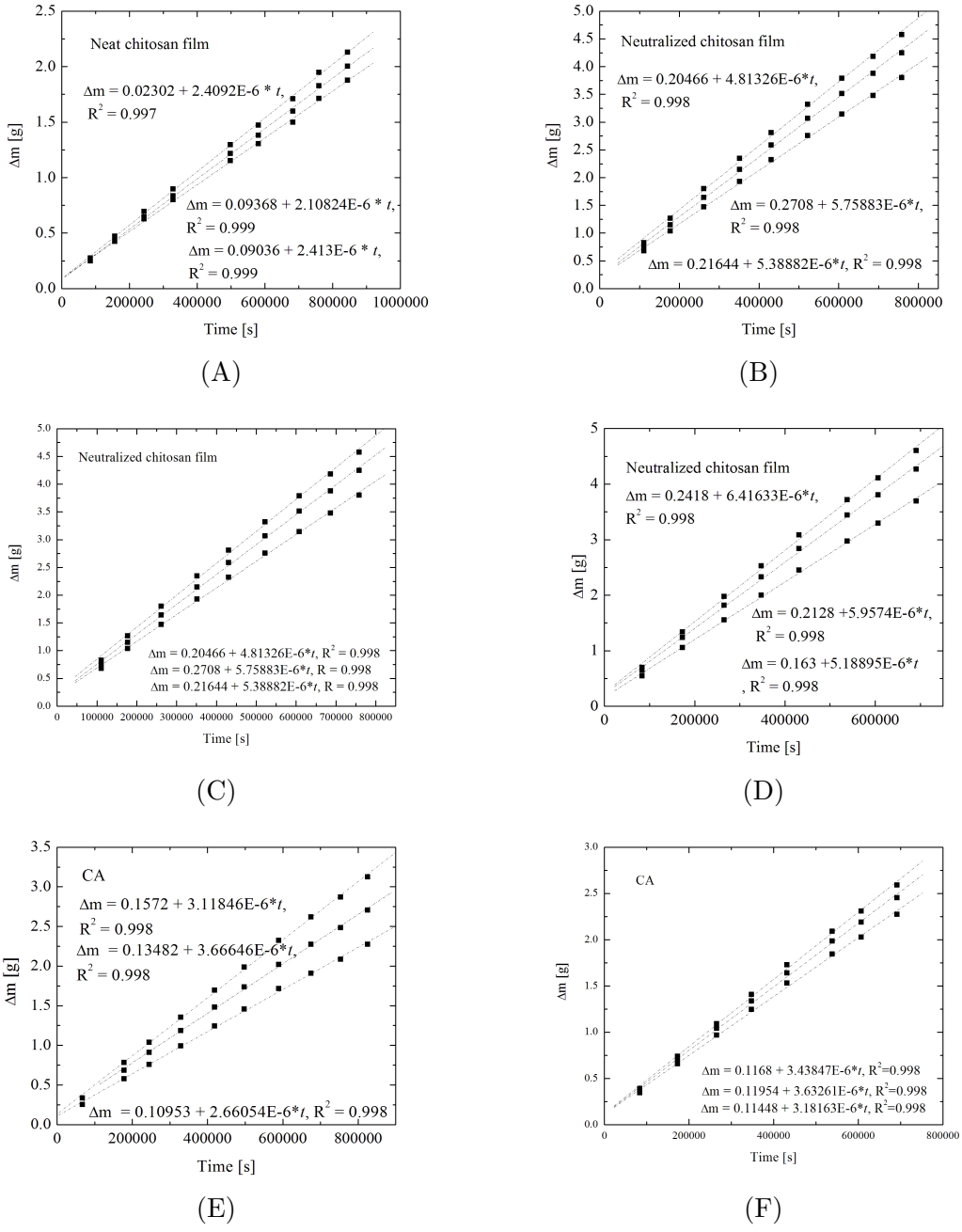

Figure A.5: Mass change with time plots with samples from (A) neat bulk film 1 (B) neat bulk film 2 (C) neutralized bulk film 1 (D) neutralized bulk film 2 (E) CA bulk film 1 and (F) CA bulk film 2.

A.4.2 Film Orientation in WVP Test Cup

From Section 6.3.2: The WVP could be influenced by surface roughness of the films, as the surface characteristics depend on the drying conditions and casting tray material. Here, the air - exposed side of the films have a rougher contour than the one from the film - glass tray interface. To test if there is bias in the WVP measurement stemming from the orientation of the sample in the test cup, the WVP of two neat specimens, cut from the same film, were measured, one with the rough surface facing inwards towards the desiccant, the other with the smooth surface facing inwards. The difference in WVP between the two samples of different orientation in the sample cup was small, 0.23×10^{-11} g/m·s·Pa, or 3.9 %. Since this value is less than the standard deviation for the WVP of neat films (10.5 % COV, Section 6.3.2), film orientation does not appear to bias the WVP value.

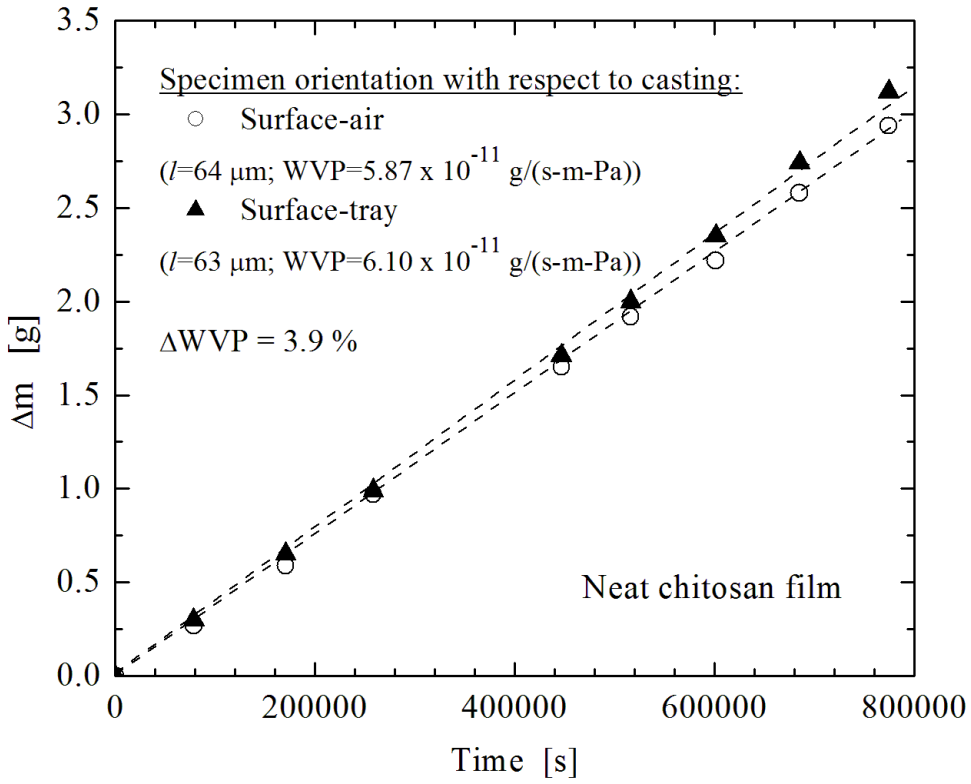

Figure A.6: The mass change of two neat chitosan specimens with time for a WVP measurement. The specimens came from the same film. The orientation of the specimens in the test cup were: film surface-air interface side (rough) facing inwards, and film surface-tray interface side (smooth) facing inwards. No significant difference was observed for WVP between these two specimens, < 4 %.

A.4.3 Stagnant Air Correction

Stagnant Air Correction - Method 1 (ASTM E96) [167]:

The measured WVP is inversely proportional to the resistance of moisture diffusion. The film specimen, stagnant air, and surfaces inside and outside of the specimen account for the paths of resistance.

$$R_{\text{mea}} = R_{\text{sp}} + R_{\text{air}} + R_{\text{surface}} \tag{A.1}$$

where R_{i} is resistance of source i, and subscripts *sp* and *mea* correspond to 'test specimen' and 'measured', respectively. Each resistance term is the inverse of its respective permeance, $R_{\text{i}} = \Pi_{\text{i}}^{-1}$, where i is the form of resistance or permeance. The permeance of still air, Π_{air}, is equal to permeability, P_{air}, divided by the thickness of the still air layer (as with Eq. 3.20). The relationship of permeability of moisture from the layer of air between film underside and desiccant to temperature and pressure is given by:

$$\text{P}_{\text{air}} = \frac{2.306 \times 10^{-5}\ \text{m}^2/\text{s} \times p_{\text{o}}}{p \times R \times T} \left(\frac{T}{273.15\ \text{K}} \right)^{1.81} \tag{A.2}$$

where P_{air} is the permeability of still air [g/m·s·Pa], T is temperature (in Kelvin), p is ambient pressure, p_{o} is standard ambient pressure (101,325 Pa), R is the ideal gas constant for water, 0.461 Pa·m^3/(K·g), and the value 2.306 $\times 10^{-5}$ m^2/s is the diffusivity constant. The surface resistance, R_{surface} can be approximated to be 4 $\times$ 10^4 Pa·s·m^2·g by Lewis' relation [167]. Using Equation A.1 to estimate R_{sp}, the corrected water vapor permeability, WVP_{cor} (the permeability of the test specimen, of thickness l, calculated without resistances, Eq. A.1), is

$$WVP_{\text{cor}} = l \cdot R_{\text{sp}}^{-1} \tag{A.3}$$

Stagnant Air Correction - Method 2 (Krochta, Gennadios) [168, 222]:

This method is based on the vapor pressures along the trajectory of the diffusing water molecules, as per Figure A.7. The computation here assumes no stagnant air exists above the test cup ($h_{\text{o}} = 0$, Figure A.7). The individual partial pressure values at specific interfaces along the path of diffusion are estimated as:

$$p_{\text{w0}} = S \times \text{RH}_1/100 \tag{A.4}$$

$$p_{\text{w2}} = S \times \text{RH}_2/100 \tag{A.5}$$

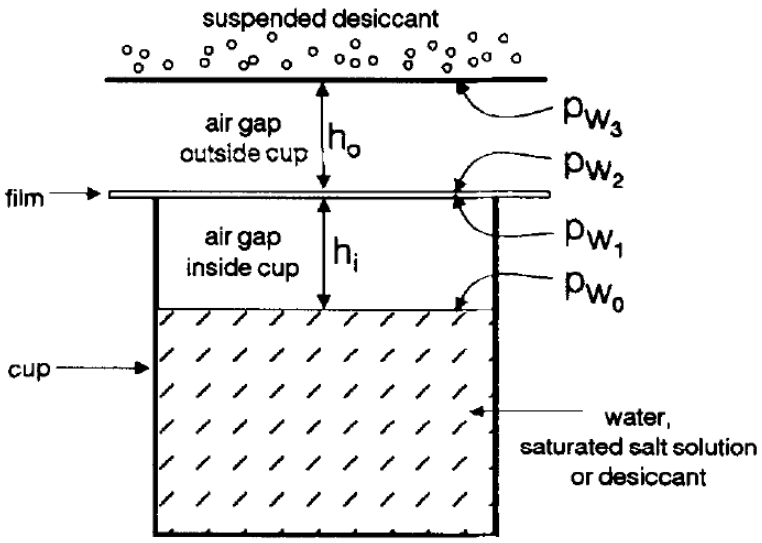

Figure A.7: Illustration of a WVP test cup showing air gap heights, h, and water vapor partial pressures, p_{w}, along the path of diffusion. Figure taken from Gennadios et al. [168].

$$p_{\mathrm{w1}} = p - (p - p_{\mathrm{w0}})\exp(-\mathrm{WVTR}_{\mathrm{mea}} h_{\mathrm{i}}/cD) \tag{A.6}$$

$$\mathrm{WVTR}_{\mathrm{cor}} = \mathrm{WVTR}_{\mathrm{mea}}\left[(p_{\mathrm{w2}} - p_{\mathrm{w0}})/(p_{\mathrm{w2}} - p_{\mathrm{w1}})\right] \tag{A.7}$$

where the partial pressures, p, are shown in Figure A.7, WVTR is water vapor transmission rate for either corrected (cor) or measured (mea) value, RH_1 and RH_2 are relative humidity values, h_{i} is the distance between specimen and desiccant, c is molar concentration, D is diffusivity, and S is the water vapor pressure. Molar concentration, c, is estimated using the ideal gas relation:

$$c = S \times R \times T \tag{A.8}$$

The diffusion coefficient at standard ambient pressure, D, is estimated by,

$$D = 0.26 \cdot (T/298)^{1.8} \tag{A.9}$$

$$WVTR_{\mathrm{cor}} = WVTR_{\mathrm{mea}}(p_{\mathrm{w2}} - p_{\mathrm{w0}})/(p_{\mathrm{w2}} - p_{\mathrm{w1}}) \tag{A.10}$$

A.4.4 WVP Change With Film Thickness

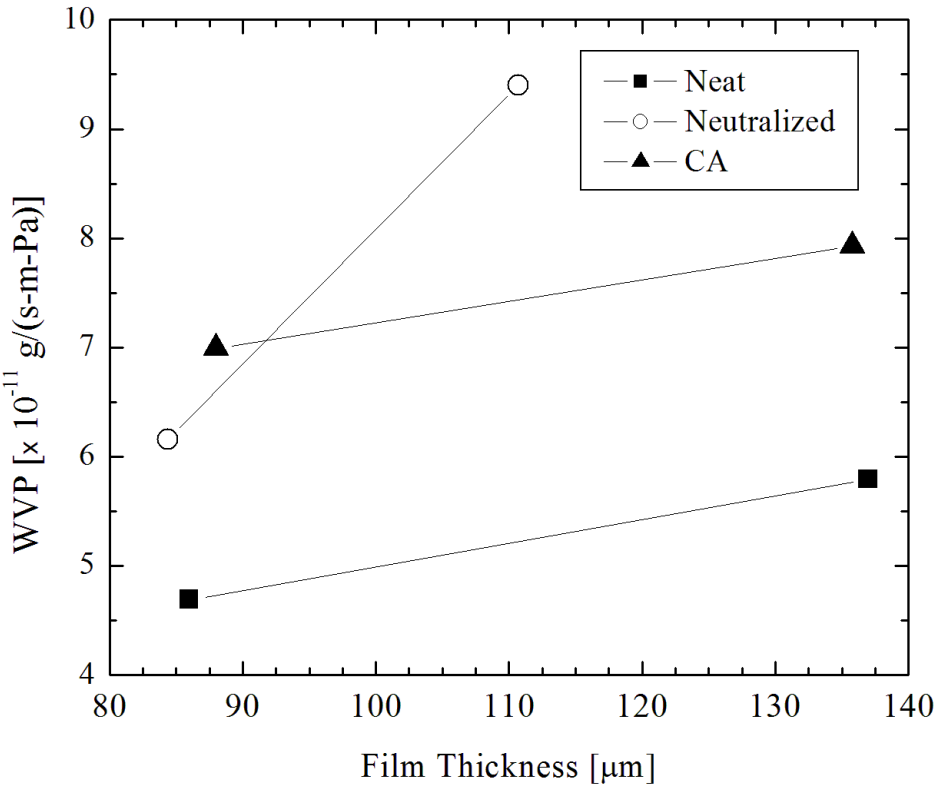

Figure A.8: The WVP change with film thickness.

A.5 Stoichiometric Ratios of Reactive Groups

Estimation of the molar ratio of reactive groups, COOH for citric acid, and CHO for GLU, to NH_2 for amine, per 1 g chitosan powder, using the DD provided by the chitosan manufacturer. Molecular weights and functionality (i.e. number reactant groups per molecule) of chitosan monomer units, citric acid, and GLU are given in the table below.

Monomer	Formula	M [g/mol]	f
Glucosamine	$C_6H_{11}O_4N_1$	161.15	$NH_2 = 1$
Acetylated-glucosamine	$C_8H_{13}O_5N_1$	203.19	$NH_2 = 1$
Citric Acid	$C_6H_8O_7$	192.10	COOH = 3
Glutaraldehyde	$C_5H_8O_2$	100.10	CHO = 2

$$n_{r,i} = f_r, i \times m_i / M_i \tag{A.11}$$

where n is number of moles, f is functionality, m is mass, M is molecular weight, and subscripts r is the reactive group, i is the compound.

For $m_{\text{chtsn}} = 1$ g: $n_{NH_2} = 4.37 \times 10^{-3}$ (75 % DD), $n_{NH_2} = 5.08 \times 10^{-3}$ (85 % DD).

Compound	Conc. [%] (w/w)	$n_{f,i}$ [mol]	Ratio (% DD given in brackets)
Citric acid	15	2.34×10^{-3}	$[NH_2]$:[COOH] = 2.17 (85), 1.87 (75)
GLU	3.12	6.24×10^{-4}	$[NH_2]$:[CHO] = 8.13 (85), 6.99 (75)
GLU	6.25	1.25×10^{-3}	$[NH_2]$:[CHO] = 4.065 (85), 3.49 (75)
GLU	12.5	2.50×10^{-3}	$[NH_2]$:[CHO] = 2.03 (85), 1.75 (75)

A.6 Surface Energy Calculation

Fowke's method was used to estimate the individual polar and dispersion surface tension components of the films as described in Section 3.8. Equation 3.27 is interpreted as a linear equation (y = mx + b) with the parts:

$y = \gamma_L \frac{(1+cos\theta)}{2(\gamma_L^D)^{1/2}}$, $m = (\gamma_S^P)^{1/2}$, $x = \frac{(\gamma_L^P)^{1/2}}{(\gamma_L^D)^{1/2}}$, and $b = (\gamma_S^D)^{1/2}$.

By plotting the respective x and y values, where θ is obtained experimentally, the parameters γ_L^P and γ_L^D from a database, and γ_S^P and γ_S^D are obtained from the slope and intercept, respectively. See Figure A.9.

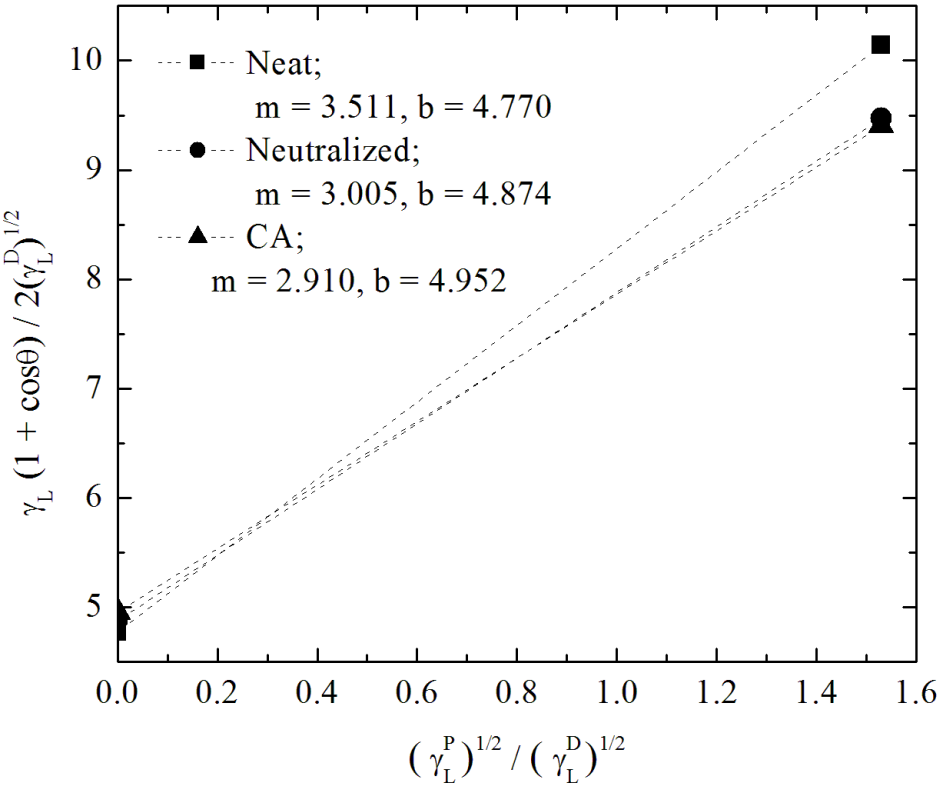

Figure A.9: Plot of respective y and x components from the Owens/Wendt method of estimating polar and dispersive components of surface tension, for neat, neutralized and CA films.

A.7 GAB Model Parameter Estimation

The following methodology for estimating the GAB model parameters (as described in Section 3.9) is provided below, and is taken from the article by Timmerman [176]. The model is converted to a quadratic formula, and the parameters of that parabolic expression are estimated using a least-square regression. The GAB parameters are then calculated from their relation to the quadratic formula parameters, as shown below:

$$a_{\mathrm{w}}/X = \alpha + \beta a_{\mathrm{w}} + \gamma a_{\mathrm{w}}^2 \tag{A.12}$$

where,

$$\alpha = 1/x_{\mathrm{m}} C_{\mathrm{G}} K_{\mathrm{G}} \tag{A.13}$$

$$\beta = (C_{\mathrm{G}} - 2)/x_{\mathrm{m}} C_{\mathrm{G}} \tag{A.14}$$

$$\gamma = -(C_{\mathrm{G}} - 1) K_{\mathrm{G}}/x_{\mathrm{m}} C_{\mathrm{G}} \tag{A.15}$$

The GAB constants are then calculated:

$$k = (f^{1/2} - \beta)/2\alpha \tag{A.16}$$

$$x_{\mathrm{m}} = f^{-1/2} \tag{A.17}$$

$$C_{\mathrm{G}} = 1 - \gamma/K_{\mathrm{G}}^2 \alpha \tag{A.18}$$

where,

$$f = \beta^2 - 4\alpha\gamma \tag{A.19}$$

Estimating the parameters for the second order model ($y = \beta_1 + \beta_2 x + \beta_3 x^2 + \epsilon$),

$$\hat{\beta} = (X_{\mathrm{m}}' X_{\mathrm{m}})^{-1} X_{\mathrm{m}}' Y \tag{A.20}$$

where X_{m} is the matrix for the input variable $a_{\mathrm{w,i}}$,

$$X_{\mathrm{m}} = \begin{bmatrix} 1 & a_{\mathrm{w,i}} & a_{\mathrm{w,i}}^2 \\ 1 & a_{\mathrm{w,i+1}} & a_{\mathrm{w,i+1}}^2 \\ . & . & . \\ 1 & a_{\mathrm{w,n}} & a_{\mathrm{w,n}}^2 \end{bmatrix} \tag{A.21}$$

and Y is the matrix for the response variable $a_{\mathrm{w,i}}/X$,

$$Y = \begin{bmatrix} 0 \\ a_{\mathrm{w,i}}/X_{\mathrm{i}} \\ . \\ . \\ a_{\mathrm{w,n}}/X_{\mathrm{n}} \end{bmatrix} \tag{A.22}$$

Appendix B

Additional XRD Analysis and Data

B.1 Degree of Crystallinity

The methods of estimating CrI, based on integration of the diffractogram (Area Methods; Method 1), or peak intensity values (Intensity Method; Method 2), are listed below.

B.1.1 Area Methods

Distinction between amorphous and crystalline segments represented by the diffractogram can be achieved by integration in four different ways, denoted as Methods 1A to 1D. Sources of variation in analysis differ by the choice of baseline and regions which separate the crystalline and non-crystalline segments. Sakurai [225] differentiated crystalline and amorphous regions by a linear baseline when analyzing chitosan films, as shown in Figure B.1A (Method 1A). This method, however, erroneously assumes the contributions from amorphous scattering are linear. This may be adjusted by estimating a non-linear baseline up to the base of the peaks [244, 245] as shown in Figure B.1B (Method 1B); the preferred approach is to measure the diffraction of a completely amorphous standard of the material. One criticism of this method is that part of the background scatter includes amorphous scattering and reduces the estimated crystallinity [246].

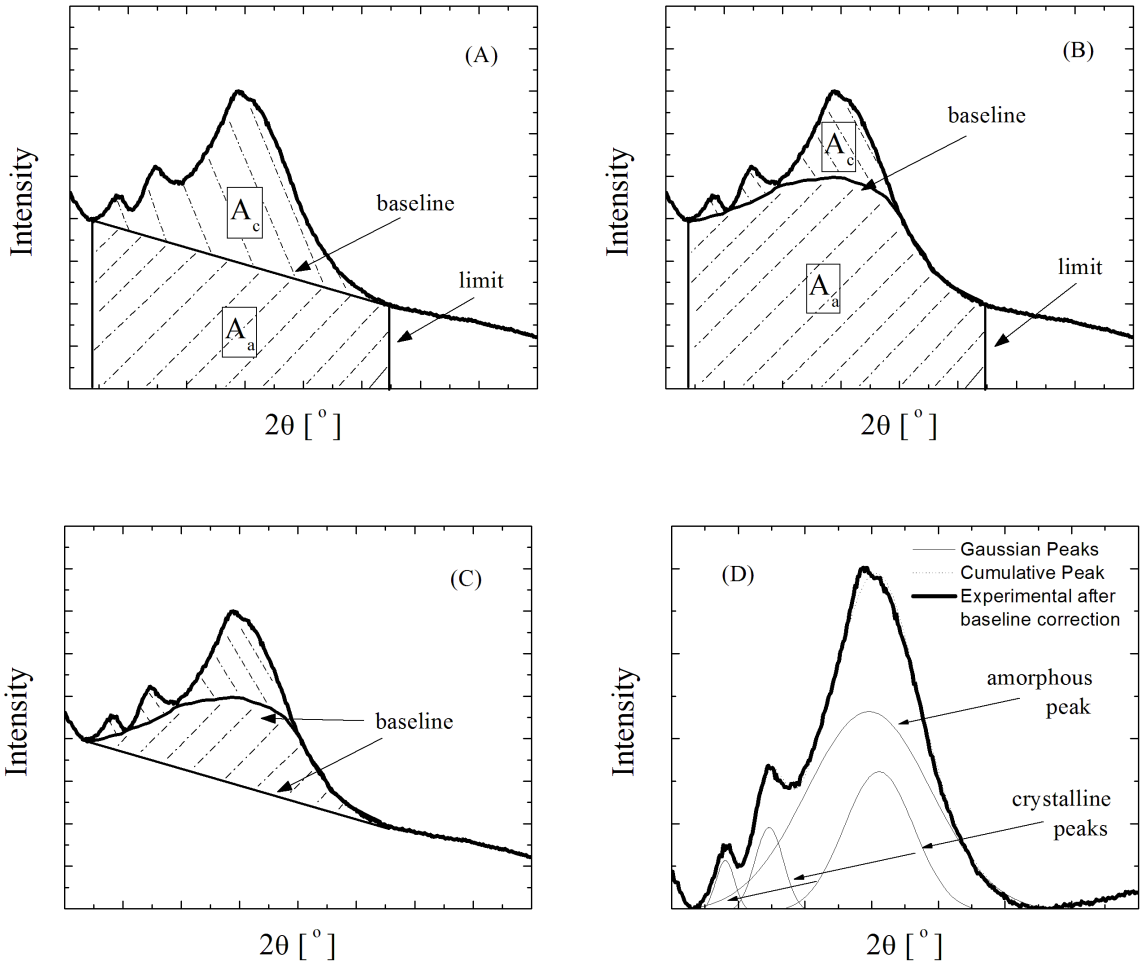

Figure B.1: Methods for estimating crystallinity index by peak integration (A_c = crystalline area, A_a = amorphous area). (A) Linear separation of crystalline and amorphous areas; integration taken to 0 intensity. (B) Non-linear separation of crystalline and amorphous regions; integration taken to 0 intensity. (C) Linear baseline; integration taken to baseline. (D) Peak fitting using Gaussian distribution after data corrected with linear baseline - same baseline as in (B).

The analysis method proposed by Nara and Komiya [247] for powdered starch utilizes Hermans-Weidinger method developed for cellulose, shown in Figure B.1C (Method 1C). Estimation of crystallinity index can also be performed by subtracting the background noise signal, and performing peak deconvolution on the remaining signal as shown in Figure B.1D (Method 1D). The sum of the areas of deconvoluted peaks corresponding to the crystalline peaks becomes A_c. The drawback to this method is the inherent assumptions made about the size of the amorphous peak, as multiple combination of peak sizes and shapes may yield the same net fit ratio, and the choice of peak fitting (i.e. Gaussian, Lorentzian and Voigt). A summary of crystallinity index estimation methods is given by Park et al. [245].

B.1.2 Intensity Method

One of the more common methods for estimating crystallinity is by taking the relative ratio of maximum crystalline peak intensity to the maximum intensity of the amorphous scatter, as per Equation B.1. It was developed for cellulose I by Segal in 1959 (see reference within [245]), and has been adopted for chitin and chitosan [55–57, 248]. The highest intensity peak between 19 and 21° in chitosan film and powder diffractorgrams correspond to the 110 lattice. The amorphous height is arbitrarily selected, but the local minimum between the 020 (15°) and 110 (20°) peaks for chitosan is a convenient choice. A 2θ of 16° is often cited [56, 57, 248] for this designation. See Figure B.2. (For reference on Miller indices of chitosan powder, see [49].)

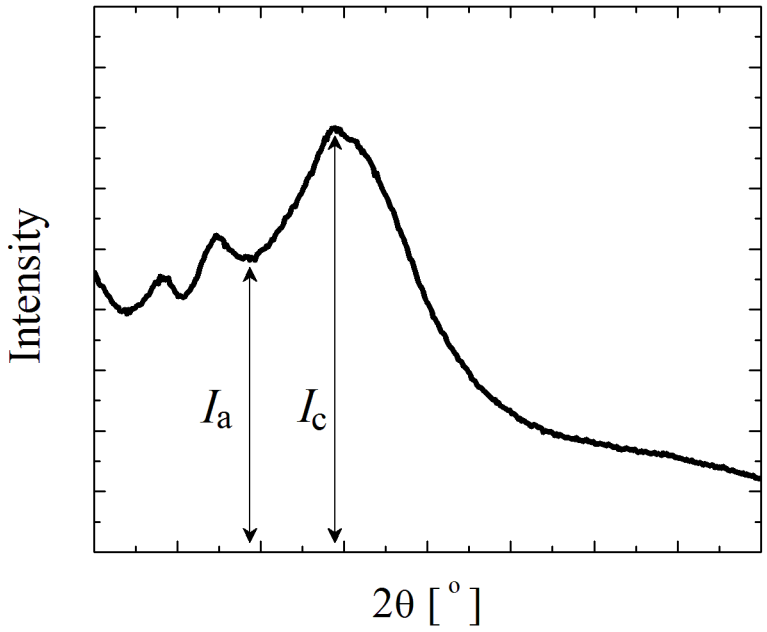

Figure B.2: Estimation of crystallinity index by relative heights of highest crystalline peak (I_c) and maximum height corresponding to amorphous scatter (I_a).

$$\text{crystallinity} = (I_c - I_a)/I_c \times 100\% \tag{B.1}$$

where I_c and I_a are the diffractogram intensities of 110 and amorphous bands, respectively.

B.1.3 Comparison of Methods

The degree of crystallinity values of the films were estimated using the methods outlined in the preceding figures and are given in Table B.1. Methods 1A - D correspond with the area methods, and method 2 is the intensity method. The trends of changes in crystallinity differ depending on the method used. Method 1A erroneously underestimates the crystallinity of the chitosan powder and neutralized films relative to neat films, while Method 1D yields the relatively highest COV of all the methods. Methods 1C and 2 offer more reliable and accurate reflection of the interpretation of the diffractogram. Method 1C was selected to represent the crystallinity index in the analysis.

Table B.1: Degree of crystallinity [%] of chitosan films computed using the various area and peak intensity methods

		Method				
Film Type	**Calc**	**1A**	**1B**	**1C**	**1D**	**2**
Neat	Average	33.8	9.0	19.3	34.1	26.4
	±	1.0	1.7	2.4	8.0	3.8
	COV [%]	3.0	18.6	12.4	23.3	14.3
Neutralized	Average	29.1	11.5	26.2	40.7	41.3
	±	3.9	0.5	2.2	5.2	1.3
	COV [%]	13.6	4.5	8.4	12.8	3.1
CA	Average	34.9	13.9	20.4	35.9	36.5
	±	5.3	1.8	2.1	6.6	2.7
	COV [%]	15.1	12.6	10.3	18.3	7.3
Powder chitosan	n = 1	32.0	15.1	51.5	N/a	48.2

B.2 Additional XRD Data and Plots

B.2.1 Chitosan Powder and Chitosan-Citrate Film

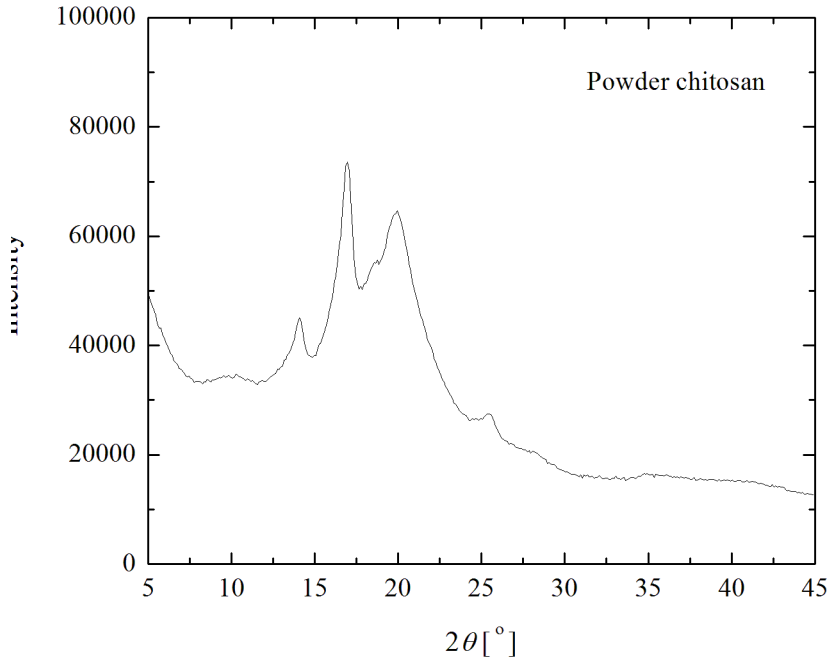

Figure B.3: Diffractogram of chitosan powder.

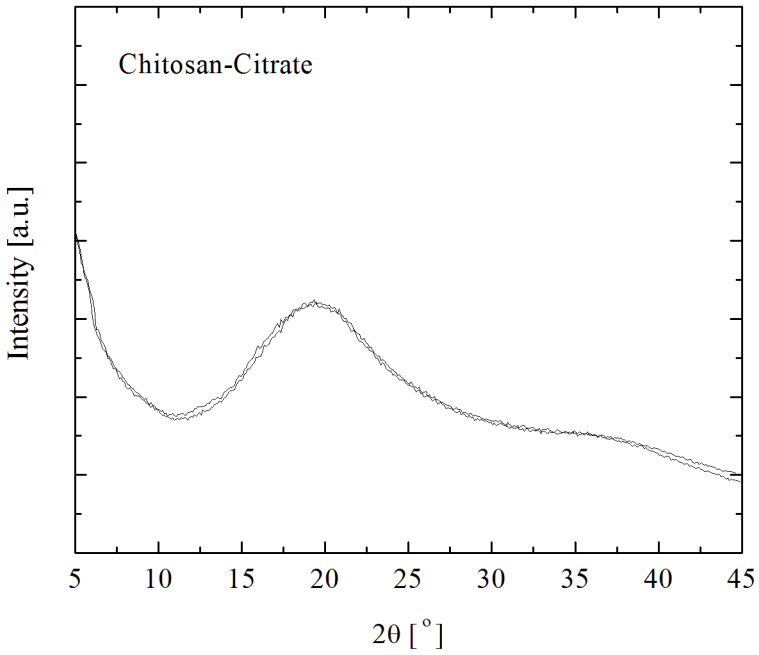

Figure B.4: Diffractogram of chitosan-citrate film.

B.2.2 Crystalline Diffraction Data of Citric Acid

The 16 ° 2θ peak in the diffractogram of CA films (B.5C, pg. 159) is likely due to citric acid on the film surface. The diffraction data of pure citric acid is presented in Table B.2. Row 7 in the table has been bolded to highlight the diffraction peak of pure citric acid that most probably correlates with the 16 ° 2θ peak of the CA films.

Data Source: de Wolff, P., Technisch Physische Dienst, Delft, The Netherlands., ICDD Grant-in-Aid.

Table B.2: Diffraction peaks of citric acid

No.	h	k	l	d [Å]	2 θ[deg]	I [%]
1	0	0	1	10.700	8.257	2.0
2	-2	0	1	6.270	14.114	35.0
3	2	0	0	5.970	14.827	2.0
4	0	0	2	5.340	16.588	18.0
5	1	1	0	5.090	17.409	2.0
6	0	1	1	4.980	17.796	35.0
7	**-1**	**1**	**1**	**4.890**	**18.127**	**100.0**
8	2	0	1	4.560	19.451	25.0
9	2	1	0	4.090	21.712	10.0
10	-1	1	2	4.000	22.206	4.0
11	0	1	2	3.870	22.962	2.0
12	-2	1	2	3.730	23.836	12.0
13	-2	0	3	3.710	23.967	4.0
14	0	0	3	3.560	24.993	12.0
15	1	1	2	3.430	25.956	25.0
16	2	0	2	3.420	26.033	35.0
17	3	1	0	3.250	27.421	2.0
18	-3	1	2	3.230	27.594	2.0
19	-4	0	1	3.190	27.947	4.0
20	-1	1	3	3.160	28.218	2.0
21	-4	0	2	3.130	28.494	1.0
22	-2	1	3	3.090	28.871	30.0
23	4	0	0	2.986	29.899	4.0
24	3	1	1	2.881	31.016	6.0
25	-3	1	3	2.858	31.272	45.0
26	-4	1	2	2.736	32.705	2.0
27	1	1	3	2.727	32.816	1.0
28	0	2	1	2.718	32.927	1.0
29	-1	2	1	2.706	33.077	4.0
30	0	0	4	2.672	33.511	8.0

B.2.3 Replicate Runs

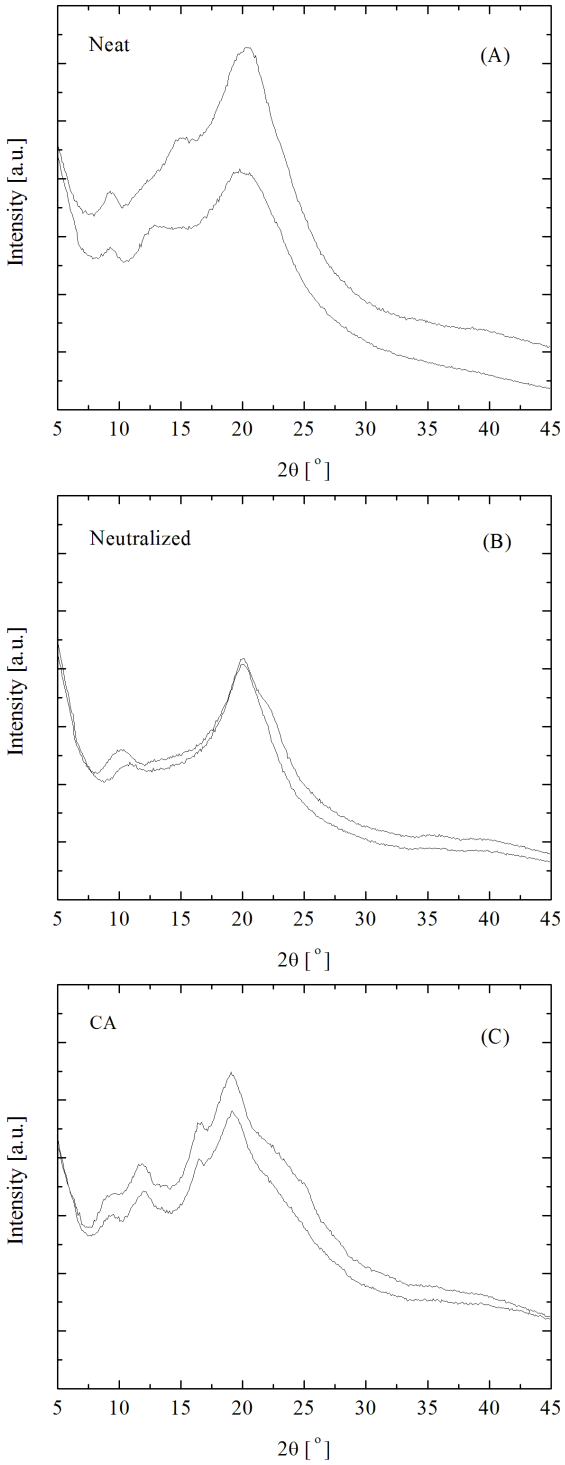

Figure B.5: Replicate diffractograms of (A) neat, (B), neutralized, and (CA) films. Two specimens were scanned for each film type; two from the same bulk film for neat and CA specimens, and one from two different films for the neutralized specimens.

Appendix C

Statistical Analysis

C.1 Statistical Analysis Equations

The statistical analysis performed on the experimental data, namely viscoelastic, WVP, tensile, and XRD. The analysis was performed using analysis of variance (ANOVA). Fisher's least significance (LSD) test to compare multiple means.

The computation of the ANOVA inputs, the sum of squares (SS), degrees of freedom (df), and mean square (MS), and the construction of the ANOVA (Table C.1) are outlined below.

Correction for mean:

$$CFM = \frac{1}{\sum_{t=1}^{k} n_t} \left(\sum_{t=1}^{k} \sum_{i=1}^{n_t} y_{ti} \right)^2 \tag{C.1}$$

Total sum of squares:

$$S_{\text{total}} = \sum_{t=1}^{k} \sum_{i=1}^{n_t} y_{ti}^2 - \text{CFM} \tag{C.2}$$

Sum of squares corresponding to 'signal' (between treatments)

$$S_{\text{b}} = \sum_{t=1}^{k} \frac{\left(\sum_{i=1}^{n_t} y_{ti} \right)^2}{n_t} - \text{CFM} \tag{C.3}$$

Sum of squares corresponding to 'noise' or residuals (within treatments)

$$S_{\text{w}} = S_{\text{total}} - S_{\text{b}} \tag{C.4}$$

where y_{ti} denotes an individual value of treatment number, t, out of a total of k treatments, and n_t is the total number of observations for a specific treatment.

Table C.1: ANOVA Table - Sample

Source	df	SS	MS	F
Signal	df_b	SS_b	SS_b / df_b	MS_b / MS_w
Noise	df_w	SS_w	SS_w / df_w	-
Total	df_{total}	SS_{total}	-	-

Fisher's LSD is used to compare multiple means without performing $k(k\text{-}1)/2$ student t-tests, as outlined below. When the difference between two means exceeds the computed LSD value, the means are considered significantly statistically difference.

$$\text{standard error} : s.e. = \sqrt{\frac{2s^2}{n}} \tag{C.5}$$

where n is the number of samples per treatment type, or if the number is different per treatment the average $\overline{n}$ may be used.

$$LSD = s.e \times t_{n_{total}-k,\alpha/2} \tag{C.6}$$

C.2 Analysis of DMA Data

For data on DMA measurements of non-preheated films, refer to Section 5.3.1.

Table C.2: ANOVA - DMA Measurements - E'(35 °C)

Source	df	SS	MS	F_{obs}
Film Types	3	20832903	6944301	16.7
Within Film	14	5806944	414782	
Total	17	26639847		

E'(35 °C) means comparison by LSD: $\alpha = 1$ %; $se = 303.6$ ($n = 5$); $t_{14,0.005} = 2.977$; $\therefore$LSD = 904

Pairs	$\Delta E'$(35 °C)	Sig. Diff.
Neat - Neutralized	1594	Y
Neutralized - CA	924	Y
Neutralized - CA-HT	941	Y
CA - CA-HT	17	N

Table C.3: ANOVA - DMA Measurements - E'(195 °C)

Source	df	SS	MS	F_{obs}
Film Types	3	16979987	5659996	40.0
Within Film	14	1980061	141433	
Total	17	18960048		

E'(195 °C) means comparison by LSD: $\alpha = 1$ %; $se = 177.3$ (n= 5); $t_{14,0.005} = 2.977$; $\therefore$LSD = 528

Pairs	$\Delta E'$(195 °C)	Sig. Diff.
Neat - Neutralized	1761	Y
Neutralized - CA	583	Y
Neutralized - CA-HT	336	N
CA - CA-HT	248	N

Table C.4: ANOVA - DMA Measurements - $T(\tan\delta$ peak 1)

Source	df	SS	MS	F_{obs}
Film Types	3	81.2	27.1	0.41
Within Film	14	926.6	66.2	
Total	17	1007.8		

$T(\tan\delta$ peak 1) means comparison by LSD: $\alpha = 1$ %; $se = 3.84$ $(n = 5)$; $t_{14,0.005} = 2.977$; $\therefore$LSD = 11

Pairs	$\Delta T(\tan\delta$ peak 1)	Sig. Diff.
Neat - Neutralized	4.8	N
Neutralized - CA	0.19	N
Neutralized - CA-HT	2.59	N
CA - CA-HT	2.77	N

Table C.5: ANOVA - DMA Measurements - $T(\tan\delta$ peak 2)

Source	df	SS	MS	F_{obs}
Film Types	3	5605	1868	42.1
Within Film	9	400	44	
Total	12	6005		

$T(\tan\delta$ peak 2) means comparison by LSD: $\alpha = 1$ %; $se = 3.70$ $(n = 3)$; $t_{9,0.005} = 3.250$; $\therefore$LSD = 12.01

Pairs	$\Delta T(\tan\delta$ peak 2)	Sig. Diff.
Neat - Neutralized	23	Y
Neutralized - CA	57	
Y [0.5ex] heightNeutralized - CA-HT	56.5	Y
CA - CA-HT	0.9	N

C.3 Analysis of Tensile Data

For data on tensile measurements, refer to Section 6.3.3.

Table C.6: ANOVA - Tensile Measurements - Tensile Strength

Source	df	SS	MS	F_{obs}
Film Type	5,250	2	2625.1	65.7
Within film	959	24	40.0	
Total	6,209	26		

TS means comparison by LSD: $\alpha = 5$ %; $se = 2.166$ ($n = 16$); $t_{0.025,46} = 2.021$; $\therefore$ LSD = 4.377

Pairs	ΔTS	Sig. Diff.
Neat-Neutralized	25.0	Y
Neat-CA	34.6	Y
Neutralized-CA	9.6	Y

Table C.7: ANOVA - Tensile Measurements - Elongation Before Break

Source	df	SS	MS	F_{obs}
Film Type	10.49	2	5.247	0.97
Within film	247.8	46	5.39	
Total	258.3	48		

EBB means comparison by LSD: $\alpha = 5$ %; $se = 0.812$ ($n = 16$); $t_{0.025,46} = 2.021$; $\therefore$ LSD = 1.641.

Pairs	ΔEBB	Sig. Diff.
Neat-Neutralized	1.1	N
Neat-CA	0.9	N
Neutralized-CA	0.2	N

Table C.8: ANOVA - Tensile Measurements - Young's Modulus

Source	df	SS	MS	F_{obs}
Film Type	0.836	2	0.418	14.32
Within film	1.342	46	0.0292	
Total	2.178	48		

E means comparison by LSD: $\alpha = 5\ \%$; $se = 0.060$ $(n = 16)$; $t_{0.025,46} = 2.021$; $\therefore$ LSD $= 0.121$

Pairs	ΔE	Sig. Diff.
Neat-Neutralized	0.26	Y
Neat-CA	0.29	Y
Neutralized-CA	0.03	N